STRATIGRAPHY, PALEOHYDROLOGY, AND SOIL VARIABILITY IN LATE QUATERNARY RIVER VALLEYS OF THE SOUTHEASTERN ATLANTIC COASTAL PLAIN, USA

by

BRADLEY EDWARD SUTHER

(Under the Direction of David S. Leigh)

ABSTRACT

Southeastern Atlantic Coastal Plain river valleys contain a diverse assemblage of late Quaternary fluvial landforms and deposits that provide important information about past river behavior and constitute geomorphic frameworks for chronosequence studies that evaluate changes in soils over time. However, most geologic maps fail to resolve the complexity of surficial deposits in Coastal Plain river valleys, and the hydrologic implications of large meandering paleochannels preserved in these settings remain poorly understood. Furthermore, previous chronsequence studies have not evaluated the extent of soil variability on fluvial landforms in these environments. To address these problems, three separate but inter-related studies were conducted. In the first study, the Quaternary sediments of the lower Oconee River valley were mapped using allostratigraphy. The Oconee valley was found to contain eight Oconee River-derived alloformations ranging from early-middle Pleistocene to Holocene age. The Oconee River had a braided morphology during the late Wisconsin interval (35-17 ka), a large meandering morphology during the terminal Pleistocene (17-11 ka), and modern-sized meanders during the Holocene (11 ka-present). These distinct morphological phases produced

unique alloformations. In the second study, the bankfull discharge of large, terminal Pleistocene meandering paleochannels ("mega-meanders") along six Coastal Plain rivers was estimated using channel boundaries determined from stratigraphy and hydraulic modeling. Mega-meander bankfull discharge was found to be similar to the discharge of present-day Coastal Plain rivers. The modest discharge of mega-meanders results from their lower hydraulic efficiency relative to modern rivers, which is due to a high width-to-depth ratio and a correspondingly reduced hydraulic radius. In the third study, soil variability and development were evaluated across a chronosequence of optically-dated meandering channel scroll bars in the Pee Dee River valley in South Carolina that range in age from Holocene to 119±30 ka. Soil morphology and chemistry show increasing development with time across the chronosequence, but soil variability resulting from intra-landform variations in parent material and relief is considerable, indicating the importance of understanding of soil variability within individual geomorphic surfaces when evaluating chronosequences in these settings. Together, these studies improve understanding of fluvial behavior, paleohydrology, and soil evolution within Coastal Plain valleys during the late Quaternary.

INDEX WORDS: allostratigraphy, Carolina, Coastal Plain, chronosequence, fluvial, Georgia, Holocene, late Pleistocene, optically-stimulated luminescence, paleochannel, paleodischarge, paleomeander, soil variability, Ultisols

STRATIGRAPHY, PALEOHYDROLOGY, AND SOIL VARIABILITY IN LATE QUATERNARY RIVER VALLEYS OF THE SOUTHEASTERN ATLANTIC COASTAL PLAIN, USA

by

BRADLEY EDWARD SUTHER

B.S., North Carolina State University, 2000.

M.S., The University of Georgia, 2006.

A Dissertation Submitted to the Graduate Faculty of The University of Georgia in Partial Fulfillment of the Requirements for the Degree

DOCTOR OF PHILOSOPHY

ATHENS, GEORGIA

2013

STRATIGRAPHY, PALEOHYDROLOGY, AND SOIL VARIABILITY IN LATE QUATERNARY RIVER VALLEYS OF THE SOUTHEASTERN ATLANTIC COASTAL PLAIN, USA

by

BRADLEY EDWARD SUTHER

Major Professor:	David S. Leigh
Committee:	George A. Brook Steven M. Holland Marguerite Madden Larry T. West

Electronic Version Approved:

Maureen Grasso
Dean of the Graduate School
The University of Georgia
August 2013

ACKNOWLEDGEMENTS

Support for my dissertation research was provided by the Educational Component of the U.S. Geological Survey's National Cooperative Mapping Program (EDMAP grant #G11AC20162); a National Geographic Society Committee for Research and Exploration grant (#8850-10); a National Science Foundation Doctoral Dissertation Research Improvement Grant (#1202846); and by the University of Georgia Graduate School's Dean's Award and Dissertation Completion Award.

I would like to extend my most sincere thanks to my advisor, David Leigh, who has provided critical guidance and insight throughout the design and completion of this project. His assistance in the field, in the laboratory, and in data analysis and manuscript review has greatly improved this research. I would also like to thank my committee members, George Brook, Steve Holland, Marguerite Madden, and Larry West, who provided valuable feedback and advice throughout the process of completing this project. I would like to acknowledge Art Schultz of the U.S. Geological Survey for his support for the geologic mapping component of this project, and thank David Shelley and the National Park Service for their support of the paleohydrologic component of this research.

The following private landowners provided property access that was essential for the completion of this project, and they are all gratefully acknowledged: Frank Baumgartner; Hardy Brown; Hal Goodwin and David Schuetrum of the Kingville Hunt Club; Durwood Graham and Consolidated Investment Properties, LLC; Jessie Hartley; Danny Howell; Robert Mace; Plum Creek Timberlands; George Roundtree; Dan Taulbee; L.A. Waters; and Kennie Woodard. I

would like to extend a special thanks to Campbell Coxe and the staff of Roblyn's Neck Trophy Club, and Pennie and Lloyd Moses, of Uvalda, Georgia, who provided not only property access but valuable logistical support for this research.

James Rogers, Jacob McDonald, Jessie Hughes, Seth Younger, Zack Sanders, Sean Cameron, Dustin Menhart, Amy Woodell, Jason Rumfelt, Caleb Snyder, and Mike Grimaldi provided field assistance. Jacob McDonald and Sergio Bernardes provided valuable cartographic assistance, and Sean Cameron and Cole Perry served as laboratory assistants. Four *pro bono* OSL dates were provided by the University of Georgia Luminescence Dating Laboratory, and Fong Brook's efforts to provide timely OSL dating results are gratefully recognized. Jane Worley provided accounting support, and Graham Pickren assisted with the formatting of this document.

Finally, but most importantly, I would like to thank my wife, Amy, and my family and friends for the love, encouragement, and patience that they have extended to me throughout my graduate education and the completion of this research. This work would not have been possible without their steadfast support.

TABLE OF CONTENTS

Page

ACKNOWLEDGEMENTS iv

LIST OF TABLES viii

LIST OF FIGURES x

CHAPTER 1 - INTRODUCTION 1

1.1 Introduction and Objectives 1

1.2 Literature Review 5

1.3 References 14

CHAPTER 2 – QUATERNARY ALLOSTRATIGRAPHY OF THE LOWER OCONEE RIVER VALLEY, UVALDA QUADRANGLE, GEORGIA 19

2.1. Introduction 22

2.2. Map Area and Geologic Setting 24

2.3. Methods 26

2.4. Results: Geologic Map Units 32

2.5. Discussion 64

2.6. Conclusions 70

2.7. References 71

CHAPTER 3 – DISCHARGE OF "MEGA-MEANDER" PALEOCHANNELS OF THE SOUTHEASTERN ATLANTIC COASTAL PLAIN, USA 85

3.1. Introduction 87

3.2. Study Area 88
3.3. Methods 90
3.4. Results 95
3.5. Discussion 106
3.6. Conclusions 113
3.7. References 114
CHAPTER 4 – SPATIO-TEMPORAL SOIL VARIABILITY ON LATE QUATERNARY FLUVIAL SURFACES OF THE PEE DEE RIVER VALLEY, SOUTHEASTERN ATLANTIC COASTAL PLAIN, USA 133
4.1. Introduction 135
4.2. Study Area 137
4.3. Methods 140
4.4. Results and Discussion 146
4.5. Conclusions 172
4.6. References 174
CHAPTER 5 - CONCLUSION 199
5.1. Conclusions 199
5.2. References 204
APPENDIX A – PROFILE DESCRIPTIONS FROM STRATIGRAPHIC CROSS-SECTIONS A, B, AND C, UVALDA, GEORGIA QUADRANGLE 206
APPENDIX B – PROFILE DESCRIPTIONS FROM ALLOFORMATIONS Qp2 AND Qp1, UVALDA QUADRANGLE, GEORGIA 239

LIST OF TABLES

Page

Table 2.1: Radiocarbon dates and supporting data. 84

Table 2.2: Optically-stimulated luminescence (OSL) dates and supporting data. 84

Table 3.1: Discharge estimates for modern rivers 127

Table 3.2: Bankfull discharge estimates at selected gaging stations in the Georgia Coastal Plain using the slope-area method and comparison with discharges calculated from gage records. 128

Table 3.3: Slope estimates derived from paleochannel geomorphic components and river valley gradients 129

Table 3.4: Radiocarbon dates and supporting data. 130

Table 3.5: Optically-stimulated luminescence (OSL) dates and supporting data. 131

Table 3.6: Bankfull discharge estimates for mega-meanders and small paleomeanders. 132

Table 4.1: Optically-stimulated luminescence (OSL) dates and supporting data. 189

Table 4.2: Descriptive statistics for selected soil morphological properties 190

Table 4.3: Selected statistics for linear regressions of soil properties versus downstream distance (m) along scroll bar ridge crests 191

Table 4.4: Descriptive statistics for selected chemical properties of the <2 mm fraction of the most pedogenically well-expressed B-horizon per pedon 192

Table 4.5: Descriptive statistics for selected chemical properties of the fine sand (0.125-0.250 mm) fraction of the most pedogenically well-expressed B-horizon per pedon 194

Table 4.6: Results of difference of means t-tests for selected soil morphological properties among soils of scroll bars on the same paleomeander surface 195
Table 4.7: Results of difference of means t-tests for selected soil chemical properties of the <2 mm fraction among soils of scroll bars on the same paleomeander surface.....196
Table 4.8: Results of difference of means t-tests for selected soil chemical properties of the fine sand (0.125-0.250 mm) fraction among soils of scroll bars on the same paleomeander surface 197
Table 4.9: Selected statistics for linear regressions of soil properties versus mean age (ka) 198

LIST OF FIGURES

Page

Figure 2.1: Map area location: Uvalda, Georgia 7.5-minute quadrangle. 74

Figure 2.2: Huddleston's (1988) generalized map of marine terraces in Georgia..... 75

Figure 2.3: Geologic map of the Quaternary sediments of the lower Oconee River valley, Uvalda quadrangle, Georgia..... 76

Figure 2.4: Quaternary sediments of the lower Oconee River valley in the Uvalda, Georgia and adjacent 7.5-minute quadrangles 77

Figure 2.5: Allostratigraphic cross-sections of the lower Oconee River valley, Uvalda, Georgia quadrangle..... 78

Figure 2.6: Modern point bar sediments of the Oconee River..... 79

Figure 2.7: Cut bank exposure, Clarks Bluff of the Oconee River..... 80

Figure 2.8: Road cut exposing Qp3 alluvium 81

Figure 2.9: Qp2 alluvium exposed in borrow pit..... 82

Figure 2.10: Photo-mosaic of a strongly developed Ultisol, map unit TQu 83

Figure 3.1: Location of mega-meander study sites.....119

Figure 3.2: Planimetric view and stratigraphic cross-sections of the Uvalda mega- and small meanders of the Oconee River.....120

Figure 3.3: Planimetric view and stratigraphic cross-sections of the Mouzon mega- and small meanders of the Black River.....121

Figure 3.4: Planimetric views and stratigraphic cross-sections of the Cooperville FP-2 mega-meander (Ogeechee River) and the Running Creek mega-meander (Congaree River). 122

Figure 3.5: Planimetric views and stratigraphic cross-sections of the Damon mega-meander (Pee Dee River) and the Moccasin Creek mega-meander (Neuse River).....123

Figure 3.6: Plot of radiocarbon and optically-stimulated luminescence (OSL) dates for mega-meanders and small paleomeanders.....124

Figure 3.7: Mega-meander bankfull discharge (Paleo-Q_{BKF}) and discharge of the 2-year recurrence interval flood (Q_2) on modern rivers adjacent to mega-meander sites 125

Figure 3.8: Mega-meander bankfull discharge compared to mean annual discharge of modern Coastal Plain rivers 126

Figure 4.1: Study area.....179

Figure 4.2: Locations of scroll bar study sites and sampling transects.....180

Figure 4.3: Field-sheet quality longitudinal cross-section depicting topography and soil variability along the PD1-2 pilot study scroll bar.....181

Figure 4.4: Resampled standard deviations of field-measured A+E horizon thickness, Bt horizon thickness, solum thickness, and rubification as quantified by the Buntley-Westing Index for pilot study scroll bar PD1-2 plotted against sample size 182

Figure 4.5: Longitudinal topographic profile of scroll bar PD1-2 (A) and selected soil morphological and chemical properties from the most well-expressed B-horizon per pedon plotted against downstream distance along the scroll bar ridge crest 183

Figure 4.6: Longitudinal topographic profile of scroll bar PD2-1 (A) and selected soil morphological and chemical properties from the most well-expressed B-horizon per pedon plotted against downstream distance along the scroll bar ridge crest.. 184

Figure 4.7: Longitudinal topographic profile of scroll bar PD3-2 (A) and selected soil morphological and chemical properties from the most well-expressed B-horizon per pedon plotted against downstream distance along the scroll bar ridge crest.. 185
Figure 4.8: Soil morphological properties plotted as a function of age. 186
Figure 4.9: Soil chemical properties of the <2 mm fraction plotted as a function of age.....187
Figure 4.10: Soil chemical properties of the fine sand (0.125-250 mm) fraction plotted as a function of age.. 188

CHAPTER 1 - INTRODUCTION

1.1 Introduction and Objectives

Fluvial landforms and deposits preserved in alluvial valleys of the southeastern Atlantic Coastal Plain provide important information about past river behavior and fluvial response to external drivers, like climate change (Leigh, 2008). These features also constitute potential geomorphic and chronologic frameworks for soil chronosequence studies that evaluate changes in soil development over time by examining properties of soils developed on similar fluvial landforms of different age (Markewich et al., 1987, 1988, 1989; Howard et al., 1993; Shaw et al., 2003). Recent research indicates that many alluvial valleys in the region contain multiple late Quaternary fluvial terraces that preserve braided and meandering channel patterns and source-bordering riverine eolian dunes that reflect extreme natural variation in past river channel pattern and depositional style (Ivester and Leigh, 2003; Leigh et al., 2004; Leigh, 2006). These features and their underlying deposits are believed to indicate regional-scale fluvial adjustments to late Quaternary climate changes and provide important insights into terrestrial response to climate forcing in a middle latitude, unglaciated, humid subtropical region that is otherwise only represented by global proxy records (e.g., ice or deep sea cores) and pollen sections from isolated localities (Leigh, 2008).

Although a chronological framework for late Quaternary river behavior in the southeastern Atlantic Coastal Plain has been established, this chronology is limited to the last 30,000 years (30 ka) and has relatively coarse resolution with respect to the last 16 ka, a time characterized by meandering channels of widely ranging sizes (Leigh and Feeney, 1995; Leigh,

2006; Leigh, 2008). Furthermore, alluvial stratigraphic investigations of these environments have been limited in scope, and most existing geologic maps fail to resolve the variety and complexity of late Quaternary valley fills in the region (Georgia Department of Natural Resources, 1976; Owens, 1989; Richmond et al., 1986; Richmond et al., 1987). This lack of geologic framework information greatly limits the ability of policy makers, regulatory agencies, and land managers to make informed decisions about surface and groundwater quality and protection, flood control, sustainable land use planning, and river management and restoration in the face of projected climate and sea level change. Thus, there is a clear need for more detailed, higher resolution stratigraphic, sedimentologic, geochronologic, and paleohydrologic information from Coastal Plain alluvial settings.

Alluvial valleys of the southeastern Coastal Plain also contain important soil resources and serve as agricultural and silvicultural hotspots within the region. Soil chronosequence studies conducted in these settings have provided valuable insights into the genesis of Coastal Plain soils (Markewich et al., 1986; 1987; 1988; Howard et al., 1993; Shaw et al., 2003). However, previous Coastal Plain alluvial chronosequences have not explicitly addressed soil spatial variability on individual fluvial landforms, a phenomenon which is not well-resolved by the scale of existing soil survey mapping in the region. Within a chronosequence framework, adequate representation of soil spatial variability on isochronous surfaces is necessary before dominant pedogenic processes can be ascertained (Harrison et al., 1990), models of pedogenesis can be tested (Huggett, 1998), the effect of time on soil formation can be estimated (Eppes and Harrison, 1999), and temporal changes in soil variability can be assessed (Barrett and Schaetzl, 1993). A better grasp of the extent and causes of soil variability in Coastal Plain alluvial valleys is needed before soil chronosequence research in the region can advance.

In order to improve our understanding of the geomorphic and geologic framework, paleohydrology, and soils of southeastern Atlantic Coastal Plain alluvial landscapes, this dissertation research has the following main objectives:

1. Generate a high resolution geologic map of Quaternary sediments in the lower Oconee River valley, within the Uvalda, Georgia 7.5-minute quadrangle at a 1:24,000 scale.
2. Model the channel-forming (bankfull) discharge represented by exceptionally large ("mega-meander") terminal Pleistocene paleomeanders as compared to modern bankfull discharge along six Coastal Plain rivers, including the lower Oconee.
3. Assess the degree and drivers of soil spatial variability and development on different age fluvial surfaces within the Pee Dee River valley, with a focus on soils developed on the scroll bar components of these surfaces.

Within the above research design, mapping and dating along the lower Oconee River serve as a foundation for the other research components by providing a detailed, high resolution stratigraphic and chronologic framework for Quaternary sediments from a representative setting that facilitates the paleohydrologic investigations in the Oconee map area and along other rivers in the region. Within the broader geomorphic and geochronologic context provided by the Oconee mapping, the paleohydrologic research presented here primarily focuses on the fluvial processes of the terminal Pleistocene interval, which generated a particularly unique set of landforms and deposits across the Southeast in the form of mega-meander paleochannels that remain poorly understood. Finally, the geomorphic, geologic, and geochronologic investigations associated with the proposed mapping and paleohydrologic research provide the geologic and temporal framework for the assessment of soil variability and development within a chronosequence context in the Pee Dee River valley, which is centrally located in the study

region. Together, these three lines of investigation contribute to our over-all understanding of fluvial behavior, paleohydrologic conditions, and soil and landscape evolution within the alluvial valleys of the southeastern Atlantic Coastal Plain during the late Quaternary.

Following the literature review provided below, this dissertation reports the findings, major implications, and conclusions of the individual research components discussed above in the format of individual, manuscript-style chapters. Chapter two presents results from geologic mapping of the Quaternary sediments of the lower Oconee River valley in southeast Georgia. The allostratigraphic mapping approach employed by the study is evaluated in terms of its suitability for delineation of Quaternary fluvial sediments in the southeastern Coastal Plain, and interpretations about the late Quaternary history of the Oconee River derived from the mapping are provided. Chapter three presents findings from a paleohydrologic investigation of large, terminal Pleistocene abandoned meandering river channels ("mega-meanders") along six rivers in the Coastal Plain of Georgia and the Carolinas. Estimates of bankfull discharge for mega-meander channels are reported and compared to bankfull flood-sizes of modern Coastal Plain Rivers, factors potentially responsible for the unusually large planform dimensions of mega-meanders are evaluated, and the paleohydrologic and paleoenvironmental implications of these features are discussed. In chapter four, soil variability and development are evaluated across a chronosequence of meandering channel scroll bar deposits that range in age from Holocene to 119±30 ka. The degree and drivers of soil variability are assessed at the scale of individual scroll bars, among scroll bars of the same fluvial surface, and among fluvial surfaces of different age. Age-related trends in soil morphology and chemistry that occur across the chronosequence are evaluated, and implications of soil variability for soil chronosequence studies are discussed. Finally, chapter five summarizes the major conclusions of the above studies and discusses their

contributions to our over-all understanding of late Quaternary landscape evolution in alluvial valleys of the Atlantic Coastal Plain.

1.2 Literature Review

This section provides a review of previous geomorphic and geologic mapping studies in the vicinity of the Oconee River valley, as well as background information about the "mega-meander" paleochannels of southeastern Coastal Plain river valleys that are investigated by this study. Three sub-sections follow that address drivers of soil variability, soil spatial variability within documented chronosequences, and spatio-temporal variation in Atlantic Coastal Plain soils.

1.2.1 Previous geomorphic and geologic studies of the Oconee River valley

The lower Oconee River valley contains a diverse assemblage of late Quaternary fluvial and eolian landforms, including multiple fluvial terraces that preserve former braided and meandering channel patterns (Leigh et al., 2004) and source-bordering riverine dunes (Ivester and Leigh, 2003). These landforms and their associated deposits provide important information about the behavior of the Oconee River during the late Quaternary in terms of variability in channel pattern, depositional style, lateral migration, and incision, as well as its response to external drivers, like climate change. The Oconee River is a tributary to the Altamaha River (Georgia), and features similar to those found in the Oconee valley occur downstream along the Altamaha and are also present along other rivers of the southeastern Atlantic Coastal Plain, including the Canoochee, Ogeechee and Savannah Rivers (Georgia), the Pee Dee and Little Pee Dee Rivers (South Carolina), and the Cape Fear River (North Carolina). In sum, these landforms

and their underlying deposits are believed to indicate a regional response of southeastern Coastal Plain fluvial systems to late Quaternary climate changes (Leigh, 2008).

While previous studies have characterized and dated some of the fluvial deposits along the lower Oconee River (Leigh et al., 2004), no detailed Quaternary geologic mapping of the valley has been conducted. Published geologic and/or geomorphic maps that encompass the lower Oconee valley are general in nature and include the Geologic Map of Georgia (Georgia Department of Natural Resources, 1976); The Quaternary Geologic Map of the Jacksonville 4X6 degree Quadrangle, United States (Richmond et al., 1986); The Quaternary Geologic Map of the Savannah 4X6 degree Quadrangle, United States (Richmond et al., 1987); and the Generalized Map of Marine Terraces and the Dissected Marine Terrace Region of Georgia (Fig. 56 of Huddlestun, 1988). These maps typically represent all fluvial sediments along the Oconee and other rivers by a single undifferentiated map unit of Quaternary or Holocene alluvium. Elsewhere in the region, more detailed mapping that subdivides Quaternary alluvium into multiple units is available along the Pee Dee and Cape Fear Rivers (Owens, 1989). However, comparison with satellite imagery, aerial photography, and elevation data indicates there is more variety and complexity to late Quaternary alluvium than this mapping resolves. In the case of the Pee Dee valley, geomorphic mapping by Leigh et al. (2004, Figure 6, p. 74) based on elevation data, surface morphology, and cross-cutting relationships evident in Landsat imagery revealed three distinct braided terraces, as well as eolian dunes, located within a single map unit of Owens (1989), the fluvial facies of the upper Pleistocene Wando Formation. Given the high degree of variability of late Quaternary deposits in the river valleys of the southeastern Atlantic Coastal Plain and the relatively low resolution of existing maps, there is a clear need for mapping

that provides a high-resolution three-dimensional geologic and geomorphic framework for these sediments.

1.2.2 "Mega-meander" paleochannels in river valleys of the southeastern Atlantic Coastal Plain

Many river valleys of the Atlantic Coastal Plain in the southeastern United States contain exceptionally large terminal Pleistocene and early Holocene meandering paleochannels ("mega-meanders") that have been recognized and dated by Leigh and colleagues in the age range from 16,000 to 5,000 years before present (16-5 ka; Leigh and Feeney, 1995; Leigh et al., 2004; Leigh, 2006; Leigh, 2008). Close temporal correspondence between shifts in channel pattern and paleoclimatic episodes documented by fossil pollen and eolian sedimentary deposits indicates climate was the primary driver of channel change during the last 30,000 years (Leigh, 2008); and previous research has suggested that large paleomeanders may represent times of greater runoff and larger-than-modern bankfull floods (Gagliano and Thom, 1967; Leigh and Feeney, 1995; Leigh, 2006). Leigh (2008) argued that the large bankfull floods attributed to mega-meanders could be the product of multiple hydroclimatological drivers, including higher levels of effective precipitation due to cool temperatures and low rates of evapotranspiration (Leigh, 2008), a pronounced snowmelt runoff season or rainfall on frozen ground (Dury, 1965), seasonal flooding due to increased magnitude and frequency of tropical storms (Alford and Holmes, 1985), and/or increased springtime frontal precipitation in response to temperature contrasts between tropical and high-latitude oceans (Bard, 2002; Lea et al., 2003).

Interestingly, morphologically similar "mega-meander" scars exist in the Gulf Coastal Plain of Texas, referred to as the "Deweyville" meander scars, but their ages are less known than in Georgia and the Carolinas (Alford and Holmes, 1985; Blum et al., 1995; Blum and Aslan,

2006; Sylvia and Galloway, 2006). Previous paleohydrologic investigations of all "mega-meander" scars have been limited in scope and based on crude retrodiction of paleodischarge using planform meander geometry, which is subject to considerable error (Ethridge and Schumm, 1978; Dury, 1985), thus warranting further research.

1.2.3 Soil variability

1.2.3.1 Drivers of soil variability

Soils are known to vary systematically as a function of landform, geomorphic component (e.g., summit, shoulder, backslope, toeslope), and soil forming factors, including climate, biota, parent material, relief, and time (Wilding and Drees, 1983). Within the context of a soil chronosequence, soil age is allowed to differ while variation in the other factors is, at least in theory, minimized. However, finding sites that conform to this design can be challenging (Schaetzl et al., 2006). On a geomorphic surface of uniform age underlain by unconsolidated sediments, parent material may vary in three dimensions, due to spatial variation in the sedimentology and stratigraphy of the original deposit. Textural and mineralogical differences in the parent material often result in soil variability because they influence many processes and properties, including: the depth and rate of leaching; the potential for argillic horizon formation by illuviation of fines; surface area, water holding capacity, and their mutual effect on secondary clay formation by weathering or precipitation from solution; and the type of secondary clay minerals and oxides formed (Birkeland, 1999, pp. 155-156). Relief may also vary within a single landform, as a function of spatial variation in primary depositional topography or, in the case of older surfaces, degradation of depositional topography by surficial processes. This can influence depth to water table and, as a consequence, redoximorphic conditions and pedogenic

processes affected by soil drainage (Daniels et al., 1971a). Through careful site selection, variation in parent material and relief can typically be minimized or at least integrated into chronosequence interpretations (Barrett and Schaetzl, 1993). However, the effects of macro- and micro-climate and biota, which vary interdependently over time and space, are much more difficult to assess. Daniels et al. (1971b) point out that soils whose ages span different intervals of Quaternary time certainly experienced different paleoenvironmental histories, which may be poorly known or have impacts on soil development that are difficult to ascertain and factor into chronosequence studies. Even on surfaces of uniform age, Schaetzl et al. (2006) caution that variability in soil development may result from climatic and biotic drivers, if such surfaces are large enough to span climatic and biotic gradients. At the pedon scale, floralturbation, in the form of tree uprooting (Schaetzl, 1986) and faunalturbation, by insects and mammals, can regress some well-developed soils to a simpler state while leaving neighboring soils unaffected (Johnson and Watson-Stegner, 1987). This may result in a wide range of soil development within a given geomorphic surface that may be difficult to disentangle once the primary evidence of such processes (like pit and mound topography, in the case of tree throw) is gradually destroyed over time by surficial processes. Thus, both climatic and biotic drivers may be responsible for within- and among-surface variation in soil chronosequence studies, but this variation is often difficult to account for and is a potential contributor to the error term in many soil chronofunctions (Schaetzl et al., 2006).

Soil spatial variability that cannot be attributed to a known cause has been traditionally described as random (Wilding and Drees, 1983). According to Wilding and Drees (1983), this variation is not necessarily random in the stochastic sense, as some or all of it might be explained by systematic factors if sampling resolution and the accuracy of analytical measurements were

perfect. Phillips (1993a; 2001) and Phillips et al. (1996), whose thinking is based in deterministic uncertainty theory, offer another explanation of why soils may exhibit apparently random spatial patterns in the absence of (or independently of) practicably measurable changes in soil-forming factors. These authors argue that the soil system is unstable and sensitive to initial conditions and minor perturbations. As such, slight differences during the life of a soil might have a disproportionately large, long-lasting impact on pedogenic processes and result in a diverse soil cover on a given landform or landscape over time, even where soil-forming factors have been relatively uniform. Thus, our current understanding of the soil system indicates that soils may vary both predictably and unpredictably on geomorphic surfaces (Schaetzl et al., 2006). This must be taken into account when designing soil chronosequence studies (Eppes and Harrison, 1999) and interpreting chronosequence data (Harrison et al., 1990).

1.2.3.2 Soil spatial variability in documented chronosequences

Although soil spatial variability has important theoretical and practical implications for the soil chronosequence approach, it has been addressed by relatively few studies. Sondheim and Standish (1983) characterized the soil variability of a chronosequence of six alpine moraines in British Columbia that spanned the last 200 years. They found that while organic carbon, nitrogen, and pH varied significantly with age and soil depth, variation in percent sand, percent clay, and numerous soil chemical properties was best explained by parent material variability. Harrison et al. (1990) analyzed soil spatial variability of terminal Pleistocene to Holocene age alluvial terraces near Cajon Pass in Southern California. While some systematic variation was recognized between bar versus swale soils, the degree of random variation among soils on a given geomorphic component of a surface led the authors to question the utility of univariant soil

chronofunctions for identifying time-dependent pedogenic processes and dating surficial deposits. Barrett and Schaetzl (1993) concluded that biotic processes play an important role in the variability of podzolic soils on Holocene terraces of Lake Michigan. Spatio-temporal trends in these soils were attributed to local-scale, spatially random treethrow processes acting upon surfaces that were otherwise experiencing overall podzolization. On basalt flows of mid- to late Pleistocene age in the Potrillo volcanic field, southern New Mexico, Eppes and Harrison (1999) demonstrated that soil variability was strongly linked to landscape position relative to ridges and swales in the initial basalt flow topography. Ridge soils had minimal variability and were well-suited to further chronosequence study, while swale soils that formed in eolian dust exhibited greater variability, owing to hydrologic differences related to swale size and shape. Taken together, the above studies illustrate that soil spatial variability is ubiquitous, even in soil-geomorphic settings that have been selected to minimize its influence on variation in soil properties, and underscore the importance of accounting for spatial variability in any chronosequence study.

1.2.3.3 Spatio-temporal variation in Atlantic Coastal Plain soils

Numerous workers have noted a high degree of short-range spatial variability in soils of the southeastern Coastal Plain (Daniels and Gamble, 1967; Anderson and Cassel, 1986; Phillips, 1993a). Foundational soil-geomorphic studies of Ultisol landscapes in the North Carolina Coastal Plain in the late 1960s and early 1970s demonstrated that much of this variability results from the influence of water table regime, topography, and landscape dissection on pedogenic processes (Daniels and Gamble, 1967; Daniels et al., 1967; Daniels et al., 1968; Daniels et al., 1971). On fluviomarine terraces of the region, spatial variability is greatest in the vicinity of the

dissected edge of a surface ("dry edge") and at the transition from moderately-well drained to poorly drained soils located in shallow depressions within the surface ("wet edge"). These phenomena, which occur over horizontal distances of several meters (wet edge) to 10s to several hundred meters (dry edge) are termed "edge effects". Later, Phillips et al. (1994) re-affirmed the general soil-landscape relationships predicted by the edge effect model but observed extreme local-scale variability in surface (A+E) horizon thickness superimposed on these patterns that the model did not explain. They attributed this variability to small bioturbations acting on a potentially unstable and chaotic soil system, whereby initially minor disturbances from tree throw and faunal activity persist and grow to result in large differences in soil morphology over very short distances.

Recent research suggests such short-range variability may increase over time. In North Carolina, Phillips (1993a) documented only one soil series along a 0.5 km transect on the late Pleistocene Pamlico Terrace, while seven series were present along an adjoining 0.5 km transect on the older, mid- to late Pleistocene Talbot Terrace, despite among-site similarities in soil-forming factors. According to a soil genesis model developed by Phillips, such increasing local-scale soil variability over time in the absence of differences in soil forming factors is consistent with an unstable, chaotic soil system. Findings were thus interpreted as empirical evidence for chaotic pedogenesis. More recent work indicates that the greater local-scale soil variability apparent on the older Talbot Terrace is also evident at the landscape scale, and that this variability increases over time independently of increasing landscape dissection (Phillips, 2001).

Most soil chronosequence studies from the southeastern Coastal Plain do not explicitly address spatial variability but have focused instead on characterizing age-related trends in soil development at the pedon scale (Markewich et al., 1987, 1988, 1989; Howard et al., 1993; Shaw

et al., 2003; Suther, 2006). Nevertheless, these studies provide useful information about rates and directions of pedogenic processes through time, as well as age-related weathering characteristics of surficial deposits in the region. The findings of Markewich et al. (1989), which draw from chronosequence data compiled from numerous geomorphic surfaces throughout the southeastern United States, suggest that certain morphological and chemical properties of soils in the Inceptisol-Alfisol-Ultisol developmental pathway, such as solum thickness and argillic horizon thickness, rubification, clay mass, and $Fe_2O_3 + Al_2O_3 / SiO_2$, increase with time and are the most reliable parameters for estimating order of magnitude ages (e.g., 10 ka vs. 100 ka vs. 1 Ma) of surficial deposits. However, Howard et al. (1993) indicate that some soil properties may not exhibit unidirectional development with age. Argillic horizon development, for example, appears to be a self-terminating process that reverses direction after $>10^7$ years of weathering in alluvial soils along the James River (Virginia), probably because illuviation eventually so plugs the soil that Bt thickening stops and degradation ensues. Furthermore, these soils appear to evolve in an episodic, not gradual, manner related to stability thresholds of primary sand- and silt-sized minerals and secondary clay minerals and do not appear to reach pedogenic steady state, even after $>10^7$ years of weathering. In a much younger alluvial chronosequence spanning the last ~100 ka in the Upper Coastal Plain of North Carolina, Suther (2006) found that solum thickness, argillic horizon thickness, and subsoil rubification, free iron content, and clay content increased with age, while whole soil (<2 mm) bases/resistant oxide ratios and whole soil and fine sand fraction $\%K_2O$ decreased. All of these properties had strong correlations with terrace age as determined by optically-stimulated luminescence (OSL) dating, and most allowed for clear separation between the younger (≤17.4±4.2 ka) and older (≥74.6±10.1 ka) terraces in the sequence. Similar to Howard et al.'s findings, soil morphological and chemical properties and

clay mineral assemblages showed nonlinear trends with age suggestive of episodic development (Suther, 2006). However, all properties exhibited unidirectional trends over the 100 ka timescale studied, and general soil development increased, indicating the dominance of progressive pedogenetic vectors over regressive ones in these soils. Incorporation of soil variability analysis into the chronosequence framework utilized by the above studies has the potential to refine chronosequence interpretations and advance our understanding of pedogenesis in the region.

1.3 References

Alford, J.J., Holmes, J.C., 1985. Meander scars as evidence of major climate changes in southeast Louisiana. Annals of the Association of American Geographers 75, 395-403.

Anderson, S.H. & Cassel, D.K., 1986. Statistical and autoregressive analysis of soil physical properties of Portsmouth sandy loam. Soil Science Society of America Journal 50, 1096-1104.

Bard, E., 2003. North Atlantic sea surface temperature reconstruction, IGBP PAGES/ World Data Center for Paleoclimatology Data Contribution Series #2003-026. NOAA/NGDC Paleoclimatology Program, Boulder CO, USA.

Barrett, L. R. and Schaetzl, R. J., 1993. Soil development and spatial variability on geomorphic surfaces of different age. Physical Geography 14, 39-55.

Beckett, P.H.T., Webster, R., 1971. Soil variability: a review. Soils and Fertility 34, 1-15.

Birkeland, P.W., 1999. Soils and Geomorphology. 3rd edn. Oxford Univ. Press, New York.

Blum, M.D., Törnqvist, T.E., 2000. Fluvial responses to climate and sea-level change: a review and look forward. Sedimentology 47, 2-48.

Blum, M.D., Aslan, A., 2006. Signatures of climate vs. sea-level change within incised valley fill successions: Quaternary examples from the Texas Gulf Coast. Sedimentary Geology 190, 177-211.

Blum, M.D., Morton, R.A., Durbin, J.M., 1995. “Deweyville” terrace and deposits of the Texas Gulf Coastal Plain. Gulf Coast Association of Geological Societies Transactions 45, 53-60.

Bockheim, J. G., 1980. Solution and use of chronofunctions in studying soil development. Geoderma 24, 71-85.

Campbell, J. B., 1979. Spatial variability of soils. Annals of the Association of American Geographers 69, 544-556.

Daniels, R.B., Gamble, E.E., 1967. The edge effect in some Ultisols in the North Carolina Coastal Plain. Geoderma 1, 117-124.

Daniels, R.B., Gamble, E.E., 1967. Relation between A2 horizon characteristics and drainage in some fine-loamy Ultisols. Soil Science 104, 364-369.

Daniels, R.B., Gamble, E.E., Bartelli, L.J., 1968. Eluvial bodies in the B horizons of some Ultisols. Soil Science 106 (3), 200-206.

Daniels, R.B., Gamble, E.E., Nelson, L.A., 1971a. Relations between soil morphology and water-table levels on a dissected North Carolina Coastal Plain surface. Soil Science Society of America Proceedings 35, 781-784.

Daniels, R.B., Gamble, E.E., Cady, J.C., 1971b. The relations between geomorphology and soil morphology and genesis. Advances in Agronomy 23, 51-88.

Dury, G.H., 1965. Theoretical implications of underfit streams, US Geological Survey Professional Paper 452-C.

Dury, G. H., 1985. Attainable standards of accuracy in the retrodiction of paleodischarge from channel dimensions. Earth Surface Processes and Landforms 10, 205-213.

Eppes, M. C. and Harrison, J. B. J., 1999. Spatial variability of soils developing on basalt flows in the Potrillo volcanic field, southern New Mexico: Prelude to a chronosequence study. Earth Surface Processes and Landforms 24, 1009-1024.

Ethridge, F.G., Schumm, S.A., 1978. Reconstructing paleochannel morphologic and flow characteristics: methodology, limitations and assessment. In Miall, A.D. (Ed.), Fluvial Sedimentology. Canadian Society of Petroleum Geologists, Calgary. Memoir 5. pp. 703- 721.

Harrison, J. B. J., McFadden, L. D., and Weldon, R. J., III, 1990. Spatial soil variability in the Cajon Pass chronosequence: Implications for the use of soils as a geochronological tool. Geomorphology 3, 399-416.

Howard, J.L., Amos, D.F., and Daniels, W.L., 1993. Alluvial soil chronosequence in the inner Coastal Plain, central Virginia. Quaternary Research 39, 201-213.

Huggett, R. J., 1998. Soil chronosequences, soil development, and soil evolution: A critical review. Catena 32, 155-172.

Jenny, H., 1941. Factors of Soil Formation. New York, NY: McGraw-Hill.

Johnson, D.L., Watson-Stegner, D., 1987. Evolution model of pedogenesis. Soil Science 143, 349-366.

Gagliano, S.M., Thom, B.G., 1967. Deweyville terrace, Gulf and Atlantic Coasts. Louisiana State University, Coastal Studies Bulletin, Vol. 1, 23-41.

Georgia Department of Natural Resources (1976). "Geologic Map of Georgia." Georgia Department of Natural Resources, Atlanta.

Huddleston, P.F. (1988). A Revision of the Lithostratigraphic Units of the Coastal Plain of Georgia: The Miocene Through Holocene. Georgia Department of Natural Resources, Georgia Geologic Survey Bulletin 104, 162 pp.

Ivester, A.H., and Leigh, D.S., 2003. Riverine Dunes on the Coastal Plain of Georgia, U.S.A. Geomorphology 51, 289-311.

Lea, D.W., Pak, D.K., Peterson, L.C., Hughen, K.A., 2003. Synchroneity of tropical and high-latitude Atlantic temperatures over the last glacial termination. Science 301, 1361-1364.

Leigh, D.S., Feeney, T.P., 1995. Paleochannels indicating wet climate and lack of response to lower sea level, southeast Georgia. Geology 23, 687-690.

Leigh, D.S., 2006. Terminal Pleistocene braided to meandering transition in rivers of the Southeastern USA. Catena 66, 155-160.

Leigh, D.S., 2008. Late Quaternary climates and river channels of the Atlantic Coastal Plain, Southeastern USA. Geomorphology 101, 90-108.

Leigh, D.S., Srivastava, P., Brook, G.A., 2004. Late Pleistocene braided rivers of the Atlantic Coastal Plain, USA. Quaternary Science Reviews 23, 65-84.

Owens, J.P., 1989. Geologic Map of the Cape Fear Region, Florence 1 × 2 degree Quadrangle and Northern Half of the Georgetown 1 × 2 degree Quadrangle, North Carolina and South Carolina. US Geological Survey Miscellaneous Investigations Series Map I-1948-A (Sheet 1/2).

Markewich, H.W., Pavich, M.J., 1991. Soil chronosequence studies in temperate to subtropical, low-latitude, low-relief terrain with data from the eastern United States. Geoderma 51, 213-239.

Markewich, H.W., Pavich, M.J., Mausbach, M.J., Stuckey, B.N., Johnston, R.G., Gonzalez, V.M., 1986. Soil development and its relation to the ages of morphostratigraphic units in Horry County, South Carolina: U.S. Geological Survey Bulletin 1589-B. U.S. Government Printing Office, Washington DC, USA, pp. B1-B61.

Markewich, H.W., Pavich, M.J., Mausbach, M.J., Hall, R.L., Johnston, R.G., Hearn, R.P., 1987. Age relationships between soil and geology on the Coastal Plain of Maryland and Virginia. U.S.

Geological Survey Bulleting 1589-A. U.S. Government Printing Office, Washington DC, USA, pp. A1-A34.

Markewich, H.W., Lynn, W.C., Pavich, M.J., Johnston, R.G., Meetz, J.C., 1988. Analysis of four Inceptisols of Holocene age, east-central Alabama. U.S. Geological Survey Bulletin 1589-C. U.S. Government Printing Office, Washington, D.C., USA, pp. C1-C29.

Markewich, H.W., Pavich, M.J., Mausbach, M.J., Johnson, R.G., and Gonzalez, V.M., 1989. A guide for using soil and weathering profile data in chronosequence studies of the Coastal Plain of the eastern United States. U.S. Geological Survey Bulletin 1589-D. U.S. Government Printing Office, Washington, D.C., USA, pp. D1-D39.

Phillips, J.D., 1993a. Chaotic evolution of some Coastal Plain soils. Physical Geography 14, 566-580.

Phillips, J.D., 1993b. Progressive and regressive pedogenesis and complex soil evolution. Quaternary Research 40, 169-176.

Phillips, J. D., 2001. Divergent evolution and the spatial structure of soil landscape variability. Catena 43, 101-113.

Phillips, J.D., Gosweiler, J., Tollinger, M., Mayeux, S., Gordon, R., Altieri, T., Wittmeyer, M., 1994. Edge effects and spatial variability in coastal plain Ultisols. Southeastern Geographer 34, 125-137.

Phillips, J. D., Perry, D., Garbee, A. R., Carey, K., Stein, D., Morde, M. B., and Sheehy, J. A., 1996. Deterministic uncertainty and complex pedogenesis in some Pleistocene dune soils. Geoderma 73, 147-164.

Richmond, G. M., Fullerton, D. S., and Weide, D. L. (1986). “Quaternary Geologic Map of the Jacksonville 4° x 6° Quadrangle, United States.” U.S.G.S. Quaternary Geologic Atlas of the United States.

Richmond, G. M., Fullerton, D. S., and Weide, D. L. (1987). “Quaternary Geologic Map of the Savannah 4° x 6° Quadrangle, United States.” U.S.G.S. Quaternary Geologic Atlas of the United States.

Saldaña, A., Ibáñez, J.J., 2004. Pedodiversity analysis at large scales: an example of three fluvial terraces of the Henares River (central Spain). Geomorphology 62, 123-138.

Schaetzl, R.J., 1986. Complete Soil Profile Inversion by Tree Uprooting. Physical Geography 7, 181-189.

Schaetzl, R. J. and Anderson, S. N., 2005. Soils: Genesis and Geomorphology. Cambridge, UK: Cambridge University Press.

Schaetzl, R.J., Mikesell, L.R., and M.A. Velbel. Expression of Soil Characteristics Related to Weathering and Pedogenesis Across a Geomorphic Surface of Uniform Age in Michigan. Physical Geography 27, 170-188.

Schaetzl, R. J., Barrett, L. R., and Winkler, J. A., 1994. Choosing models for soil chronofunctions and fitting them to data. European Journal of Soil Science 45, 219-232.

Shaw, J.N., Odom, J.W., Hajeck, B.F., 2003. Soils on Quaternary terraces of the Tallapoosa River, Central Alabama. Soil Science 168 (10), 707-717.

Sondheim, M. W. and Standish, J. T., 1983. Numerical analysis of a chronosequence including an assessment of variability. Canadian Journal of Soil Science 63, 501-517.

Stevens, P. R. and Walker, T. W., 1970. The chronosequence concept and soil formation. Quarterly Review of Biology 45, 333-350.

Suther, B.E., 2006. Soil Chronosequence of the Little River valley, Atlantic Coastal Plain, North Carolina. Unpublished MS Thesis, University of Georgia, Athens, Georgia, USA.

Switzer, P. S., Harden, J. W., and Mark, R. K., 1988. A statistical method for estimating rates of soil development and ages of geologic deposits: A design for soil-chronosequence studies. Mathematical Geology 20, 49-61.

Sylvia, J.P.M., and Galloway, W.E., 2006. Morphology and stratigraphy of the late Quaternary lower Brazos valley: implications for paleoclimate, discharge, and sediment delivery. Sedimentary Geology 190, 159-175.

Wilding, L. P. and Drees, L. R., 1983. Spatial variability and pedology. In: L. P. Wilding, N. E. Smeck, and G. F. Hall, (Eds.), Pedogenesis and Soil Taxonomy. New York, NY: Elsevier, 83-116.

Yaalon, D. H., 1975. Conceptual models in pedogenesis. Can soil-forming functions be solved? Geoderma 14, 189-205.

CHAPTER 2 – QUATERNARY ALLOSTRATIGRAPHY OF THE LOWER OCONEE RIVER VALLEY, UVALDA QUADRANGLE, GEORGIA[1]

[1]Suther, B.E., Leigh, D.S., and Brook, G.A. To be submitted to *Sedimentary Geology*.

Abstract

Allostratigraphic mapping indicates that the Quaternary valley of the lower Oconee River contains eight informal alloformations within the Uvalda, Georgia 7.5-minute quadrangle, an area that previously lacked detailed surficial geologic mapping. Each alloformation is bounded by: 1) a basal contact with either pre-Quaternary sediment or older, Oconee-River derived alluvium; 2) an upper boundary that is defined by a laterally traceable geomorphic surface; and 3) lateral boundaries characterized by cross-cutting relationships in the geomorphology and lithofacies of adjacent map units.

Alloformations Qh2 and Qh1 respectively date to the late and early Holocene, have geomorphic surfaces characterized by meandering paleochannels with modern-like planform dimensions, and consist of normally graded alluvium that is composed of loamy to clayey overbank and clayey channel fill vertical accretion facies that abruptly overlie sandy lateral accretion and bedload deposits. Alloformation Qp6 dates to the terminal Pleistocene (ca. 11-17 ka), is characterized by exceptionally large, meandering paleochannels ("mega-meanders"), and contains normally graded meandering channel deposits comprised of lithofacies that are similar to those of Qh1 and Qh2. Alloformation Qp5 is of late Wisconsin age (17-34 ka), exhibits well-defined, interwoven braid bar and swale topography, and consists of alluvial deposits composed of loamy to clayey vertical accretion, sandy to loamy braided channel fill, and sandy upper braid bar lithofacies that overlie a gravelly sand bedload lithofacies that was deposited by the Oconee River when it had a braided channel pattern. Alloformation Qp4 returned a middle Wisconsin age (52 ka), preserves evidence of both meandering and braided channel patterns on its surface, and contains alluvium composed of a variety of weakly to strongly weathered lithofacies that were probably deposited by both meandering and braided phases of the Oconee River. No

absolute numerical age control is available of alloformations Qp3, Qp2, and Qp1, which all pre-date 52 ka. Cross-cutting geometries and surface elevations indicate a relative age relationship of Qp3<Qp2<Qp1 for these units, which are assigned to the Pleistocene because their surface elevations indicate that they must postdate the nearby late Pliocene to Pleistocene Hazlehurst marine terrace. Qp3, Qp2, and Q1 lack distinct fluvial topography and consist of alluvial deposits with a wide range of textures that exhibit crude normal grading and extensive alteration by weathering and pedogenesis.

Results indicate that allostratigraphy is effective for delineating Quaternary sediments in this setting, and allostratigraphic mapping appears to be equally applicable to other alluvial valleys in the southeastern Coastal Plain and elsewhere. However, as deposits become more weathered and fluvial topography degrades with age, confident identification of bounding discontinuities and accurate delineation of alloformation boundaries becomes more difficult. Scrutiny of alloformation surface morphology, sedimentology, and stratigraphy, along with chronologic data provided by radiocarbon and optically-stimulated luminescence (OSL) dating, indicate that the lower Oconee River exhibited a braided morphology during the late Wisconsin interval, a mega-meandering morphology during the terminal Pleistocene, and a meandering morphology with modern-like planform dimensions during the early to late Holocene. These results are generally consistent with the major morphological phases exhibited by rivers elsewhere in the southeastern Atlantic Coastal Plain during the late Quaternary and further improve our understanding of the evolution of fluvial systems in the region during this time period.

2.1. Introduction

The lower Oconee River valley contains a diverse assemblage of late Quaternary fluvial landforms, including multiple terraces that preserve former braided and meandering channel patterns (Leigh et al., 2004). These landforms and their associated deposits provide important information about the behavior of the Oconee River during the late Quaternary in terms of variability in channel pattern, depositional style, lateral migration, and incision, as well as its response to external drivers, including climatic change and tectonics. The Oconee River is a tributary to the Altamaha River (Georgia), and features similar to those found in the Oconee valley occur downstream along the Altamaha and are also present along other rivers of the southeastern Atlantic Coastal Plain, including the Canoochee, Ocmulgee, Ogeechee and Savannah Rivers (Georgia), the Black, Congaree, Lynches, Pee Dee and Little Pee Dee Rivers (South Carolina), and the Cape Fear and Neuse Rivers (North Carolina). In sum, these landforms and their underlying deposits are believed to indicate a regional response of southeastern Coastal Plain fluvial systems to late Quaternary climate changes (Leigh, 2008).

While previous studies have characterized and dated some of the fluvial deposits along the lower Oconee River (Leigh et al., 2004), no detailed Quaternary geologic mapping of the valley has been conducted. Published geologic and/or geomorphic maps that encompass the lower Oconee valley are general in nature and include the Geologic Map of Georgia (Georgia Department of Natural Resources, 1976); The Quaternary Geologic Map of the Jacksonville 4×6 degree Quadrangle, United States (Richmond et al., 1986); The Quaternary Geologic Map of the Savannah 4×6 degree Quadrangle, United States (Richmond et al., 1987); and the Generalized Map of Marine Terraces and the Dissected Marine Terrace Region of Georgia (Fig. 56 of Huddlestun, 1988). These maps typically represent all fluvial sediments along the Oconee and

other rivers by a single undifferentiated map unit of Quaternary or Holocene alluvium. Elsewhere in the region, more detailed mapping that subdivides Quaternary alluvium into multiple units is available along the Pee Dee and Cape Fear Rivers (Owens, 1989). However, comparison with satellite imagery, aerial photography, and elevation data indicates there is more variety and complexity to late Quaternary alluvium than this mapping resolves. In the case of the Pee Dee valley, geomorphic mapping by Leigh et al. (2004, Figure 6, p. 74) based on elevation data, surface morphology, and cross-cutting relationships evident in Landsat imagery revealed three distinct braided terraces, as well as eolian dunes, located within a single map unit of Owens (1989), the fluvial facies of the upper Pleistocene Wando Formation. Given the high degree of variability of late Quaternary deposits in the river valleys of the southeastern Atlantic Coastal Plain and the relatively low resolution of existing maps, there is a clear need for mapping that provides a high-resolution three-dimensional geologic and geomorphic framework for these sediments.

This study provides a high-resolution geologic map of the Quaternary sediments of the lower Oconee River valley within the Uvalda, Georgia 7.5-minute quadrangle at a 1:24,000 scale. It also presents stratigraphic cross-sections, as well as new radiocarbon and optically-stimulated luminescence (OSL) dates, that indicate that the Oconee River experienced major changes in planform and depositional style, including transitions from braided, to large meandering, to modern-sized meandering morphologies, during the late Pleistocene and Holocene. Map units were delineated informally as alloformations, which consist of three-dimensional bodies of genetically-related lithofacies differentiated by bounding discontinuities (NACSN, 2005). Mapping was conducted as an EDMAP component of the U.S. Geological Survey's (USGS) *Geology of Atlantic Watersheds Project* and is intended to complement

ongoing cooperative mapping by the South Carolina Geological Survey and USGS in the Savannah River valley. The Uvalda quadrangle was selected for mapping because it contains a wide array of late Quaternary landforms and deposits that are similar to those found along other rivers of the southeastern Atlantic Coastal Plain. In this respect, it constitutes an ideal location for investigating the geomorphic, stratigraphic, and chronologic relationships among late Quaternary fluvial deposits in the region, and the results presented here should be useful for interpreting the fluvial sediments and alluvial architecture of other river valleys elsewhere in the Coastal Plain.

Following overviews of the map area and project methodology, this paper provides detailed map unit descriptions for each informal alloformation delineated by the study that include radiocarbon and optically-stimulated luminescence (OSL) age estimates in cases where they are available. A brief discussion follows that evaluates of the utility of allostratigraphy for delineation of Quaternary fluvial sediments in the Coastal Plain and provides interpretations about the late Quaternary evolution of the lower Oconee River based on data from the Uvalda locality. The document concludes with a summary of major project findings.

2.2. Map Area and Geologic Setting

The map area is contained within the Uvalda, Georgia 7.5-minute quadrangle and is located in the Coastal Plain of southeastern Georgia along the Oconee River (Figs. 2.1, 2.2, and 2.3). The Oconee originates on the saprolite-mantled Paleozoic crystalline rocks of the Georgia Piedmont and flows across the Cretaceous and younger sedimentary rocks of the Coastal Plain until it joins the Ocmulgee River to form the Altamaha River, approximately 5 km south of the

map area. The modern Oconee River has a sandy bed, a meandering pattern, and a channel width of 80-150 m in the vicinity of the map area.

Uplands in the Uvalda quadrangle and surrounding areas range from somewhat flat to relatively dissected, with the majority of present relief formed from incision of the Oconee River and its tributaries. Huddlestun (1988) identifies the Miocene Altamaha Formation as the lithostratigraphic unit immediately underlying uplands in this part of the Georgia Coastal Plain, although in some places it is locally overlain by undifferentiated alluvium, colluvium, surficial sands, and lacustrine deposits. The Altamaha Formation consists of "…thin to thick bedded or crossbedded, well-sorted to very poorly sorted, variably feldspathic, sporadically pebbly or gravelly, argillaceous sand, sandstone, sandy clay, clay, and claystone" (Huddlestun, 1988; p. 103) and its depositional environment is interpreted to have been fluvial to upper estuarine. The late Pliocene to early Pleistocene Hazlehurst terrace, the oldest, highest, and most landward of the marine terraces mapped in the Georgia Coastal Plain (Huddleston, 1988), overlies sediments in the southern part of the quadrangle, although in this area the original terrace surface has been so obscured by dissection that is difficult to recognize (Fig. 2.2).

The Oconee River valley ranges from four to nine km wide in the vicinity of the map area and contains multiple fluvial surfaces of Quaternary age (Figs. 2.3 and 2.4). Optically-stimulated luminescence (OSL) age estimates from a prior study indicated an 18-32 ka two-sigma age range for alluvium beneath a braided terrace in the southwestern portion of the Uvalda quadrangle (Leigh et al., 2004). This braided terrace is located on the east side of the valley axis and stands at 4-8 m above river level. An exceptionally large paleochannel ("mega-meander" scar), with a width and radius of curvature substantially greater than the modern river, crosscuts the northern end of the braided terrace. This mega-meander paleochannel occurs at a slightly

lower elevation than the braided terrace and bears a striking resemblance to large paleomeanders that have been documented along other southeastern Coastal Plain rivers (Leigh, 2008). The mega-meander and its associated terrace are in turn cross-cut to the northwest by a lower surface that constitutes the first terrace above the modern floodplain of the Oconee River. This first terrace occurs on both sides of the valley and ranges from 3-6 m above river level. The floodplain, which is located adjacent to the Oconee River along its entire course through the quadrangle, stands at 1-4 m above river level. Both the floodplain and first terrace contain meandering paleochannels with modern-like planform dimensions that are laterally incised into higher surfaces. Four higher fluvial terraces that pre-date the 18-32 ka braided terrace occur in the map area and have heights above river level that range from 5-35 m. With the exception of paleochannel scars that occur on the lowest of the four higher terraces, distinct fluvial topography (e.g., scrollwork, ridges and swales, paleochannels) has not been preserved on these surfaces. Previously published geologic maps do not subdivide the alluvium underlying any of the aforementioned geomorphic surfaces and report surficial sediments within the valley as undifferentiated Quaternary alluvium (Georgia Department of Natural Resources, 1976) or Holocene alluvial gravelly sand (Richmond et al., 1987).

2.3. Methods

2.3.1 Mapping methods

Quaternary sediments of the lower Oconee River valley were delineated as alloformations, which are the fundamental units of allostratigraphic classification and consist of three-dimensional bodies of related lithofacies that are differentiated based on bounding discontinuities (NACSN, 2005). Alloformations were delineated based on interpretation of

geomorphic surfaces, topography, lithofacies, soils, and bounding discontinuities at a scale of 1:24,000 in a manner similar to that adopted by Autin (1992).

This study also delineated paleochannels with present day topographic expression because these features provide valuable insight into the evolution of the Oconee River and the processes of alloformation development. Paleochannels were mapped as surface morphological features (e.g., meandering paleochannels, braided paleochannels and swales, indeterminate paleochannels) in cases where they could be clearly recognized in the field and on remote sensing imagery. Although these paleochannels typically contain fill that is separated from underlying alloformations by a bounding discontinuity, paleochannel fills were not delineated as separate alloformations by this study because they could not be consistently delineated as three dimensional geologic units throughout the entire map area. On older surfaces, paleochannel fills lack geomorphic expression, owing to degradation of depositional topography by surficial processes, which makes them impossible to identify without extensive subsurface data. This precludes consistent treatment of paleochannel fills among older and younger deposits at the level of resolution represented by this study. Furthermore, even on younger fluvial surfaces where paleochannels appear to have strong geomorphic expression, additional paleochannels may exist that are buried by vertical accretion sediments that are likewise difficult to identify without a dense coverage of subsurface data.

Geomorphic and topographic interpretations used to guide delineation of alloformations and surface morphological features were conducted by ground reconnaissance, survey, and manual interpretation of USGS 7.5 minute topographic quadrangles, U.S. Geological Survey National Elevation Database (NED) one-third arc-second (10 meter) digital elevation models (DEMs) and their slope derivatives, digital soil survey mapping (Soil Survey Staff, 2011), and

remote sensing imagery within ArcGIS 10®. Remote sensing imagery included a 1998 Landsat image (LT50170381998052AAA02), 1999 USGS color infrared digital orthophoto quarter quadrangles, and 2010 National Agricultural Imagery Program (NAIP) natural color ortho-rectified aerial photography.

Subsurface field data were provided by borings ranging from 1-13 m in depth that were collected by a Giddings hydraulic soil probe or with a manual bucket auger. Supplementary subsurface observations were made in road cuts, pre-existing borrow bits, and along cutbanks of the Oconee River and its tributaries. Morphological characteristics of soil and sediment were described according to USDA Soil Survey terminology (Soil Survey Division Staff, 1993), and lithologic properties and the nature of stratigraphic contacts were noted. Three stratigraphic cross-sections were constructed to illustrate the relationships between lithofacies, geomorphic surfaces, and alloformations that are based on data from a total of 59 borings. Borings were conducted at approximately 100 to 300 m intervals along these cross-sections, depending upon the variability encountered on each transect. One mega-meander and one smaller meandering paleochannel were cored at much shorter distance intervals (about one-tenth of channel width) to illustrate channel cross-sectional dimensions. An additional 45 borings were collected to guide delineation of alloformations elsewhere in and immediately surrounding the Uvalda quadrangle during ground reconnaissance that involved visual inspection of the landscape at over 80 localities.

The final map was constructed by digitizing alloformation boundaries in ArcMap 10® based on interpretations made from the above data and consists of a 1:24,000 scale map of the spatial extent of the alloformations that comprise the Quaternary sediments of the lower Oconee

River valley within the Uvalda, Georgia 7.5-minute quadrangle (Fig. 2.3). Figure 2.5 depicts three stratigraphic cross-sections from the map area.

2.3.2 Radiocarbon dating methods

Radiocarbon samples were collected with either a hand-held bucket auger or a Giddings hydraulic soil probe. Uncarbonized plant macrofossils that appeared fresh (e.g., seeds, nuts, leaves) and not reworked by fluvial transport were used for radiocarbon dating wherever possible. Samples were inspected in the field and any obvious contaminating material was removed. Samples were then wrapped in aluminum foil, bagged, and transported to the University of Georgia (UGA) Geomorphology laboratory, where any remaining contaminating macro-organics were removed following a rinse in 50 g/L sodium metaphosphate solution. Samples were then rinsed in distilled water and oven dried at 105˚C. All radiocarbon samples were measured by the accelerator mass spectrometry (AMS) method at the UGA Center for Applied Isotope Studies following an acid-alkali-acid (HCl-NaOH-HCl) cleaning procedure. The resulting radiocarbon ages are given in radiocarbon years before 1950 (yr BP), using the ^{14}C half-life of 5,568 years. Calibrated ages are provided in calendar years before present and take into account fluctuations in ^{14}C production. Calibrated ages were generated with the radiocarbon calibration program Oxcal 4.2 using the IntCal 09 calibration curve (Ramsey, 2009).

2.3.3 Optically-stimulated luminescence (OSL) dating methods

2.3.3.1 Principles of OSL dating

OSL dating estimates the time elapsed since sediment was last exposed to sunlight (Stokes and Walling, 2003). The OSL signal emitted by a quartz sand grain upon exposure to

light is proportional to the amount of radiation it received since its last exposure to sunlight, which is assumed to be immediately prior to burial. OSL dating relies on reconstructing the amount of irradiation necessary to produce a given luminescence signal (equivalent dose); estimating the annual dose rate that results from the decay of naturally occurring radionuclides (U, Th, ^{40}K) in surrounding sediment, and to a lesser extent from cosmic rays; and using this information to calculate a sample age that approximates the time of deposition according to the following equation (modified from Forman et al., 2000)

age (ka) = equivalent dose (Gy) / dose rate (Gy/ka) Eq. 1

An underlying assumption of OSL dating is that a sample's luminescence signal is zeroed (bleached) prior to burial (Stokes and Walling, 2003). While OSL dating is ideal for eolian sediments, a number of studies indicate that reliable OSL age estimates can also be obtained from fluvial sediments similar to those sampled along the Oconee River (Colls et al., 2001; Leigh et al., 2004; Rittenour et al., 2003, 2005; Srivastava et al., 2001; Stokes et al., 2001; Suther et al., 2011; Wallinga et al., 2001). Wherever possible, OSL age estimates were cross-checked by radiocarbon dating for corroboration, and we generally regard the OSL dates presented in this report to be reliable age estimates. All OSL ages are reported with two standard errors (± 2 sigma).

2.3.3.2 OSL dating procedures

Samples for OSL dating were collected either by pounding an 7 cm diameter light-tight metal tube into sediments at the base of a hand-augered hole or by driving a metal tube laterally into the face of a hand-dug pit. In all cases, OSL dating was conducted on unweathered (C horizon) alluvium that consisted of quartz-rich, medium to coarse sand sampled from below the

depth of bioturbation. Following sample collection, tubes were sealed immediately to prevent exposure to light.

Sample preparation and handling for OSL dating were carried out in subdued red-light conditions. Five centimeters of sediment were removed from each end of the sample tubes for dose rate estimation. Luminescence measurements were made on samples from the central section of the cylinder that was least likely to have been exposed to sunlight during sampling. All samples were treated with 10% HCl and 30% H_2O_2 to remove carbonates and organic matter. Samples were sieved to extract the 125-250 μm-size fraction. Quartz and feldspar grains were separated by density with Na-polytungstate (ρ=2.58 g cm^{-3}). The quartz fraction was etched using 48% HF for 80 min followed by 36% HCl for 30 min to remove the outer surface affected by alpha radiation. The quartz grains were mounted on stainless steel discs using Silkospray™.

Light stimulation of the quartz was achieved using a RISØ array of blue LEDs centered at 470 nm. Detection optics consisted of two Hoya 2.5 mm thick U340 filters and a 3 mm thick Schott GG420 filter coupled to an EMI 9635 QA photomultiplier tube. Measurements were taken with a RISØ TL-DA-15 reader. A 25-mCi $^{90}Sr/^{90}Y$ built-in source was used for sample irradiation.

The single aliquot regenerative dose (SAR) protocol (Murray and Wintle, 2000) used to determine equivalent dose involved a five-point regenerative dose strategy, with three dose points to bracket the equivalent dose, a fourth zero dose to test for recuperation effects, and a fifth repeat dose, usually of the smallest change correction incorporated in the SAR protocol. All measurements were made at 125°C for 100 s after a pre-heat to 220°C for 60 s. For all aliquots, the recycling ratio between the first and the fifth point ranged within 0.95-1.05. Data were analyzed using the ANALYST program of Duller (1999).

Equivalent dose measurements were made on single aliquots of 9.6 mm diameter. Typically 21to 24 aliquots per sample were analyzed. The dose rate calculation relied on the thick source ZnS (Ag) alpha counting technique for elemental concentration of uranium and thorium. Potassium was measured by ICP90, with a detection limit of 0.01%, using the Sodium Peroxide Fusion technique at the SGS Laboratory in Toronto, Canada. The cosmic ray Gamma contribution was assumed to be 150 ± 30 μGy/yr, as recommended for sediments located below an altitude of 1000 m between latitudes 0° - 40° (Prescott and Stephan, 1982). Sample ages were calculated using a pore-water content for the dated sediment that was either directly measured or estimated using the best available data.

2.4. Results: Geologic Map Units

Eight informal alloformations consisting of Oconee River-derived Quaternary alluvium were mapped within the Uvalda, Georgia quadrangle (Figs. 2.3 and 2.4). These map units can be traced both upstream and downstream of the map area and some extend into the neighboring Jordan quadrangle that is located to the immediate west (Fig. 2.4). Alloformations have been differentiated by bounding discontinuities and geomorphic, lithologic, pedologic, and stratigraphic criteria. Each alloformation of the Oconee River is bounded by 1) a basal contact with either pre-Quaternary Coastal Plain sediments or older Oconee River-derived alluvium; 2) an upper boundary that is defined by a laterally traceable geomorphic surface; and 3) lateral boundaries characterized by cross-cutting relationships in the geomorphology and lithofacies of adjacent map units. Figure 2.5 provides stratigraphic cross-sections that illustrate relationships between lithofacies, geomorphic surfaces, and alloformations at three locations in the valley. Descriptions for each alloformation, in order from youngest to oldest, along with available

radiocarbon (Table 2.1) and OSL (Table 2.2) age estimates, are provided below. Appendix A contains profile descriptions from each boring location along the cross-sections depicted in Figure 2.5, and Appendix B provides descriptions from alloformations Qp2 and Qp1, which do not occur at cross-section locations. This mapping effort focused on Quaternary sediments within the Oconee River valley. Upland sediments outside of the valley margins were beyond the scope of the study and were generalized into a single undifferentiated map unit that contains a variety of sediments with a wide range of Quaternary and Tertiary ages. Differentiation of tributary alluvium within the Oconee valley was also beyond the project scope, and these sediments were generalized into one undifferentiated map unit of Quaternary stream alluvium.

2.4.1 Map unit Qh2

The Qh2 alloformation is the youngest map unit, and its spatial extent corresponds with that of the Oconee River floodplain, which represents the alluvial surface being constructed by the modern Oconee River. Qh2 is located at the center of the valley axis and is distributed nearly continuously along both sides of the Oconee River within the map area (Figs. 2.3 and 2.4). The cross-sectional width of Qh2 ranges from 300 m in the central part of the valley to a maximum of 2,700 m in the northern valley, where it extends off the map area into the Jordan quadrangle. In most locations, Qh2 extends from the Oconee River channel, to proximal scrollbar and natural levee environments, then across a relatively low, flat floodplain surface that in some places is characterized by muted scrollwork topography. Outer portions of Qh2 are generally low, very wet, and occupied by backswamp environments or more typically by meandering paleochannels with modern or slightly smaller-than-modern planform dimensions that have muted scrollwork on the insides of their meander bends. The outer boundaries of Qh2 in many places are

scalloped, reflecting cross-cutting of Qh2 paleochannels into adjacent units, and are characterized by a well-defined scarp that may range from 1-2 m in height at the boundary with the next older map unit, Qh1, to as much as 9 m where Qh2 is cross-cut into the much higher Qp2 surface in the southwestern corner of the map area. Qh2 stands 1-4 m above the elevation of the base flow Oconee River, with variation in elevation reflecting differences in local relief among higher natural levee and scrollbar ridge settings versus lower scrollbar swale, backswamp, and paleochannel scar/oxbow environments.

Qh2 sediments typically consist of normally graded (fining upward) alluvium that is composed of loamy to clayey overbank and clayey channel fill vertical accretion lithofacies that abruptly overlie a sandy lithofacies comprised of lateral accretion and bedload deposits (Fig. 2.5). Qh2 was drilled to its base at one location in the map area (Fig. 2.5A, core 3), where bedload sands and gravels unconformably overlie gleyed, clayey pre-Quaternary sediment. In this location, Qh2 is 4.8 m thick, but vertical sections exposed in cutbanks of the Oconee River indicate this alloformation may be more than 5-6 m thick in some areas.

The sandy lithofacies of Qh2 (Fig. 2.5, lithofacies #1) consists of light gray (10YR 7/1) to light brown (10YR 6/4) coarse sand with infrequent, thin beds of very fine to medium gravels and often fines upward to medium sand in its upper meter. This lithofacies represents lateral accretion and bedload sediments that aggraded in channel lag, channel bar, and point bar environments, and the sedimentology and stratification of this facies are similar to modern Oconee River point bars (Fig. 2.6). The sandy lithofacies comprises the bottom stratum of Qh2 across the entire spatial extent of the alloformation. Limited stratigraphic data indicate that in Qh2 the sandy lithofacies ranges from 2 to >5 m in thickness and that this facies is thinnest

beneath abandoned paleochannels and thickest beneath scrollbar ridges that represent former point bars (Fig. 2.5A).

For the majority of its spatial extent, the sandy lithofacies is abruptly overlain by a dark brown (7.5YR 3/4) to dark yellowish brown (10YR 4/4) loamy to clayey vertical accretion facies (Fig. 2.5, lithofacies #2) that occurs directly beneath the ground surface and ranges in texture from sandy loam to clay. Where they are not obscured or obliterated by pedogenesis, sedimentary structures in this lithofacies are either massive or consist of thin, laminar, horizontal beds of interstratified loamy and sandy sediments located immediately above the contact with the underlying sandy lithofacies. The clayey to loamy lithofacies is characterized by weak pedogenic development, with soils consisting of Inceptisols with A-Bw or Bg-C horizon sequences and cambic horizons that typically exhibit weak subangular blocky structure and lack argillans. Low chroma, light brownish gray (10YR 6/2) and gray (10YR 6/1) matrix colors that reflect reducing conditions become more prevalent in this lithofacies with increasing depth from the ground surface and in low-lying swale and backswamp landscape positions. This lithofacies consists of vertical accretion sediments derived from suspended load that were deposited in natural levee, proximal overbank, and backswamp environments. It ranges from 0.4 to >2.0 m in thickness and tends to be thickest at swale and backswamp landscape positions.

The loamy to clayey vertical accretion lithofacies is laterally bounded in some locations within Qh2 by a clayey channel fill facies (Fig. 2.5, lithofacies #3) that directly underlies the ground surface within abandoned meandering paleochannel scars. The channel fill lithofacies is typically composed entirely of massive clay or consists of thinly, horizontally bedded interstratified sandy loam, silty clay, and clay that grade upward into massive clay. The contact between the channel fill facies and the underlying sandy bedload facies is typically abrupt, but it

has a more gradational character in locations where basal fill is composed of interstratified sand and clay. This lithofacies is typically gray (10YR 5/1) to light gray (10YR 7/1) in color and is characterized by hydric soils with weak development. Soils range from Inceptisols with Ag-Bg-Cg horizon sequences and Bg horizons that exhibit weak to moderate subangular blocky structure to Entisols with Ag over Cg profiles. This lithofacies consists of vertical accretion sediment derived largely from slackwater sedimentation in abandoned meandering channel environments (e.g., meander scars and oxbow lakes), although the sandy components of the interstratified sediments found near the base of some paleochannel fills probably reflect deposition during floods when the channel became reoccupied by the Oconee River. The channel fill lithofacies typically has a relatively narrow, arcuate shape in planform and ranges in thickness from ~1-3 m within Qh2. It is typically thickest near the outside bends of abandoned paleochannels and thinnest near the inside bends.

A paleochannel from the outer margin of Qh2, known as the "Uvalda small meander" was selected for radiocarbon and OSL dating to approximate the maximum age of the alloformation (Fig. 2.4, #13; Fig. 2.5C, core 57). Leaf fragments obtained from basal channel fill immediately above the contact with bedload sand in the thalweg of this paleochannel returned a calibrated radiocarbon date with a 2-sigma age range of 4.4-4.5 ka (Table 2.1). OSL dating of upper lateral accretion sand obtained from the point bar of this paleochannel returned a correlative date of 5.5±1.2 ka (Table 2.2; Fig. 2.4, #12; Fig. 2.5C, core 48). Given the 2-sigma error of the OSL age and that point bar sediment should be slightly older than post-abandonment channel fill, we consider these ages to be in good agreement. When taken together with early Holocene radiocarbon dates obtained from the next older map unit, Qh1 (UGAMS #11797 &

10683, reported below), the Qh2 dates suggest that formation of Qh2 began in the middle Holocene, and the entire age range of this alloformation spans from that time to the present.

To provide an additional check on the reliability of OSL ages obtained from Oconee River alluvium, sediment obtained from a depth of 70 cm beneath the crest of a modern Oconee River point bar was also dated by OSL (Fig. 2.6). This sample returned an essentially modern OSL date of 0.23±0.06 ka (Table 2.2; Fig. 2.4, #11), indicating complete (or nearly complete) bleaching of grains prior to sample burial, and lending credence to the generally reliability of OSL age estimates presented in this study.

2.4.2 Map unit Qh1

The Qh1 alloformation consists of alluvium that immediately predates Qh2, and its spatial extent corresponds with that of the first terrace of the Oconee River. Qh1 is distributed discontinuously along both the eastern and western sides of the valley, where it typically flanks the outer margins of Qh2 (Figs. 2.3 and 2.4). Qh1 remnants range from 250-1,200 m in cross-valley width and indicate that the original cross-valley extent of this unit was much greater (~1,000-2,700 m) prior to its erosional removal by the Oconee River during Qh2 time. In most places, Qh1 extends from its boundary with Qh2 across a relatively low, flat terrace surface characterized by muted to moderately well-expressed scrollwork and ridge-and-swale topography. Similar to the outer margins of Qh2, the outer parts of Qh1 are generally, low, wet, and occupied by meandering paleochannels with modern-like planform dimensions that have muted to moderately well-expressed scrollwork on the insides of their meander bends. The outer boundaries of Qh1 in many places are scalloped, reflecting cross-cutting of Qh1 paleochannels into adjacent units, and are characterized by a well-defined scarp that may range from 1-2 m in

height at the boundary with the next older map unit, Qp6, to as much as 3 m where Qh1 is cross-cut into the higher Qp4 surface in the central part of the map area. Qh1 stands 3-6 m above the elevation of the base flow Oconee River, with variation in elevation reflecting differences in local relief among higher natural levee and scrollbar ridge settings versus lower scrollbar swale and paleochannel scar/oxbow environments.

Qh1 sediments typically consist of normally graded (fining upward) alluvium that is composed of loamy to clayey overbank and clayey channel fill vertical accretion lithofacies that abruptly overlie a sandy lithofacies comprised of lateral accretion and bedload deposits (Fig. 2.5). These lithofacies are very similar to the loamy to clayey overbank, clayey channel fill, and sandy lateral accretion lithofacies found in Qh2 and cannot be differentiated from their Qh2 counterparts based on lithologic criteria. In some places in Qh1, a gradational sandy to loamy overbank lithofacies occurs between the sandy lateral accretion and the loamy to clayey overbank vertical accretion facies that was not observed in Qh2. Qh1 was drilled to its base at one location in the map area (Fig. 2.5A, core 5), where bedload sands and gravels unconformably overlie gleyed, pre-Quaternary sediments with a fine sandy clay texture. In this location, Qh1 has a thickness of 5.8 m.

The sandy lithofacies of Qh1 is nearly identical to that of Qh2 and consists of light gray (10YR 7/1) to yellowish brown (10YR 5.5/6) coarse sand with infrequent, thin beds of very fine to medium gravel and often fines upward to medium sand in its upper meter (Fig. 2.5, lithofacies #1). This lithofacies represents lateral accretion and bedload sediment that aggraded in channel lag, channel bar, and point bar environments, and, as observed in Qh2, the sedimentology and stratification of this facies are similar to modern Oconee River point bars (Fig. 2.6). The sandy lithofacies comprises the bottom stratum of Qh1 across the entire spatial extent of the

alloformation. Limited stratigraphic data indicate that in Qh1 the sandy lithofacies ranges from ~3 to >4 m in thickness and that this facies is thinnest beneath abandoned paleochannels and thickest beneath scrollbar ridges that represent former point bars (Fig. 2.5A).

For much of its spatial extent, the sandy lithofacies is abruptly overlain by a yellowish brown (10YR 5/6) to brown (10YR 5.5/3) loamy to clayey vertical accretion facies (Fig. 2.5, lithofacies #2) that occurs directly beneath the ground surface and ranges in texture from clay to silty clay loam. The clayey to loamy lithofacies is characterized by slightly greater pedogenic development in Qh1 than in Qh2, with soils consisting of Inceptisols with A-Bw or Bg-C horizon sequences and cambic horizons that typically exhibit slightly stronger subangular blocky structure than their Qh2 counterparts. The sedimentary structures observed in this lithofacies in Qh2 are not evident in Qh1 and appear to have been destroyed by pedogenesis. As observed in Qh2, low chroma, gray (10YR 6/1) and grayish brown (10YR 5/2) matrix colors that reflect reducing conditions become more prevalent in this lithofacies in Qh1 with increasing depth from the ground surface and in low-lying swale and backswamp landscape positions. This lithofacies, which consists of vertical accretion sediments derived from suspended load that were deposited in natural levee, proximal overbank, and backswamp environments, ranges from ~1 to >2 m thick in Qh1 and tends to be thickest at swale and backswamp landscape positions, although its thickness appears to be less landscape dependent than in Qh2.

In some locations in Qh1, a gradational sandy to loamy lithofacies (Fig. 2.5, lithofacies #4) occurs between the sandy lateral accretion and the loamy to clayey overbank vertical accretion facies. This lithofacies consists of very pale brown (10YR 7/3) to yellowish brown (10YR 5/8) medium sand that fines upward to loamy sand or sandy loam. This facies exhibits little alteration by pedogenesis other than iron oxide staining and in some cases contains thin,

horizontal beds of interstratified sand, finer-grained sediments, and organics. The sandy to loamy lithofacies is interpreted as consisting of vertical accretion sediments that were deposited in proximal overbank environments during foods.

In Qh1, the loamy to clayey vertical accretion lithofacies is laterally bounded in some areas by a clayey channel fill facies (Fig. 2.5, lithofacies #3) that directly underlies the ground surface within abandoned meandering paleochannel scars. With the exception of exhibiting slightly greater pedogenic development in Qh1, this lithofacies has nearly identical characteristics to its counterpart in Qh2, and the reader is referred to the description provided in section 2.4.1 for its typical lithologic properties, geometry, thickness, and interpreted depositional environment.

An initial effort to radiocarbon date Qh1 deposits from cross-section B-B' "MB2" site using wood fragments obtained from channel bed sediments returned an infinite age of 53,580±900 ^{14}C yr BP (Table 2.1; Fig. 2.4, #2; Fig. 2.5B, core 29). Because radiocarbon and OSL dates from the immediately adjacent Qh2 and Qp6 alloformations suggested that Qh1 was deposited during the early Holocene, two paleochannels from the outer margin of Qh1 were selected for radiocarbon dating to more precisely determine its age. A nut hull obtained from basal channel fill immediately above the contact with bedload sand in the thalweg of the Qh1 "Uvalda A 349469 m" paleochannel in the southern part of the valley returned a calibrated radiocarbon date of 10.7±0.1 ka (Table 2.1; Fig. 2.4, #7; Fig. 2.5A, core 6). Radiocarbon dating of an acorn collected from the base of channel fill in a second Qh1 paleochannel, known as the "Loblolly" paleochannel, which is located the central part of the valley and is similarly situated on the margin of the alloformation, yielded a very correlative date of 10.5±0.1 ka (Table 2.1; Fig. 2.4, #1). When taken together with middle Holocene radiocarbon and luminescence dates

obtained from Qh2 (see section 2.4.1) and terminal Pleistocene dates obtained from the next older map unit, Qp6 (Tables 2.1 & 2.2; reported below), the dated Qh1 paleochannels indicate that the Qh1 alloformation is of early Holocene age and that the wood obtained from the B-B' locality greatly pre-dates Qh1 sediments. This "radiocarbon-dead" wood is interpreted as having been eroded from older sediments and then re-deposited with channel bed sediments during the construction of Qh1.

2.4.3 Map unit Qp6

The Qp6 alloformation comprises the map unit that immediately predates Qh1, and its spatial extent coincides with that of the second terrace above the Oconee River. Qp6 occurs in only one location within the Uvalda quadrangle, to the east of the Oconee River in the south-central portion of the valley (Fig. 2.3), but a second Qp6 map unit exists on the western side of the valley, <1 km south of the map area, in the Hazlehurst, North quadrangle (Fig. 2.4). Qp6 is unique among alloformations of the Oconee River in that it is the only map unit characterized by exceptionally large, meandering paleochannel scars ("mega-meanders") that are clearly evident both in the field and on satellite imagery and aerial photography. Qp6 paleochannels have widths and radii of curvature several times larger than the modern river. Similar large paleomeanders occur along other rivers in the southeastern Atlantic Coastal Plain, and previous workers have interpreted these features as evidence that rivers in the region once conveyed greater bankfull discharge than they do today (Leigh and Feeney, 1995; Leigh, 2006; Leigh, 2008). Qp6 occurs as isolated remnants flanking the outer margins of Qh2 and Qh1 that range in cross-valley extent from 1,000-1,400 m, but its spatial relationship with these and immediately older units suggest that it was formerly positioned near the center of the valley axis prior to its

erosional removal by concurrent and later phases of the Oconee River. Qp6 extends from its inner boundary with Qh2 and Qh1 deposits, across scrollwork topography that ranges from weakly to well-expressed, to its outer boundary, which is characterized by a mega-meander paleochannel that is laterally incised into adjacent older map units. This outer boundary is sharply scalloped and associated with a well-defined scarp that rises about 3 m above the paleochannel ground surface. Qp6 stands about 3-7 m above the base flow Oconee River, with variation in elevation reflecting differences among scrollbar ridge, swale, and paleochannel landscape positions.

Like Qh2 and Qh1, Qp6 sediments consist of normally graded (fining upward) meandering channel deposits composed of loamy to clayey overbank and clayey channel fill vertical accretion lithofacies that overlie a sandy lithofacies comprised of lateral accretion and bedload sediments (Fig. 2.5). Similar to Qh1 deposits, Qp6 contains a gradational sandy to loamy overbank lithofacies that occurs between the sandy lateral accretion and the loamy to clayey overbank vertical accretion facies. Although no complete vertical sections of Qp6 could be recovered by drill rig or located in outcrop, a boring from the B-B' locality (Fig. 2.5B, core 32) indicates that Qp6 in this area is at least 8.4 m thick.

The sandy lithofacies of Qp6 (Fig. 2.5, lithofacies #1) is very similar to those of Qh1 and Qh2, and the reader is referred to sections 2.4.1 and 2.4.2 for a description of the lithologic properties and sedimentary structures characteristic of these deposits. The sandy lithofacies comprises the bottom stratum of Qp6 across its entire spatial extent. This lithofacies represents lateral accretion and bedload sediments that aggraded in channel lag, channel bar, and point bar environments of larger-than-modern meandering channels. In this respect, its total thickness, which is >6.0 m in the B-B' vicinity (Fig. 2.5B), as well as the individual thickness and planform

extent of the individual point bar and channel bar components of this lithofacies, appear to be somewhat greater than in Qh1 and Qh2.

The loamy to clayey overbank vertical accretion lithofacies of Qp6 (Fig. 2.5, lithofacies #2) is lithologically very similar to its counterparts in Qh1 and Qh2 but displays a greater degree of pedogenic development and has retained no sedimentary structures. Ultisols with yellowish brown (10YR 5/4) to strong brown (7.5YR 5/8), ~0.5 m thick argillic horizons to Inceptisols with incipient argillic horizon development characterize this lithofacies in Qp6, with soils developed in swales exhibiting lower chroma matrix colors and redoximorphic features. The loamy to clayey lithofacies abruptly overlies sandy lateral accretion sediments in the central part of Qp6 in the B-B' vicinity (Fig. 2.5B), but it gradationally overlies a sandy to loamy overbank vertical accretion lithofacies (Fig. 2.5, lithofacies #4) that occurs in the western part of the unit in this locality. This sandy to loamy lithofacies can be as much as 1.5 m thick in Qp6 and is interpreted to represent sandy vertical accretion sediments that accumulated in proximal overbank environments and swales during floods. With the exception of exhibiting slightly more weathering in its upper part, the Qp6 sandy to loamy lithofacies is very similar to its counterpart in Qh1, and the reader is referred to section 2.4.2 for a detailed description of its lithologic properties and sedimentary structures.

The clayey channel fill facies (Fig. 2.5, lithofacies #3) that occurs within the abandoned mega-meander paleochannel scars of Qp6 is very similar in terms of lithology, sedimentary structures, stratigraphic character, and pedogenic development to its counterpart facies in Qh1 and Qh2. Its thickness, which ranges from ~1.5-2.0 m and thins toward the insides of meander bends, is similar to that of Qh1 and Qh2 abandoned channel fills, but its planform shape, which

tends to be arcuate to crescent-shaped, has a much greater width that reflects the greater-than-modern width-to-depth ratios of Qp6 mega-meander paleochannels.

Radiocarbon and OSL dating of respective basal channel fill and upper lateral accretion point bar sediments were conducted on the Qp6 mega-meander paleochannels located within and to the immediate south of the Uvalda quadrangle. Radiocarbon dating of seeds obtained from basal channel fill situated immediately above the contact with bedload sand in the thalweg of the Uvalda mega-meander returned a calibrated age of 12.3±0.2 ka (Table 2.1; Fig. 2.4, #4; Fig. 2.5B, core 45). OSL dating of upper lateral accretion sand collected from the point bar of this paleochannel yielded a date of 17.3±3.4 ka (Table 2.2; Fig. 2.4, #3; Fig. 2.5B, core 34). We consider these age estimates to be in good agreement, considering the 2-sigma error of the OSL date (14.0-20.7 ka) and that channel fill should post-date meander abandonment. Relatively fresh-looking seeds collected from unoxidized, peaty sediments at the base of channel fill of the second Qp6 paleochannel, the "Leware mega-meander", returned a similar calibrated radiocarbon date of 11.6±0.2 ka (Table 2.1; Fig. 2.4, #14), while OSL dating of upper lateral accretion sands beneath the adjacent point bar yielded a slightly younger age of 9.0±2.6 ka (Table 2.2; Fig. 2.4, #15). We regard the 11.6 ka radiocarbon date to better approximate the time of channel abandonment at the second Qp6 mega-meander locality, given its stratigraphic context, the high quality of the dated material, and the lesser degree of statistical and experimental uncertainty associated with AMS radiocarbon versus OSL dating. However, we nonetheless consider the radiocarbon and OSL ages obtained from this site to be in rough agreement, considering that the radiocarbon age estimate coincides with the upper boundary of the 2-sigma error in the OSL date (6.4-11.6 ka). We interpret radiocarbon and OSL dates obtained from Qp6 to indicate a terminal Pleistocene age for this alloformation. This age

assignment is supported by respective late Wisconsin and early Holocene dates obtained from the immediately adjacent Qp5 and Qh1 alloformations that are indicated by cross-cutting relationships to respectively pre- and postdate Qp6.

2.4.4 Map unit Qp5

The Qp5 alloformation constitutes the map unit that immediately predates Qp6, and its spatial extent coincides with that of the third terrace above the Oconee River. Qp5 occurs on both sides of the Oconee valley in the southern part of the quad and on the western side of the valley it extends south into the Hazlehurst, North quadrangle (Figs. 2.3 and 2.4). Qp5 is unique among the alloformations of the Oconee River in that it is only map unit whose surface is characterized by interweaving linear sand ridges separated by silty to clayey swales that are clearly evident and mappable both in the field and on remote sensing imagery. The interwoven ridge-and-swale topography of the Qp5 surface bears strong resemblance to the late Pleistocene braided terraces of the lower Mississippi River valley described by Saucier (1994) and modern rivers with sandy bar-braided morphologies and indicates that the Qp5 alloformation was deposited when the Oconee River had a braided channel pattern (Leigh et al., 2004). In the southern part of the valley, Qp5 occurs as large but discontinuous remnants that are cross-cut by Qp6, Qh1, and Qh2. Its spatial relationships with these younger units, as well as with older adjacent units, indicate that, prior to its erosional removal from the central and northern parts of the valley, it was located near the center of the valley axis and occupied at least a portion of the area where Qp6, Qh1, and Qh2 now occur. The most well expressed braid bar morphology is found on the Qp5 unit on the eastern side of the valley (Plate 1; Plate 2, A-A'). In this location, the Qp5 surface extends from its inner boundary with Qh1, eastward across high, north-northeast

to south-southwest trending linear sand ridges that stand 3 to >4 m above intervening braided paleochannels, to an area of more subdued topography, characterized by lower ridges and shallower braid swales with 0.5-1.0 m of local relief. The outer boundary of Qp5 in this locality is characterized by a relatively well-defined scarp ~1.5 m in height. Qp5 stands about 4-8 m above the base flow Oconee River, with this range of relief resulting from the ridge and swale features described above. Although on the eastern side of the valley extensive subsurface and geomorphic data indicate that Qp5 is entirely composed of braided river deposits (Fig. 2.5), the outermost parts of the Qp5 map unit on the western side of the valley contain paleochannels with both meandering and indeterminate morphologies that extend south into the Hazlehurst, North quadrangle. In this location, it should be noted that inclusions may occur of meandering channel deposits that could not be differentiated from Qp5 with the available resolution of topographic and subsurface data.

Qp5 sediments primarily consist of alluvial deposits composed of loamy to clayey vertical accretion, sandy to loamy braided channel fill, and sandy upper braid bar lithofacies that overlie a gravelly sand bedload lithofacies that was deposited by the Oconee River when it had a braided channel pattern (Fig. 2.5A). Similar to Qp6 and Qh1, Qp5 contains a gradational sandy to loamy lithofacies that occurs between the loamy to clayey vertical accretion and gravelly sand bedload deposits. Qp5 was drilled to its base at one location in the map area (Fig. 2.5A, core 7), where coarse bedload sand unconformably overlies gleyed, loamy pre-Quaternary sediment. In this location, Qp5 is 9.2 m thick, but further east along the A-A' cross-section in the vicinity of core 19, it is more than 13.2 m thick.

The gravelly sand bedload lithofacies (Fig. 2.5, lithofacies #5) predominantly consists of gray (10YR 6/1) to light brownish gray (10YR 6/2) gravelly coarse sand that is interstratified

with lesser amounts of gravelly to very gravelly very coarse sand. Gray (N /5) gley colors typically occur in the lower part of this facies. Sedimentary structures evident in borings at the A-A' locality include thin beds of interstratified fine to medium, subrounded gravels and infrequent, thin (3-20 cm) beds of clay that are scattered throughout the lower and middle sections of the lithofacies. A more complete characterization of the sedimentary structures that likely occur in this lithofacies is provided by descriptions of sand bar architectural elements observed by Leigh et al. (2004) in the cutbank of a correlative braided channel deposit along the Altamaha River, located about 14 km downstream of the Uvalda quadrangle A-A' vicinity. Sedimentary structures at this location included tabular and trough cross beds, horizontally laminated sand beds, and thin, horizontal beds of gravel and silt that resemble the "Platte River Type" braided channel facies of Miall (1977). Although at the A-A' locality the majority of the vertical section of this lithofacies exhibited no fining upward trend, the upper 1-3 m are composed of medium sand that displays strong brown (7.5YR 5/6) to light yellowish brown (10YR 6/6) colors that reflect slight accumulations of pedogenic iron oxides. While the majority of the lithofacies is interpreted as braided river bedload sediments that aggraded in channel bed and lower bar environments, the medium sand component of the facies is interpreted to reflect deposition in lower energy settings, including middle to upper braid bar and low flow swale and channel environments. The gravelly sand lithofacies comprises the bottom stratum of Qp5 for the entire spatial extent of the alloformation and ranges in thickness from 8.2 m at the core 7 location on A-A' to >10 m in cores 16 and 19 (Fig. 2.5A).

For the majority of Qp5's spatial extent, the gravelly sand bedload facies is overlain by a coarse loamy to clayey vertical accretion lithofacies (Fig. 2.5, lithofacies #6) that occurs immediately beneath the ground surface in areas characterized by subdued ridge-and-swale

topography of ~0.5-1.0 m of local relief (Fig. 2.5A-C). An intervening gradational sandy to loamy lithofacies (Fig. 2.5, lithofacies #4), similar to those observed in Qp6 and Qh1, commonly occurs between this facies and the underlying bedload facies (Fig. 2.5A). The texture of the coarse loamy to clayey vertical accretion lithofacies typically ranges from sandy loam to clay, and this facies is generally coarser in its upper part than the vertical accretion facies that mantle Qp6, Qh1, and Qh2. This lithofacies has greater pedogenic development than the vertical accretion sediments of Qp6 and is characterized by Ultisols with A-E-Bt or Btg horizon sequences and argillic horizons with moderate structure and matrix colors that range from yellowish brown (10YR 5/6) to yellowish red (5YR 5/8) on ridges to (10YR 5/1) in swales. Soil color appears to be controlled by landscape position (i.e., ridge vs. swale), and, although texture appears to be less landscape dependent, clayey sediments are more common beneath swales. Pedogenesis appears to have destroyed any sedimentary structures that may have existed in this facies, which is interpreted as an overbank, vertical accretion flood drape that slowly accumulated following the abandonment of braided channels in this vicinity. Because no soil development is evident in the top of the gravelly sand bedload facies where it is directly overlain by vertical accretion, it appears that little time passed between the deposition of braid bar sediment and the initiation of vertical accretion sedimentation. The thickess of the loamy to clayey vertical accretion facies in the Qp5 deposit at the A-A' vicinity ranges from 2.4 m along its eastern, outer boundary to ~1.0 m near its western, inner margin, possibly indicating westward lateral migration of the Oconee River in this area during Qp5 time.

The sandy to loamy lithofacies (Fig. 2.5, lithofacies #4) that occurs in Qp5 between the finer-grained vertical accretion facies described above and bedload sediments has lithologic properties similar to its counterparts in Qp6 and Qh1. It typically exhibits faint to distinct

stratification and fines upward from medium sand to sandy loam. Cross-section A-A' (Fig. 2.5A) indicates that this facies occupies depressions in the surface of the underlying gravelly sand bedload facies that are interpreted to represent paleochannels and flood chutes within the former braided channel pattern of the Oconee River. In this context, this lithofacies is interpreted as coarse-grained sediments that were deposited in these channels and swales during flood events that post-dated braiding. The sandy to loamy lithofacies has a maximum thickness of 0.7 m and occurs in isolated bodies that in vertical section are crudely lenticular in shape.

Qp5 contains two additional lithofacies of limited spatial extent: a sandy, upper braid bar facies and a sandy to loamy braided channel fill facies. The sandy, upper braid bar lithofacies (Fig. 2.5, lithofacies #7) directly underlies the ground surface beneath the higher, interwoven braid bar ridges that occur near the western, inner margin of Qp5 in the A-A' vicinity (Figs. 2.3 and 2.5A). Similar deposits occur south of the map area on the inner margin of a Qp5 unit in the Hazlehurst, North quadrangle on the western side of the valley (Fig. 2.4). This facies consists of yellowish brown (10YR 5/6) to brownish yellow (10YR 6/6), well to moderately-well sorted, lower medium sand that lacks coarser particles, displays a slight fining upward trend, exhibits little pedogenic development, and gradationally overlies lower braid bar components of the gravelly sand bedload facies. We interpret this facies to either represent extremely well sorted, upper braid bar sediment of fluvial origin or bodies of eolian sediment that were blown from surrounding braid plains during Qp5 time and subsequently sculpted by flood flows into their present linear, paleo-flow oriented planform shapes. This facies ranges in thickness from 1.4-2.4 m in the A-A' vicinity.

The braided channel fill facies (Fig. 2.5, lithofacies #8) occurs in the well-defined, relatively deeply incised braided paleochannels that are present along the western margin of the

Qp5 unit on the eastern side of the Oconee valley in the Uvalda quadrangle (Figs. 2.3 and 2.5A). This lithofacies abruptly overlies the gravelly sand bedload facies, is typically about 1.0 m thick, and consists of black (10YR 2/1) to dark grayish brown (10YR 4/2), stratified sands and loamy sediments that exhibit Ag over Cg soil profiles which sometimes contain buried A horizons. This lithofacies represents channel fill that accumulated in abandoned braided paleochannels following their abandonment. It should be noted that braided paleochannels and swales have been mapped as morphological features in other areas of Qp5, such as in the central and eastern parts of Qp5 in the A-A' vicinity (Fig. 2.5A). However, the sediments underlying these areas comprise part the loamy to clayey vertical accretion lithofacies, and cannot be lithologically differentiated from similar adjacent sediments that underlie ridges and terrace flats in this area. Thus, the braided channel fill facies is not mapped in these localities.

Leigh et al. (2004) reported two OSL age estimates for Qp5, which included one date of 27.9±4.4 ka obtained from a braid bar at the core 10 location on cross-section A-A'(Fig. 2.4, #9 and Fig. 2.5A) and a second date of 22.4±4.2 ka obtained from an adjacent braid bar located about 900 m to the north-northwest (Fig. 2.4, #6). To further refine age estimates for the Qp5 alloformation in the A-A' vicinity, radiocarbon dates were obtained from both the eastern part of the unit, at the core 19 location, where no prior dating had been conducted, and from the western part of the unit, near its inner boundary with Qh1 at the core 7 location (Fig. 2.5A). Leaf fragments obtained from a depth of 400 cm within bedload sediments in core 19, at the "Uvalda A 349560 m" locality, yielded a calibrated radiocarbon date with a 2-sigma age range of 34.5-34.8 ka (Table 2.1; Fig. 2.4, #10; Fig. 2.5A), which is in good agreement with the OSL age of Leigh et al. Radiocarbon dating of a well-preserved pine log collected from a depth of 430-450 cm within bedload sediments further west, in core 7 at the "Uvalda A 351398 m" locality,

returned a calibrated age with a 2-sigma range of 17.5-18.0 ka (Table 2.1; Fig. 2.4, #8; Fig. 2.5A). We consider this date to also compare well with the OSL ages of Leigh et al., even though it is somewhat younger, given the fact that it is not unusual for sediments of varying age to occur in close proximity to one another in laterally shifting braided channel environments that have complex cut-and-fill sedimentary architectures. To provide an estimate for Qp5 deposits on the western side of the valley, OSL dating was conducted on upper braid bar sediments on the inner margin of a Qp5 unit, at the "Leware Braid Bar" locality, immediately south of the map area in the Hazlehurst, North quadrangle (Fig. 2.4, #16). These sediments returned an OSL age of 31.5±7.19 ka, which is in strong agreement with the ages reported by Leigh et al. (Table 2.2). Taken together, the above radiocarbon and OSL dates indicate a late OIS 3 to OIS 2 age for Qp5, which is consistent with late Wisconsin dates reported from braided river deposits that occur downstream along the Altamaha River and along other rivers in the Southeast (Leigh et al., 2004; Leigh, 2008).

2.4.5 Map unit Qp4

The Qp4 alloformation comprises the map unit that immediately predates Qp5, and its spatial extent corresponds to that of the fourth terrace of the Oconee River. Qp4 occurs as two long, continuous paired remnants extending from the north-central to the south-central parts of the valley that in some places are dissected by units of Quaternary stream alluvium (Fig. 2.3; see section 2.4.10 below). Smaller units of Qp4 are present in the eastern valley at the southern boundary of the Uvalda quadrangle and elsewhere, both upstream and downstream of the map area (Fig. 2.4).

The Qp4 surface typically stands 5-10 m above the Oconee River, has a cross-sectional extent of 700-1,800 m, and extends from an inner boundary that is cross-cut by adjacent, younger alloformations to its outer margin, which is cross-cut into older alloformations or surrounding uplands. In the eastern valley, the outer boundary of Qp4, which borders Qp3, is in some places characterized by a subtly to moderately defined ~1.5 m scarp. In other places, the boundary between these units has no geomorphic expression, and the Qp3 and Qp4 surfaces together comprise a relatively flat terrace that slopes gently downhill from adjacent uplands towards the valley bottom. In the western valley within the Uvalda quadrangle, Qp4 is cross-cut into the higher Qp2 surface, and its outer boundary is characterized by a scarp that ranges from 3-5 m in height.

Immediately north of its lateral boundary with Qp5 in the eastern valley, the Qp4 surface contains a higher-elevation component that exhibits weakly expressed ridge-and-swale patterns that are evident on color-infrared aerial photography, as well as in the field, that resemble degraded forms of the braided channel patterns on the Qp5 surface. Inspection of sediments underlying this surface revealed a lithofacies assemblage similar to that of the braided river Qp5 alloformation, comprised of a sandy, braid bar lithofacies overlain by a fining upward, sandy to clayey vertical accretion facies. Just to the north of this area, the higher component of Qp4 is cross-cut by a meandering paleochannel that occupies a lower-elevation component of the Qp4 surface (Figs. 2.3 and 2.4). Three additional meandering paleochannels occur to the northwest of this feature. Sediments underlying these localities consist of loamy to clayey overbank and mucky to clayey channel fill lithofacies overlying sandy lateral accretion and bedload facies that, although more weathered, bear a strong resemblance to the meandering channel lithofacies of Qp6, Qh1, and Qh2. Based on this evidence, we consider Qp4 to be comprised of alluvium

derived from both braided and meandering phases of the Oconee River. However, expression of geomorphic boundaries on the Qp4 surface is too poor, and the available coverage of subsurface data in this area is too sparse, to allow delineation of bounding discontinuities that would subdivide Qp4 into discrete braided channel and meandering channel alloformations. Thus, the Qp4 alloformation should be considered as a generalized map unit composed of both braided and meandering channel deposits.

In the A-A' vicinity (Fig. 2.5A), Qp4 is characterized by a 3.5-5.0 m thick upper lithofacies that is primarily composed of gray (10YR 5/1 to 6/1), extremely plastic, backswamp or paleochannel clay (Fig. 2.5, lithofacies #9) that gradationally overlies a gray (10YR 6/1) to red (2.5YR 5/6) medium to coarse sand lithofacies that is similar to the lateral accretion/bedload facies of Qp6, Qh1, and Qh2 (Fig. 2.5, lithofacies #1). Although drilling revealed that Qp4 is at least 8.4 m thick in the A-A' locality, its total thickness in this location as well as elsewhere in the valley is unknown. In general, Qp4 is characterized by greater pedogenic development than Qp5, with soils formed on both the braided and meandering channel components of this unit consisting of Ultisols with A-E-Bt-C horizon sequences, well-expressed elluvial (E) horizons, and multiple, underlying argillic horizons with a cumulative thickness of ~0.5-1.0 m, moderate structure, distinct clay films, and (in well-drained landscape positions) 10YR to 2.5YR hues (Fig. 2.7). On outer, older parts of Qp4, soils tend to be thicker and the extent of pedogenesis precludes recognition of the discrete lithofacies that originally composed these deposits.

OSL dating of light gray, medium to coarse, C-horizon sand recovered from a depth of 270-300 cm within a Qp4 deposit overlain by muted braided topography returned an age of 52.3±12.2 ka (40.1-64.5 ka; Table 2.2; Fig. 2.4, #5). We consider this age to compare well with the oldest age obtained from Qp5 (34 ka), the immediately younger alloformation as indicated by

cross-cutting relationships, and consider it to be a reliable estimate. However, given the 2-sigma error in the OSL age and the fact that the dated sediments occupy a component of Qp4 that is cross-cut by younger Qp4 meandering channel deposits, it is most reasonable to view Qp4 as containing multiple deposits that span a range of late OIS 4 and early to middle OIS 3 ages.

2.4.6 Map unit Qp3

The Qp3 alloformation constitutes the map unit that immediately predates Qp4, and its spatial extent coincides with that of the fifth terrace of the Oconee River. In the Uvalda quadrangle, one extensive remnant of Qp3 occurs on the eastern margin of the Oconee valley, and smaller remnants of the unit also occur upstream and downstream of this location within and beyond the map area (Figs. 2.3 and 2.4). The Qp3 surface stands 7-14 m above the base flow Oconee River, has a cross-sectional width of 250-1,000 m, and extends from an inner boundary that is cross-cut by Qp4 and adjacent, younger alloformations, to its outer margin, which is cross-cut into adjacent uplands or, less frequently, into the older Qp2 alloformation. Within the Uvalda quadrangle, on the eastern side of the Oconee valley, the outer boundary of Qp3 coincides in most locations with the boundary of mappable Oconee River-derived Quaternary alluvium recognized by this study. In these areas, the outer boundary of Qp3 typically occurs at the 40 m contour that marks the toe of the uplands. Although in some places the ascent into the adjacent uplands is gradual, in most cases it is relatively abrupt. The Qp3 surface slopes gently from its outer boundary down to its inner boundary with Qp4, and is relatively flat, containing only slight rises and depressions. Stream dissection of this surface is modest, and no distinct fluvial topography (e.g., paleochannel scars, scrollwork topography) has been preserved.

Qp3 sediments typically consist of alluvial deposits of a wide range of textures that display a crude fining upward trend and extensive alteration by weathering and pedogenesis. For this reason, clearly identifiable, discrete lithofacies, as they occur in map units Qp5-Qh2, cannot be recognized in this alloformation. In the A-A' vicinity (Fig. 2.5A), Qp3 contains an upper stratum of coarse loamy alluvium 2.5-3.7 m thick that fines upward from coarse sandy loam basal sediments to sandy loam and sandy clay loam in its upper part (Fig. 2.5, lithofacies #10). Soils with A-E-Btg or Btgx-BC profiles ranging from ~2.0-2.5 m in total thickness have developed in these sediments, and no sedimentary structures have been preserved. This coarse loamy upper stratum unconformably overlies a bottom stratum (Fig. 2.5, lithofacies #11) composed of older, clayey deposits of indeterminate origin that due to refusal could not be drilled to its base. The bottom stratum is brown (7.5YR 5/2) to very dark gray (10YR 3/1) in its upper part, but it displays an oxidized, yellowish brown (10YR 5.5/8) color at greater depth and may consist of a paleosol developed in pre-Quaternary Coastal Plain sediments or older, Oconee River-derived alluvium. Thus, at the A-A' locality, the total thickness of Qp3 is unclear, since its lower boundary could either be placed at the base of the coarse loamy alluvium upper stratum or beneath the clayey bottom stratum, depending upon whether or not the bottom stratum is comprised of Oconee River alluvium. The stratigraphic relationship between Qp3 deposits and underlying sediments is more clear at the Dead River Road roadcut locality, located immediately south of the map area in the Hazlehurst North quadrangle (Figs. 2.4 and 2.8). Here, basal gravel lag unconformably overlies pre-Quaternary Coastal Plain sediments, and Qp3 has a total thickness of ~2.1 m.

Given its elevation range, spatial extent, and the diverse assemblage of alloformations that comprise more recent Oconee River deposits, it is highly likely that Qp3 originally consisted

of multiple, recognizable alloformations separated by bounding discontinuities. However, because no distinct fluvial topography has been preserved on the Qp3 surface and extensive weathering has rendered discrete lithofacies unrecognizable in most locations, Qp3 alluvium is mapped as a single alloformation by this study. The age of Qp3 is beyond the range of radiocarbon dating, and, in every location where Qp3 sediments were examined, they were too weathered to be suitable for OSL dating. Thus, no absolute numerical age estimate is available for this alloformation. However, cross-cutting relationships with Qp4 indicate that Qp3 must be the older of the two units. Given that Qp4 sediments returned an OSL date 52.3±12.2 ka, Qp3 must be greater in age than 52.3±12.2 ka.

2.4.7 Map unit Qp2

The Qp2 alloformation is the map unit that immediately predates Qp3, and its spatial extent coincides with that of the sixth terrace of the Oconee River (Fig. 2.3). Qp2 occupies its greatest extent in the southwestern corner of the quad, where it extends westward into the neighboring Jordan quadrangle and continues to the south into the Hazlehurst, North quadrangle (Fig. 2.4). Qp2 occupies a valley margin or near-valley margin position, and its surface extends from an inner lateral boundary marked by a well- to moderately-defined scarp, where it has been cross-cut by younger map units, to an outer lateral boundary with Qp1 deposits or adjacent uplands. In the southwestern corner of the Uvalda quadrangle, this outer boundary with Qp1 is characterized by a 5-6 m scarp that, although typically well-defined, in some places has been smoothed by erosion to constitute a more gradual, sloping boundary. In the southwestern Uvalda and northwestern Hazlehurst, North quadrangles, the Qp2 surface stands 13-20 m above the Oconee River and is remarkably flat, though it is deeply dissected by Crooked Creek and other

tributaries to the Oconee River. The Qp2 surface contains no distinct fluvial topography (e.g., paleochannel scars, scrollwork), but it does exhibit numerous, circular- to ovoid-shaped, closed depressions of various sizes. Long-axis orientations of these depressions range widely, from northwest to southeast, as typical of Carolina Bays, to east-to-west, to northeast-to-southwest. The fact that much of the Qp2 surface is composed of loose sand that would have been subject to possible eolian reworking during windier, drier, more sparsely-vegetated paleoenvironmental conditions may suggest an eolian origin for these features. However, this study did not explicitly investigate these landforms, and together they may comprise a mixed assemblage of blow-outs, Carolina Bays, and incipient sinkhole features.

Qp2 sediments primarily consist of alluvial deposits that display a wide range of textures, a crudely fining upward trend, and extensive alteration by weathering and pedogenesis. In many places, pale brown (10YR 6/3) loamy sand to sandy loam, with a loose, single-grained character, occurs at the Qp2 surface. Qp2 soils display similar to slightly greater pedogenic development relative to those of Qp3, with A-E-Bt1-Bt2-(Bt3)-(Bt4)-C profiles that contain two or more argillic horizons that exhibit sandy loam to clay textures; distinct, discontinuous clay films; brownish yellow (10YR 6/5) to strong brown (7.5YR 5/8) matrix colors; and 0.7-2.0 m of cumulative thickness (Appendix B, Tables B1 and B2). In most locations, clearly identifiable, discrete lithofacies, as they occur in map units Qp5-Qh2, cannot be recognized in Qp2 due to severe alteration by weathering. However, in one locality in the western valley immediately south of the Uvalda quadrangle, a borrow pit exposure reveals Qp2 deposits that are interpreted to consist of an intensively weathered, fine to coarse loamy vertical accretion lithofacies that abruptly overlies a sandy, lateral accretion and bedload facies (Fig. 2.9). This sandy facies is characterized by indeterminate cross-bedding; moderately to poorly sorted, medium to coarse

loamy sand to sandy loam with infrequent granules; evidence of weathering in its upper part; and weak cementation throughout its exposed thickness. In this location, Qp2 deposits are at least 2.3 m thick. However, because no complete exposures of Qp2 could be located and auger refusal prevented drilling to its base, the total thickness of Qp2 is unknown.

Given its elevation range, spatial extent, and the diverse assemblage of alloformations that comprise more recent Oconee River deposits, it is highly likely that Qp2, like Qp3, originally consisted of multiple, recognizable alloformations separated by bounding discontinuities. However, because no primary fluvial topography has been preserved on the Qp2 surface and extensive weathering has rendered discrete lithofacies unrecognizable in many locations, Qp2 alluvium is mapped as a single alloformation by this study. The age of Qp2 is beyond the range of radiocarbon dating, and Qp2 sediments are too weathered to be suitable for OSL dating. Given that cross-cutting and elevation relationships indicate Qp2 is older than Qp4, which returned a 52.3±12.2 ka OSL age, an age of >52.3±12.2 ka is assigned to the Qp2 alloformation.

2.4.8 Map unit Qp1

The Qp1 alloformation constitutes the map unit that immediately pre-dates Qp2, and its spatial extent corresponds to that of the seventh terrace above the Oconee River (Fig. 2.3). Although Qp1 only occupies a small area in the southwestern corner of the Uvalda quadrangle, its surface comprises an extensive, flat to gently rolling, deeply dissected terrace in the eastern part of the neighboring Jordan quadrangle and the respective northeast and northwest corners of the Lumber City and Hazlehurst, North quadrangles (Fig. 2.4). Qp1 occupies a valley margin position, and its surface extends from an inner lateral boundary with younger, adjacent map units

to an outer lateral boundary with surrounding uplands that is located outside the Uvalda quad (Fig. 2.4). Although in some places it has distinct topographic expression, in most places the boundary between Qp1 and adjacent uplands is best described as a zone of gradually increasing elevation that extends from the relatively flat Qp1 surface to higher, more densely dissected upland areas. In this sense, its placement in Figure 2.4 is somewhat arbitrary and represents a best approximation.

The Qp1 surface displays a wider elevation range than do the surfaces of other map units and contains a higher-elevation component that stands 25-35 m above the Oconee River, as well as a lower-elevation component that is 20-25 m above river level. The Qp1 surface contains no distinct fluvial topography (e.g., paleochannel scars, scrollwork), but it does exhibit numerous, circular- to ovoid-shaped, closed depressions of various sizes. Long-axis orientations of these depressions range widely, from northwest to southeast, as typical of Carolina Bays, to east-to-west, to northeast-to-southwest. This study did not explicitly investigate these landforms, and together they may comprise a mixed assemblage of blow-outs, Carolina Bays, and incipient sinkhole features.

Qp1 sediments primarily consist of alluvial deposits that display a wide range of textures, a crudely fining upward trend, and extensive alteration by weathering and pedogenesis. In locations on Qp1 where profiles were described, soils consist of Ultisols with A-E-Bt1-Bt2-Btv-BC-C profiles that are similar in development to Qp2 soils, except for the fact that they contain plinthite within their argillic horizons and sometimes have rounded to subrounded ironstones in their upper meter (Appendix B, Tables B3 and B4). In these sections, Qp1 sediments generally fine upward, from gravelly coarse sand or sandy loam at depth to finer-grained loamy and clayey textures in their upper part, but are so altered by pedogenesis that they are difficult to distinguish

from soils that are developed in older Coastal Plain sediments on surrounding uplands. Clearly identifiable, discrete lithofacies and sedimentary structures, as they occur in map units Qp5-Qh2, cannot be recognized in Qp1 due to severe alteration by weathering. Qp1 deposits range from >2.7 to >4.0 m thick in the localities where they were examined. However, because no complete exposures of Qp1 could be located and auger refusal prevented drilling to its base, the total thickness of Qp1 is unknown.

Given its elevation range, spatial extent, and the diverse assemblage of alloformations that comprise more recent Oconee River deposits, it is highly likely that Qp1, like Qp2 and Qp3, originally consisted of multiple, recognizable alloformations separated by bounding discontinuities. However, because no distinct fluvial topography has been preserved on the Qp1 surface and extensive weathering has rendered discrete lithofacies unrecognizable in many locations, Qp1 alluvium is mapped as a single alloformation by this study. Qp1 sediments are too weathered to be suitable for OSL dating. Qp1 is older than 52.3±12.2 ka, given that cross-cutting and elevation relationhips indicate that it is older than Qp4, which returned a 52.3±12.2 ka OSL date. The Hazlehurst terrace, the highest, oldest, and most landward of the marine terraces recognized in Georgia, is mapped by Huddlestun (1988) as extending into the southern part of the Uvalda quadrangle (Fig. 2.2). The Hazlehurst terrace has an absolute elevation that ranges from 70-79 masl and is thought to be no older than late Pliocene to early Pleistocene (Huddlestun, 1988, pp. 153-154). Because Qp1, which has surface elevations that range from 48-62 masl, is inset within the Oconee River valley beneath the Hazlehurst terrace, it must post-date the Hazlehurst terrace. Therefore, we consider Qp1 to be of Quaternary age, with an early to middle Pleistocene age being most likely.

2.4.9 Map unit Qals

The Qals map unit is comprised of alluvium deposited by major tributaries of the Oconee River and smaller streams (Figs. 2.3 and 2.4). Although detailed delineation of tributary alluvium is beyond the scope of this study, this generalized unit was mapped because tributary alluvium in some cases dissects, and in other cases is super-posed on, Oconee River-derived alloformations. In this respect, it constitutes a meaningful part of the valley's geomorphology and alluvial architecture.

Within the margins of the Oconee valley, units of Qals typically emerge from adjacent uplands and extend along stream courses that cross-cut successively younger, laterally adjacent Oconee River-derived alloformations in route to the Oconee River. However, in many locations, tributaries debouch onto lower surfaces, splay out into paleochannels, backswamps, or terrace environments, and become unrecognizable relative to surrounding deposits and therefore unmappable. Thus, the Qals unit is shown as terminating in these areas, and this phenomenon is commonly observed on the outer margins of Qh1 and Qh2. The Qals unit is shown as deviating from the courses of blue line streams in instances where field checks or inspection of aerial photography revealed differences in the locations of drainageways and tributary alluvium from base map hydrography. The Qals unit is not mapped outside the boundaries of the Oconee valley, but it should be noted that tributary alluvium often extends along drainageways into surrounding uplands for substantial distances upstream of this boundary.

The Qals map unit consists of loamy to sandy, stratified sediments ranging from less than one to several meters in thickness that occupy tributary valley bottoms within the greater Oconee River valley. Because tributary valleys are narrow and not well-suited to long-term storage of sediment, a large proportion of tributary alluvium probably correlates to Holocene alloformations

Qh1 and Qh2 of the Oconee River. However, older sediments do occur in tributary valleys, and this map unit contains deposits that span a range of Quaternary ages that could not be confidently separated at the resolution and scale of this study.

2.4.10 Map unit TQu

The TQu map unit consists of a variety of undifferentiated sediments that immediately underlie areas outside the margins of the Oconee River valley (Figs. 2.3, 2.4, and 2.5) and span a wide range of Tertiary and Quaternary ages. This unit includes the Miocene Coastal Plain sediments that underlie uplands in this area and their weathering residuum, as well as younger Quaternary sediments of eolian, alluvial, colluvial, and lacustrine origin that locally overlie these older deposits. Thus, TQu contains Pleistocene and Holocene stream alluvium that occupies tributary valley bottoms; colluvial and slope wash deposits of Quaternary age that occur in lower backslope, footslope, and toeslope landscape positions; sediments associated with Carolina Bays and other closed depressions; and surficial eolian sediments. It is worth noting that residual soils formed in the Miocene Coastal Plain sediments that underlie upland summit positions display the greatest pedogenic development of any soils in the map area, and typically consist of strongly developed Ultisols with A-E-Btx1-Btx2-(Btx3)-C profiles with multiple argillic horizons that exhibit variegated colors; moderate to strong subangular to angular blocky structure; common, well expressed argillans; and sometimes contain fragipans (Fig. 2.10).

TQu also contains small remnants of Oconee River-derived alloformations that are too limited in extent to map at the 1:24,000 scale. Beyond the eastern margin of the Oconee River valley, in the central part of the Uvalda quadrangle, upland areas are deeply and densely dissected and stand in strong contrast to the relatively flat topography that characterizes the

western valley in the southwestern corner of the Uvalda and eastern part of the Jordan quadrangles (Figs. 2.3 and 2.4). Here, TQu is mapped at elevations between ~40-60 masl, an elevation range that is occupied by Oconee River-derived alloformations on the western side of the valley. Although thin caps of alluvium sometimes occur in this area that may correlate to map units Qp2 and Qp1, these deposits are too patchy, thin and discontinuous to map at the resolution and scale of this study, and, in some cases, are so severely altered by pedogenesis that they are often difficult to distinguish from surrounding upland weathering residuum. Therefore, these deposits have been incorporated into the TQu map unit and are recognized as inclusions that occur therein.

Finally, for the sake of simplicity, all pre-Quaternary sediments that underlie and/or laterally bound the Oconee River-derived alloformations depicted in Figure 2.5A-C have been classified as part of the TQu unit. Although these sediments were not characterized by this study and their lithostratigraphic classification was not confirmed, they may be comprised of more than one formal lithostratigraphic unit. According to the spatial extents and stratigraphic relationships among lithostratigraphic units in this part of the Georgia Coastal Plain described by Huddlestun (1988), the pre-Quaternary sediments that immediately underlie uplands in the map area and laterally bound Oconee River Quaternary alluvium along the valley margin most likely belong to the Miocene Altamaha Formation (Huddlestun, 1988, pp. 100-107). However, at elevations near or below the bed of the modern Oconee River in this area, where pre-Quaternary sediments immediately underlie Oconee River alluvium, deposits may belong to the Miocene Meigs Member of the Coosawhatchie Formation, which immediately underlies the Altamaha Formation in this part of Georgia (Huddlestun, 1988, pp. 87-92).

2.5. Discussion

2.5.1 Utility of allostratigraphy for delineation of Quaternary fluvial sediments

Allostratigraphic mapping of Quaternary sediments of the lower Oconee River valley has identified eight informal alloformations within the Uvalda, Georgia 7.5-minute quadrangle. This represents a substantial improvement over previous geologic maps in the area, which fail to resolve any of the aforementioned units and report all surficial sediments within the Oconee valley as either undifferentiated Quaternary alluvium (Georgia Department of Natural Resources, 1976) or Holocene alluvial gravelly sand (Richmond et al., 1987).

This study demonstrates that allostratigraphy is effective for delineating Quaternary sediments in the Oconee valley and suggests that the method is equally applicable to other alluvial valleys within the southeastern Atlantic Coastal Plain and elsewhere. These findings affirm those of prior studies that have successfully employed allostratigraphy for the delineation of Quaternary fluvial sediments (Autin, 1992; Blum and Valstro, 1994). In settings like the Oconee valley, allostratigraphy is preferable to other mapping approaches because it facilitates the delineation of alloformations. In this context, in cases where bounding discontinuities can be confidently recognized by geomorphic surfaces, cross-cutting relationships in geomorphic and lithologic features, and subsurface unconformities, an alloformation consists of a three dimensional body of sediment composed of heterogeneous but genetically related lithofacies that were deposited within a discrete period of time and associated with a given regime of the Oconee River. Thus, allostratigraphic mapping delineates map units composed of sediments derived from a related suite of fluvial processes and establishes relative age relationships for the map units it defines (Autin, 1992). In contrast, if geomorphic mapping were adopted as an alternative to the allostratigraphic approach, and Quaternary deposits of the Oconee valley were mapped

simply as terraces, relative age relationships among geomorphic surfaces could be established and interpretations about past channel pattern and depositional style could be inferred, but relationships between surface morphology and underlying lithofacies would be unclear, information about depositional environments would be limited, and the alluvial architecture of the valley would remain unknown. If lithostratigraphy were adopted as an alternative to the allostratigraphy, and Oconee deposits were mapped as lithostratigraphic units, map units would provide information about sedimentary processes and depositional environments. However, genetically related, contemporaneous but lithologically distinct vertical accretion and lateral accretion lithofacies deposited by the same regime of the Oconee River would be mapped as two separate units, while similar lithofacies that clearly belong to separate alloformations based on cross-cutting relationships (e.g., the sandy lateral accretion and bedload lithofacies that comprises the lower stratum of Oconee River alloformations Qh2, Qh1, and Qp6), would be generalized into one lithoformation. As such, lithostratigraphic mapping would severely limit interpretations about relative age relationships among map units and the fluvial evolution of the lower Oconee River.

Although allostratigraphy has many benefits, there are some scenarios encountered in the Oconee valley that pose challenges for the allostratigraphic approach. Oconee River alloformations were mapped based on bounding discontinuities, and each alloformation is bounded by 1) a basal unconformable contact with either pre-Quaternary Coastal Plain sediments or older Oconee River-derived alluvium; 2) an upper boundary that is defined by a laterally traceable geomorphic surface; and 3) lateral boundaries characterized by cross-cutting relationships in the geomorphology and lithofacies of adjacent map units. However, in areas

where bounding discontinuities cannot be confidently identified, accurate delineation of alloformations becomes uncertain.

In younger alloformations (e.g., Qh2, Qh1, Qp6, and Qp5), distinct fluvial topography (like scarps, paleochannels, and scrollwork), as well as individual lithofacies, are well-preserved, facilitating recognition of lateral bounding discontinuities and allowing confident delineation of lateral alloformation boundaries. However, in older alloformations, degradation of fluvial topography and obliteration of discrete, identifiable lithofacies by weathering in some instances makes lateral discontinuities difficult to identify and results in map unit boundaries being somewhat interpretive. This is the case in some areas along the lateral contact between Qp4 and Qp3, on the eastern side of the Oconee valley, where sediments are highly weathered, the boundary between map units lacks geomorphic expression, and the Qp3 and Qp4 surfaces together comprise a flat terrace that slopes gently downhill from adjacent uplands toward the valley bottom. Furthermore, when compared with younger alloformations, it appears that the lack of distinct fluvial topography and clearly identifiable lithofacies also reduces the resolution at which older alloformations can be mapped. For example, Qp4 contains evidence of both meandering and braided river deposits that must have been originally separated by recognizable bounding discontinuities. However, expression of geomorphic boundaries is too poor, and preservation of lithofacies is too spotty, to allow confident subdivision of Qp4 into discrete braided and meandering channel alloformations with a reasonable amount of subsurface data. Based on this information, we regard it likely that Qp3, Qp2, and Qp1 also once consisted of multiple alloformations separated by lateral bounding discontinuities that can no longer be recognized and mapped. Confident identification of the lower boundaries of these older alloformations is also difficult, because weathering and pedogenesis often extend completely

through the Oconee River-derived alluvium, into underlying pre-Quaternary Coastal Plain sediments and so overprint the unconformity that marks the base of the alloformation that it is difficult to identify, particularly in auger borings. This problem is compounded by the fact that the Altamaha Formation, which underlies uplands in the map area and is of fluvial origin (Huddlestun, 1988), consists of weathered sand, clay, and rounded quartz gravels that bear a strong resemblance to weathered Oconee River alluvium in many places. These complications pose further challenges to the accurate delineation of older alloformations within the map area.

A final challenge to the allostratigraphic approach in the Oconee valley and similar settings relates to the definition of the upper boundaries of alloformations. Following its abandonment by the Oconee River, a given alloformation, such as Qh1, may continue to receive sediment deposition via overbank flooding on its upper boundary during the time interval that spans the deposition of the next younger map unit (Qh2). However, in the Oconee valley, pedogenesis appears to have kept pace with sedimentation, and recognition of the true upper boundary of the alloformation (in the allostratigraphic sense) is, in most cases, not possible because it is located somewhere within a soil profile developed in vertical accretion sediments and has been obliterated by pedogenesis. For this reason, we recognize that Qh1, and to varying degrees the other alloformations, contain sediments in their upper part that were deposited following primary allounit emplacement. These observations are similar to the findings of Autin (1992), who noted that overbank sedimentation and pedogenesis on Holocene meander belts of the Amite River in the Louisiana Gulf Coastal Plain resulted in alloformations with indistinct upper boundaries.

2.5.2 Late Quaternary fluvial evolution of the lower Oconee River

Previous studies indicate that, during the past 30 ka, rivers of the southeastern Atlantic Coastal Plain experienced major transitions in channel pattern and depositional style from braided, to large meandering, to modern-sized meandering planforms, in response to late Quaternary climatic shifts that drove changes in terrestrial sediment yield and the amount, and possibly the seasonal distribution, of runoff (Leigh, 2008; Leigh, 2006; Leigh et al., 2004; Leigh and Feeney, 1995). Leigh (2008) indicates that southeastern Coastal Plain rivers exhibit four distinct morphological phases over the past 30 ka that closely correspond to major climatic and paleoenvironmental episodes. These include: 1) a late Wisconsin (30-16 ka) braided phase; 2) a terminal Pleistocene (16-11 ka) phase characterized by large meandering paleochannels (mega-meanders) with pronounced scrollbars; 3) an early Holocene (11-5.5 ka) phases with mega-meanders that typically lack pronounced scrollbars; and 4) a late Holocene (5.5 ka-present) phase with meandering channels with modern-size dimensions. Findings from the Oconee River, including the surface morphologies, sedimentologies, and radiocarbon and OSL age estimates of alloformations, generally affirm this succession of morphological phases, and indicate that the Oconee River exhibited similar behavior to that of other southeastern Atlantic Coastal Plain rivers during the late Quaternary.

Alloformation Qp5 has interwoven, ridge-and-swale topography and a lithofacies assemblage that indicate that it was deposited by a braided river channel (see section 2.4.4). New radiocarbon and OSL dates generated by this study indicate Qp5 experienced sedimentation between 17.8-34.6 ka. These age estimates are in good agreement with previous dates of 22.4 and 27.9 ka reported for this deposit by Leigh et al. (2004) and demonstrate that this alloformation is correlative to 13-31 ka braided deposits that have been documented downstream

on the Altamaha River (Leigh et al., 2004) and similar in age to late Wisconsin braided terraces that have been dated along the Canoochee and Ogeechee Rivers (Leigh, 2008) and the Pee Dee River (Leigh et al., 2004).

Qp6, the alloformation that immediately postdates Qp5, contains scrolled "mega-meander" paleochannels and returned radiocarbon and OSL age estimates that place it in the terminal Pleistocene (see section 2.4.3). These results affirm previous studies that indicate the terminal Pleistocene was a time when many rivers in the southeastern Coastal Plain had mega-meandering morphologies. However, within the Uvalda quadrangle and adjoining areas, no mega-meander paleochannels could be confidently dated to the early Holocene. Alloformation Qh1, which dates to this time, contains many meandering paleochannels along its outer margins, but these have modern-like planform dimensions. This may indicate that the Oconee River did not exhibit the mega-meandering planform that was typical of some other rivers in the region during the early Holocene. However, it may simply reflect that no mega-meander paleochannels from this time interval are preserved in the segment of valley studied, and more data probably are needed to fully resolve the early Holocene history of the lower Oconee River. Qh2 contains numerous modern to slightly-smaller-than modern meandering paleochannels and spans the middle to late Holocene. This finding is consistent with that of Leigh (2008) that the late Holocene was a time of meandering channels with modern-like morphologies.

Details regarding the channel pattern and depositional style of the Oconee River prior to about 30-40 ka are sketchy, but limited interpretations are possible. An OSL sample recovered from beneath very muted braided topography on Qp4 returned an age of 52.3±12.2 ka (40.1-64.5 ka). These sediments occupy a higher-elevation component of Qp4 that is cross-cut by a meandering paleochannel that occupies a lower-elevation component of Qp4 located to the

immediate north. These data suggest that the Oconee River may have had a braided pattern sometime between ~40-65 ka, during terminal Oxygen Isotope Stage (OIS) 4 through middle OIS 3, then transitioned to a meandering planform before it established the distinctive braided pattern during the late Wisconsin that is evident on the Qp5 surface. Limited observations from elsewhere in the region (Leigh, 2008), including the Big Hammock locality of the Altamaha River (Leigh et al., 2004), indicate that the Sangamon through middle Wisconsin interval of 130-30 ka was a time of both braided and meandering channel patterns, and data from the Uvalda locality support this interpretation.

2.6. Conclusions

This study has identified eight informal alloformations of Quaternary age within the Oconee River valley in the Uvalda quadrangle, an area that previously lacked detailed surficial geologic mapping. Results indicate that allostratigraphy provides an effective framework for delineating Quaternary sediments in this setting, and the allostratigraphic approach appears to be equally applicable to geologic mapping in other alluvial valleys in the southeastern Coastal Plain and elsewhere. However, as deposits become more weathered and fluvial topography degrades with age, confident identification of bounding discontinuities and accurate delineation of alloformation boundaries becomes more difficult. Scrutiny of alloformation surface morphology, sedimentology, and stratigraphy, along with chronologic data provided by radiocarbon and OSL dating, indicate that the lower Oconee River exhibited a braided morphology during the late Wisconsin interval, a mega-meandering morphology during the terminal Pleistocene, and a meandering morphology with modern-like planform dimensions during the early to late Holocene. These results are generally consistent with the major

morphological phases exhibited by rivers elsewhere in the southeastern Atlantic Coastal Plain during the late Quaternary and further improve our understanding of the evolution of fluvial systems in the region during this time period.

2.7. References

Autin, W.J., 1992. Use of alloformations for definition of Holocene meander belts in the middle Amite River, southeastern Louisiana. Geological Society of America Bulletin 104, 233-241.

Blum, M.D., Valastro, S., 1994. Late Quaternary sedimentation, lower Colorado River, Gulf Coastal Plain of Texas. Geological Society of America Bulletin 106, 1002-1016.

Colls, A.E., Stokes, S., Blum, M.D., Straffin, E., 2001. Age limits on the Late Quaternary evolution of the upper Loire River. Quaternary Science Reviews 20, 743-750.

Duller, G.A.T., 1999. Luminescence Analyst computer programme, V2.18. Department of Geography and Environmental Sciences. University of Wales, Abersystwyth, UK.

Forman, S.L., Pierson, J., and Lepper, K., 2000. Luminescence Geochronology. In: Noller, J.S.., Sowers, J.M., and Lettis, W.R. (Eds.) Quaternary Geochronology: Methods and Applications. American Geophysical Union, Washington, DC, pp. 157-176.

Georgia Department of Natural Resources (1976). “Geologic Map of Georgia.” Georgia Department of Natural Resources, Atlanta.

Huddleston, P.F. (1988). A Revision of the Lithostratigraphic Units of the Coastal Plain of Georgia: The Miocene Through Holocene. Georgia Department of Natural Resources, Georgia Geologic Survey Bulletin 104, 162 pp.

Leigh, D.S., 2006. Terminal Pleistocene braided to meandering transition in rivers of the Southeastern USA. Catena 66, 155-160.

Leigh, D.S., 2008. Late Quaternary climates and river channels of the Atlantic Coastal Plain, Southeastern USA. Geomorphology 101, 90-108.

Leigh, D.S., Srivastava, P., Brook, G.A., 2004. Late Pleistocene braided rivers of the Atlantic Coastal Plain, USA. Quaternary Science Reviews 23, 65-84.

Leigh, D.S., Feeney, T.P., 1995. Paleochannels indicating wet climate and lack of response to lower sea level, southeast Georgia. Geology 23, 687-690.

Miall, A.D., 1985. Architectural element analysis: A new method of facies analysis applied to fluvial deposits. Earth Science Reviews 22, 261-308.

Murray, A.S., Wintle, A.G., 2000. Luminescence dating of quartz using an improved single-aliquot regenerative-dose protocol. Radiation Measurements 32, 57-73.

North American Commission on Stratigraphic Nomenclature, 2005. North American Stratigraphic Code. AAPG Bulletin, 89 (11), 1547 – 1591.

Owens, J.P., 1989. Geologic Map of the Cape Fear Region, Florence 1 × 2 degree Quadrangle and Northern Half of the Georgetown 1 × 2 degree Quadrangle, North Carolina and South Carolina. US Geological Survey Miscellaneous Investigations Series Map I-1948-A (Sheet 1/2).

Prescott, J.R., Stephan, L.G., 1982. Contribution of cosmic radiation to environmental dose. PACT, 6, 17-25.

Ramsey, B.C., 2009. Bayesian analysis of radiocarbon dates. Radiocarbon, 51 (1), 337-360.

Richmond, G. M., Fullerton, D. S., and Weide, D. L. (1986). "Quaternary Geologic Map of the Jacksonville 4° x 6° Quadrangle, United States." U.S.G.S. Quaternary Geologic Atlas of the United States.

Richmond, G. M., Fullerton, D. S., and Weide, D. L. (1987). "Quaternary Geologic Map of the Savannah 4° x 6° Quadrangle, United States." U.S.G.S. Quaternary Geologic Atlas of the United States.

Rittenour, T.M., Goble, R.J., Blum, M.D., 2003. An optical age chronology of Late Pleistocene fluvial deposits in the northern lower Mississippi valley. Quaternary Science Reviews 22, 1105-1110.

Rittenour, T.M., Goble, R.J., Blum, M.D., 2005. Development of an OSL chronology for Late Pleistocene channel belts in the lower Mississippi valley, USA. Quaternary Science Reviews 24, 2539-2554.

Saucier, R.T., 1994. Geomorphology and Quaternary Geologic History of the Lower Mississippi River Valley. President of the Mississippi River Commission by the US Army Corps of Engineers, Waterways Experiment Station, Vicksburg, MS, 364 pp.

Soil Survey Division Staff, 1993. Soil Survey Manual. USDA Handbook 18. U.S. Government Printing Office, Washington, D.C., USA, 437 p.

Soil Survey Staff, Natural Resources Conservation Service, United States Department of Agriculture, 2011. Soil Survey Geographic (SSURGO) Database for Montgomery, Toombs, and Wheeler Counties, Georgia. Available online at http://soildatamart.nrcs.usda.gov. Accessed 10/1/2011.

Srivastava, P., Juyal, N., Singhvi, A.K., Wasson, R., Bateman, M.D., 2001. Luminescence chronology of river adjustment and incision of Quaternary sediments in the alluvial plain of the Sabarmati River, north Gujurat, India. Geomorphology 36, 217-229.

Stokes, S. and Walling, D.E., 2003. Radiogenic and Isotopic Methods for the Direct Dating of Fluvial Sediments. In: Kondolf, M. and Piegay, H. (Eds.) Tools in Fluvial Geomorphology. John Wiley and Sons, Ltd, West Sussex, England, p. 233-267.

Stokes, S., Bray, H.E., Blum, M.D., 2001. Optical resetting in large drainage basins: tests of zeroing assumptions using single-aliquot procedures. Quaternary Science Reviews 20, 879-885.

Suther, B.E., Leigh, D.S., Brook, G.A., 2011. Fluvial terraces of the Little River valley, Atlantic Coastal Plain, North Carolina. Southeastern Geology 48 (2), 73-93.

Wallinga, J., Murray, A.S., Duller, G.A.T., Törnqvist, T.E., 2001. Testing optically stimulated luminescence dating of sand-sized quartz and feldspar from fluvial deposits. Earth and Planetary Science Letters 193, 617-630.

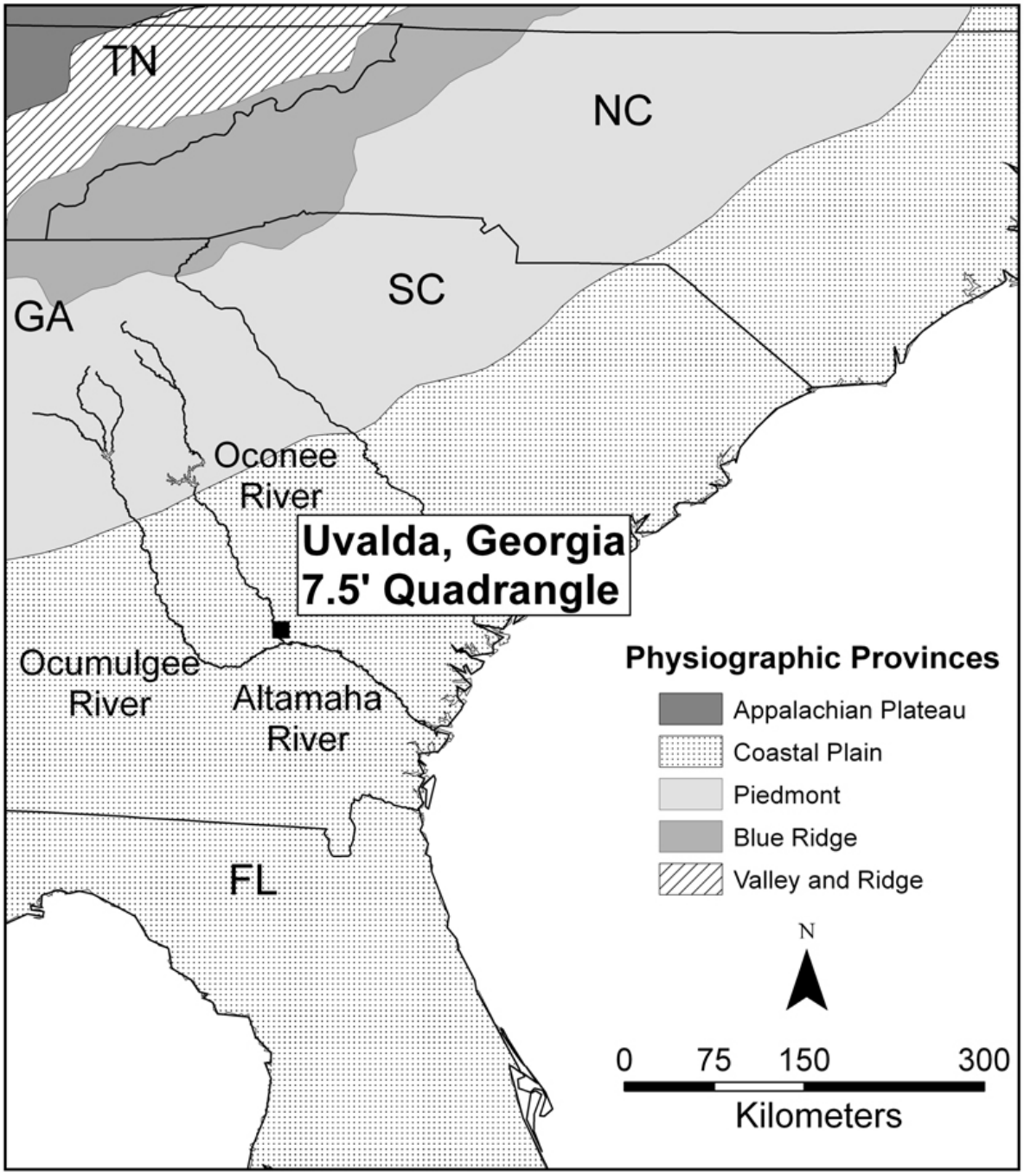

Figure 2.1. Map area location: Uvalda, Georgia 7.5-minute quadrangle.

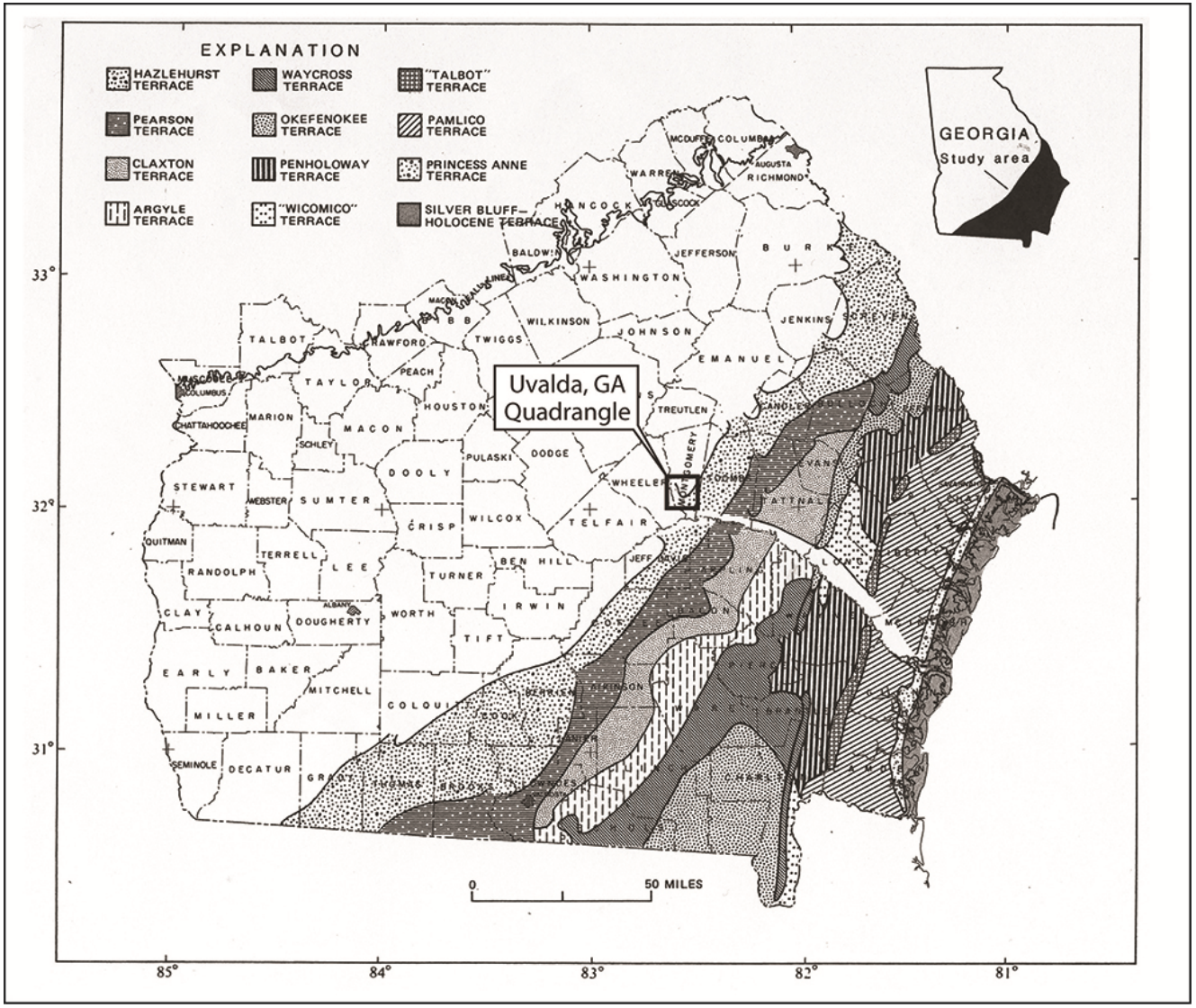

Figure 2.2. Huddleston's (1988) generalized map of marine terraces in Georgia. The map has been modified to show the location of the Uvalda, Georgia 7.5-minute Quadrangle.

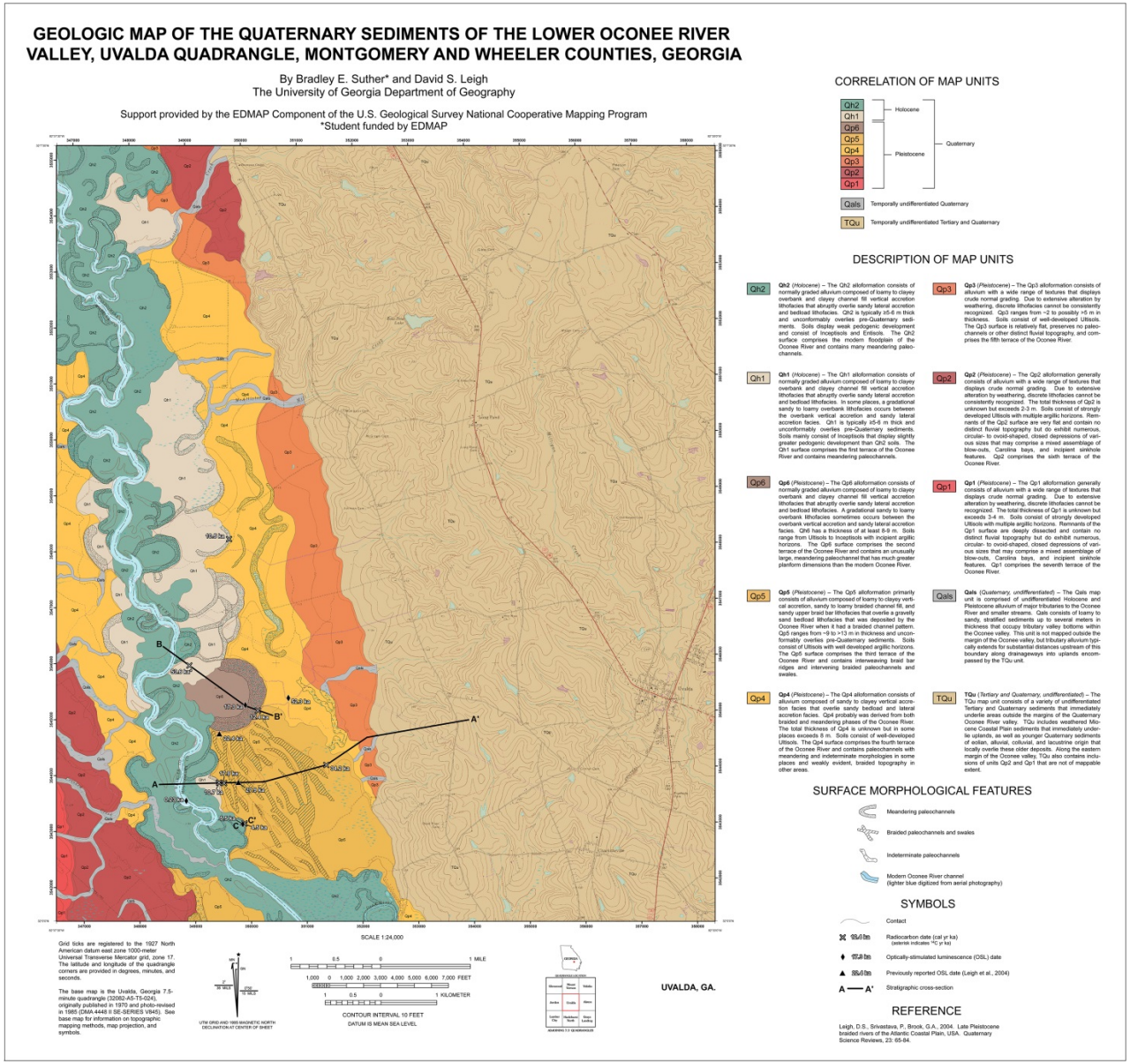

Figure 2.3. Geologic map of the Quaternary sediments of the lower Oconee River valley, Uvalda quadrangle, Georgia.

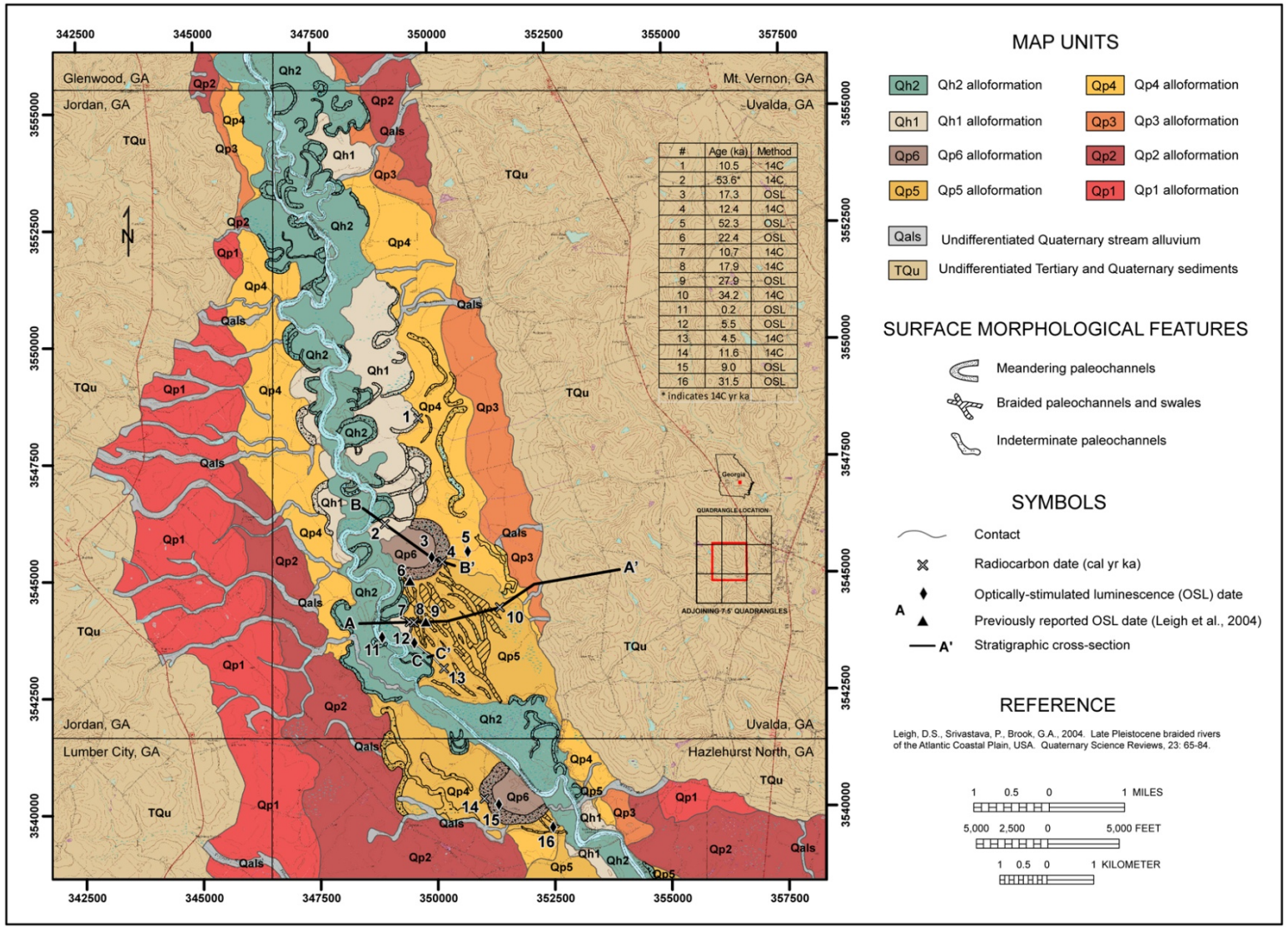

Figure 2.4. Quaternary sediments of the lower Oconee River valley in the Uvalda, Georgia and adjacent 7.5-minute quadrangles. Along the map's southern margin, Oconee River deposits grade laterally into correlative deposits of the Ocmulgee and Altamaha Rivers.

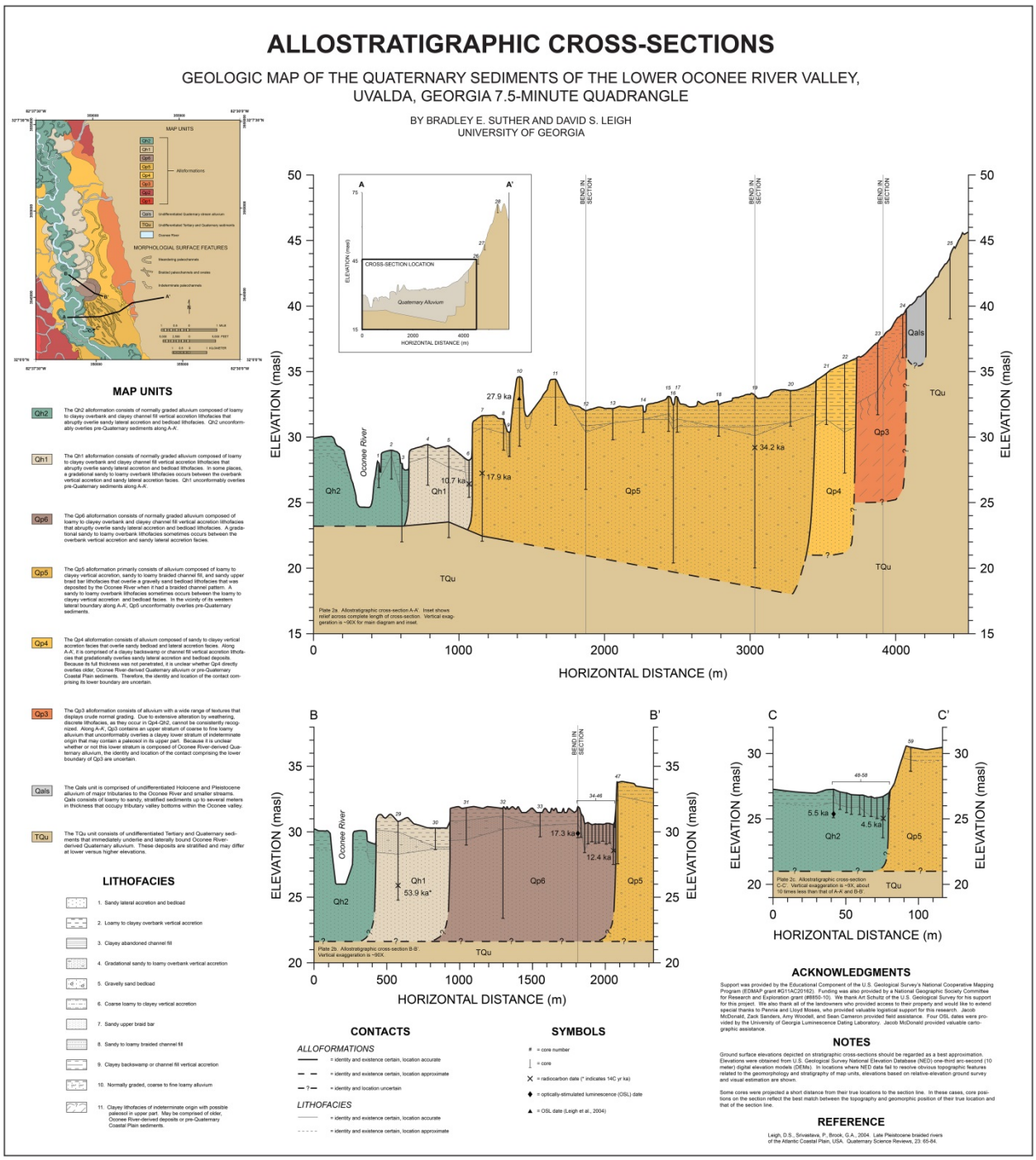

Figure 2.5. Allostratigraphic cross-sections of the lower Oconee River valley, Uvalda, Georgia quadrangle.

Figure 2.6. Modern point bar sediments of the Oconee River. Pit is located at UTM NAD 83 Zone 17 coordinates 348879 m E, 3543723 m. Pit is located on the crest of the point bar and the pit face is oriented approximately perpendicular to flow. View is in the upstream direction. 125-180 μm quartz obtained from a depth of 70 cm returned an OSL date of 0.23±0.056 ka (2-sigma error), indicating complete (or nearly complete) bleaching of grains prior to sample burial. See Table 2.2 for supporting data related to the OSL age.

Figure 2.7. Cut bank exposure, Clarks Bluff of the Oconee River. Here, the Oconee River is eroding Qp4 deposits. View is downstream. The inset photograph shows an Ultisol with an A-E-Bt1-Bt2-Bt3-C horizon sequence developed in Qp4 alluvium. This profile is located at UTM NAD 83 coordinates 346733 m E, 3550843 m N, Zone 17

Figure 2.8. Road cut exposing Qp3 alluvium. Exposure is located along Dead River Road, on the eastern side of the Oconee valley immediately south of the Uvalda, Georgia quadrangle. Here, basal lag gravels unconformably overlie weathered deposits with a silty clay to silty clay loam texture that are interpreted to be pre-Quaternary Coastal Plain sediments. This profile is located at UTM NAD 83 coordinates 353923 m E, 3539525 m N, Zone 17.

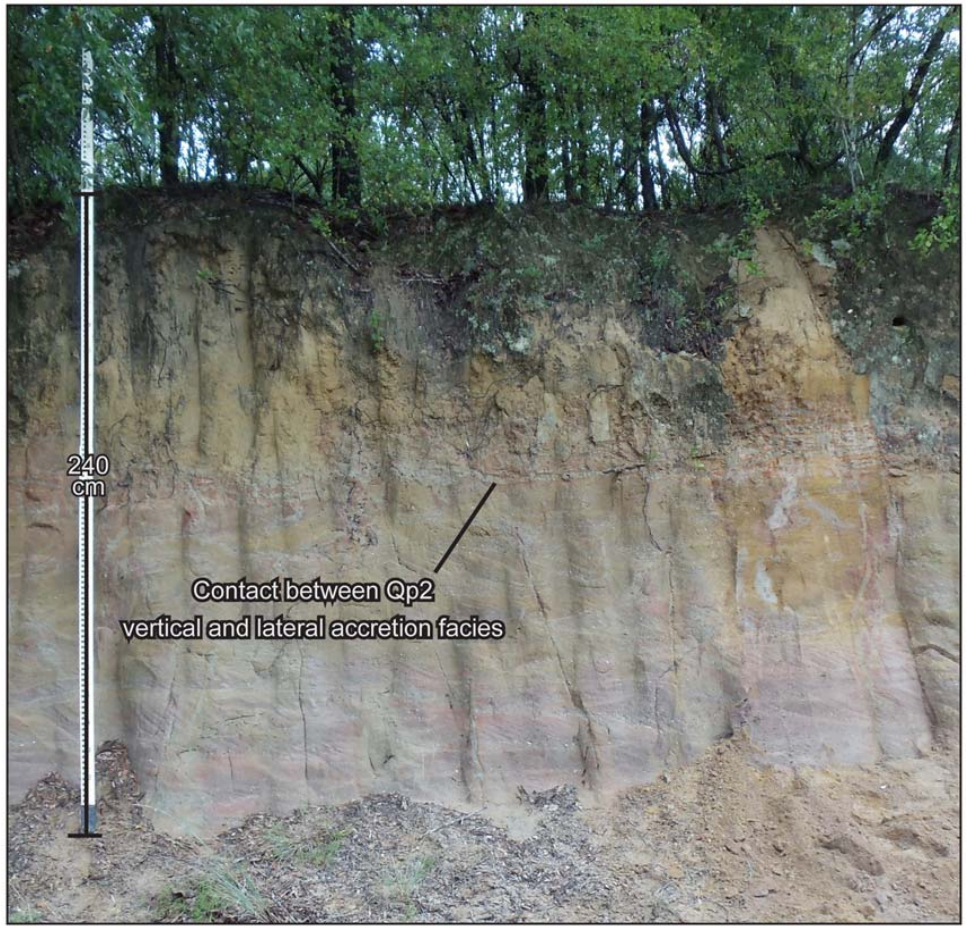

Figure 2.9. Qp2 alluvium exposed in borrow pit. This site is located on the western side of the Oconee valley, immediately south of the Uvalda, Georgia quadrangle at UTM NAD 83 coordinates 349165 m E, 3540718 m N, Zone 17. Here, a vertical accretion facies exhibiting strong pedogenic development abruptly overlies a weathered, sandy lateral accretion facies that displays indeterminate cross-bedding.

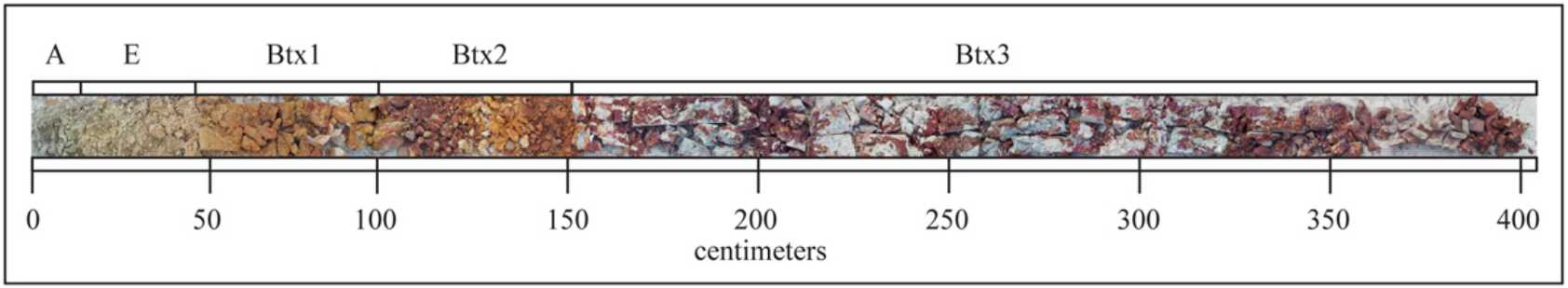

Figure 2.10. Photo-mosaic of a strongly developed Ultisol, map unit TQu. Core was obtained from an upland summit on transect A-A' at the core 28 location, at UTM NAD 83 coordinates 353560 m E, 35450289 m N, Zone 17.

Table 2.1. Radiocarbon dates and supporting data.

Map Unit, Site, and Fig. 2 Cross-reference	Lab No.	Sample depth (cm)	Material dated	$\delta^{13}C$ corrected age ± 1 sigma (^{14}C yr BP)	Calendar age[a] (ka)	2-Sigma calendar age (ka)
Qh2, Uvalda Small Meander (Fig. 2, #13)	UGAMS 9718	164-168	leaves	3,970±25	**4.5**	4.4-4.5
Qh1, Loblolly paleochannel, (Fig. 2, #1)	UGAMS 11797	282-283	acorn	9270±30	**10.5**	10.3-10.6
Qh1, Uvalda A 349469 m, (Fig. 2, #7)	UGAMS 10683	193-195	nut	9,450±30	**10.7**	10.6-10.8
Qh1, MB2 (Fig. 2, #2)	UGAMS 9554	490	wood	53,580±900	---	---
Qp6, Leware Mega-meander (Fig. 2, #14)	UGAMS 11796	213-216	seeds	10,060±30	**11.6**	11.4-11.8
Qp6, Uvalda Mega-meander (Fig. 2, #4)	UGAMS 9553	198-203	seeds	10,430±30	**12.3**	12.1-12.5
Qp5, Uvalda A 349560 m (Fig. 2, #8)	UGAMS 9719	430-450	log	14,620±35	**17.8**	17.5-18.0
Qp5, Uvalda A 351398 m (Fig. 2, #10)	UGAMS 10684	400	leaves	29,910±80	**34.6**	34.5-34.8

[a]All dates were calibrated to calendar years using the OxCal 4.2 program and the IntCal 09 calibration curve (Ramsey, 2009).

Table 2.2. Optically-stimulated luminescence (OSL) dates and supporting data.

Map Unit, Site, and Fig. 2 Cross-reference	Sample name/Lab No.	Age (ka) ± 2 sigma[e]	Sample depth (cm)	U (ppm)	Th (ppm)	K (%)	Water content (% by wt.)	Equivalent Dose (Gy)	Dose rate (Gy/ka)
Oconee River Point Bar (Fig. 2, #11)	UGA12OSL-840	**0.23±0.06**	70	2.31±0.42	7.30±1.45	0.8	10±5	0.43±0.04	1.89±0.18[a]
Qh2, Uvalda Small Meander (Fig. 2, #12)	UGA11OSL-805	**5.5±1.2**	185-217	1.22±0.16	2.98±0.6	0.7±0.1	17.75±5.0	6.15±0.12	1.12±0.12[b]
Qp6, Leware Mega-meander (Fig. 2, #15)	UGA12OSL-850	**9.0±2.6**	191-222	2.73±0.87	14.3±2.98	0.7	15.0±5.0	19.73±0.59	2.18±0.31[b]
Qp6, Uvalda Mega-meander (Fig. 2, #3)	UGA11OSL-789	**17.3±3.4**	205-237	1.4±0.3	3.8±0.9	0.7±0.1	14.7±5.0	21.9±0.8	1.3±0.1[b]
Qp5, Leware Braid Bar (Fig. 2, #16)	UGA12OSL-851	**31.5±7.2**	165-196	2.19±0.32	5.45±1.11	0.5	15±5	42.93±0.68	1.36±0.15[c]
Qp4, Millionaire 0735 m E (Fig. 2, #5)	UGA12OSL-841	**52.3±12.2**	270-301	2.25±0.45	8.64±1.58	0.7	16.65±5	88.37±1.98	1.69±0.19[d]

[a]Cosmic ray contribution assumed to be 0.19±0.02 Gy/ka.
[b]Cosmic ray contribution assumed to be 0.16±0.02 Gy/ka.
[c]Cosmic ray contribution assumed to be 0.17±0.02 Gy/ka.
[d]Cosmic ray contribution assumed to be 0.16±0.02 Gy/ka.
[e]Two times 1-sigma error.

CHAPTER 3 – DISCHARGE OF "MEGA-MEANDER" PALEOCHANNELS OF THE SOUTHEASTERN ATLANTIC COASTAL PLAIN, USA[1]

[1]Suther, B.E., Leigh, D.S., and Brook, G.A. To be submitted to *Quaternary Research*.

Abstract

Paleodischarge estimates based on the slope-area method and channel boundaries determined from stratigraphic cross-sections indicate that large, terminal Pleistocene meandering paleochannels ("mega-meanders") in river valleys of the southeastern Atlantic Coastal Plain represent bankfull flood sizes that were similar to, or at most only modestly larger than, the discharge of low magnitude, high frequency floods on present-day Coastal Plain rivers. These data indicate that bankfull discharges on the order of two to four times modern values previously attributed to mega-meanders based on planform meander dimensions are likely overestimates that need to be reconsidered. Mega-meander paleochannels were wide and shallow, and their relatively modest discharge reflects their comparatively lower hydraulic efficiency relative to modern rivers, which resulted from a high width to depth ratio and a correspondingly reduced hydraulic radius. Rather than reflecting extremely large bankfull floods, the unusually large planform dimensions of terminal Pleistocene mega-meanders appear to be the product of a sediment discharge regime characterized by large quantities of bedload sand, relatively little vertical accretion, and the influence of these factors on the composition of bed and bank material and channel shape. Regional increases in moisture and runoff indicated by fossil pollen records for the southeastern Coastal Plain during the terminal Pleistocene provide a possible explanation for modestly increased discharge in cases where mega-meanders may have conveyed slightly larger than modern bankfull floods, but the precise climatic mechanisms that influenced precipitation delivery and runoff during this time period remain poorly known. In the broader context of the late Quaternary evolution of southeastern Coastal Plain fluvial systems, scrolled terminal Pleistocene mega-meanders likely represent a transitional meandering planform that

was still influenced by large volumes of sandy bedload immediately following the braided, sand bed channels of the late Wisconsin interval, ca. 30-17 ka.

Comparison of paleodischarge estimates presented in this study with prior estimates based on paleochannel width, radius of curvature, and meander wavelength demonstrates the amount of potential error involved when paleohydrologic interpretations are based solely on channel planform dimensions and casts doubt on paleodischarge estimates that rely on regression relationships between discharge and meander geometry established on modern rivers. This has important implications for the discipline of paleohydrology, given that such techniques are still in common use, both on Earth and in extraterrestrial settings.

3.1. Introduction

Many river valleys of the southeastern Atlantic Coastal Plain contain unusually large terminal Pleistocene and early Holocene meandering paleochannels ("mega-meanders") that exhibit planform dimensions much larger than those of late Holocene paleochannels and modern rivers in the region (Gagliano and Thom, 1967; Leigh and Feeney, 1995; Leigh, 2006; Leigh, 2008). Because the planimetric and cross-sectional dimensions of alluvial channels are strongly correlated with the discharge of low magnitude, high frequency (one- to five-year recurrence interval) floods (Dury, 1976; Knox, 1985; Williams, 1988), mega-meander paleochannels can be used to estimate past discharge. Regression equations that model paleodischarge based on relationships between discharge and channel width, radius of curvature, and meander wavelength established on modern, gaged rivers indicate that mega-meanders may have conveyed channel-forming (bankfull) discharges that were 1.3 to 4.7 times larger than those of modern rivers (Leigh and Feeney, 1995; Leigh, 2006). Previous workers have used these paleodischarge

estimates, along with fossil pollen records, to suggest that the terminal Pleistocene and early Holocene were times of greater runoff and (at least seasonally) wetter paleoclimate in the southeastern United States (Goman and Leigh, 2004; Leigh, 2006; Leigh, 2008). However, standard errors associated with discharge estimates derived from regression models based on planform meander dimensions are large (43-53%, Leigh and Feeney, 1995), and more accurate estimates of paleodischarge are needed if the paleohydrology of this period is to be better understood.

This study tests the hypothesis that mega-meanders conveyed larger-than-modern bankfull discharge using paleodischarge estimates that are based on field-surveyed paleochannel cross-sectional dimensions, estimates of paleochannel slope, and hydraulic modeling by the slope-area method. This study also presents new radiocarbon and optically-stimulated (OSL) age estimates for four previously undated mega-meanders and two smaller paleomeanders, along with high-resolution sedimentologic and stratigraphic data, that improve our understanding of the timing of mega-meander paleochannels in the southeastern US and the stratigraphy of their fills and bounding deposits.

3.2. Study Area

Study sites include mega-meander paleochannels along the Oconee, Ogeechee, Congaree, Black, Pee Dee, and Neuse Rivers in the southeastern Atlantic Coastal Plain, USA (Fig. 3.1). With the exception of the Black River, which originates near the Fall Line, these rivers head on the saprolite-mantled Paleozoic crystalline terranes of the Southern Blue Ridge Mountains or Piedmont provinces and flow across the Cretaceous and younger sediments of the Coastal Plain. For the Oconee, Congaree, Pee Dee, and Neuse Rivers, the majority of the drainage area

upstream of study sites is contained within the Piedmont, while the drainage areas of the Ogeechee and Black River sites are respectively located either predominantly or entirely within the Coastal Plain. Study sites were distributed among these six basins to provide a regional perspective on the paleohydrology represented by mega-meanders and to facilitate comparisons between catchments of differing drainage area and physiography.

Modern rivers in the study area typically have single-thread, meandering channels with sand beds that are sometimes interspersed with gravelly riffles. In the vicinity of study sites, modern channels have slopes that range from 0.00014-0.00024, sinuosities of 1.3-1.8, and bankfull widths that range from 25-40 m on the Black River to 100-190 m on the Congaree. The bedload of modern channels consists of sand and fine to medium gravel, but suspended load probably comprises the majority of the sediment load transported by rivers with large drainage areas in the Piedmont (Meade et al., 1990). Study area rivers have stable, cohesive, heavily vegetated banks and vertical accretion floodplains that are characterized by clayey to loamy soils, and backswamp, oxbow, natural levee, and crevasse splay depositional environments. Meandering paleochannels with modern-like dimensions occur on the modern floodplain in the vicinity of all six study sites. Table 3.1 provides discharge estimates for modern rivers in the vicinity of study sites and at the nearest U.S. Geological Survey (USGS) gaging stations.

Mega-meander paleochannels in the study area commonly contain cypress-gum swamp forests and are clearly evident as large meander scars on color-infrared aerial photography and satellite imagery (Fig. 3.1). They typically occur on low terraces slightly higher than the modern floodplain, are cross-cut into older alluvial deposits or valley walls, and are associated with well-expressed to muted, sandy scroll bars. In some localities, including the Damon mega-meander of

the Pee Dee River (Fig. 3.1E this paper; Leigh et al., 2004), relict, eolian dunes occur on the scrolled topography and apparently were blown from the scroll bars (Leigh, 2008).

The climate of the study area is humid subtropical. Mean annual precipitation ranges from 1100 to 1400 mm/yr. Maximum precipitation occurs in January, February, and March (100-130 mm mean monthly totals), due to frontal precipitation, and during July and August (120-200 mm mean monthly totals), as a result of tropical storms and convective thunderstorms. Mean annual temperature ranges from approximately 15-20° C. Native vegetation cover consists of deciduous, mixed, and southern pine forests and has been altered by agriculture, silviculture, and urbanization during historical time.

3.3. Methods

3.3.1 Paleodischarge estimation

Six large meandering paleochannels with planform dimensions typical of mega-meanders in their respective valleys were identified on 1999 USGS color-infrared digital orthophoto quarter quadrangles and Landsat imagery. Two additional, smaller paleomeanders were selected for study from the floodplains of the Oconee and Black Rivers to facilitate pairwise comparison between the older mega-meanders and younger, more modern-like paleochannels along one large (Oconee) and one small (Black) Coastal Plain river.

Mega-meander discharge was estimated by the slope-area method, which has been successfully applied to alluvial paleochannels in similar settings (Rotnicki, 1991). The slope-area method relies on flow resistance formulae, channel cross-sectional area, and slope (Whiting, 2003). Here, discharge was calculated using the product of channel cross-sectional area and flow velocity, as determined by the Manning equation (Knighton, 1998):

$$v = kR^{2/3}s^{1/2} / n \qquad \text{Eq. 1}$$

Where:

v = velocity

k = 1 (if SI units are used)

R = hydraulic radius (channel cross-sectional area divided by wetted perimeter)

s = slope of the energy gradient

n = Manning's roughness coefficient

Cross-sectional area was determined for each mega-meander from channel boundaries delineated by stratigraphy observed along coring transects, using a procedure slightly modified from that of Knox (1985). Transects were situated near the apex of meander bends and oriented perpendicular to paleo-flow direction. Cores were spaced at intervals no coarser than one-tenth of channel width, and sampling was performed with either a bucket auger or Russian corer. In cases where the stratigraphy of paleochannel fill was fairly uniform, a steel tile probe was used in conjunction with coring to measure the depth to the contact between fine-grained channel fill sediment and channel bed sand. Morphological characteristics of soils and sediment were described according to USDA Soil Survey terminology (Soil Survey Division Staff, 1993), and lithologic properties and stratigraphic contacts were noted. Ground surface elevations along transects were surveyed with an electronic total station or a rotary laser level.

Paleochannel slope was estimated using field-surveyed, paleochannel bed elevations for the Oconee, Ogeechee, and Neuse River mega-meanders, or was derived from the longitudinal gradient of the mega-meander terrace surface (Congaree, Black, and Pee Dee River mega-meanders) or the modern floodplain (Oconee and Black River small meanders). Field-measured slopes were calculated from channel bed elevations along the main cross-sectional coring

transect and along upstream and downstream cross-sections that were surveyed by the methods described above. Longitudinal gradients of the mega-meander terraces (or modern floodplains, in the case of small meandering paleochannels) were calculated using the tops of prominent scroll bar ridges identified on either 2 or 3 m horizontal resolution LIDAR elevation data (Congaree, Black, Pee Dee, and Neuse sites) or by using the prevailing treads of paleomeander surfaces identified on USGS 7.5-minute topographic quadrangles, where LIDAR data were unavailable (Oconee and Ogeechee sites). To account for meandering, a sinuosity of 1.7, derived from well-preserved mega-meander paleochannels on the Ogeechee and Black Rivers of one to greater than three wavelengths, was applied to all mega-meander terrace gradients to better approximate channel slope. Respective sinuosities of 1.5 and 1.8, based on the sinuosities of the modern Oconee and Black rivers in the vicinities of the study sites, were applied to the floodplain gradients associated with the Oconee and Black River small paleomeanders. To account for uncertainty in slopes derived from valley gradients, the longitudinal gradient of the mega-meander terrace (or modern floodplain) was used as a maximum estimate, while the sinuosity-corrected gradient served as a minimum estimate. To bracket uncertainty in field-measured channel bed slopes, estimates calculated from elevations of the predominant surface and the lowest 20% of the channel bed were employed, and justification for the use of these components of the channel bed is provided in the following section.

Because the roughness of paleochannels cannot be precisely known, a best estimate (0.0375) and range (0.030-0.045), of Manning's roughness coefficient (n) values were used in paleodischarge calculations. Manning's n values were estimated using criteria specified in Arcement and Schneider (1989) and by comparison of paleochannel morphological characteristics with photographs of modern channels of known roughness (Barnes, 1967). Based

on pollen data that indicate mega-meanders were active during a period of cool moist deciduous to warm mixed forest, roughness estimates assume that mega-meanders had forested banks that in some localities may have lacked vegetation on the point bar side, as indicated by relict eolian dunes that appear to have blown from the scroll bars of some mega-meanders (Leigh, 2008).

Discharge estimates by the slope-area method typically have a percentage uncertainty of 10-20% at the 95% confidence level (p. 509, Herschy, 1985). To evaluate the reliability of this technique on southeastern alluvial rivers, bankfull discharge was estimated at five USGS gaging stations in the Georgia Coastal Plain using field-surveyed cross-sections provided by the USGS (personal communication, A.J. Gotvald, 2013) and slope estimates obtained from the best available elevation data. Ratios of slope-area to gaged estimates of bankfull discharge range from 0.82-0.99 (Table 3.2) and fall within the envelope of error expected for the slope-area method. These results indicate that this technique yields reasonable bankfull discharge estimates for modern rivers in the study area and lends credence to the paleodischarge estimates presented in this study. For all paleomeanders, a best estimate and minimum and maximum values for discharge are reported that reflect the best estimate and associated uncertainties for channel roughness and slope.

3.3.2 Radiocarbon and optically-stimulated luminescence (OSL) dating

To best approximate the timing of channel abandonment, samples for radiocarbon dating were collected at or near the thalweg of paleochannels from unoxidized, basal channel fill located immediately above channel bed sand. Only uncarbonized plant macrofossils (e.g., seeds, nuts, leaves) that appeared fresh and not reworked by fluvial transport were used. All radiocarbon samples were measured by the accelerator mass spectrometry method (AMS) at the

University of Georgia (UGS) Center for Applied Isotope Studies following an acid-alkali-acid (HCl-NaOH-HCl) pretreatment.

Optically-stimulated luminescence (OSL) dating of paleomeander alluvium was conducted to provide additional age control for paleochannels. At each site, samples for OSL dating were obtained from lateral accretion or upper bedload sediment, beneath the scroll bar immediately adjacent to the paleochannel that functioned as the active point bar at the time of channel abandonment. OSL samples were collected by pounding a 7-cm diameter light-tight metal tube into the base of a hand-augered hole. In all cases, OSL dating was conducted on unweathered (C horizon) quartz-rich sand sampled from below the depth of bioturbation. Equivalent dose was determined at the UGA Luminescence Dating Laboratory by the single aliquot regenerative dose (SAR) protocol (Murray and Wintle, 2000) from either 125-180, 125-250, or 180-250 μm quartz sand that was pretreated to remove carbonates, organic matter, and the alpha skin. For all samples, 21-24 aliquots were analyzed following placement on 9.6 mm diameter disks. Dose rate calculation was based on the thick source ZnS (Ag) alpha counting technique for elemental concentration of uranium and thorium, and potassium was measured by ICP90 with a detection limit of ±0.1%, using the Sodium Peroxide fusion technique at the SGS Laboratory in Toronto, Canada. Cosmic ray gamma contribution was calculated according to the guidance of Prescott and Stephan (1982). Water content was directly measured and used to generate an estimate and uncertainty for pore water content since the time of sample deposition. Additional details regarding OSL dating procedures are provided in Section 2.3.3.2 of Chapter 2 of this document.

3.4. Results

3.4.1 Paleochannel morphology and stratigraphy

Paleochannels are filled with 1.0-5.0 m of either massive, gray clay or thin, horizontally bedded, interstratified sand and clay that grade upward to muck, peat, or loamy sediments (Figures 3.2-3.5). Typically, fine-grained paleochannel fill abruptly overlies and is readily distinguishable from light gray, coarse sand. This sand is interpreted as channel bed sediment based on its stratigraphic position and its textural similarity to the bedload of modern rivers in the study area. In cases where bedload sands are gradationally overlain by interstratified sand and clay, channel bed sand was discriminated from overlying, sandy paleochannel fill on the basis of its lack of interstratified clay and organic material, lighter color (10YR 5/1-7/1), higher gravel content, and greater resistance to penetration with a manual tile probe, thus facilitating accurate delineation of paleochannel boundaries.

On the outsides of paleomeander bends, paleochannel fill is bounded by sand associated with older fluvial deposits, whereas on the insides lateral accretion sediments overlain by finer-grained vertical accretion deposits typically less than one meter thick bound channel fill. Because vertical accretion facies lacked evidence of buried ground surfaces or lithologic discontinuities indicative of continued sedimentation following channel abandonment, bankfull stage for all paleomeanders was defined as coinciding with the top of vertical accretion sediments (i.e., the ground surface) on the crest of the point bar immediately adjacent to the paleochannel (Figures 3.2-3.5). However, we recognize the possibility that this placement may represent a slight overestimate of bankfull stage in instances where rates of pedogenesis equaled or exceeded overbank sedimentation rates following meander abandonment.

Because the slope of a paleochannel is not necessarily equivalent to that of its modern river counterpart (Rotnicki, 1991), paleochannel slope was field-surveyed at the Oconee, Ogeechee, and Neuse mega-meander sites (Table 3.3), and field-measured estimates were used to evaluate the validity of slopes derived from valley gradients. Paleochannel slopes based on the entire set of channel bed elevations per cross-section vary by a factor of 2.5, from 0.00016 (Ogeechee River, Cooperville FP-2 mega-meander) to 0.00041 (Oconee River Uvalda mega-meander). To evaluate how different geomorphic components of the channel bed influenced variability in slope estimates, slopes were also calculated using the predominant channel bed surface, the tops of fluvial bars, the thalweg, and the lowest 20% of bed elevations per cross-section. For a given paleochannel, slope estimates from individual channel bed geomorphic components vary by as little as 0.00010 (a factor of 1.5), between the gradients of the predominant bed surface (0.00020) and mid-channel bars (0.00030) of the Neuse River Moccassin Creek mega-meander, to as much as 0.00068 (a factor of 3.8) between the gradient of mid-channel bars (0.00024) and the gradient of the thalweg (0.00092) of the Oconee River Uvalda mega-meander (Table 3). However, no single geomorphic element of the channel bed results in consistent maximum or minimum slope values.

To account for uncertainty in mega-meander slope estimates resulting from variability in channel bed topography, minimum and maximum estimates based on the predominant channel bed surface and the lowest 20% of the channel bed were used in paleodischarge calculations. Slopes derived from the predominant bed surface (0.00020-0.00061, Table 3.3) exclude elements of the channel bed that may be subject to extreme variability at the reach or cross-section scale (e.g., sand bars, thalweg scour holes) that are not representative of the overall channel gradient. Slope estimates based on the lowest 20% of channel elevations (0.00020-0.00078, Table 3.3) are

intended to provide an estimate of gradient derived from the lowest part of the channel bed, while simultaneously dampening the influence of localized variability in thalweg elevations. This estimate serves as the maximum gradient at two of the three sites where mega-meanders were field-surveyed (Table 3.3).

In all cases where mega-meander channel slopes were field-measured, the longitudinal valley gradient of the mega-meander terrace and the sinuosity-corrected valley gradients are either entirely bracketed by or are within 20% of minimum and maximum slope estimates based on the predominant channel bed surface and lowest 20% of the channel bed (Table 3.3), suggesting that reliable estimates of paleochannel slope can be derived from valley gradients. Therefore, for mega-meanders where field-measured slopes are unavailable (Congaree, Black, and Pee Dee River sites), maximum slope estimates (0.00028-0.00068) are based on the gradient of the mega-meander terrace, while sinuosity-corrected gradients (0.00016-0.00040) serve as minimum slope estimates (Table 3.3). The longitudinal gradient of the modern floodplain (0.00026) and the sinuosity-corrected floodplain gradients (0.00016-0.00018) similarly serve as respective maximum and minimum slope estimates for the small meandering paleochannels examined along the Oconee and Black Rivers.

3.4.2 Paleochannel ages

3.4.2.1 Mega-meanders

Tables 3.4 and 3.5 respectively report radiocarbon and OSL age estimates for paleomeanders, and Figure 3.6 provides a graphical depiction of age estimates and their associated uncertainties. Three of the four previously undated mega-meanders (Oconee, Congaree, and Neuse River sites) returned calibrated radiocarbon ages that range from 11.8-17.1

ka, if the full breadth of the 2-sigma error is considered. These estimates are in good agreement with previously published radiocarbon and OSL dates of 13.4-13.8 ka for the Damon mega-meander of the Pee Dee River (Leigh et al., 2004; Fig. 3.5, this paper) and dates reported from other sites in North Carolina and Georgia that indicate southeastern Coastal Plain rivers exhibited mega-meandering planforms during the terminal Pleistocene (Leigh, 2006, 2008). A terminal Pleistocene age is also indicated for the Cooperville FP-2 mega-meander of the Ogeechee River, based on a high quality seed obtained from a depth of 195-200 cm, at the base of mucky channel fill, immediately atop channel bed sands, that yielded a calibrated date of 13.8-14.1 ka (Table 3.4, Fig. 3.4). Although this estimate is considerably older than an 8.2-8.8 ka date reported by Leigh and Feeney (1995) from a fragment of unidentified wood obtained from a higher stratigraphic position elsewhere in the paleochannel, we believe that it provides a better estimate for the timing of meander abandonment than the early Holocene age, based on the quality of the dated material and its position at the very base of the paleochannel fill.

In contrast to the terminal Pleistocene dates discussed above, a middle Holocene calibrated radiocarbon age of 5.1-5.5 ka was obtained from a seed situated approximately 90 cm above channel bed sand in the thalweg of the Mouzon mega-meander of the Black River (Table 3.4, Fig. 3.3). Although this age may not seem unreasonable, given that mega-meanders of early- to middle Holocene age have been reported along the Ogeechee (Leigh & Feeney, 1995) and Canoochee (Leigh, 2006) Rivers in Georgia, it is likely that this date underestimates the time elapsed since meander abandonment, given its relatively high position within the paleochannel fill at the thalweg location (Fig. 3.3), and we regard it with caution.

Mean OSL age estimates obtained from lateral accretion and bedload sands beneath mega-meander point bars range from 13.8-19.1 ka (Table 3.5, Figure 3.6) and in all cases pre-

date counterpart radiocarbon ages obtained from channel fill, while the full breadth of the 2-sigma error considered for all mega-meander OSL dates spans from 11.6-25.1 ka. Slightly older OSL age estimates are expected due to the fact that point bar sediments pre-date paleochannel abandonment and sedimentary filling, but also may reflect a degree of "inherited" age resulting from incomplete bleaching of grains during transport. OSL dating was conducted on upper lateral accretion sand obtained from 70 cm beneath the crest of a modern point bar of the Oconee River, near the Uvalda mega-meander site, to qualitatively evaluate the degree of re-setting experienced by modern point bar sediments in the study area during fluvial transport. Although the inherited luminescence signal of this individual sample appears to have been nearly cleared prior to burial, based on an essentially modern OSL date of 0.23±0.06 ka, fluvial sediments sometimes suffer from incomplete bleaching during transport (Stokes and Walling, 2003), and this possibility must be considered when interpreting the OSL age estimates presented here. The fact that the mean ages (and majority of the 2-sigma error) of the Oconee, Ogeechee, Congaree, Black, and Neuse River mega-meander OSL dates fall within the 16-25 ka time frame (Fig. 3.6), a period known to have been characterized by braided channels on the Oconee and other southeastern rivers (Leigh et al., 2004; Leigh, 2008; Chapter 2, this document), provides further evidence that mega-meander OSL dates are likely slight over-estimates, given that in many localities (including the Oconee, Congaree, Black, and Neuse sites) mega-meanders cross-cut, and therefore must be younger than, braided river deposits. For this reason, and due to the generally higher uncertainties associated with OSL relative to AMS radiocarbon dating, we believe that the radiocarbon dates of basal channel fill reported here provide the best estimates of when mega-meanders last functioned as active channels. For the Oconee, Ogeechee, Congaree, Pee Dee, and Neuse mega-meanders, this appears to have been during the terminal Pleistocene,

ca. 11.8-17.1 ka. Given that the mean OSL dates reported here appear to slightly overestimate the ages of mega-meanders as a result of possible partial bleaching, future work will explore the application of a minimum age model that relies on the aliquot in each sample with the minimum measured equivalent dose in order to improve the accuracy and precision of mega-meander OSL age estimates.

The age of the Mouzon mega-meander of the Black River remains unresolved, given the discrepancy between OSL and radiocarbon age estimates and the fact that the radiocarbon sample was obtained from sediments relatively high in the channel fill that may substantially post-date meander abandonment. Additional dating to refine the age estimate of this mega-meander will be conducted in the course of future research.

3.4.2.2 Small paleomeanders

The smaller paleomeanders examined along the Oconee and Black Rivers are believed to be of Holocene age. Leaf fragments obtained from basal channel fill immediately above the contact with bedload sand in the thalweg of the Uvalda small meander of the Oconee River returned a calibrated radiocarbon date of 4.4-4.5 ka (Table 3.4; Fig. 3.2; Fig. 3.6). OSL dating of bedload sand obtained beneath the point bar of this paleochannel returned a very correlative date of 5.5±1.2 ka (Table 5; Figures 2 and 8). Given the 2-sigma error of the OSL age and the fact that point bar sediment should slightly pre-date abandoned channel fill, we regard these ages to be in good agreement.

Lateral accretion sand beneath the point bar of the Mouzon small meander yielded an OSL age of 30.2±12.6 ka, while radiocarbon dating of an acorn from 170 cm above the base of channel fill returned a calendar age of 1954-2005 AD (Tables 3.4 and 3.5; Figs. 3.3 and 3.6).

Although no additional absolute dating of Black River floodplain paleochannels has been conducted, similar, modern-sized paleochannels on the floodplains and first terraces of many other Coastal Plain rivers, including the Oconee, Ogeechee, Canoochee, and Pee Dee Rivers (Leigh and Feeney, 1995; Leigh et al., 2004; Leigh, 2006; Chapter 2, this document), cross-cut well dated, terminal Pleistocene or early Holocene mega-meander deposits, indicating that such paleochannels must be of Holocene age. Thus, based on correlation with other southeastern rivers, and given that the 30.2 ka OSL age was obtained from lateral accretion sediment in clear association with a paleochannel on the active floodplain of the Black River rather than older, underlying strata (Fig. 3.3), we favor a Holocene age for this paleochannel and regard the OSL date as an overestimate that likely reflects inherited age resulting from partial bleaching prior to sample burial. Although the Mouzon small meander is clearly cross-cut into and must be younger than the Mouzon mega-meander, uncertainties surrounding the age of this mega-meander (see Section 3.4.2.1, above) preclude establishing a more precise maximum age for the smaller paleomeander. However, a modern radiocarbon date from the upper half of the fill in the smaller channel suggests that it has experienced sedimentation during historical time and provides further evidence of the relatively youthful age of this paleomeander.

3.4.3 Paleodischarge estimates

3.4.3.1 Mega-meanders

Paleodischarge estimates by the slope-area method indicate that the bankfull flood size of mega-meanders was similar to, or only modestly larger than, the discharge of low magnitude, high frequency floods on present-day Coastal Plain Rivers (Table 3.6; Figs. 3.7 and 3.8). This finding is significant, given that previous estimates based on planform meander dimensions have

indicated that mega-meanders conveyed bankfull discharges on the order of two to four times the bankfull flood sizes of modern rivers. Ratios of mega-meander paleo/modern discharge range from 0.6 (Cooperville FP-2 mega-meander, Ogeechee River) to 1.5 (Damon mega-meander, Pee Dee River), while the average of the ratios from all six mega-meanders is 1.1 (Table 3.6). Modern river discharges used in these ratios use the two-year recurrence interval flood at ungaged sites adjacent to each respective mega-meander paleochannel, which were estimated using regional flood frequency prediction techniques (Gotvald et al., 2006; Feaster et al., 2009; Weaver et al., 2009; Table 3.2, this paper) and are assumed to be reasonable approximations of bankfull discharge at the ungaged locations.

The Ogeechee, Oconee, and Black River mega-meanders have paleo/modern discharge ratios of 0.6 to 0.9, and scrutiny of the uncertainties associated with discharge estimates suggests little difference between paleo and modern discharge on the these rivers. Paleochannels that may have conveyed larger-than-modern discharges include the mega-meanders at the Neuse, Congaree, and Pee Dee River sites. The ratio of paleo to modern discharge for these mega-meanders ranges from 1.3 to 1.5, and the lower limits of the error associated with their paleodischarge estimates either approximately equal or slightly exceed mean estimates of the two-year recurrence interval discharge for their modern river counterparts (Fig. 3.7). However, given the full breadth of uncertainty in both paleo and modern discharge estimates, it is possible that these mega-meanders, like those on the Ogeechee, Oconee, and Black Rivers, may have had bankfull discharges no greater than those of modern rivers.

Comparison of mega-meander discharge estimates with the mean annual flood size of other modern rivers of comparable drainage area in the Coastal Plain of Georgia and South Carolina yields similar results. Mean annual flood discharge calculated by Leigh and Feeney

(1995) for unregulated rivers at 30 USGS gaging stations in the Coastal Plain was regressed against drainage area, and results are depicted in Figure 3.8. Mega-meanders with drainage areas within the applicable limits of the regression model, including the Neuse mega-meander, have bankfull discharge estimates that fall within or nearly within the prediction intervals of the regression, lending support to the interpretation that mega-meander channel forming discharges did not vary substantially from those of modern rivers. While the bankfull discharge estimates for the Pee Dee and Congaree mega-meanders would exceed the predicted mean annual flood size for their respective drainage areas were the regression extrapolated to include drainage areas greater than 15,000 km^2, this exercise is speculative and of limited use, given that it violates the assumptions of regression by applying the model to drainage areas well beyond empirical observations.

Previous studies have reported paleo to modern discharge ratios of 1.3 to 4.7 for mega-meanders in the southeastern Coastal Plain using regression relationships established on modern, gaged rivers that retrodict discharge based on planform meander dimensions, including bankfull channel width, radius of curvature, and meander wavelength (Leigh and Feeney, 1995; Leigh, 2006). To evaluate how paleodischarges predicted by this technique compare to the estimates presented in this paper, mega-meander channel widths were measured from 1999 color-infrared aerial photographs and discharge was calculated using equation three of Leigh and Feeney (1995), which predicts mean annual flood discharge (Q_{maf}) based on bankfull width (W_b), according to the following equation:

$$Q_{maf} = 10.24Wb^{1.1012} \quad \text{Eq. 2}$$

Paleodischarges estimated by the bankfull width equation of Leigh and Feeney are three to 10 times greater than discharge estimates by the slope-area method, and, in all cases, the lower

bound of the 95% confidence limit associated with the channel width-based estimate greatly exceeds the maximum estimate associated with the slope-area approach (Fig. 3.7). Given that mega-meander channel boundaries were clearly delineated by paleochannel stratigraphy, that uncertainties in channel slope and roughness could be reasonably accounted for, and that the slope-area method generates reliable estimates of dicharge when these variables are properly estimated (Herschy, 1985; Jarrett et al., 1987; Section 3.3.1 of this paper), we consider the mega-meander paleodischarge estimates by the slope-area method presented herein to be reasonable and regard the discharges based on the predictive equation of Leigh and Feeney as overestimates.

3.4.3.2 Small paleomeanders

Best estimates of bankfull flood size for the Oconee and Black River small meanders result in paleo to modern discharge ratios of 0.03 to 0.5, respectively (Table 3.6). Although the lower than modern discharge estimates of the small paleomeanders may appear to cast doubt on mega-meander estimates, we regard them to be of limited interpretive value from a paleohydrological standpoint, given that channel cross-sectional area probably was underestimated in both instances.

In the case of the Black River small meander, and in contrast to the stratigraphy of mega-meander channel fills, the lower half of the palochannel fill was composed entirely of stratified sands that were probably deposited when the channel was re-occupied by post-abandonment floods. These sands are difficult to differentiate from channel bed and lateral accretion sediments typical of modern rivers in the study area, and while Figure 3.3 reflects the best interpretation of channel boundaries possible given the available data, underestimation of

bankfull cross-sectional area may account for the discrepancy between paleo and modern discharge at this location. The comparatively sandier fill of this paleochannel relative to those of the mega-meanders discussed above likely reflects its position relative to the modern river, which is ideally situated to capture flood waters as they round a tight bend in the modern channel (Fig. 3.3).

In the case of the Uvalda small meander of the Oconee River, because the paleochannel bed is well defined by gray clay that abruptly overlies compact, very coarse sand, low paleodischarge is not thought to reflect misinterpretation of paleochannel boundaries. Rather, the possibility must be recognized that the Uvalda small meander represents one channel within a bifurcated reach that did not convey the entire discharge of the river at the time it was active, given that channel bifurcations occur in the modern Oconee River (see northwest corner of Uvalda quadrangle, Plate1 and Fig. 2.2, Chap. 2 of this document). Although the available geomorphic and stratigraphic data are insufficient to confirm or refute this interpretation, this paleochannel has a bankfull width one third to one half of the typical width of the modern channel, and scrutiny of the modern Oconee River floodplain reveals that the Uvalda small meander is among one of the smallest paleochannels in the valley (see meandering paleochannels of map unit Qh2, Plate 1 and Fig. 2.2, Chap. 2 of this document). Given uncertainties surrounding the Oconee and Black River small meanders, more data are needed before meaningful comparisons can be made between the paleodischarge of mega-meanders and that of younger, more modern-like paleochannels in the southeastern Coastal Plain.

3.5. Discussion

3.5.1 Mega-meander paleodischarge

Mega-meander bankfull discharge during the terminal Pleistocene appears to have been similar to, or at most only modestly larger than, the discharge of low magnitude, high frequency floods on present-day Coastal Plain rivers. These findings indicate that previous mega-meander discharge magnitudes derived from channel planform dimensions are likely overestimates and suggest that previous interpretations attributing anomalously high discharge to mega-meanders require re-evaluation.

Although the modest discharge of mega-meanders may seem counter-intuitive given their large planimetric dimensions, it is attributable to basic parameters that influence open channel flow. Because all available evidence indicates that mega-meanders had channel gradients similar to or slightly greater than their modern channel counterparts (Tables 3.2 and 3.3), it is unlikely that modest paleodischarge values reflect underestimation of channel slope. It is also unlikely that overestimation of channel roughness accounts for low discharge, given that the paleodischarge estimates presented here incorporate a wide range of Manning's *n* values (0.030-0.045) that well represent the lower range of possible channel roughness that could have been associated with mega-meanders. The modest discharge of mega-meander paleochannels is instead thought to reflect their comparatively lower hydraulic efficiency relative to modern channels, which results from a high width to depth ratio and a correspondingly reduced hydraulic radius.

The hydraulic radius quantifies the hydraulic efficiency of a channel by providing a measure of how much contact there is between flow and the channel boundary (Charlton, 2008) and is expressed by cross-sectional area divided by the wetted perimeter (see Equation 1, Section

3.3.1). Assuming that other factors are equal, including channel roughness and slope, channels like mega-meanders that are wide and shallow will have a greater length of their boundary in contact with flow (as represented by the wetted perimeter term) and in turn experience frictional energy losses that reduce their hydraulic efficiency, and thus their discharge, relative to narrower, deeper channels of comparable (or in some cases less) cross-sectional area.

Although channel cross-sectional data are unavailable for modern rivers immediately adjacent to mega-meander study sites, meaningful morphological comparisons can be made between cross-sections of mega-meanders and modern Coastal Plain rivers of roughly similar characteristics (Table 3.2) that illustrate these hydraulic relationships. The modern channel of the Ohoopee River at Reidsville, Georgia has a drainage area, basin physiography, cross-sectional area, slope and estimated roughness similar to that of the Mouzon mega-meander of the Black River (Tables 3.1, 3.2 and 3.6). Although the Mouzon mega-meander has a bankfull width nearly double that of the Ohoopee channel (114 m vs. 61 m), it also has a considerably shallower mean depth (2 m vs. 4 m). In turn, the Ohoopee River channel has a hydraulic radius that is 1.8 times greater than that of the Mouzon mega-meander, which results in greater hydraulic efficiency and a discharge at the bankfull stage slightly greater than that of the mega-meander. A similar contrast in channel morphology is provided by the Uvalda mega-meander of the Oconee River and the modern Oconee River at Dublin, Georgia. Although twice as wide as the modern channel, the mega-meander has a bankfull discharge similar to that of the modern river, due in part to its lower hydraulic radius. While admittedly it would be preferable to compare mega-meanders with modern channels of the same river, at locations of equivalent drainage area, these examples nonetheless demonstrate the influence of cross-sectional shape on the hydraulic

efficiency of the channels in this study and illustrate how rivers with very different planform dimensions may have relatively comparable bankfull discharge.

3.5.2 Mega-meander channel morphology

The cross-sectional shape of alluvial channels is controlled not only by water discharge, but also by the discharge and size of sediment and the composition of bed and bank material (Bridge, 2003). Early work by Schumm (1960) recognized the influence of bed and bank material on channel morphology, indicating that the width to depth ratios of alluvial channels decreases as the silt and clay content of the channel perimeter increases and that this relationship occurs independent of changes in discharge. More recently, Blum et al. (1995) observed that many data sets used to relate discharge to planform meander geometry, such as those of Carlston (1965) and Dury (1965), exhibit substantial variability in meander dimensions for a given discharge, and hypothesized that such scatter may reflect the influence of bank material, with larger channel widths, meander wavelengths, and radii of curvature resulting from a lack of bank-stabilizing muds, and lower values reflecting more clay-rich, cohesive floodplain settings.

Given that mega-meanders register discharges similar to or only modestly larger than modern values, it appears that their exceptionally large planform dimensions are more likely a product of a sediment discharge regime characterized by large quantities of bedload sand, relatively low amounts of fine-grained vertical accretion, and the influence of these factors on bed and bank composition and channel shape, and not necessarily unusually large bankfull floods. Mega-meandering planforms were established during the terminal Pleistocene, following a late Wisconsin phase of sand-bed braiding, in response to the onset of warmer, more moist climatic conditions that drove afforestation and decrease in upland sediment yield, while

simultaneously stabilizing river banks with vegetation and causing incision beneath braided floodplains (Leigh, 2006, 2008). The distinctive, scrolled floodplains of terminal Pleistocene mega-meanders, which are underlain by large volumes of lateral accretion sand but comparatively little fine-grained vertical accretion sediment (Leigh, 2006; Figs. 3.2-3.5, this paper), confirm that mega-meanders transported large volumes of bedload sediment and suggests that these paleochannels may represent a transitional meandering planform that was still heavily influenced by large quantities of bedload sand following sand-bed braiding during the late Wisconsin, ca. 30-17 ka (Leigh, 2006, 2008), as they laterally eroded sandy braided river deposits. This geomorphic and sedimentologic context would readily satisfy the conditions required to yield the wide, shallow sand bed channels typical of mega-meanders, given current understanding of relationships between sediment supply, bank material composition, and channel morphology. Increased bank stability possibly resulting from an increase in density of riparian vegetation during the terminal Pleistocene also likely contributed to the development of mega-meander morphologies and may in part explain why southeastern Coastal Plain rivers, while still transporting large quantities of sandy bedload, developed wide, shallow, highly sinuous, mega-meandering forms that were less hydraulically efficient than the preceding braided channels of the late Wisconsin interval.

The scrolled mega-meandering planform of terminal Pleistocene channels may also reflect the influence of a paleoflood regime characterized by overbank flooding that was either less frequent or of shorter duration than in the Holocene, given the relative lack of vertical accretion facies associated with terminal Pleistocene mega-meanders in comparison to later meandering forms (Leigh, 2008). However, lower amounts of vertical accretion on terminal Pleistocene floodplains may alternatively reflect that lateral migration of mega-meanders was so

rapid that thick vertical accretion packages failed to accumulate (Leigh, 2008). Regardless, reduced quantities of fine-grained, overbank sediment on terminal Pleistocene mega-meander floodplains would have resulted in less cohesive banks that favored wider channels and larger meander dimensions than later meandering forms.

One might wonder if the slopes of mega-meander channels, which, like the slopes of braided channels of the late Wisconsin interval (Leigh et al., 2004), appear to have been larger than slopes of modern rivers and graded to lower sea levels on the now submerged continental shelf, also contributed to the sandy, scrolled pattern of terminal Pleistocene mega-meanders. The larger than modern slopes of these channels may have resulted in enhanced stream power and thereby greater capacity to transport bedload sediment. However, slope was probably not a primary driver responsible for the transitional, sandy scrolled mega-meander pattern, given that Leigh et al. (2004) indicate that modern floodplain gradients and 2-year discharges already place present-day large Coastal Plain rivers within the field of sand-bed braided streams of Kellerhalls (1982) and in close proximity to the classic boundary line between braided and meandering streams of Leopold and Wolman (1957).

Blum et al. (1995) provide a model of channel formation for the "Deweyville" meander scars of the Gulf Coast similar to the model described above that lacks need for greater discharge. The Deweyville meanders were active during Oxygen Isotope Stages (OIS) 4-2 (Blum and Aslan, 2006) and have very similar planform characteristics to mega-meanders of the southeastern Atlantic Coastal Plain. Although some previous workers inferred much larger than modern channel-forming discharges for Deweyville paleochannels (Gagliano and Thom, 1967; Alford and Holmes, 1985), Blum et al. (1995) argue that the large Deweyville channels represent hydraulic adjustments to a lack of bank-stabilizing muds that resulted from an absence of

overbank floods during OIS 4-2. They contend that the smaller dimensions of Holocene Gulf Coast rivers simply reflect the presence of thick, bank-stabilizing muds that have accumulated in response to the more pronounced overbank flood regime that is characteristic of Holocene climatic conditions of the Texas Gulf Coast.

3.5.3 Paleoenvironmental implications

Paleodischarge estimates derived from planform dimensions of mega-meanders have been used in conjunction with interpretations derived from fossil pollen records to infer (at least seasonally) wetter paleoclimatic conditions, greater runoff, and larger bankfull floods for the terminal Pleistocene and early Holocene versus late Holocene and modern time in the southeastern Coastal Plain (Leigh, 2008; Leigh, 2006; Leigh and Feeney, 1995). While pollen records clearly indicate cooler, wetter conditions for the terminal Pleistocene time interval when most of the paleochannels documented by this study were active (Watts, 1980; Hussey, 1993; LaMoreaux et al., 2009), results presented here indicate that such conditions do not appear to have been manifested by extremely large bankfull flood discharge on the order of two to four times that of modern rivers, as previous studies have suggested. Where best estimates of paleodischarge indicate the possibility of larger than modern floods (Congaree, Pee Dee, and perhaps the Neuse River sites), magnitudes are more modest, on the order of 30 to 50 percent larger than modern.

If bankfull discharge were slightly larger for some rivers in the study area during the terminal Pleistocene, Leigh (2008) notes that multiple paleoclimatic phenomena could have been responsible, including: higher levels of effective precipitation resulting from relatively cool temperatures and corresponding lower rates of evapotransporation; snow melt runoff or rain on

frozen ground, in a manner similar to that invoked by Dury (1965); increased frequency or magnitude of tropical storms, driven by high tropical sea surface temperatures that occurred during this time (Lea et al., 2003); and intensified springtime frontal precipitation due to strong temperature contrasts between tropical and high latitude oceans (Lea et al., 2003; Bard, 2003). Interestingly, the three mega-meander channels with the greatest possibility of representing larger than modern discharge (Congaree, Pee Dee, and Neuse River sites) have the most northerly drainage areas of the rivers evaluated in this study. Whether these basins, which are mainly contained in the Piedmont and inner Coastal Plain of South and North Carolina, were more subject than the southerly sites to paleoenvironmental conditions that increased regional moisture and runoff is unknown, and several questions of this sort cannot be resolved by the limited number of paleochannels evaluated by this study.

3.5.4 Methodological implications

Retrodiction of discharge from the planform dimensions of meandering channels has a long history in fluvial geomorphology (Dury, 1965; Dury, 1976; Dury, 1985; Alford and Holmes, 1985; Sylvia and Galloway, 2006). However, because channel geometry does not depend only on water discharge but also on sediment supply and other factors, this technique has major conceptual flaws, and the large standard errors reported for regression equations used to retrodict discharge from channel dimensions likely results in part from failure to account for all the controlling variables (Bridge, 2003). Comparison of mega-meander paleodischarge estimates presented in this study with prior estimates demonstrates the amount of error that is possible when only planform channel geometry is considered and casts doubt on paleodischarge estimates based on bivariate regression relationships between discharge and planform dimensions that are

established on modern rivers. This has important implications for the practice of paleohydrology in alluvial settings, given that such techniques continue to be used in paleohydrologic investigations to estimate discharge (e.g., Sylvia and Galloway, 2006). Recent studies have also used planform dimensions to estimate the discharge of relict channels on the surface of Mars (Irwin et al., 2005; Burr et al., 2010), and these estimates must be subject to considerable error as they lack field data on channel bed and bank sediment. Findings presented in this paper provide a terrestrial example that illustrates the limitations of planform-based discharge estimation that should help improve understanding of the uncertainty associated with discharge estimates for channels in extraterrestrial settings.

3.6. Conclusions

The bankfull discharges of terminal Pleistocene mega-meander paleochannels of the southeastern Atlantic Coastal Plain were similar to, or at most only modestly larger than, bankfull flood sizes of modern rivers in the region. Cross-sectional coring transects reveal that mega-meander paleochannels were very wide but relatively shallow, and the modest discharge associated with these paleomeanders reflects their comparatively lower hydraulic efficiency relative to modern channels, which resulted from a high width to depth ratio and a correspondingly reduced hydraulic radius. Within the broader context of the late Quaternary evolution of fluvial systems in the region, scrolled terminal Pleistocene mega-meanders likely represent a transitional meandering planform that was still influenced by large volumes of sandy bedload sediment immediately following the braided, sand bed channels of the late Wisconsin interval (ca. 30-17 ka). Rather than reflecting extremely large bankfull floods, the unusually large planform dimensions and distinctive scrollwork of these paleomeanders apparently are the

result of a sediment discharge regime characterized by transport of large quantities of bedload sand, relatively little vertical accretion sedimentation, and the influence of these factors on bed and bank composition and channel shape. Regional increases in moisture and runoff indicated for the terminal Pleistocene by fossil pollen records provide a possible explanation for modestly increased discharge in cases where mega-meanders may have conveyed slightly larger than modern bankfull floods, but the precise climatic controls that influenced precipitation delivery and runoff during this time period remain poorly known. Comparison of paleodischarge estimates presented in this study with prior estimates based on paleochannel width, radius of curvature, and meander wavelength demonstrates the amount of error that is possible when paleohydrologic interpretations are based solely on planform channel dimensions and casts doubt on paleodischarge estimates that rely on regression relationships between discharge and channel geometry established on modern rivers. This has important implications for the discipline of paleohydrology, given that such techniques are still in common use, both on Earth and in extraterrestrial settings.

3.7 References

Alford, J.J., Holmes, J.C., 1985. Meander scars as evidence of major climate changes in southeast Louisiana. Annals of the Association of American Geographers 75, 395-403.

Arcement, G.J., Schneider, V.R., 1989. Guide for selecting Manning's roughness coefficients for natural channels and flood plains.Water supply paper 2339. United States Geological Survey. 38 pp.

Bard, E., 2003. North Atlantic sea surface temperature reconstruction, IGBP PAGES/ World Data Center for Paleoclimatology Data Contribution Series #2003-026. NOAA/NGDC Paleoclimatology Program, Boulder CO, USA.

Barnes, H.H., 1967. Roughness characteristics of natural channels. U.S. Geological Survey Water-Supply Paper 1849. U.S. Government Printing Office, Washington, D.C. 213 p.

Blum, M.D., Aslan, A., 2006. Signatures of climate vs. sea-level change within incised valley fill successions: Quaternary examples from the Texas Gulf Coast. Sedimentary Geology 190, 177-211.

Blum, M.D., Morton, R.A., Durbin, J.M., 1995. "Deweyville" terrace and deposits of the Texas Gulf Coastal Plain. Gulf Coast Association of Geological Societies Transactions 45, 53-60.

Bridge, J.S., 2003. Rivers and Floodplains: Forms, Processes, and Sedimentary Record. Blackwell Publishing, Malden, MA, 491 p.

Burr, D. M., R. M. E. Williams, K. D. Wendell, M. Chojnacki, and J. P. Emery (2010), Inverted fluvial features in the Aeolis/Zephyria Plana region, Mars: Formation mechanism and initial paleodischarge estimates, J. Geophys. Res. 115, E07011, doi:10.1029/2009JE003496.

Carlston, C. A., 1965. The relation of free meander geometry to stream discharge and its geomorphic implications. Am. J. Sci. 263, 864-885.

Charlton, R., 2008. Fundamentals of Fluvial Geomorphology. Routledge, New York, NY. 234 p.

Dury, G.H., 1965. Theoretical implications of underfit streams. US Geological Survey Professional Paper 452-C.

Dury, G. H., 1976. Discharge prediction, present and former, from channel dimensions. Journal of Hydrology 30, 219-245.

Dury, G. H., 1985. Attainable standards of accuracy in the retrodiction of paleodischarge from channel dimensions. Earth Surface Processes and Landforms 10, 205-213.

Feaster, T.D., and Tasker, G.D., 2002. Techniques for estimating the magnitude and frequency of floods in rural basins of South Carolina, 1999: U.S. Geological Survey Water-Resources Investigations Report 02-4140, 34 p.

Feaster, T.D., Gotvald, A.J., and Weaver, J.C., 2009. Magnitude and frequency of rural floods in the Southeastern United States, 2006-Volume 3, South Carolina: U.S. Geological Survey Scientific Investigations Report 2009-5156, 226 p.

Gagliano, S.M., Thom, B.G., 1967. Deweyville terrace, Gulf and Atlantic Coasts. Louisiana State University, Coastal Studies Bulletin, Vol. 1., 23-41.

Goman, M., Leigh, D.S., 2004. Wet early to middle Holocene conditions on the upper Coastal Plain of North Carolina, USA. Quaternary Research 61, 256-264.

Gotvald, A.J., Feaster, T.D., and Weaver, J.C., 2009. Magnitude and frequency of rural floods in the southeastern United States, 2006-Volume 1, Georgia: U.S. Geological Survey Scientific Investigations Report 2009-5043, 120 p.

Gotvald, A.J., Feaster, T.D., and Weaver, J.C., 2009. Flood-frequency applications tool for use on streams in Georgia, South Carolina, and North Carolina, Version 1.3. Avaiable at : http://pubs.usgs.gov/sir/2009/5156/, accessed on June 3rd, 2013.

Herschy, R.W., 1985. Streamflow Measurement. Elsevier, London. 553 p.

Hussey, T.C. 1993. A 20,000-year history of vegetation and climate at Clear Pond, northeastern South Carolina. M.S. Thesis. University of Maine, Orono, Maine, USA.

Irwin, R. P., III, R. A. Craddock, and A. D. Howard, 2005. Interior channels in Martian valley networks: Discharge and runoff production. Geology, 33, 489-492, doi:10.1130/G21333.1.

Jarrett, R.D., 1987. Errors in slope-area computations of peak discharges in mountain streams. Journal of Hydrology 96, 53-67.

Kellerhals, R., 1982. Effect of river regulation on channel stability. In: Hey, R.D., Bathhurst, J.C., Thorne, C.R. (Eds.), Gravel-bed Rivers. Wiley, Chichester, pp. 685-705.

Knighton, D., 1998. Fluvial Forms and Processes: A New Perspective. Arnold, London. 383 p.

Knox, J. C., 1985. Responses of floods to Holocene climate change in the Upper Mississippi Valley: Quaternary Research 23, 287-300.

LaMoreaux, H.K., Brook, G.A., Knox, J.A., 2009. Late Pleistocene and Holocene environments of the Southeastern United States from the stratigraphy and pollen content of a peat deposit on the Georgia Coastal Plain. Palaeogeography, Palaeoclimatology, Palaeoecology 280, 300-312.

Lea, D.W., Pak, D.K., Peterson, L.C., Hughen, K.A., 2003. Synchroneity of tropical and high-latitude Atlantic temperatures over the last glacial termination. Science 301, 1361-1364.

Leigh, D.S., 2006. Terminal Pleistocene braided to meandering transition in rivers of the Southeastern USA. Catena 66, 155-160.

Leigh, D.S., 2008. Late Quaternary climates and river channels of the Atlantic Coastal Plain, Southeastern USA. Geomorphology 101, 90-108.

Leigh, D.S., Feeney, T.P., 1995. Paleochannels indicating wet climate and lack of response to lower sea level, southeast Georgia. Geology 23, 687-690.

Leigh, D.S., Srivastava, P., Brook, G.A., 2004. Late Pleistocene braided rivers of the Atlantic Coastal Plain, USA. Quaternary Science Reviews 23, 65-84.

Leopold, L.B., Wolman, M.G., 1957. River channel patterns: braided, meandering, and straight. US Geological Survey Professional Paper 282-B. US Government Printing Office, Washington, pp. 39-85.

Meade, R.H., Yuzyk, T.R., Day, T.J., 1990. Movement and storage of sediment in rivers ofthe United States and Canada. In: Wolman, M.G., Riggs, H.C. (Eds.), Surface Water Hydrology. Geological Society of America, The Geology of North America, Vol. O-1, Boulder, pp. 255-280.

Murray, A.S., Wintle, A.G., 2000. Luminescence dating of quartz using an improved single-aliquot regenerative-dose protocol. Radiation Measurements 32, 57-73.

Pope, B.F., Tasker, G.D., and Robbins, J.C., 2001. Estimating the magnitude and frequency of floods in rural basins of North Carolina-Revised: U.S. Geological Survey Water- Resources Investigations Report 01-4207, 44 p.

Prescott, J.R., Stephan, L.G., 1982. Contribution of cosmic radiation to environmental dose. PACT 6, 17-25.

Ramsey, B.C., 2009. Bayesian analysis of radiocarbon dates. Radiocarbon, 51 (1), 337-360.

Rotnicki, K., 1991. Retrodiction of palaeodischarges of meandering and sinuous alluvial rivers and its palaeohydrologic implications, in Starkel, L., et al., eds., Temperate palaeohydrology, fluvial processes in the temperate zone during the last 15,000 years: New York, Wiley, p. 431-470.

Schumm, S.A., 1960. The shape of alluvial channels in relation to sediment type: erosion and sedimentation in a semiarid environment. US Geological Survey Professional Paper 352-B. US Government Printing Office, Washington, pp. 17-30.

Soil Survey Division Staff, 1993. Soil Survey Manual. U.S. Department of Agriculture Handbook 18. U.S. Government Printing Office, Washington, D.C., USA, 437 pp.

Stokes, S. and Walling, D.E., 2003. Radiogenic and Isotopic Methods for the Direct Dating of Fluvial Sediments. In: Kondolf, M. and Piegay, H. (Eds.) Tools in Fluvial Geomorphology. John Wiley and Sons, Ltd, West Sussex, England, p. 233-267.

Stuiver, M., Reimer, P.J., Braziunas, T.F., 1998. High-precision radiocarbon age calibration for terrestrial and marine samples. Radiocarbon 40, 1127-1151.

Sylvia, J.P.M., and Galloway, W.E., 2006. Morphology and stratigraphy of the late Quaternary lower Brazos valley: implications for paleoclimate, discharge, and sediment delivery. Sedimentary Geology 190, 159-175.

Watts, W.A., 1980. Late-Quaternary Vegetation History at White Pond on the Inner Coastal-Plain of South-Carolina. Quaternary Research 13, 187-199.

Weaver, J.C., Feaster, T.D., and Gotvald, A.J., 2009. Magnitude and frequency of rural floods in the Southeastern United States, through 2006-Volume 2, North Carolina: U.S. Geological Survey Scientific Investigations Report 2009–5158, 111 p.

Whiting, P.J., 2003. Flow Measurement and Characterization. In: Kondolf, M. and Piegay, H. (Eds.) Tools in Fluvial Geomorphology. John Wiley and Sons, Ltd, West Sussex, England, p. 323-346.

Williams, G.P., 1988. Paleofluvial estimates from dimensions of former channels and meanders. In: Baker, V.R., Kochel, R.C., Patton, P.C. (Eds.), Flood geomorphology. John Wiley and Sons, New York, pp. 357-376.

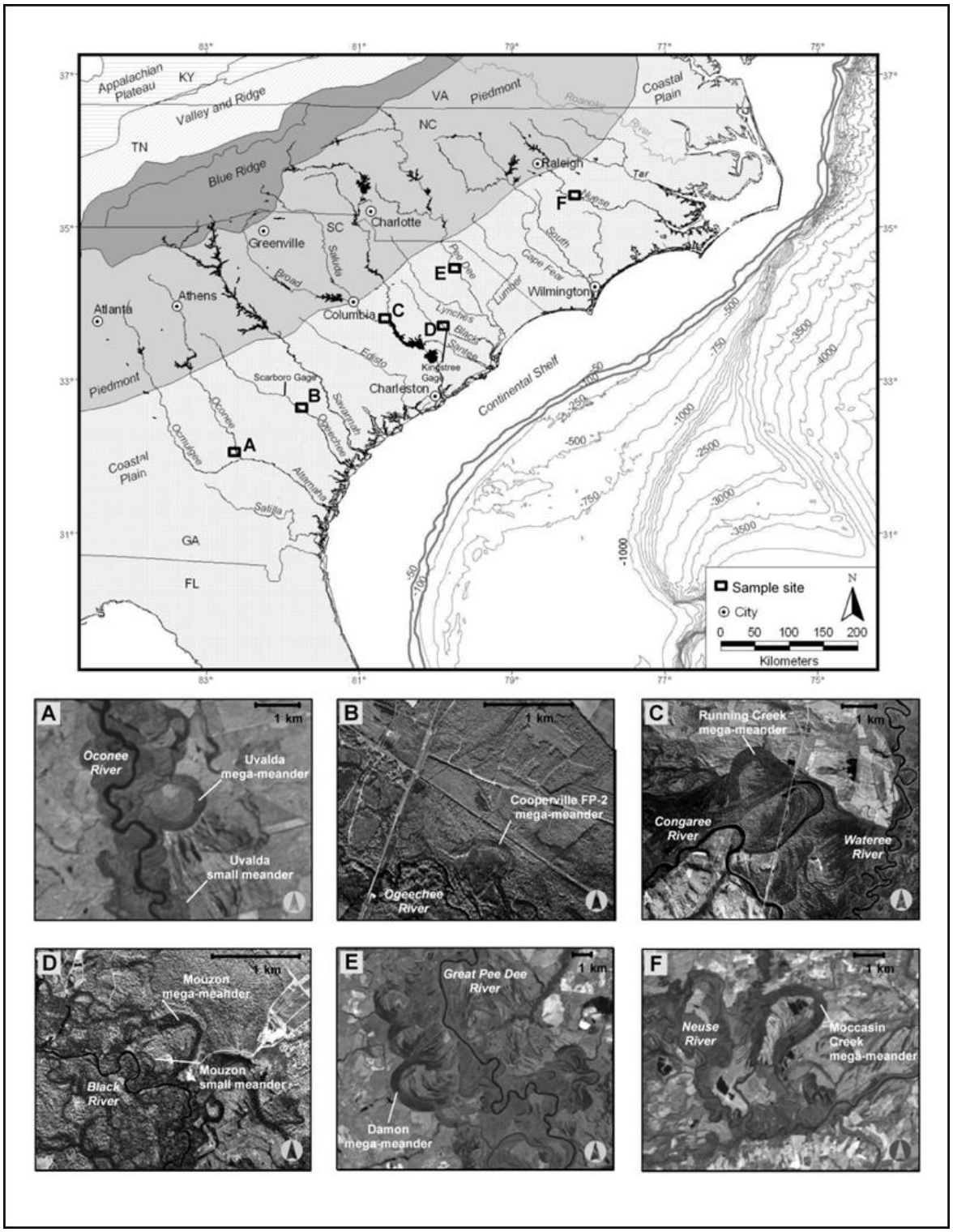

Figure 3.1. Location of mega-meander study sites. On satellite imagery and high altitude aerial photography, the planform dimensions of "mega-meanders" dwarf the late Holocene paleochannels, exhibiting much greater widths and radii of curvature.

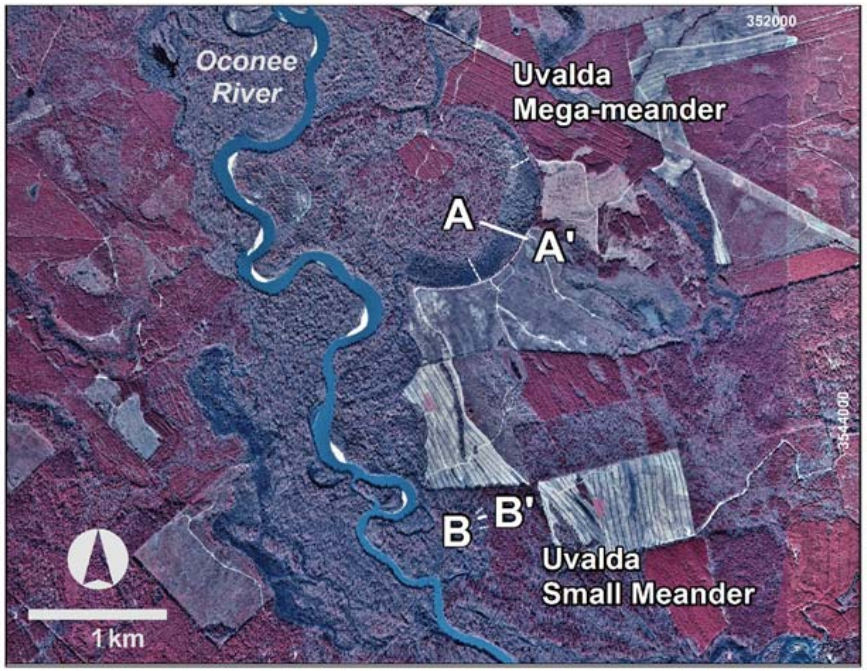

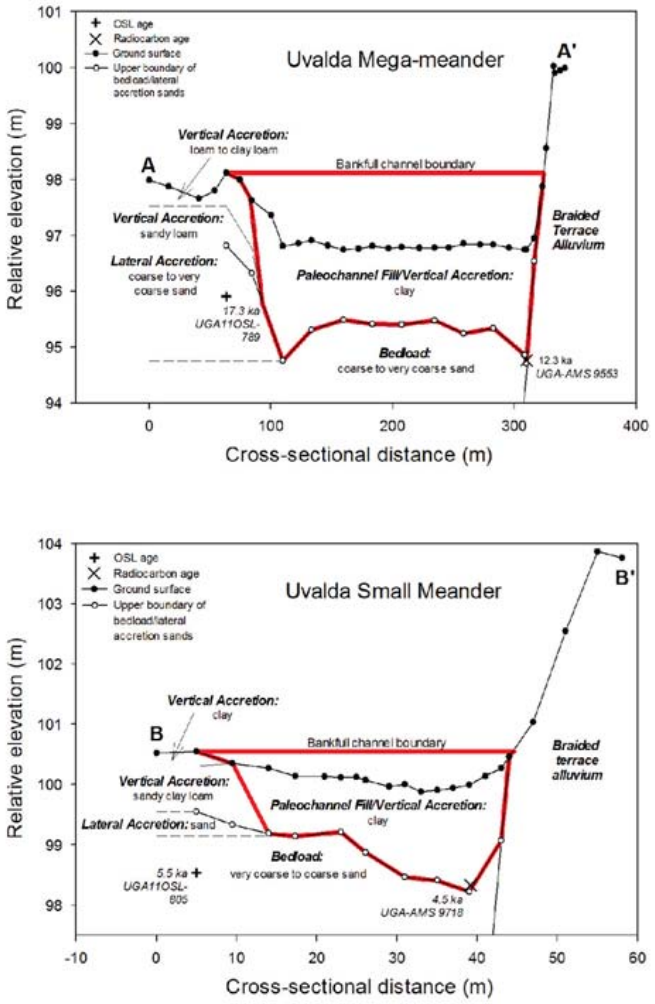

Figure 3.2. Planimetric view and stratigraphic cross-sections of the Uvalda mega- and small meanders of the Oconee River. Additional cross-sections used to estimate paleochannel slope are shown on the planimetric figure with dashed lines (only ground surface slope was surveyed for the small meander). The base map for this figure, as well as for Figures 3.3-3.5, is a 1 m color-infrared digital orthophotograph registered to the North American Datum of 1983 and UTM grid zone 17.

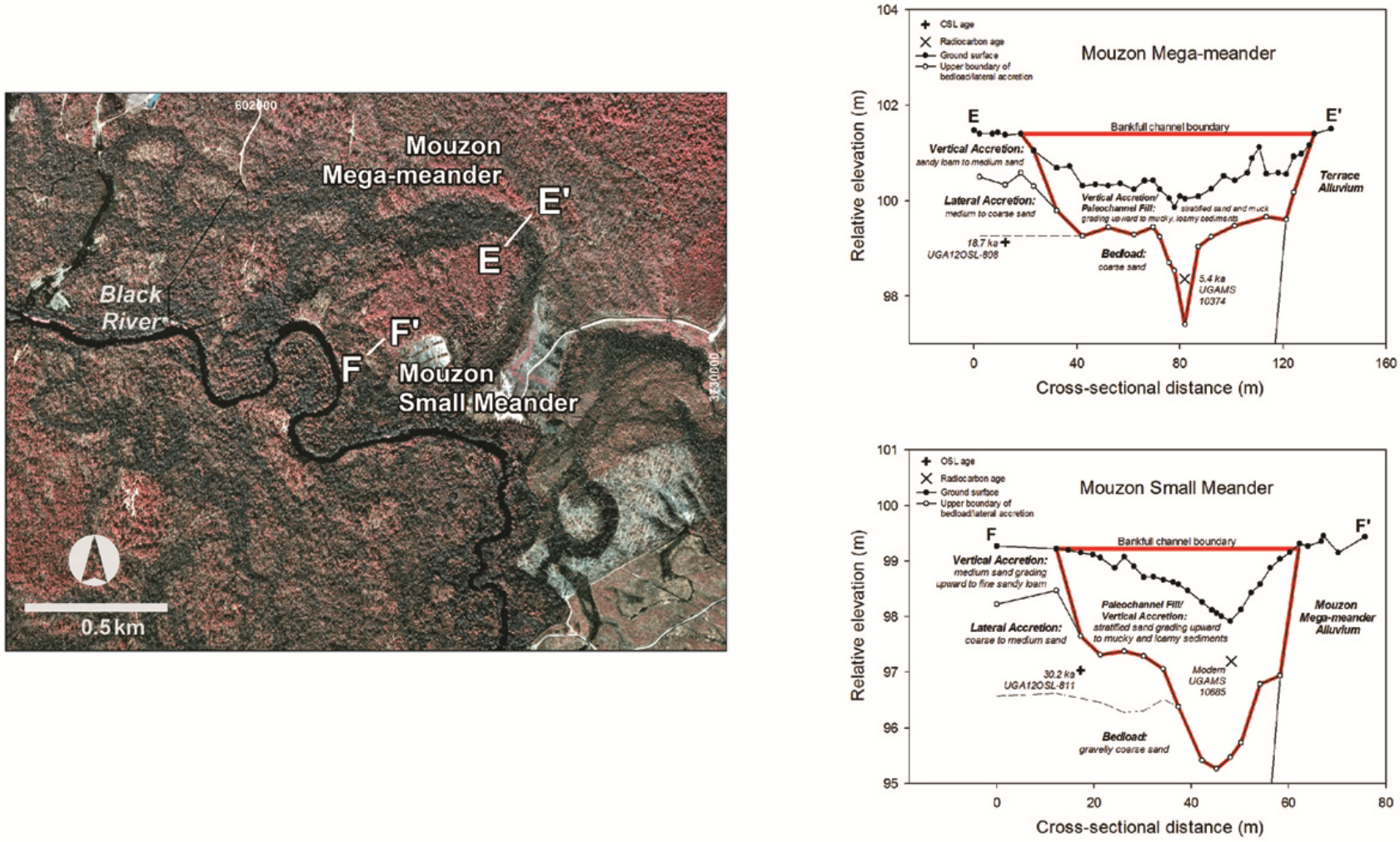

Figure 3.3. Planimetric view and stratigraphic cross-sections of the Mouzon mega- and small meanders of the Black River.

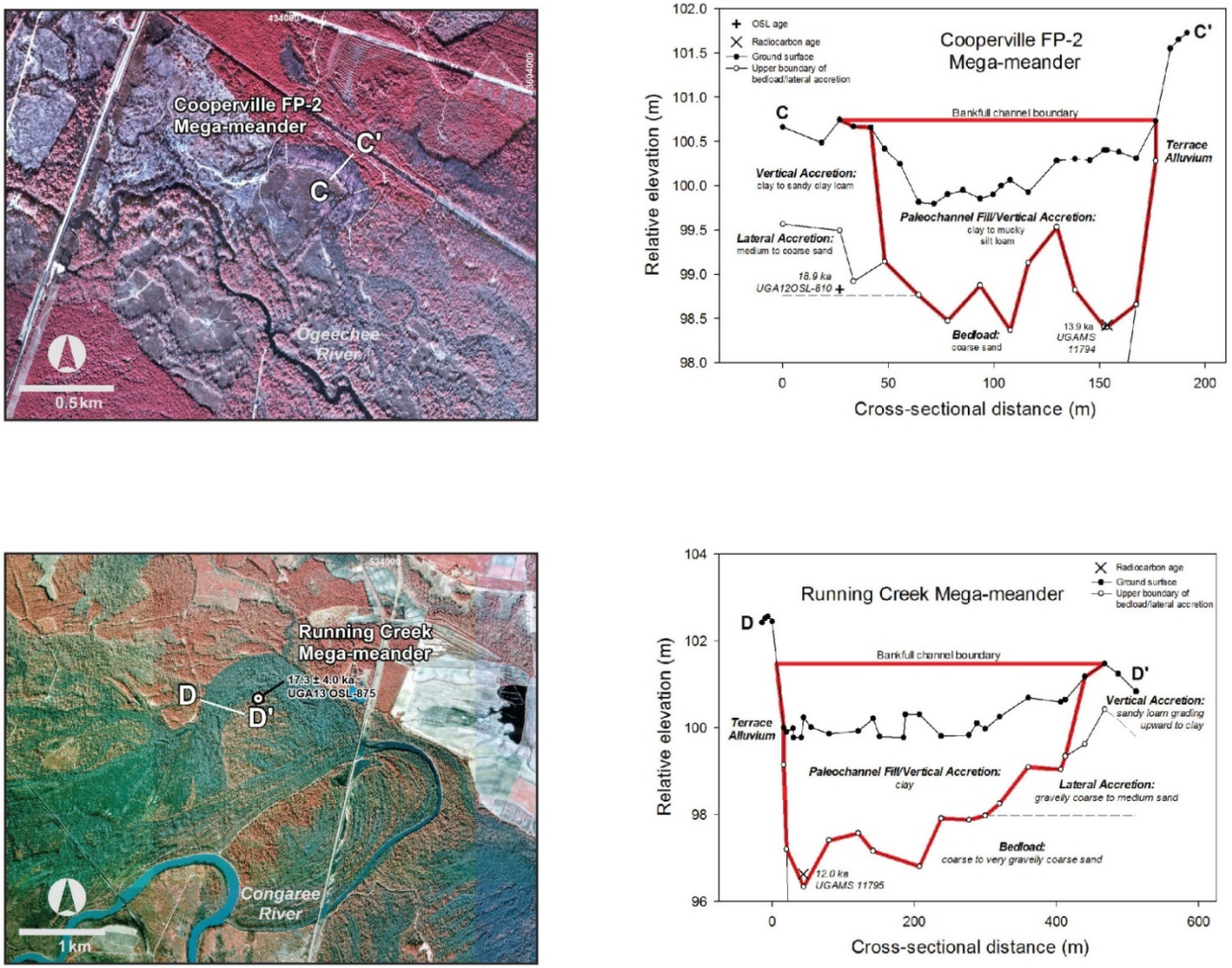

Figure 3.4. Planimetric views and stratigraphic cross-sections of the Cooperville FP-2 mega-meander (Ogeechee River) and the Running Creek mega-meander (Congaree River). Additional cross-sections used to estimate paleochannel slope for the Cooperville FP-2 mega-meander are shown with dashed lines. Because the OSL date for the Running Creek mega-meander (17.3 ± 4.0 ka) is located off the stratigraphic cross-section at the apex of the mega-meander bend, it is shown on the planview diagram.

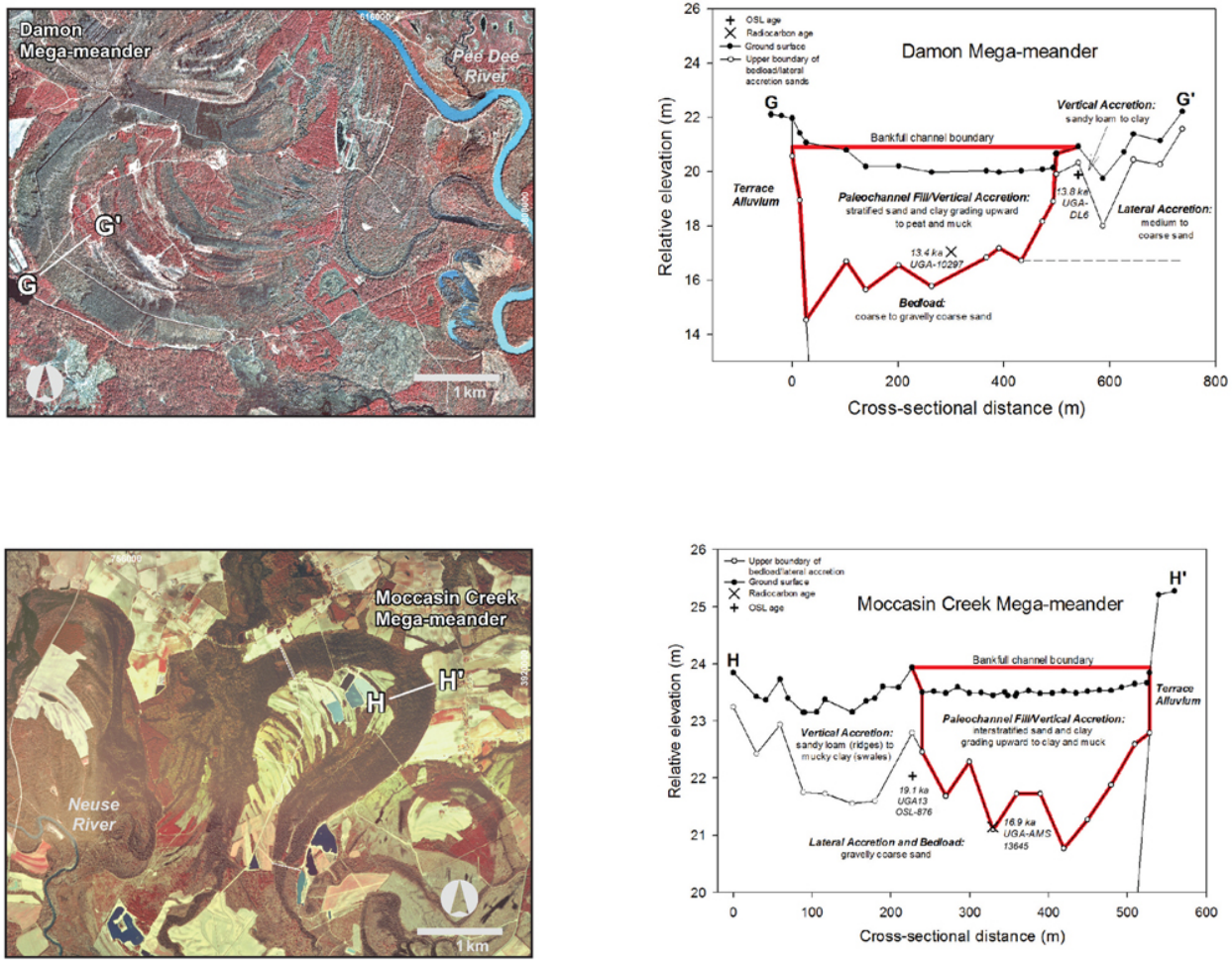

Figure 3.5. Planimetric views and stratigraphic cross-sections of the Damon mega-meander (Pee Dee River) and the Moccasin Creek mega-meander (Neuse River). Additional cross-sections used to estimate paleochannel slope for the Moccasin Creek mega-meander are shown with dashed lines. For the Damon mega-meander, the radiocarbon and OSL dates of Leigh et al. (2004) were projected a short distance from their true locations to the G-G' section line. Their positions on section reflect the best match between the topography and stratigraphy of their true locations and that of section line.

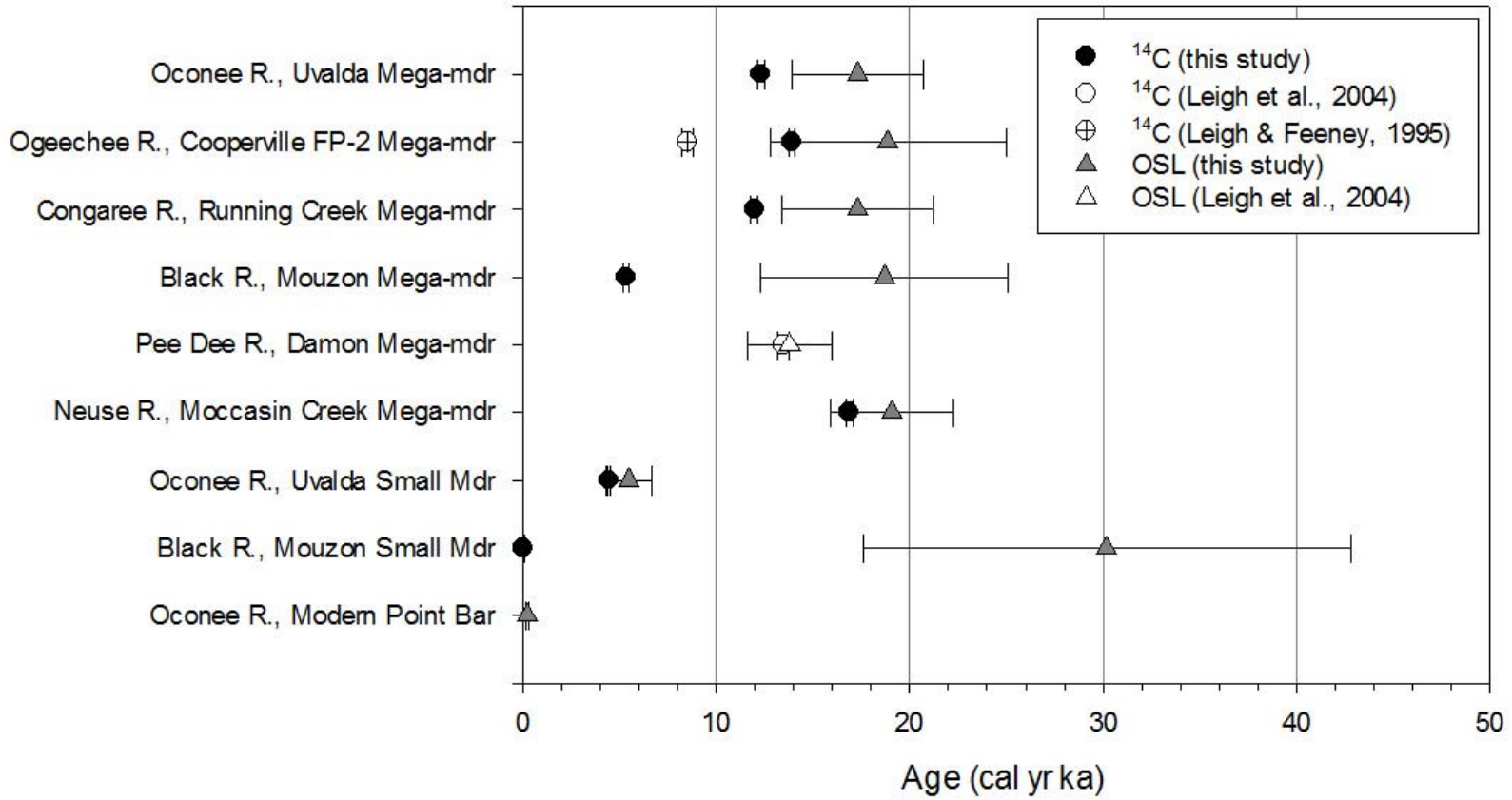

Figure 3.6. Plot of radiocarbon and optically-stimulated luminescence (OSL) dates for mega-meanders and small paleomeanders. The OSL date shown for a modern point bar of the Oconee River was obtained in close proximity to the Uvalda mega- and small paleomeanders. Previously published dates for the Cooperville FP-2 mega-meander of the Ogeechee River (Leigh and Feeney, 1995) and the Damon mega-meander of the Pee Dee River (Leigh et al, 2004) are also shown. The error bars represent two standard deviations of the age estimates.

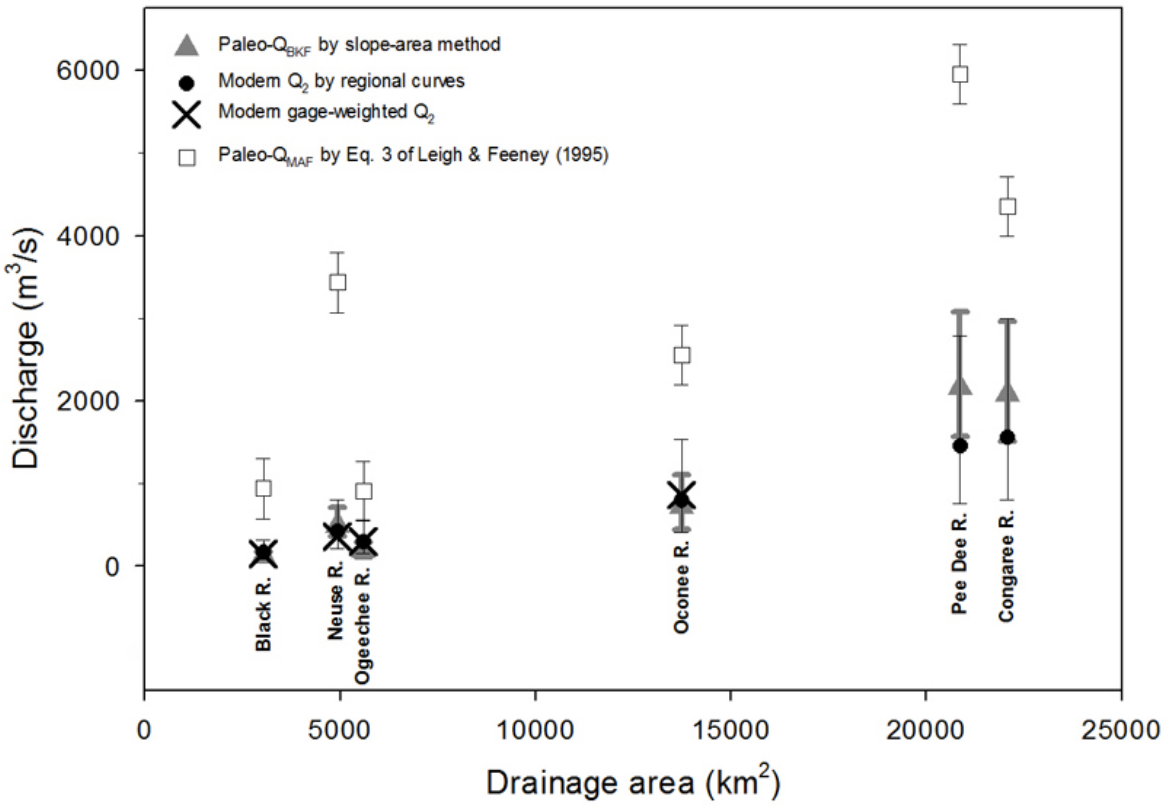

Figure 3.7. Mega-meander bankfull discharge (Paleo-Q_{BKF}) and discharge of the 2-year recurrence interval flood (Q_2) on modern rivers adjacent to mega-meander sites. Modern Q_2 was estimated at ungaged mega-meander sites using both the regional flood frequency regression model (black circles) and the weighted discharge technique (black X's) of Gotvald et al. (2006). The gage-weighted discharge provides a slightly more accurate estimate of discharge at ungaged sites by incorporating flood frequency data from the nearest gage with the regional regression estimate. Mega-meander mean annual flood discharge (Paleo-Q_{MAF}) estimates retrodicted by equation 3 of Leigh and Feeney (1995) are provided for comparison. Error bars for mega-meander bankfull discharge represent minimum and maximum discharges based on minimum and maximum estimates of channel roughness and slope. Error bars for modern Q_2 predicted by the regional curve reflect the lower and upper limits of the 95% prediction interval, while error bars for Paleo-Q_{MAF} by the Leigh and Feeney equation represent ±2 standard errors.

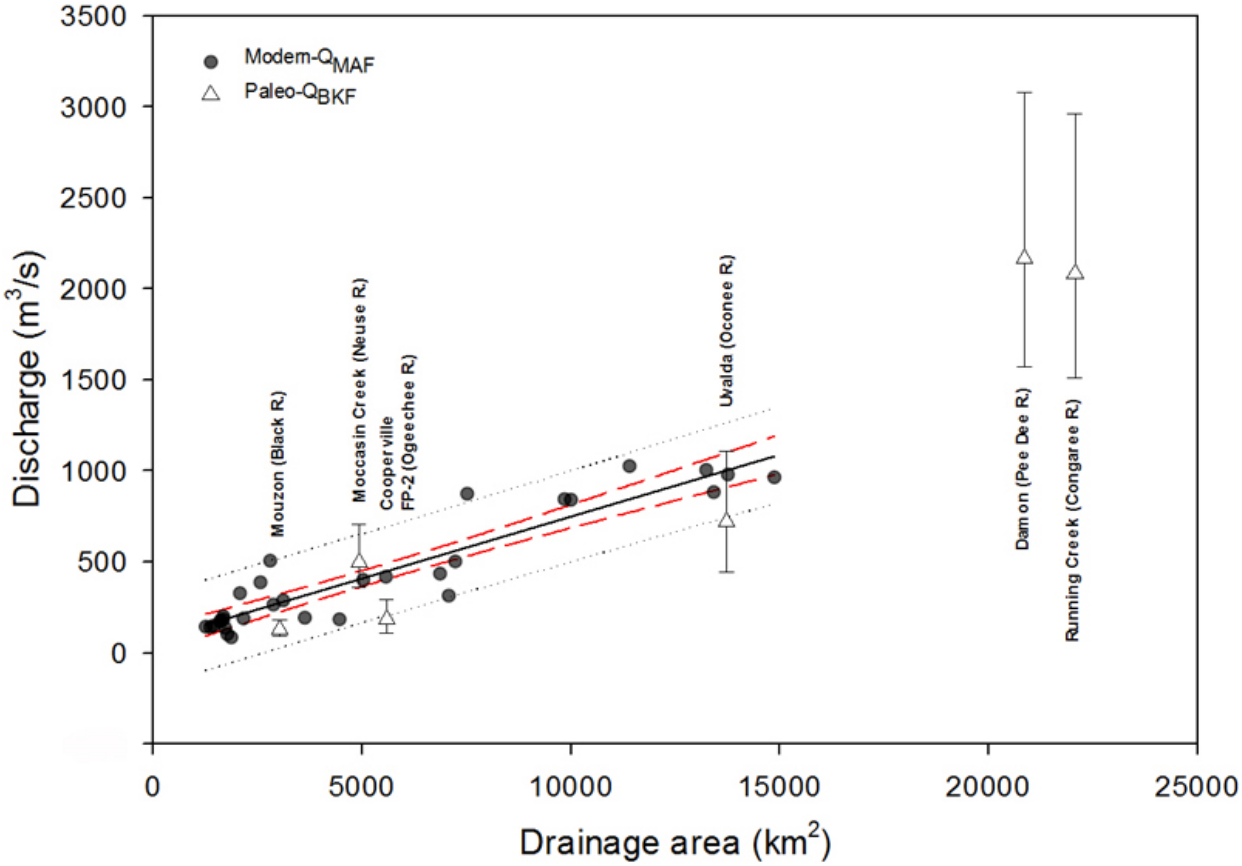

Figure 3.8. Mega-meander bankfull discharge compared to mean annual discharge of modern Coastal Plain rivers. Mean annual flood discharge (Q_{MAF}) as calculated by Leigh and Feeney (1995) regressed against drainage area for unregulated rivers at 30 U.S. Geological Survey gaging stations in the Coastal Plain of Georgia and South Carolina ($r^2 = 0.87$; significance level of F-ratio <0.0001). The 95% confidence intervals and the prediction intervals for the regression are respectively depicted by the red dashed and black dotted lines. Mega-meander bankfull paleodischarge, with error bars that indicate minimum and maximum estimates, are shown for comparison. Because available gages in the study area with drainage areas greater than ~15,000 km^2 are located on regulated rivers, these sites were excluded from the analysis to avoid the influence of impoundments on flood regime. Therefore, the regression terminates at a drainage area of ~15,000 km^2.

Table 3.1. Discharge estimates for modern rivers. Discharge is provided for modern rivers near mega-meander study sites and the nearest USGS gaging stations with >20 years of record.

	Ungaged mega-meander sites					Nearest USGS gaging station					
		Discharge (m^3/s) predicted by regional flood frequency curves[a]		Weighted discharge (m^3/s)[a]				Discharge (m^3/s)[c,d]			
River	Drainage area (km^2)	Q_2	Q_5	Q_2	Q_5	Gage name and number	Drainage area (km^2)	$Q_{1.5}$	Q_2	Q_{maf}	Q_5
Oconee	13,736	799	1,270	864	1,390	Mt. Vernon, 02224500	13,235	700	917	1,017	1,458
Ogeechee	5,590	292	490	302	518	Scarboro, 02202000	5,025	220	305	397	568
Congaree	22,071	1,555[b]	2,373[b]	---	---	Columbia, 02169500	20,332	2,122	2,757	3,424	4,724
Black	3,032	166	289	150	289	Kingstree, 02136000	3,243	100	141	209	289
Pee Dee	20,865	1,450[b]	2,215[b]	---	---	Pee Dee, 02131000	22,870	939	1,120	1,411	1,559
Neuse	4,928	422[b]	688[b]	359	555	Goldsboro, 02089000	6,213	296	352	402	514

[a]Calculated using the *Flood-frequency applications tool for use on streams in Georgia, South Carolina, and North Carolina, Version 1.3,* (Gotvald et al., 2009), based on the methods described in Gotvald et al. (2006), Feaster et al. (2009), and Weaver et al. (2009). Weighted discharge provides an estimate of discharge for a given recurrence interval flood based on both the regional flood frequency curve and data from the nearest gage. Data required to calculate weighted discharge were not available for the Congaree and Pee Dee Rivers, so estimating weighted discharge for these sites was not possible.

[b]Present-day flood regimes of the Congaree, Pee Dee, & Neuse Rivers are regulated by impoundments. Thus, flood sizes derived from regional curves may not accurately reflect the post-impoundment regimes of these rivers. Discharges provided here are intended as estimates of pre-dam flood sizes.

[c]$Q_{1.5}$, Q_2, & Q_5 = discharge of the 1.5, 2, & 5 year flood as calculated by the Log Pearson Type III method from the annual peak flood record at gaging stations. Qmaf = mean annual discharge.

[d]Discharges were calculated for the pre-reservoir record where possible: Congaree, 1892-1929, prior to completion of Lakes Murray & Greenwood (Feaster and Tasker, 2002); Pee Dee, 1939-1961, prior to completion of W. Kerr Scott & Tuckertown Reservoirs (Feaster and Tasker, 2002); Neuse, 1930-1980, prior to completion of Falls Lake (Pope et al., 2001).

Table 3.2. Bankfull discharge estimates at selected gaging stations in the Georgia Coastal Plain using the slope-area method and comparison with discharges calculated from gage records.

							n			v (m/s)			Q_{BKF} (m^3/s) by slope-area			Discharges calculated from gage records (m^3/s)				
River name and USGS Gage #	Drainage area (km^2)	W/D	CSA (m^2)	WP (m)	R	S	min	max	best estimate	min	max	best estimate	min	max	best estimate	Q_{BKF}	Slope area/ Gaged Q_{BKF}	Q_{BKF} recurrence interval (yr)	$Q_{1.5}$	Q_2
Ogeechee @ Eden, #02202500	6,864	25.6	152.1	70.2	2.2	0.00030	0.030	0.040	0.035	0.72	0.96	0.83	110	147	**126**	**152**	**0.83**	1.1	242	324
Ohoopee near Reidsville, #02225500	2,875	14.1	205.7	63.8	3.2	0.00023	0.030	0.040	0.035	0.82	1.09	0.94	168	224	**192**	**234**	**0.82**	2.3	162	213
Altamaha near Baxley, #02225000	30,044	65.9	1171.9	301.2	3.9	0.000143	0.030	0.040	0.035	0.74	0.99	0.85	868	1157	**992**	**1100**	**0.90**	1.4	1170	1549
Oconee @ Dublin, 02223500	11,396	19.0	644.3	124.5	5.2	0.000188	0.030	0.040	0.035	1.03	1.37	1.17	661	881	**755**	**770**	**0.98**	1.7	669	872
Ocmulgee @ Lumber City, 02215500	13,416	32.2	515.8	133.1	3.9	0.00020	0.030	0.040	0.035	0.86	1.15	0.99	445	593	**508**	**515**	**0.99**	1.4	566	738

Notes: W/D = width to depth ratio; CSA = cross-sectional area; WP = wetted perimeter; R = hydraulic radius; S = slope; n = Manning's roughness coefficient; v = velocity; Q_{BKF} = bankfull flood discharge; $Q_{1.5}$, Q_2, Q_5 = discharge of 1.5 yr, 2 yr, and 5 yr recurrence interval floods calculated by the Log Pearson Type III method, respectively; Qmaf = mean annual flood discharge. Bankfull discharge at gage locations was estimated using a discharge-stage rating curve constructed from gage data and inspection of USGS field-surveyed channel cross-sections provided by A.J. Gotvald (personal communication, 2013). Slope was measured from USGS 7.5-minute topographic quadrangles for all gages except the Ogeechee River at Eden, where 3 m horizontal resolution LIDAR data were used. Manning's *n* values were estimated by criteria specified in Arcement and Schneider (1989) and by visual comparison with the viewbook of Barnes (1967).

Table 3.3. Slope estimates derived from paleochannel geomorphic components and river valley gradients. Values in bold represent the minimum and maximum estimates of channel slope used in paleodischarge calculations.

Site	Channel Bed	Bar Tops[a]	Thalweg	Predominant Bed Surface[b]	Lowest 20% of Bed[c]	Paleochannel Ground Surface[d]	Valley Gradient[e]	Sinuosity-corrected Valley Gradient[f]
Mega-meander Paleochannels								
Uvalda, Oconee R.	0.00041	0.00024	0.00092	**0.00028**	**0.00078**	0.00044	0.00039	0.00023
Cooperville FP-2, Ogeechee R.	0.00016	+	0.00029	**0.00061**	**0.00020**	0.00012	0.00038	0.00022
Running Creek, Congaree R.	---	---	---	---	---	---	**0.00068**	**0.00040**
Mouzon, Black R.	---	---	---	---	---	0.00023	**0.00030**	**0.00018**
Damon, Great Pee Dee R.	---	---	---	---	---	0.00016	**0.00028**	**0.00016**
Moccasin Creek, Neuse R.	0.00028	0.00030	0.00027	**0.00020**	**0.00026**	0.00043	0.00041	0.00024
Small Meandering Paleochannels								
Uvalda, Oconee R.	---	---	---	---	---	0.00135	**0.00026**	**0.00018**
Mouzon, Black R.	---	---	---	---	---	0.00009	**0.00026**	**0.00014**

[a]Tops of mid-channel bars. Plus sign indicated for the Cooperville FP-2 site means the slope was inverted. This was due to a pronounced mid-channel bar that was present at the middle and downstream cross-sections but absent at the upstream cross-section.

[b]The prevailing channel bed surface. Excludes the thalweg and tops of pronouced mid-channel bars.

[c]The lowest 20% of bed elevations per paleochannel cross-section.

[d]Determined by field survey (Oconee, Ogeechee, and Neuse R. sites) or derived from Light Detection and Ranging (LIDAR) elevation data with a horizontal resolution of either 2 m (Pee Dee R. site) or 3 m (Congaree and Black R. sites).

[e]Longitudinal valley gradient of the mega-meander terrace (for mega-meander paleochannels) or the modern floodplain (for small meandering paleochannels). See text for further explanation.

[f]The slope that results if a meandering planform of typical sinuosity is superimposed on the valley gradient. See text for further explanation.

Notes: --- = No data.

Table 3.4. Radiocarbon dates and supporting data.

River and Site	Lab No.	Sample depth (cm)	Height above bedload (cm)	Material dated	$\delta^{13}C$ corrected age ± 1 sigma (^{14}C yr BP)	Calendar age (ka)[a]	2-Sigma cal age (ka)
Oconee River							
Uvalda Mega-meander	UGAMS 9553	198-203	2.5	seeds	10,430±30	**12.3**	12.1-12.5
Uvalda Small Meander	UGAMS 9718	164-168	8	leaves	3,970±25	**4.5**	4.4-4.5
Ogeechee River							
Cooperville FP-2 Mega-meander	Beta-66163[b]	135	5	wood	7,700±100	**8.5**	8.2-8.8
Cooperville FP-2 Mega-meander	UGAMS 11794	195-200	2.5	seed	12,090±30	**13.9**	13.8-14.1
Congaree River							
Running Creek Mega-meander	UGAMS 11795	361	29	seed pod	10,230±30	**12.0**	11.8-12.1
Black River							
Mouzon Mega-meander	UGAMS 10374	165-170	90	seed	4600±25	**5.4**	5.1-5.5
Mouzon Small Meander	UGAMS 10685	70-75	170	acorn	modern[d]	**---**	---
Pee Dee River							
Damon Mega-meander	UGA-10297[c]	260-275	---[e]	acorn	11,470±50	**13.4**	13.2-13.8
Neuse River							
Moccasin Creek Mega-meander	UGAMS 13645	225-235	5	seeds	13790±40	**16.9**	16.7-17.1

[a]All dates were calibrated to calendar years using the OxCal 4.2 radiocarbon calibration program, IntCal 09 calibration curve (Ramsey, 2009), with the exception of two previously reported dates (Beta-66163 & UGA-10297), which were calibrated using the Calib 4.4 program (Stuiver et al., 1998). [b]Previously reported in Leigh & Feeney (1995). [c]Previously reported in Leigh et al. (2004). [d]Calibration of this sample indicates that it was growing either between 2001-2005 or between 1953-1955 AD (personal communication, Alex Cherkinsky, UGA Center for Applied Isotope Studies, 2013). [e]Height above bedload not provided by authors (Leigh et al., 2004).

Table 3.5. Optically-stimulated luminescence (OSL) dates and supporting data.

River and Site	Sample name/Lab No.	Age (ka) ± 2 sigma[f]	Sample depth (cm)	U (ppm)	Th (ppm)	K (%)	Water content (% by wt.)	Equivalent Dose (Gy)	Dose rate (Gy/ka)
Oconee River									
Uvalda Mega-meander	UGA11OSL-789	**17.3±3.4**	205-237	1.4±0.3	3.8±0.9	0.7±0.1	14.7±5.0	21.9±0.8	1.3±0.1[b]
Uvalda Small Meander	UGA11OSL-805	**5.5±1.2**	185-217	1.22±0.16	2.98±0.6	0.7±0.1	17.75±5.0	6.15±0.12	1.12±0.12[b]
Oconee River Point Bar	UGA12OSL-840	**0.23±0.06**	70	2.31±0.42	7.30±1.45	0.8	10±5	0.43±0.04	1.89±0.18[c]
Ogeechee River									
Cooperville FP-2 Mega-meander	UGA12OSL-810	**18.9±6.1**	178-210	0.79±0.24	4.0±0.84	0.2±0.1	18.28±5.0	13.54±0.14	0.72±0.12[b]
Congaree River									
Running Creek Mega-meander	UGA13OSL-875	**17.3±3.9**	147-177	3.3±0.7	11.76±2.42	1.7	14.9±5	51.74±0.98	2.99±0.33[e]
Black River									
Mouzon Mega-meander	UGA12OSL-808	**18.7±6.4**	210-242	0.8±0.09	1.16±0.35	0.2±0.1	17.09±5.0	10.02±0.21	0.54±0.09[d]
Mouzon Small Meander	UGA12OSL-811	**30.2±12.6**	198-230	0.51±0.09	1.38±0.35	<0.1	18.30±5.0	12.66±0.23	0.42±0.09[b]
Pee Dee River									
Damon Mega-meander	DL-6[a]	**13.8±2.2**	120-150	1.0±0.3	2.2±0.9	1.19	15.0±5.0	19.9±2.7	1.4±0.1
Neuse River									
Moccasin Creek Mega-meander	UGA13OSL-876	**19.1±3.2**	175-205	1.37±0.16	2.32±0.6	1.7	15.9±5	37.26±0.53	1.95±0.16[b]

[a]Previously reported in Leigh et al. (2004). Cosmic ray contribution assumed to be 0.15±0.03 Gy/ka. [b]Cosmic ray contribution assumed to be 0.16±0.02 Gy/ka. [c]Cosmic ray contribution assumed to be 0.19±0.02 Gy/ka. [d]Cosmic ray contribution assumed to be 0.15±0.02 Gy/ka. [e]Cosmic ray contribution assumed to be 0.165±0.02 Gy/ka.
[f]Two times 1-sigma errror.

Table 3.6. Bankfull discharge estimates for mega-meanders and small paleomeanders. Estimated discharge for the 2-year recurrence interval flood for modern rivers at mega-meander study sites are also provided.

	MEGA-MEANDER PALEOCHANNELS																MODERN RIVERS				
					Slope			n			v (m/s)			PaleoQ$_{BKF}$ (m^3/s) by slope-area			Q$_2$ (m^3/s) by regional flood frequency curves				
Site	W/D	CSA (m^2)	WP (m)	R	min	best estimate	max	min	best estimate	max	min	best estimate	max	min	best estimate	max	Lower limit, 95% prediction interval	Mean	Upper limit, 95% prediction interval	Weighted Q$_2$ (m^3/s)	PaleoQ$_{BKF}$/ Q$_2$ modern channel
Mega-meander Paleochannels																					
Uvalda, Oconee R.	121.2	649.6	261.4	2.5	0.00028	0.00053	0.00078	0.030	0.038	0.045	0.69	1.11	1.71	445	**723**	1110	416	**799**	1535	**864**	**0.84**
Cooperville FP-2, Ogeechee R.	95.7	251.1	150.4	1.7	0.00020	0.00041	0.00061	0.030	0.038	0.045	0.45	0.75	1.16	112	**188**	292	152	**292**	561	**302**	**0.62**
Running Creek, Congaree R.	144.3	1533.3	462.9	3.3	0.00040	0.00054	0.00068	0.030	0.038	0.045	0.99	1.36	1.93	1514	**2084**	2962	807	**1555**	3002	**---**	**1.34**
Mouzon, Black R.	55.2	210.0	114.6	1.8	0.00018	0.00024	0.00030	0.030	0.038	0.045	0.44	0.61	0.86	93	**128**	182	86	**166**	320	**150**	**0.85**
Damon, Great Pee Dee R.	166.3	2180.9	541.4	4.0	0.00016	0.00022	0.00028	0.030	0.038	0.045	0.72	0.99	1.41	1575	**2167**	3080	753	**1450**	2790	**---**	**1.49**
Moccasin Creek, Neuse R.	166.7	639.5	304.1	2.1	0.00024	0.00033	0.00041	0.030	0.038	0.045	0.57	0.78	1.11	362	**498**	709	220	**422**	810	**359**	**1.39**
																				Average =	**1.09**
Small Meandering Paleochannels																					
Uvalda, Oconee R.	30.9	56.0	40.6	1.4	0.00018	0.00022	0.00026	0.030	0.035	0.040	0.42	0.53	0.67	23	**30**	37	416	**798.62**	1534.944	**864**	**0.03**
Mouzon, Black R.	18.7	116.1	51.1	2.3	0.00014	0.00020	0.00026	0.030	0.038	0.045	0.46	0.64	0.93	53	**75**	108	86	**166.24**	320.016	**150**	**0.50**

Notes: W/D = width to depth ratio; CSA = cross-sectional area; WP = wetted perimeter; R = hydraulic radius; S = slope; n = Manning's roughness coefficient; v = velocity; Q_{BKF} = bankfull flood discharge; Q_2 = discharge of 2 yr recurrence interval flood. See Table 1 for methods used to calculate the weighted and regional flood frequency curve estimates of Q_2. The mean Q_2 predicted by the regional flood frequency curve was used for the paleoQ_{BKF}/Q_2 modern channel ratio for the Congaree and Pee Dee sites, where weighted estimates of Q_2 were unavailable. The weighted estimate of Q_2 was used in all other cases.

CHAPTER 4 – SPATIO-TEMPORAL SOIL VARIABILITY ON LATE QUATERNARY FLUVIAL SURFACES OF THE PEE DEE RIVER VALLEY, SOUTHEASTERN ATLANTIC COASTAL PLAIN, USA[1]

[1]Suther, B.E. and Leigh, D.S. To be submitted to *Catena*.

Abstract

Soil variability and development are evaluated across a chronosequence of optically-dated meandering channel scroll bar deposits in the Pee Dee River valley of the South Carolina Coastal Plain that range in age from Holocene to 119±30 ka. Soils on older and younger scroll bars of three paleomeander surfaces of different age were examined to assess soil variability within individual scroll bars, among scroll bars on the same fluvial surface, and among scroll bars on fluvial surfaces of different age. Twenty four pedons per scroll bar were characterized with respect to their gross morphology and the morphological and chemical properties of the most pedogenically well-expressed B-horizon per pedon after conducting a pilot study to determine the number of profiles required to adequately represent variability on an individual scroll bar. Pee Dee soils become more developed across the chronosequence, as indicated by increases in solum thickness, cumulative B-horizon thickness, rubification, and dithionite-iron to total iron, and decreases in the concentrations of bases in both the whole soil and fine sand fractions. B-horizon and solum thickness appear to increase gradually with time, suggesting progressive development, while changes in the bulk chemistry of the whole soil and fine sand fractions representative of mineral weathering trends, appear to change episodically.

Within individual scroll bars, soil variability is considerable and reflects variation in local relief and the thickness and texture of the vertical accretion deposits that constitute the soil parent material, with soils exhibiting increasing B-horizon and solum thickness, higher clay content, and lower rubification in the downstream direction along scroll bars characterized by downstream decreases in local relief and downstream increases in the thickness and clay content of vertical accretion sediments. Among older versus younger scroll bars of the same paleomeander surface, in some cases, variability may be linked to systematic spatial variation in

the thickness and texture of vertical accretion deposits across the surface, with thicker, more finely textured B-horizons and sola being associated with older scroll bars located on the interior of paleomeander surfaces that have been subjected to overbank sedimentation in lower energy floodplain positions for greater durations of time. In other instances, the thicker B horizons and sola of soils on scroll bars on the interiors of paleomeander surfaces may simply reflect a greater duration of pedogenesis. These findings demonstrate the importance of understanding of soil variability within geomorphic surfaces of uniform age when conducting chronosequence studies and suggest that sampling strategies designed to account for both the central tendency and range of soil development on a given surface are advisable.

4.1. Introduction

Soil geographers and pedologists have long recognized that soil spatial variability occurs in all landscapes and at multiple scales (Campbell, 1979; Barrett and Schaetzl, 1993). On a given geomorphic surface, soils may vary predictably, in response to known geomorphic and soil-forming factors (Wilding and Drees, 1983), or unpredictably, without any apparent relationship to practicably measurable changes in such conditions (Phillips, 1993a; 2001; Phillips et al., 1996). Soil spatial variability has particularly important implications for soil chronosequence studies, which evaluate the influence of time on soil development. A soil chronosequence is a group of soils developed on geomorphic surfaces of different age for which the soil-forming factors of climate, biota, relief, and parent material have been approximately equivalent (Jenny, 1941; Yaalon, 1975; Birkeland, 1999). Although these factors are never truly constant over the time period of study, the time factor in a valid chronosequence has such

disproportional influence relative to the other factors that the effect of time on soil genesis can be estimated (Schaetzl and Anderson, 2005).

Soil chronosequences are useful for dating and correlating geomorphic surfaces (Birkeland, 1999), and in this capacity chronosequence data have been used in tandem with other dating techniques to provide a chronologic framework for archaeological investigations (Holliday, 2004) and in geologic mapping (Markewich et al., 1989). Furthermore, soil chronosequences remain the pedologist's primary source for empirical data to evaluate rates of soil development (Schaetzl et al., 1994) and to test theories of pedogenesis (Huggett, 1998). However, spatial variability among soils of equivalent age can pose both theoretical and practical problems for chronosequence studies (Harrison et al., 1990; Schaetzl et al., 2006) and has been identified as a major source of error in mathematical chronofunctions used to model soil formation rates (Schaetzl et al., 1994). Within the context of a soil chronosequence, adequate representation of soil spatial variability on isochronous surfaces is needed before temporal changes in soil variability can be assessed (Barrett and Schaetzl, 1993); dominant processes (Harrison et al., 1990) and direction of pedogenesis (Johnson and Watson-Stegner, 1987) can be ascertained; competing models of pedogenesis can be tested (Huggett, 1998), and the effect of time on soil formation can be estimated (Eppes and Harrison, 1999).

Although recent empirical and theoretical research highlights the degree of spatial variability possible on an individual geomorphic surface of uniform age in the southeastern Coastal Plain and elsewhere (Phillips, 1993a; Phillips, 1993b; Phillips et al. 1996; Phillips, 2001; Schaetzl et al., 2006), relatively few studies addressing the impact of intra-landform soil variability on chronosequence interpretations have been conducted (Sondheim and Standish, 1983; Harrison et al., 1990; Barrett and Schaetzl, 1993; Eppes and Harrison, 1999; Saldaña and

Ibáñez, 2008). This study examines the range of soil development within and among late Quaternary fluvial surfaces of different age in the Pee Dee River valley in the South Carolina Coastal Plain in order to assess spatio-temporal trends of soil variability and development and evaluate potential drivers of these changes. The main objectives of this research are to 1) characterize the range of soil development within fluvial surfaces of different age, with a focus on soils developed on the scrollbar components of these surfaces; 2) assess age-related trends in soil spatial variability and pedogenic development; and 3) identify possible drivers and pedogenic processes responsible for spatial and temporal soil variation. This study is unique in that it examines soil variability at a level of spatial and temporal resolution not achieved by previously published chronosequences in the region, across an age range that spans the past approximately 100 ka. The southeastern Coastal Plain is ideally suited for this research, given that it is a region of notorious soil variability (Daniels and Gamble, 1967; Phillips et al., 1994) where soil chronosequence data have been employed to estimate the age of surficial deposits (Markewich et al., 1989) and continue to prove useful for evaluating pedogenic processes and understanding relationships between soil genesis and time (Markewich et al., 1986; 1987; 1988; Howard et al., 1993; Shaw et al., 2003; Suther, 2006).

4.2. Study Area

The soils examined by this study developed in late Quaternary alluvium of the Pee Dee River valley in the Atlantic Coastal Plain of South Carolina (Fig. 4.1). The Pee Dee valley ranges from 10 to 15 km wide and contains a wide array of late Quaternary fluvial and eolian landforms, including multiple fluvial terraces that preserve well-expressed former braided and meandering channel patterns (Leigh et al., 2004; Leigh, 2006) and source-bordering riverine

dunes (Ivester and Leigh, 2003). Alluvium underlying these terraces is sourced from the saprolite that mantles Paleozoic crystalline rocks of the Appalachian Piedmont and Blue Ridge provinces and the sandy, unconsolidated Late Cretaceous and younger marine and fluvial sediments of the Atlantic Coastal Plain. In this setting, parent sediments are similar enough to allow comparisons of alluvial soils among different fluvial terrace levels. The climate of the southeastern Coastal Plain is humid subtropical, with a mean annual temperature of about 15-20 °C and mean annual precipitation of 1100-1200 mm/yr. The soil temperature regime is thermic (USDA-NRCS, 1997a), and the soil moisture regime is udic (USDA-NRCS, 1997b). Native vegetation consists of deciduous, mixed, and southern pine forests and has been altered by agriculture and silviculture during historical time. Soil development in the region is thought to progress along an Inceptisol to Alfisol to Ultisol genetic pathway in moderately to well sorted sediments like those of the Oconee-Altamaha and Pee Dee valleys that have mixed mineralogies (Markewich and Pavich, 1991). In such environments, Ultisols predominate and Alfisols are uncommon, due to the intensity of leaching and possibly because the transition from Alfisols to Ultisols is rapid (Markewich and Pavich, 1991).

This study examines soils developed on the scrollbar components of Sangamon to early Wisconsin, terminal Pleistocene, and Holocene age fluvial surfaces constructed by former meandering phases of the Pee Dee River (Figs. 4.1 and 4.2). Scrollbars preserved on these surfaces represent former point bars deposited by meandering channels and are 300 to >3000 m in length and 10 to 70 m wide. They are clearly evident on aerial photography, satellite imagery, and in the field. Because deposition is essentially contemporaneous along the entire length of a scrollbar relative to timescales of soil formation, an individual scrollbar constitutes a landform of uniform age.

On the terminal Pleistocene and Holocene surfaces (Figs. 4.1A-B, 4.2A-B), soil survey maps typically do not differentiate scrollbar soils from soils occupying adjacent swales and meander scars. However, field observations indicate scrollbar soils are better drained than their swale and meander scar counterparts and formed in somewhat coarser alluvial sediments. Terminal Pleistocene and Holocene scroll bars evaluated by this study are predominantly mapped as a complex of the Chastain and Chewacla series (Fine, mixed, semiactive, acid, thermic Fluvaquentic Endoaquepts, and Fine-loamy, mixed, active, thermic Fluvaquentic Dystrudepts, respectively; Morton, 2006), but portions of some scroll bars occur within units of Chewacla clay loam (same taxonomic classification as above) or Riverview silt loam (fine-loamy, mixed, active, thermic Fluvaquentic Dystrudepts; Morton, 2006). The terminal Pleistocene surface examined by this study contains relict, riverine eolian dunes that have reworked and on-lapped large tracts of scrollwork topography and occur in close spatial association with scroll bars (Figs. 4.1B and 4.2B). These dunes are thought to have formed from sand blown from scroll bars during the terminal Pleistocene (Leigh, 2008) and are mapped as either Tarboro sand (Mixed, thermic Typic Udipsamments) or Lakeland sand (thermic, coated Typic Udipsamments; Morton, 2006), and units of Tarboro sand extend onto the upstream ends of some scroll bars in this area. Soil survey map unit geometries more clearly reflect scrollwork topography on the Sangamon to early Wisconsin age paleomeander (Figs. 4.1C and 4.2C), with scrollbar positions predominantly occupied by Cahaba loamy sand (Fine-loamy, siliceous, semiactive, thermic Typic Hapludults), Persanti fine sandy loam (Fine, kaolinitic, thermic Aquic Paleudults), Hiwassee fine sandy loam (Fine, kaolinitic, thermic Rhodic Kanhapludults) and Smithboro silt loam (Fine, kaolinitic, thermic Aeric Paleaquults) (Pitts, 1980).

4.3. Methods

4.3.1 Site selection and sampling design

Soils developed on the scrollbar components of paleomeander surfaces were specifically targeted to reduce among site variation in parent material, topography, and drainage and to narrowly isolate the influence of time on soil variability and development. Paleomeander surfaces were selected for study because age relationships among their individual geomorphic components are readily inferred from spatial relationships. On the inside bend of a paleomeander, the age of scrollwork topography (and thus soil age, assuming soil formation begins immediately following scrollwork deposition), increases with distance from the paleochannel. Thus, for scrollwork of a given paleochannel, investigation of changes in soil development over short timescales (between younger and older scroll bars) and analysis of variability on a single geomorphic component of uniform age (an individual scrollbar) are both readily accomplished.

A random, linear sampling design was used to evaluate soil variability at multiple spatial and temporal scales, including variation:

-within individual scrollbars of uniform age;

-among scrollbars of different age on a the same fluvial surface; and

-among scrollbars of different age fluvial surfaces within the Pee Dee River valley.

Three paleomeander surfaces were sampled: the Holocene floodplain (Fig. 4.2A) which has yet to be precisely dated; a terminal Pleistocene surface (Fig. 4.2B) dated in the range of 13-17 ka by Leigh et al. (2004) and characterized by an unusually large meandering paleochannel, pronounced scrollwork topography, and eolian dunes; and a Sangamon to early Wisconsin paleomeander terrace (Fig. 4.2C) that predates 69 ka (Leigh et al., 2004). On each paleomeander

surface, two widely separated scrollbars of the same paleochannel were sampled to facilitate evaluation of changes in soil development over shorter timespans: an outer, younger scroll bar in relatively close proximity to the paleochannel, and an older, inner scrollbar deposited by an earlier phase of the channel (Fig. 4.2). This resulted in a total of 6 sampled scrollbars.

For the purposes of this study, the Sangamon to early Wisconsin paleomeander terrace, which is the oldest of the three paleomeander surfaces examined, is referred to as PD1, as it was deposited first. In turn, the terminal Pleistocene and Holocene paleomeander surfaces are respectively referred to as PD2 and PD3. In keeping with this convention, on each surface, the older, inner scroll bar is site one, while the younger, outer scroll bar is site two. Thus, "PD1-1" refers to the older scroll bar on the Sangamon to early Wisconsin paleomeander surface, while the younger scroll bar on this surface is referred to as "PD1-2" (Fig. 4.2C).

4.3.2 Pilot study

In January 2013, a pilot study was conducted to determine the sample size needed to characterize soil spatial variability on a single scroll bar in the Pee Dee River valley in order to guide sampling at the remaining field sites. Because previous studies suggest soil variability in the Coastal Plain increases with age (Phillips, 1993a; 2001), the pilot scroll bar (PD1-2, Fig. 4.2C) was selected from a Sangamon to early Wisconsin age terrace to avoid under-representing the potentially greater variability on such surfaces. The study examined 50 soil profiles spaced at random along a linear transect following the crest of the pilot scroll bar. To ensure that the same pedon was not sampled twice and that possible soil variation resulting from changes in scrollbar width was resolved, spacing between borings was at least twice the width of a typical pedon (~1.5 m) and less than the width of the scrollbar at its narrowest point (~40.0 m). Profiles

were sampled by hand auger, and, at each sampling location, a morphological description was recorded using standard NRCS terminology (Soil Survey Division Staff, 1993) that included: horizonation, color, texture, structure, consistence, clay films, and redoximorphic features. Soil morphological properties that have been shown by previous studies to be valuable chronosequence parameters in the Atlantic Coastal Plain, including solum thickness and the thickness and rubification of the Bt horizon (Markewich et al., 1989; Howard et al., 1993; Suther, 2006), were determined for each profile. Figure 4.3 depicts the variability in gross soil morphology, including horizonation and Bt horizon morphological properties, encountered along the pilot scroll bar transect. Soil variability observed on PD1-2 and the other scroll bars evaluated by this study are discussed in detail in section 4.4.2, and interpretations of possible drivers of intra-scroll bar variability are provided.

A resampling approach was applied to the pilot data using the statistical program R (R Core Team, 2013) to determine the appropriate sample size per scroll bar. This approach was designed to indicate how effective a given sample size is at representing the variation of a parent population (in this case, soils on the pilot scroll bar), and it relies on two assumptions: 1) that the sample of n=50 pedons is representative of the true variability among all pedons on the pilot scroll bar, and 2) that the soil variability on the pilot scroll bar is typical of scroll bar soil variability throughout the study area. Resampling was conducted as follows: 100 trials of each sample size of n=2 through n=50 were drawn with replacement from the 50 values for each soil morphological parameter obtained from the pilot study (solum thickness, A+E thickness, and Bt horizon thickness and rubification, among others), and the standard deviation of each of these trials was calculated for each parameter. Results were then interpreted graphically to determine an appropriate sample size.

Figure 4.4 plots standard deviation vs. sample size for A+E thickness, Bt horizon thickness, solum thickness, and rubification. As sample size increases, the standard error of the resampled standard deviations for each parameter decreases, and sample variation approaches that of the "parent population". However, beyond some sample size *n*, each successive sample's representation of population variation improves only slightly, and the benefit of larger sample sizes diminishes. This study considered a sample of size *n* to sufficiently represent the soil variability on the pilot scrollbar when the standard error of resampled standard deviations associated with that sample size was less than twice the standard error of standard deviations at *n*=50. Inspection of Figure 4.4 reveals that this occurs at a sample size of approximately *n*= 20 to 30. Based on these results, a sample size of *n*=24 was considered to adequately represent soil spatial variability on the pilot scroll bar, and 24 profiles per scroll bar were examined at the remaining field sites.

4.3.3 Field and laboratory methods

The morphology and chemistry of scrollbar soils were examined, with a focus on properties that have been shown to be valuable chronosequence parameters in the Atlantic Coastal Plain (Markewich et al., 1989; Howard et al., 1993; Suther, 2006). Soil morphological properties that were evaluated include: solum thickness, cumulative B and Bt horizon thickness, and the clay content and rubification of the most pedogenically well-expressed B horizon per pedon. Rubification values were calculated using the indices of Buntley-Westin (1965) and Hurst (1977). The Buntley-Westin Index increases with increasing redness by assigning a numerical value to the Munsell hue and multiplying it by the chroma, while the Hurst Index decreases with increasing redness by assigning a numerical value to the Munsell hue and

multiplying it by the fraction of value / chroma. Soil chemical properties were evaluated for the most pedogenically well-expressed B horizon per profile and consist of: dithionite-extractable iron (Fe_D) of the whole soil (<2 mm) and the total chemistry of the whole soil and the fine sand (0.125-0.250 mm) fraction.

For each scroll bar, 24 pedons were examined along a linear transect that followed the scroll bar ridge crest (Fig. 4.2). Sampling locations were spaced at random intervals and spanned the entire length of the scroll bar except in the case of scroll bars PD2-1 and PD2-2, where transects were shortened to avoid eolian sediments in order to ensure comparability in parent material among sites (Fig. 4.2B). A hand auger was used for sampling, and borings were located using a hand-held GPS unit. Profile descriptions that included horizonation, color, texture, structure, clay films, redoximorphic features, and horizon boundaries were conducted for each pedon using standard NRCS terminology (Soil Survey Staff, 1993), and the moist consistence, stickiness, and plasticity of the most well-expressed B-horizon per pedon were noted. In all cases, the entire profile, including the C horizon (unweathered alluvium) was described. One sample from the most pedogenically well-expressed B-horizon was collected per pedon and retained for particle size and chemical analysis.

Particle size analysis by the pipette method (Gee and Bauder, 1986) and determination of dithionite-extractable iron oxide content by USDA Soil Conservation Service citrate-dithionite extraction procedure 6C2 (Soil Survey Laboratory Staff, 1992) were performed at the University of Georgia (UGA) Laboratory for Environmental Analysis. Elemental analysis of the whole soil and fine sand fraction was performed by inductively coupled plasma mass spectrometry (ICP-MS) by ALS Geochemistry following a four acid “near total” digest.

4.3.4 Optically-stimulated luminescence (OSL) dating

Optically-stimulated luminescence (OSL) dating was conducted to provide numerical age estimates for scroll bars on the PD1 and PD2 surfaces. Ages for scroll bars on the PD3 surface were estimated based on chronologic context provided by well-dated bounding deposits and estimates of Holocene river channel lateral migration rates from elsewhere in the Coastal Plain (see section 4.4.1.3). For the PD1 and PD2 scroll bars, samples for OSL dating were obtained from sandy lateral accretion sediment. OSL samples were collected by pounding a 7-cm diameter light-tight metal tube into the base of a hand-augered hole. In all cases, OSL dating was conducted on unweathered (C horizon) quartz-rich sediment. Equivalent dose was determined at the UGA Luminescence Dating Laboratory by the single aliquot regenerative dose (SAR) protocol (Murray and Wintle, 2000) from 125-250 μm quartz sand that was pretreated to remove carbonates, organic matter, and the alpha skin. For all samples, 19-24 aliquots of 9.6 mm diameter were analyzed. Dose rate calculation was based on the thick source ZnS (Ag) alpha counting technique for elemental concentration of uranium and thorium, and potassium was measured by ICP90 with a detection limit of ±0.1%, using the Sodium Peroxide fusion technique at the SGS Laboratory in Toronto, Canada. Cosmic ray gamma contribution was calculated according to the guidance of Prescott and Stephan (1982). Water content was directly measured and used to generate an estimate and uncertainty for pore water content since the time of sample deposition. Additional details regarding OSL dating procedures are provided in Section 2.3.3.2 of Chapter 2 of this document.

4.4. Results and Discussion

Soil variability and development were examined at the scale of individual scroll bars, among scroll bars of the same paleomeander surface, and among scroll bars of the PD1, PD2, and PD3 paleomeander surfaces that together comprise the complete chronosequence. Soil age estimates were determined either by OSL dating or from the best available data. Results of these analyses are provided in the sections below, along with interpretations regarding the degree and drivers of soil variability encountered at each scale of the study.

4.4.1 Scroll bar age estimates

4.4.1.1 PD1 scroll bars

OSL dating indicates that the chronosequence of Pee Dee River scroll bars documented by this study spans the past approximately 100 ka (Table 4.1). Lateral accretion sand obtained from a depth of 180-210 cm at the 1.5 m distance on the pilot study transect yielded a 107.8±24.9 ka (82.9-136.7 ka) age estimate for the PD1-2 scroll bar, given the 2-sigma error associated with the date (Table 4.1, Fig. 4.2C). The paleomeander terrace that contains the PD1 site is cross-cut to the west by an extensive braided river terrace, identified and mapped by Leigh et al. (2004) as the fourth braid terrace ("BT4") of the Pee Dee River valley (see Fig. 6 of Leigh et al., 2004). Leigh et al. report an OSL age estimate of 68.6±10.5 ka from a braided braid bar at a location on the braid terrace about 10.5 km northwest of the PD1 site (see Fig. 4.1). Because PD1 deposits are cross-cut and must therefore be older than BT4 sediments, we regard the age estimates of the PD1-2 scroll bar and the BT4 braid terrace to be in good agreement and consider the 107.8± 24.9 ka date obtained from PD1-2 to be a reasonable estimate.

OSL dating of upper lateral accretion sediment from the PD1-1 scroll bar, which should slightly predate the age of PD1-2 based on the direction of lateral migration of the PD1 paleomeander indicated by scrollwork topography (Fig. 4.2C), yielded a bimodal equivalent dose distribution. The younger mode of this distribution, composed of 11 aliquots, returned a date of 61.3±14.8 ka, while the older mode, composed of 8 aliquots, yielded an age of 118.8±30.4 ka (Fong Z. Brook, University of Georgia Luminescence Dating Laboratory, personal communication, 2013). This bimodal equivalent dose distribution indicates that the PD1-1 sample contains a mixture of grains of different OSL ages. Given the context provided by the age estimates of PD1-2 (107.8±24.9 ka) and braid terrace BT4 of Leigh et al. (68.6±10.5 ka) discussed above, we consider the bimodal equivalent dose distribution of the PD1-1 sample to reflect contamination of older sediments with grains that have a younger OSL signal. In light of the high likelihood that bioturbative processes were operative throughout the late Quaternary in soils and unconsolidated sediments of the southeastern Coastal Plain based on current understanding of paleovegetation and paleoenvironments of the region (Leigh, 2008), and given that the great age of PD1 deposits would have provided ample time for such processes to operate, it is possible that bioturbation translocated bleached grains from at or near the surface of the PD1-1 profile to the depth of the OSL sample.

Given the chronologic context provided by the PD1-2 and BT4 OSL dates discussed above, and taking into account that PD1-1 sediments appear to have been contaminated by younger grains, we consider the date of 118.8±30.4 ka yielded by the older mode of the PD1-1 equivalent dose distribution to provide a more accurate age estimate for the PD1-1 scroll bar than the 61.3±14.8 ka date produced by the younger mode. Therefore, a mean age estimate of 118.8 ka has been assumed for the PD1-1 soils evaluated in this study.

4.4.1.2 PD2 scroll bars

Leigh et al. (2004) report an OSL age of 13.8±2.2 ka from lateral accretion sediment of the PD2-2 scroll bar, which they considered to be a reliable age estimate based on its close correlation to a calibrated radiocarbon date of 13.2-13.8 ka obtained from basal channel fill of the adjacent, unusually large meandering paleochannel (known as the "Damon mega-meander") that deposited the scroll bars of the PD2 surface (Fig. 4.2B). The PD2-1 scroll bar, located on the northeastern portion of the PD2 surface about 2.7 km to the northeast of the PD2-2 site, returned an OSL age of 23.1±4.5 ka (Table 4.1; Fig. 4.2B). In addition to the dates reported for the PD2-2 scroll bar and Damon mega-meander, Leigh et al. presented two radiocarbon and three OSL dates from several locations about 15 km north of the PD2 locality that collectively indicate that the Pee Dee River transitioned from a low sinuosity scroll bar pattern to the very high sinuosity pattern exhibited on the PD2 surface around 14-17 ka. This evidence suggests that the mean of the PD2-1 OSL date (23.1 ka) is likely a slight overestimate. This is also indicated by the 15.0±1.4 ka age reported by Leigh et al. for the dune overlying intervening scroll bars between the PD2-1 and PD2-2 sites, if relatively uniform rates of lateral migration are assumed (Fig. 4.2B). If the 23.1 ka date is an overestimate, it may reflect some degree of inherited age resulting from incomplete bleaching of grains during transport, given that fluvial sediments sometimes suffer from this condition (Stokes and Walling, 2003) and that sediments from similar depositional environments dated by the author elsewhere in the Coastal Plain appear to exhibit the same problem when compared to radiocarbon-dated samples known to be of relatively comparable age (see Chapter 3, this document). For the purposes of this study, the mean age of 23.1 ka is nonetheless assigned to the PD2-1 scroll bar, but the reader should be aware that soils on this surface may be slightly younger than this. Although the present study relies on mean

OSL ages for soil chronosequence interpretations (see section 4.4.4), future work will explore the use of a minimum age model that relies on the aliquot in each sample with the minimum measured equivalent dose to improve the accuracy and precision of scroll bar OSL age estimates. Future research will also attempt to better account for uncertainty in OSL age estimates by employing a Monte-Carlo approach similar to that of Switzer et al. (1988), which has the potential to improve soil chronosequence analyses by considering the full uncertainty associated with each soil age estimate.

4.4.1.3 PD3 scroll bars

OSL age estimates are not available for the PD3-1 and PD3-2 scroll bars. To facilitate soil chronosequence interpretations for PD3 soils in the absence of numerical age estimates, Holocene ages were assigned to these scroll bars based on 1) chronological context provided by adjacent deposits and 2) estimates of Holocene river channel lateral migration rates from elsewhere in the southeastern Coastal Plain. Radiocarbon and OSL dates reported by Leigh et al. (2004) indicate that the Damon mega-meander paleochannel of the PD2 surface was abandoned ca. 13.4-13.8 ka and that PD2 fluvial sediments can be no younger than 13-14 ka (see Fig. 4.2B and discussion above). Because the PD3 surface cross-cuts, and therefore must be younger than, the PD2 surface, the dates of Leigh et al. strongly indicate that the PD3 scroll bars are younger than 13-14 ka. In the absence of additional contextual dates in the area, the PD3 surface was assigned an age of 6.9 ka. This estimate reflects the arithmetic average of between the present (0 ka) and the 13.8 ka date of Leigh et al., which represents the latest date that the PD2 surface received active lateral accretion sedimentation from the Pee Dee River, as indicated by the mean OSL age estimate of the PD2-2 scroll bar (Fig. 4.2B, Table 4.1).

To account for the age difference between the two PD3 scroll bars, the 6.9 ka age estimate was assigned to a location on the PD3 surface midway between the PD3-1 and PD3-2 scroll bars. Then an average long-term lateral migration rate of 0.15 m/yr, derived from OSL-dated Holocene scroll bars of the nearby Wateree River (Whitley and Leigh, 2005), was used to estimate the age difference between the two scroll bars. This resulted in respective age estimates for PD3-1 and PD3-2 of 8.3 ka and 5.5 ka. While admittedly it would be preferable to have numerical dates for these deposits, this approach provides the best age estimates for the PD3 scroll bars given the available data. Future research will include OSL dating of the PD3 scroll bars and will incorporate resulting age estimates into analysis of the Pee Dee chronosequence. However, given that the entire chronosequence spans a timeframe of about ~100 ka, it is unlikely that age adjustments of Holocene timescales will have a substantive effect on the major chronosequence interpretations that this study provides.

4.4.2 Soil variability within individual scroll bars

4.4.2.1 Soil morphology

Within individual scroll bars, Pee Dee soils exhibit considerable variability with respect to solum thickness, cumulative B-horizon thickness, and the rubification and clay content of the most well expressed B-horizon (Table 4.2). For the six scroll bars examined, the standard deviation and interquartile ranges of B-horizon thickness respectively ranged from 16.3-31.8 cm and 18-43 cm. A similar degree of variability was observed for solum thickness. Standard deviations, interquartile ranges, and minimum-maximum ranges for rubification as measured by the Buntley-Westin Index respectively spanned 1.6-12.2, 0-24.0, and 6-32 index units. The lowest minimum-maximum range for Buntley-Westin Index unit rubification (6) was associated

with B horizons of PD3-1 soils and is represented by Munsell colors from 10YR 5/4 to 10YR 4/6. The largest minimum-maximum range for Buntley-Westin Index unit rubification (32) was associated with B horizons of PD1-1 soils and reflects Munsell colors from 2.5Y 5/4 to 5YR 4/8. Hurst index values, which incorporate not only hue and chroma but also color value, displayed even greater intra-scroll bar variability. Standard deviations for clay content in B-horizons of soils within individual scroll bars ranged from 1.7-13.8%, with inter-quartile ranges that spanned 2-27%. Variability in B-horizon thickness, rubification, and clay content as measured by standard deviation is consistently higher for scroll bar soils on the PD1 and PD2 surfaces versus soils on the PD3 scroll bars.

Field observations suggest that the gross morphology of soils on the PD1 and PD2 surfaces varies systematically from the upstream to downstream end of an individual scroll bar, with sola increasing in thickness and B-horizons exhibiting increasing thickness and clay content and decreasing matrix color rubification in the downstream direction (Fig. 4.3). Field inspection of the morphology and of soil-stratigraphic profiles of scroll bars of the PD1 and PD2 surfaces indicate that these scroll bars decrease in elevation and exhibit textural fining and an increase in the thickness of fine-grained (fine-loamy to clayey) vertical accretion sediments from their upstream to downstream ends. These changes in parent material and local relief were hypothesized to be in part responsible for the systematic trends observed between soil morphology and downstream distance along these scroll bars. To evaluate this hypothesis, individual soil properties of the most well-expressed B-horizon per profile were regressed against downstream distance as a proxy for the independent variables of parent material and scroll bar relief. This approach was used because sufficient quantitative data for the local relief and particle size distributions of scroll bar sediments were not available. The reader should note

that linear regression is used in this context simply to highlight trends in soil properties with respect to downstream distance, not as a predictive model, and that some assumptions of least squares regression, including normality of the dependent variables within their respective sample sets, normality of dependent variables about the regression line, constancy of variance, and linearity may have not been satisfied in some cases.

Among scroll bars of the PD1 and PD2 surfaces, soil morphological properties exhibit moderate to strong correlation with downstream distance in the majority of cases, with over half of the properties having R^2 values greater than 0.4 (Table 4.3). Both percent clay and B-horizon thickness showed a positive relationship with downstream distance, while B horizon rubification decreased in the downstream direction. Perhaps the best evidence for downstream trends in parent material is provided by B-horizon sand content and sand:silt ratios, which show moderate to strong, negative relationships with downstream distance on scroll bars PD1-2, PD2-1, and PD2-2 (Table 4.3). These data, which were obtained from B-horizons within the upper meter of every profile sampled, strongly indicate that vertical accretion on these three scroll bars fines in the downstream direction. Graphical depictions of regressions of soil properties versus downstream distance for scroll bars PD1-2 and PD2-1 are respectively provided in Figures 4.5 and 4.6 that give the reader with a feel for the magnitude of change displayed by soil properties from the upstream to the downstream ends of scroll bars on the PD1 and PD2 surfaces.

In contrast, regressions reveal that soil morphological properties on scroll bars PD3-1 and PD3-2 bear little to no relationship with downstream distance along the scroll bar ridge crest (Table 4.3, Fig. 4.7). Percent sand, the sand:silt ratio, and percent clay have statistically significant regression relationships with downstream distance on PD3-2, but the magnitude of the relationships are modest to negligible when compared to trends observed for PD1 and PD2

scroll bars. Relationships on PD3-1 are even weaker, with only rubification registering a significant relationship with downstream distance.

In large part, regression analysis confirms field observations of soil morphological trends along individual scroll bar ridge crests, and supports the interpretation that the character of the relationship between soil properties and downstream distance is different for scroll bars of the PD1 and PD2 surfaces versus those of the PD3 surface. Scroll bars of the PD1 and PD2 surfaces are arcuate in planform and were deposited in the context of deep meander bends within former channel reaches of the Pee Dee River that had a high degree of sinuosity (Fig. 4.2B and 4.2C). Field reconnaissance and LIDAR elevation data reveal that their longitudinal profiles are asymmetrical in cross-section and that these scroll bars decrease in elevation from their upstream to downstream ends (Fig. 4.3) relative to adjacent swales. In concert with this downstream change in relief, field inspection of numerous (n=24) soil-stratigraphic profiles per scroll bar indicates that vertical accretion sediments both thicken and fine in the downstream direction, and support for downstream fining of scroll bar sediments is provided by B horizon sand and silt fraction data, as noted above.

Based on the evidence presented above, systematic downstream changes in scroll bar relief, sedimentology, and stratigraphy are interpreted as exerting a substantial influence on the variability in gross soil morphology at the scale of individual scroll bars on the PD1 and PD2 surfaces. The negative relationship between B-horizon rubification and downstream distance exhibited by soils on the PD1-1, PD1-2, and PD2-2 scroll bars (Table 4.3), likely reflects the influence of a decrease in local relief from the upstream to downstream ends of scroll bars on soil drainage status. This systematic change in relief results in an increasingly less well-drained pedoenvironment along the scroll bar ridge crest in the downstream direction, which influences

the formation of pedogenic iron oxides and the types of iron oxide minerals present. The largest systematic changes in rubification with respect to downstream distance occurs on the PD1 scroll bars, which transition from 2.5YR (PD1-1) and 5YR (PD1-2, see Fig. 4.3) hues on their upstream ends to 10YR (PD1-1) and 10YR to 2.5Y (PD1-2) hues in the downstream direction. This color transition indicates that hematite, which characteristically has 5YR and redder hues and favors more well-drained pedoenvironments (Schwertmann and Taylor, 1989) does not occur at the scale of a major soil-matrix pigmenting agent on the downstream reaches of scroll bars, which exhibit yellow brown and orange B-horizons hues that respectively reflect the presence of goethite and possibly lepidocrocite (Schwertmann and Taylor, 1989). Interestingly, systematic changes in soil drainage status in the downstream direction along scroll bars and their effects on pedogenic iron oxide formation and soil color also appear to influence the number of B horizons present at some sites, since variation in soil matrix color and the abundance of redoximorphic features, including iron oxide concentrations and depletions, often resulted in subdivision of B horizons that were otherwise relatively similar with respect to texture, structure, and other properties. This circumstance was most pronounced on the PD1-2 scroll bar (Fig. 4.3) but was also observed elsewhere.

Perhaps the most interesting spatial trend in soil variability observed on individual scroll bars on the PD1 and PD2 surfaces is that cumulative B-horizon thickness (and Bt-horizon thickness on the PD1 surface) is greater on the middle and downstream reaches of scroll bars, which tend to have lower local relief and exhibit poorer drainage. This may seem counterintuitive, since one might suspect, based on conventional toposequence relationships, that soils would be deepest, and B- and Bt-horizons would be thickest, at locally higher landcape positions where leaching would be greatest and the weathering environment would be most

intense. However, B-horizon thickness appears to be linked to the thickness of clay-rich, vertical accretion deposits, which increases from the upstream to downstream ends of PD1 and PD2 scroll bars. On the upstream ends of these landforms, the boundary between the B- and underlying C-horizons roughly coincides with a gradational to abrupt contact between clayey to fine loamy vertical accretion sediments and underlying medium to coarse, single-grained sands. On the middle and downstream portions of scroll bars, the boundary between B- versus C- (or transitional BC and CB) horizons does not coincide with such a marked textural contrast but instead occurs at a point below which B-horizon properties, most notably subangular blocky pedogenic structure of moderate to weak grade, are no longer found, well within the larger package of vertical accretion sediments (which at these landscape positions extends to a greater depth).

These soil-stratigraphic relationships appear to indicate that the thickness of vertical accretion deposits exerts some influence on the thickness of B-horizons on the PD1 and PD2 scroll bars. Vertical accretion sediments are thinner on the upstream ends of PD1 and PD2 scroll bars, and single-grained medium to coarse lateral accretions sands occur at shallower depths within soil profiles at these landscape positions. While soils on such upstream scroll bar positions are freely drained and the textural contrast between fine-grained vertical accretion sediments and sandy lateral accretion deposits certainly would not impose hydrologic or pedologic limiations in the way that channel lag gravels or bedrock might, even on ~100 ka PD1 scroll bars, it appears that pedogenesis has not extended to sufficient depths to overprint and obscure the gradational to abrupt lithologic contact between vertical and lateral accretion sediments beyond oxidation and modest mixing of lateral accretion deposits in their upper part. These relationships suggest that pedogenic processes capable of enriching the clay content of

lateral accretion sediments and obscuring their contact with overlying vertical accretion deposits on the upstream ends of scroll bars, such as clay translocation, in-situ formation of clays by weathering, and profile mixing processes, may proceed at a slower rate than the formation of soil structure in clayey vertical accretion deposits, given that deterioration of pedogenic structure marks the boundary between B- and C- (or B and BC to CB) horizons within vertical accretion sediments on the middle and downstream reaches of scroll bars.

The virtual lack of association between soil morphological properties and downstream distance observed for the PD3-1 and PD3-2 scroll bars (Table 4.3, Fig. 4.7) probably results from the relative uniformity that these scroll bars exhibit across their entire length with respect to both local relief and the sedimentology and stratigraphy of their deposits. Figure 4.7A depicts the longitudinal topographic profile of scroll bar PD3-2, which, like scroll bar PD3-1, exhibits very little elevation change across its entire length, resulting in little change in local relief relative to the adjacent swales. PD3-1 and PD3-2 sediments also have relatively consistent properties along their respective lengths, and are characterized by thick vertical accretion deposits that exhibit modest to little downstream fining in their upper part (Table 4.3, Figure 4.7B, C, and D). Furthermore, definitive sandy, lateral accretion sediments were never encountered in PD3 profiles during field sampling, even in borings up to 3 m deep. The relative lack of variability in local relief and parent material are thought to be at least in part responsible for the lower variability that PD3 soils exhibit relative to PD1 and PD2 with respect to B-horizon thickness, rubification, and clay content. However, given the relatively youthful (Holocene) age of PD3 soils, it is likely that their lower variability may also partially reflect the fact that insufficient time has elapsed for other pedogenic processes not directly linked to systematic changes in

parent material and local relief to result in differentiation of soils across the scroll bars of this surface.

4.4.2.2 Soil chemistry

Descriptive statistics for soil chemical parameters of the <2 mm and fine sand (0.125-0.250 mm) fraction observed for the most well-expressed B horizon per pedon on individual scroll bars are provided in Tables 4.4 and 4.5. Dithionite-iron data are available for all soils in the chronosequence. Major element oxide concentrations for the whole soil and fine sand fraction are available for all soils except those of the PD3-1 scroll bar. Future research will include elemental analysis of PD3-1 soils and will incorporate PD3-1 chemical data into the assessment of soil variability and development both within and among individual scroll bars of the Pee Dee chronosequence.

In general, the coefficients of variation (standard deviation scaled to mean) of most <2 mm and fine sand chemical properties are slightly lower than those of soil morphological properties, indicating that B-horizon chemistry varies somewhat less that gross soil and B-horizon morphological properties at the scale of individual scroll bars. In order to evaluate whether B-horizon chemical properties, like morphological properties, exhibit correlations with downstream distance along scroll bar ridge crests, several key soil chemical parameters were regressed against downstream distance in the same manner as soil morphological properties, and results are shown in Table 4.3 and Figures 4.5, 4.6, and 4.7.

In general, relationships between B-horizon chemistry and longitudinal position on scroll bar ridge crests are weaker and less consistent than trends observed for soil morphological properties (Table 4.3). Whole soil (<2 mm) bases:alumina ratios exhibited moderate to strong,

negative correlations with downstream distance for four of the six scroll bars (PD1-2, PD2-2, PD2-1, and PD3-2), but regression relationships were only statistically significant at two of these sites, PD1-2 (R^2=0.66) and PD2-1 (R^2=0.74). Sites with the most pronounced decreases in B-horizon bases:alumina and bases:resistant oxide ratios also exhibited substantial increases in B-horizon clay content from upstream to downstream along scroll bar ridges, and the bases:alumina trends in these soils likely result from downstream increases in B-horizon clay content that are associated with increasing relative abundance of aluminum-rich phyllosilicate (clay) minerals, which occur in the clay fraction of soils. Dithionite-extractable iron exhibited a moderate to strong correlation with downstream distance on scroll bars PD1-2 and PD2-1, with respective R^2 values of 0.66 and 0.47, but relationships between dithionite iron and position on scroll bar ridges were weaker to non-existent on the other scroll bars. As observed for alumina content, the positive correlation between dithionite iron and downstream distance is strongest on scroll bars that exhibit considerable downstream increases in clay content. Because secondary iron oxides occur in the clay size fraction of soils (Schwertmann and Taylor, 1989), the greater dithionite iron contents of soils on downstream positions on the aforementioned scroll bars are probably simply a function of their greater clay content.

Within the fine sand fraction, individual bases (CaO, K_2O, MgO, and Na_2O) displayed relatively consistant weak to negative correlations with downstream distance, so they were summed as "total bases" and regressed against downstream distance to evaluate intra-scroll bar trends in fine sand fraction chemistry. Total bases exhibited moderate to strong, negative correlations with downstream position along three of the six Pee Dee scroll bars (PD2-1, PD2-2, and PD3-2) but exhibit little relationship with downstream distance along scroll bars of the PD1 surface (Table 4.3). Given the general trends in downstream textural fining observed for the

majority of the scroll bars in this study, a systematic decrease in total bases of the B-horizon fine sand faction along scroll bar ridges in the downstream direction may reflect a general decrease in abundance of sand-sized base-bearing heavy minerals relative to quartz as a result of hydraulic sorting, with heavy minerals being preferentially deposited in slightly higher energy locations on the upstream ends of scroll bars and excluded from lower energy downstream scroll bar positions. However, it is notable that the total bases in the fine sand fraction of Bt-horizons of the PD1-2 surface, which display downstream textural fining with respective to total sand and the sand:silt ratio, exhibit no relationship with downstream distance (Table 4.3). However this may reflect the fact that the majority of unstable, base-bearing minerals appear to have been depleted from these soils (see Section 4.4.4.2).

The above results indicate that trends exhibited by soil morphological properties along scroll bar ridges that are believed to reflect response to systematic changes in local relief and parent material are not as well expressed for B-horizon chemical properties. This may result from the fact that chemical data were obtained from samples collected from the middle to upper part of clayey to fine loamy vertical accretion deposits that, from profile to profile, are relatively similar with respect to their bulk chemistry apart from differences imparted by variations in particles size composition, in particular with respect to their clay content. This interpretation is supported by the fact that some of the strongest relationships between soil chemistry and longitudinal position along scroll bar ridge crests consist of downstream increases in dithionite iron and alumina that occur in settings that are also characterized by substantial downstream increases in clay content.

4.4.3 Soil variability within paleomeander surfaces

4.4.3.1 Soil morphology

Sample means of soil morphological properties suggest that on a given paleomeander surface, some variables show systematic trends in their central tendencies, depending upon whether or not they occur on the younger (outer) scroll bar or the older (inner) scroll bar (Table 4.2). These relationships appear to be particularly pronounced for B-horizon, Bt-horizon, and solum thickness and B-horizon clay content, as indicated by visual inspection of data in Figure 4.8, which plots morphological properties of scroll bar soils as a function of soil age. To determine whether soils on younger (outer) versus older (inner) scroll bars on an individual surface exhibit statistically significant, meaningful differences in the central tendencies of their respective morphological characteristics, parametric difference-of-means t-tests were applied to each group of younger versus older scroll bar soils within the PD1, PD2, and PD3 paleomeander surfaces. In addition to requiring random sampling, which this study provides, the t-test assumes that the means of the compared groups of soils are normally distributed. Because most of the soil morphological variables have roughly symmetrical distributions, and because sample size for each group of soils (n=24) was deemed sufficiently large to provide a normal distribution of means according to the central limit theorem, t-tests were conducted on non-transformed soil morphological data.

For each of the three paleomeander surfaces, t-tests indicate that soils on the older, inner scroll bar have greater cumulative B-horizon and solum thickness than those on the younger, outer scroll bar (Table 4.6). Bt horizons do not occur on the PD2 and PD3 surfaces, but the same relationship is observed for the cumulative Bt-horizon thickness of PD1 scroll bar soils. Generally, these differences are of meaningful magnitude, with soils on younger scroll bars

exhibiting mean cumulative B-horizon, Bt-horizon, and sola thicknesses that are respectively 14-53 cm, 60 cm, and 28-57 cm less than those on older scroll bars, based on the best estimates of t-tests (Table 4.6). The magnitude of the difference in mean rubification values for soils on older versus younger scroll bars on the same surface is less pronounced, and is only indicated by both the Buntley-Westin and Hurst Indices at a significance level of α=0.05 for the PD2 surface, where soils of the older scroll bar (PD2-1) have greater mean redness. Mean clay content appears to be greater for soils on older versus younger scroll bars for two of the three paleomeander surfaces, with soils on the younger scroll bars of the PD1 and PD3 surfaces having mean B-horizon clay contents that are respectively ~6% and ~14% lower than those of older scroll bars.

The consistently greater mean B-horizon, Bt-horizon, and sola thicknesses exhibited by soils of older scroll bars on the PD1 and PD2 surfaces may be linked to thickness of fine-grained vertical accretion deposits, which field observations indicate to be greater in these settings. As discussed above in section 4.4.2.1, at the scale of individual scroll bars, the thickness of fine grained-vertical accretion deposits appears to exert a degree of control on cumulative B horizon and solum thickness, with greater thicknesses of vertical accretion sediments being associated with thicker B (or Bt) horizons and deeper sola in the downstream direction along scroll bar ridge crests. Vertical accretion thickness may also exert control on thickness of B horizons and sola at a broader scale, among scroll bars across a paleomeander terrace surface. General increases in vertical accretion thickness observed on the PD1 and PD2 surfaces moving away from the abandoned paleomeander across younger, outer scroll bars, toward older scroll bars on the interiors of paleomeander surfaces are likely explained by the fact that inner scroll bars are older, have been subjected to overbank sedimentation for a greater duration of time, and as a

consequence have developed greater thicknesses of vertical accretion deposits. The fact that older, inner scroll bars occupy landscape positions that become progressively distal relative to the river as channels migrate laterally through time may account for the higher mean clay contents of inner scroll bar soils on the PD1 surface, given the decrease in particle size that is commonly observed with increasing distance from river channels in floodplain overbank sediments. If this explanatory model is correct, then the variability observed in B horizon thickness, solum thickness, and B horizon clay content among scroll bars of the PD1 and PD2 paleomeander surfaces does have a chronologic component, but one that more strongly reflects chronologic controls on spatio-temporal variation in parent material characteristics than differences in duration of exposure to weathering and pedogenesis. However, no difference in vertical accretion thickness was observed among scroll bars of the PD3 surface, and the greater mean B horizon and sola thicknesses exhibited by soils on the older scroll bar of this surface may simply reflect a greater duration of pedogenesis.

Mean B-horizon rubification values do not appear to differ as much as soil thickness and clay content among soils of older versus younger scroll bars on the same paleomeander surface (Table 4.6). The largest difference in rubification observed among scroll bars of the same surface, which occurs on PD2, probably results from sampling bias. In order to avoid eolian sediments on the upstream segment of the PD2-2 scroll bar, sampling on PD2-2 was forced to incorporate a larger than normal proportion of profiles with low chroma B-horizons from more poorly drained landscape positions on the downstream end of the landform. Rather than differences in parent material or duration of weathering, this difference in landscape position imparted by sampling constraints and its effects on soil drainage is the likely cause of the observed difference between mean rubification values in PD2-2 versus PD2-1 soils.

4.4.3.2 Soil chemistry

To evaluate whether soils on younger versus older scroll bars within individual paleomeander surfaces display differences in their chemical properties, difference of means t-tests were also conducted on B-horizon whole soil and fine sand fraction chemical parameters for the younger versus older scroll bar soils of the PD1 and PD2 surfaces. Because elemental data for PD3-1 soils are not available, t-tests of PD3 scroll bar soils could only be performed with respect to dithionite iron.

For all sites except PD3-1, chemical data are available for 10 profiles per scroll bar with respect to all parameters except dithionite iron, for which 24 profiles were analyzed. Because difference of means t-tests rely on the assumption that the means of the compared groups follow a normal distribution, and due to the concern that this assumption might not be met as a result of the small sample size (n=10) per scroll bar soil group along with the fact that a substantial proportion (~40%) of soil chemical variables displayed modest right-tailed (log normal) frequency distributions, results of t-tests conducted on non-transformed soil chemical data were compared to results of t-tests conducted on $\log_{10}$ transformed chemical data, as well as results from the non-parametric Wilcoxon rank sum test. Both t-tests of log-transformed chemical variables and Wilcoxon rank sum tests recognized significant differences among the same scroll bar soil chemical groups that were identified by the initial t-tests, lending confidence to the results of the t-tests on non-transformed variables. For this reason, and to retain chemical data in more easily interpretable units, differences in soil chemistry among soils on scroll bars of the same paleomeander surface are evaluated in the context of parametric t-tests conducted on non-transformed chemical data. Results are reported in Tables 4.7 and 4.8.

In general, soils on older versus younger scroll bars of the same surface appear to differ less with respect to their chemistry than they do with respect to their morphology (Tables 4.7 and 4.8). The greater dithionite iron content of PD3-1 versus PD3-2 soils appears to be the only case in which differences in clay content among soils of older versus younger scroll bars are large enough to influence bulk soil chemistry. Other notable relationships in the whole soil and fine sand fraction chemistry among soils on older versus younger scroll bars of the same surface occur with respect to the concentrations of individual bases (CaO, K_2O, MgO, Na_2O) on scroll bars of the PD1 surface. Among these soils, in the <2 mm fraction, concentrations of K_2O and MgO are greater on the older, inner scroll bar (PD1-1), while CaO and Na_2O concentrations are greater on the younger, outer scroll bar (PD1-2). The same relationships are observed within the fine sand fraction chemistry of these soils.

Although data are insufficient to precisely characterize differences in the mineralogical compositions of these soils, whole soil and fine sand chemistry may indicate variation in the relative abundances of particular minerals in the sand fractions of these soils that reflects subtle parent material differences among the older, inner PD1-1 scroll bar versus the younger, outer PD1-2 scroll bar. The mean and median sand content of Bt horizons on the PD1-2 scroll bar are respectively 42 and 40%, while Bt horizons of PD1-1 are much less sandy, with respective mean and median sand contents of 25 and 24%. These particle size data are consistent with the interpretation that the vertical accretion sediments of older, inner scroll bars are finer in their upper part as a result of their more channel-distal position on (paleo) floodplains. This difference in particle size among older versus younger scroll bars that is linked to differences in depositional environment may explain the behavior of K_2O and MgO versus CaO and Na_2O concentrations in B horizons on scroll bars on the PD1 surface.

Although it cannot be verified in the absence of sand fraction mineralogical data, the greater concentrations of CaO and Na_2O on the younger, outer PD1-2 scroll bar may result from a greater abundance of sand-sized plagioclase feldspars in PD1-2 versus PD1-1 Bt-horizons that is correlated with their higher sand content. In turn, the higher K_2O and MgO concentrations in Bt-horizons of the older, inner PD1-1 scroll bar may reflect muscovite and biotite micas, whose deposition would be favored over other sand sized minerals in the lower energy depositional environment of the interior of the paleomeander surface when it functioned as an active flood plain, because when in suspension sand-sized micas settle at rates more similar to those of silt-sized grains due to their platy form. However, an alternative, and perhaps more likely, explanation is that these relationships reflect the results of different durations of weathering among PD1-1 versus PD1-2 soils. The greater K_2O and lower CaO and Na_2O concentrations of older PD1-1 Bt-horizons relative to those of slightly younger PD1-2 Bt-horizons may simply reflect their relative enrichment with respect to more resistant potassium feldspars versus more weatherable plagioclase feldspars. More data are needed for Pee Dee scroll bar soils in order to elucidate the mineralogical trends reflected by their soil chemistry, and future research will attempt to address this issue.

4.4.4 Soil chronosequence trends

4.4.4.1 Soil morphology

Relationships between soil properties and age were evaluated using linear regression. In this capacity, regression is simply intended to highlight age-related trends in the morphology and chemistry of the soils under study. The reader should note that some soil properties are not normally distributed within their respective sample sets or about the regression line, and that

some regressions violate the assumption of constant variance. In some cases, soil properties exhibit non-linear trends with respect to time, and in these cases, possible alternative functions are suggested. Thus, the regression relationships presented here are not intended as mathematical models to predict rates of soil development, but are simply employed to illustrate chronosequence trends observed in these soils. Either the mean of the OSL date (PD1 and PD2 soils) or the best available estimate of scroll bar age (PD3) is used as the independent variable in the regressions. The reader should recognize that OSL age estimates of the oldest soils in the chronosequence, on the PD1-1 (118.8±30.4 ka) and PD1-2 (107.8±24.9 ka) surfaces, are associated with large 2-sigma errors. In this paper, relationships between soil properties and mean OSL age estimates are used to assess soil genesis trends, but it should be noted that the form of a relationship between a particular property and time might be influenced by where in the envelope of uncertainty the true soil age is located. Future research will attempt to better account for uncertainty in age estimates by employing a Monte Carlo approach similar to that of Switzer et al. (1988), which incorporates a more comprehensive consideration of the error associated with age estimates in soil chronosequence analyses.

Morphological properties of Pee Dee scroll bar soils were regressed against soil age, and results are reported in Figure 4.8 and Table 4.9. Cumulative B-horizon thickness (R^2=0.41, Fig. 4.8A) and solum thickness (R^2=0.51, 4.8C) exhibit moderate, positive correlations with age that are characterized by large degrees of scatter associated with variability in these parameters within individual scroll bars and among scroll bars on the same surface. Although B-horizon and solum thicknesses constitute soil properties that may be assumed to be zero at $time_{zero}$ in chronofunction frameworks (Schaetzl and Anderson, 2005; p. 595), regressions of these variables were not forced through the origin in this study because, with a simple linear model,

such manipulation resulted in a poor fit to the data across the majority of the chronosequence. Future analysis of these data will explore the utility of nonlinear functions for more adequeate characterization of the $time_{zero}$ boundary conditions of these parameters.

Bt-horizon thickness exhibited a strong, positive correlation with age (R^2=0.88, Fig. 4.8B), but the form of this relationship appears to be nonlinear and might be better represented by an exponential growth function, while B-horizon clay content showed only weak, positive correlation with age (R^2=0.22, Fig. 4.8D) characterized by a large degree of scatter associated with variability in clay content within individual scroll bars and among older and younger scroll bars of the same surface. Rubification as measured by the Buntley-Westin Index (R^2=0.40, Fig. 4.8E) displayed a stronger correlation with age than did the Hurst Index (R^2=0.10, Fig. 4.8F), although the increase in rubification through time indicated by trends in the former might be better modeled by an exponential growth function.

Evaluation of the above regression relationships provides several insights into age-related trends in the genesis of Pee Dee scroll bar soils. Although there is considerable overlap in the cumulative B horizon and solum thicknesses among the oldest (108-119 ka) soils in the chronosequence and those of terminal Pleistocene and Holocene age, regression results nonetheless suggest that the B-horizons and sola of scroll bar soils thicken over timescales of ~100,000 years and that this process occurs gradually through time. Given that all pedons on the PD3-1 and PD3-2 scroll bars contained cambic (Bw) horizons, it appears that B-horizons form over Holocene timescales in these pedoenvrionments. However, greater than ~19,000-27,000 years appears to be required for soils in scroll bar settings to develop well-expressed argillic horizons, given that soils on PD2-2 (23.1±4.5 ka) and younger scroll bars lack Bt horizons. This time frame for argillic horizon formation is considerably greater than estimates reported from

elsewhere in the southeastern United States, which have ranged from 4,000-17,000 years (Foss et al., 1981; Segovia, 1981; Leigh, 1996; Suther, 2006), and may be exaggerated, given that the PD2-2 OSL date is likely an overestimate (see section 4.4.1.2). Lack of data for soils within the 23-108 ka mean age range (Fig. 4.8B) prevent more precise estimation of the time required for argillic horizon formation in alluvial soils of the Pee Dee valley, but based on soils of the PD1 surface, after ~100,000 years of weathering, Bt horizons in this setting are moderately well-developed.

Most Bt horizons of PD1-2 (108 ka) and PD1-1 (119 ka) exhibit few to common, distinct, discontinuous clay films on ped faces, indicating that these soils contain illuvial clay translocated from higher positions in the profile. To the extent that there is a progressive increase in clay content with age in the Bt horizons of Pee Dee soils (Fig. 4.8D), it probably reflects such illuvial accumulations. However, the relationship between clay content and age is weak in scroll bar soils. Considerable overlap in clay content between soils on the oldest versus the youngest paleomeander surfaces suggests that the majority of clay content in B horizons is inherited from the fine-grained vertical accretion sediments that serve as their parent material and does not represent clay accumulation by pedogenic processes.

Age-related trends in B-horizon rubification are most well-expressed by the Buntley-Westin Index (Fig. 4.8E). Increases in rubification with age as expressed by PD1 (108-119 ka) versus PD2 and PD3 (Holocene-23 ka) pedons show trends similar to those of dithionite iron and dithionite to total iron (Fig. 4.9E and 4.9F) that reflect accumulation of iron oxides and oxyhydroxides in the Bt horizons of these soils, which is discussed further in the following section.

4.4.4.2 Soil chemistry

Pee Dee scroll bar soil B-horizon <2 mm and fine sand fraction chemical properties were also evaluated within a chronosequence framework using simple linear regression, and results are presented in Figures 4.9 and 4.10 and Table 4.9. Graphical interpretation of Figures 4.9 and 4.10 suggests that soil chemical properties are more strongly associated with age than are morphological properties, although this is not particularly well-reflected by the R^2 values of the regressions, since many of these soil-age relationships would be better characterized by nonlinear regression.

The molar ratios of whole soil bases:alumina and bases:resistant oxides both exhibit moderately strong, negative relationships with soil age ($R^2 \geq 0.67$, Fig. 4.9A and 4.9B). The decrease with age shown by these ratios primarily reflects trends in the concentrations of individual basses discussed below, as alumina ($R^2=0.07$) and the other resistant oxides show no substantive trends across the chronosequence. The lack of a strong association between alumina and soil age probably reflects the fact that differences in clay content across the chronosequence are relatively modest. Relationships between bases:alumina and bases:resistant oxides versus age appear to be more linear than the trends of the individual bases, but the lack of data within the ~25-108 ka time frame limits interpretations about the form of the soil-age relationships of these molar ratios. At the scale of individual scroll bars, variability in the bases:alumina and bases:resistant oxides ratios tends to decrease with age.

K_2O and CaO concentrations show strong, negative, nonlinear relationships with age. Respective linear regression R^2 values for these variables are 0.39 and 0.62, but their relationships with age would probably be better characterized by a nonlinear exponential decay function (Fig. 4.9C and 4.9D, Table 4.9). Whole soil MgO and Na_2O concentrations are not

plotted in Figure 4.9 but show similar behavior (Table 4.9). Within the fine sand fraction of scroll bar soil B horizons, concentrations of K_2O, MgO and Na_2O and the K_2O:TiO_2 molar ratio also exhibit strong, negative, nonlinear relationships with age (Fig. 4.10). The R^2 values for linear regressions of these parameters range from 0.26-0.79 and would certainly improve if an exponential decay function were fit to the data. Fine sand fraction CaO concentration shows a strong, negative relationship with age as well, but its decrease in increasingly older soils appears to follow a more linear form than it does in the whole soil fraction (Fig. 4.10B).

Plots of whole soil K_2O and CaO concentrations (Fig. 4.9C and 4.9D) suggest that these bases experience rapid depletion from scroll bar B horizons within the first ~19,000 to 28,000 years of weathering, considering the 2-sigma error associated with the PD2-2 OSL age estimate, and whole soil MgO and Na_2O concentrations (not shown) exhibit similar behavior. Beyond this time frame, weathering of bases appears to either stabilize or proceed at a much more gradual rate, apart from more minor differences among base concentrations among the older (PD1-1) and younger (PD1-2) scroll bars of the PD1 surface (discussed in section 4.4.3.2).

Age-related trends in the base concentrations of B-horizons of Pee Dee soils are thought to reflect rapid initial depletion of unstable base-bearing detrital minerals from a range of particle size fractions within the whole soil. Rapid depletion of bases within the fine sand fraction is even more pronounced than in the whole soil (Fig. 4.10), and if depletion of fine sand fraction weatherable minerals is occurring in these soils over Holocene to terminal Pleistocene timescales, it can be inferred that such weathering is transpiring at least as rapidly for unstable minerals in the very fine sand and silt fractions, given their greater relative surface area. Thus, it is likely that a substantial component of the depletion of bases in the whole soil fraction reflects rapid initial depletion of unstable silicate minerals such as potassium and plagioclase feldspars,

micas, pyroxenes, and hornblende and other amphiboles, from the silt and fine to very fine sand frations after about 19,000 to 28,000 years of weathering, and minerals within coarser sand fractions may also be involved. Whether or not the low base concentrations of Bt horizons in the 108-119 ka PD1 soils indicates that they have reached a steady state, or a pedogenically temporary meta-stable state, with respect to weathering of unstable silt and sand-sized minerals is difficult to evaluate, given that no chemical data are available from older fluvial surfaces in the Pee Dee valley. Interestingly, K_2O concentrations of ~1.0-2.0 % in PD1 soils may indicate that a small quantity of potassium-bearing minerals, like orthoclase, microcline, and muscovite mica, may persist in scroll bar B-horizons for timescales of ~100,000 years. However, it is notable that timespans of only ~20,000 to 100,000 years appear to be sufficient for weathering to dampen the intra-scroll bar spatial variability in most bases.

Whole soil dithionite-extractable iron (R^2=0.28) and the ratio of dithionite to total iron (R^2=0.39) respectively exhibit weak to moderate, positive relationships with age (Fig. 4.9E and 4.9F, Table 4.9). Both variables exhibit roughly linear relationships with age, although slight curvilinearity may be indicated for the plot of dithionite to total iron. In general, among soil chemical properties depicted in Figure 4.9, dithionite iron exhibits the greatest variability at the scale of individual scroll bars, but neither dithionite iron nor dithionite iron to total iron display the systematic decrease in variability through time shown by individual bases or the bases:alumina and bases:resistant oxide ratios.

As discussed in Section 4.4.2.2, variability in B-horizon dithionite iron at the scale of individual scroll bars may in part reflect variations in the inherited secondary iron oxide contents of the alluvial parent material along scroll bar ridge crests. Localized variations in scroll bar relief that affect soil drainage status also likely influence the variability in dithionite iron shown

in Figure 4.9E. As observed above, the correlation of dithionite iron with age is modestly improved when it is expressed as a proportion of total iron (Fig. 4.9F). The progressive increase in dithionite to total iron across the chronosequence suggests that pedogenic iron oxides comprise a gradually increasing proportion of the total iron in Pee Dee scroll bar soils over ~100,000 years of development, as pedogenic iron oxides are formed from the weathering of detrital iron-bearing sand- and silt-sized silicate minerals and possibly iron-bearing clay minerals.

4.5. Conclusions

Central tendencies of the morphological and chemical properties of Pee Dee soils become increasingly developed over the ~100 ka timescale of the chronosequence, as illustrated by increases in solum thickness, cumulative B-horizon thickness, rubification, and dithionite-iron to total iron and decreases in the concentrations of bases in both the whole soil and fine sand fractions. Some properties, like B-horizon and solum thickness appear to increase gradually with time, suggesting progressive development, while others, such as changes in the bulk chemistry of the whole soil and fine sand fractions that reflect mineral weathering trends, appear to change episodically. To varying degrees, the general directions of the age-related trends observed in Pee Dee scroll bar soils agree with those documented by other chronosequence studies in the southeastern Coastal Plain (Markewich et al., 1987, 1988, 1989; Howard et al., 1993; Shaw et al., 2003; Suther, 2006), though the magnitude and rates of change among Pee Dee soils versus those examined by previous studies may vary from property to property, depending upon the particular geomorphic, geologic, and climatic settings and timescales involved.

Nevertheless, data indicate a large degree of soil spatial variability within the Pee Dee chronosequence, both at the scale of individual scroll bars and among older versus younger scroll bars of the same paleomeander surface. Within individual scroll bars, soil variability appears to bear a strong linkage to variation (or lack of variation) in local relief and the thickness and texture of vertical accretion deposits that is most strongly expressed by soil morphological properties, with soils exhibiting increasing B (or Bt) and solum thickness, higher B horizon clay content, and lower B horizon rubification in the downstream direction along scroll bars characterized by downstream decreases in local relief and downstream increases in the thickness and clay content of their vertical accretion sediments. Among older versus younger scroll bars of the same paleomeander surface, in some cases, variability in gross soil morphology may be linked to systematic spatial variation in the thickness and grain size of vertical accretion deposits across an individual paleomeander surface, with thicker, more finely textured B-horizons and sola being associated with older scroll bars located on the interior of paleomeander surfaces that have been subjected to overbank sedimentation in lower energy floodplain positions for greater durations of time. In other instances, the thicker B horizons and sola of soils on the interiors of paleomeander surfaces may simply reflect a greater duration of pedogenesis.

While the variability among scroll bar soils is not so great that it invalidates the chronosequence approach in this setting, Pee Dee data demonstrate the necessity of a thorough understanding of soil variability within geomorphic surfaces of uniform age prior to undertaking a soil chronosequence study. These findings support the recommendation of Schaetzl et al. (2006) that researchers sample large numbers of profiles and focus on central tendency values, while incorporating data pertaining to soil variability or "range of expression" within individual landforms, when developing chronosequence interpretations.

Several recent studies have investigated soil landscape relationships in settings in the southeastern Coastal Plain where extreme short-range spatial variability has been observed among soils of equivalent age, where variability in gross morphology could not be adequately explained by variation in parent material, topography, soil drainage, or vegetation (Phillips, 1993a; Phillips et al., 1994; Phillips et al., 1996). These studies have used a deterministic uncertainty conceptual framework to explain such short-range variability, whereby unstable growth of minor perturbations in the soil system ultimately results in disproportionately large variations in soil morphology among neighboring pedons. Such chaotic behavior has been cited as a confounding factor for soil chronosequence research, since it has the potential produce vastly different degrees of pedogenic development among soils that occur in close spatial association within surfaces of uniform age (Phillips, 1993b). Findings from the Pee Dee chronosequence stand in contrast to these studies, in that for the settings evaluated they indicate that 1) a substantial proportion of the variability among soils on the same geomorphic surface can be accounted for by systematic variation in factoral drivers like parent material, local relief, and soil drainage status, and 2) reasonable chronosequence interpretations can be made within the context of such intra-surface variability if the size of sample pedons is sufficiently large and the character of the intra-surface variability is sufficiently understood.

4.6 References

Barrett, L. R., Schaetzl, R. J., 1993. Soil development and spatial variability on geomorphic surfaces of different age. Physical Geography 14, 39-55.

Birkeland, P.W., 1999. Soils and Geomorphology. 3rd edn. Oxford Univ. Press, New York.

Buntley, B.T., Westin, F.C., 1965. A comparative study of developmental colour in a Chestnut-Chernozem-Brunizem soil climosequence. Soil Sci. Soc. Am. Proc. 29, 579-582.

Campbell, J. B., 1979. Spatial variability of soils. Annals of the Association of American Geographers 69, 544-556.

Daniels, R.B., Gamble, E.E., 1967. The edge effect in some Ultisols in the North Carolina Coastal Plain. Geoderma 1, 117-124.

Eppes, M. C., Harrison, J. B. J., 1999. Spatial variability of soils developing on basalt flows in the Potrillo volcanic field, southern New Mexico: Prelude to a chronosequence study. Earth Surface Processes and Landforms, Vol. 24, 1009-1024.

Foss, J.E., Wagner, D.P., and Miller, F.P., 1981. Soils of the Savannah River Valley. Russell Papers, 1985, Archeological Services and the National Park Service, Atlanta, Georgia, USA, 93 p.

Gee, G.W., Bauder, J.W., 1986. Particle Size Analysis. In: Klute, A. (Ed.), Methods of Soil Analysis: Part I, Physical and Mineralogical Methods Second Edition. Agronomy Monograph No. 9, American Society of Agronomy – Soil Science Society of America, Madison, Wisconsin, USA, p. 383-411.

Harrison, J. B. J., McFadden, L. D., and Weldon, R. J., III, 1990. Spatial soil variabil¬ity in the Cajon Pass chronosequence: Implications for the use of soils as a geochronological tool. Geomorphology 3, 399-416.

Holliday, V.T., 2004. Soils in Archaeological Research. Oxford University Press, 448 pp.

Howard, J.L., Amos, D.F., Daniels, W.L., 1993. Alluvial soil chronosequence in the inner Coastal Plain, central Virginia. Quaternary Research 39, 201-213.

Huggett, R. J., 1998. Soil chronosequences, soil development, and soil evolution: A critical review. Catena 32, 155-172.

Hurst, V.J., 1977. Visual estimation of iron in saprolite. Geological Society of America Bulletin 88, 174- 176.

Jenny, H., 1941. Factors of Soil Formation. New York, NY: McGraw-Hill.

Johnson, D.L., Watson-Stegner, D., 1987. Evolution model of pedogenesis. Soil Science 143, 349-366.

Leigh, D.S., 1996. Soil chronosequence of Brasstown Creek, Blue Ridge Mountains, USA. Catena 26, 99-114.

Leigh, D.S., 2006. Terminal Pleistocene braided to meandering transition in rivers of the Southeastern USA. Catena 66, 155-160.

Leigh, D.S., 2008. Late Quaternary climates and river channels of the Atlantic Coastal Plain, Southeastern USA. Geomorphology 101, 90-108.

Leigh, D.S., Srivastava, P., Brook, G.A., 2004. Late Pleistocene braided rivers of the Atlantic Coastal Plain, USA. Quaternary Science Reviews 23, 65-84.

Markewich, H.W., Pavich, M.J., 1991. Soil chronosequence studies in temperate to subtropical, low-latitude, low-relief terrain with data from the eastern United States. Geoderma 51, 213-239.

Markewich, H.W., Pavich, M.J., Mausbach, M.J., Stuckey, B.N., Johnston, R.G., Gonzalez, V.M., 1986. Soil development and its relation to the ages of morphostratigraphic units in Horry County, South Carolina: U.S. Geological Survey Bulletin 1589-B. U.S. Government Printing Office, Washington DC, USA, pp. B1-B61.

Markewich, H.W., Pavich, M.J., Mausbach, M.J., Hall, R.L., Johnston, R.G., Hearn, R.P., 1987. Age relationships between soil and geology on the Coastal Plain of Maryland and Virginia. U.S. Geological Survey Bulleting 1589-A. U.S. Government Printing Office, Washington DC, USA, pp. A1-A34.

Markewich, H.W., Lynn, W.C., Pavich, M.J., Johnston, R.G., Meetz, J.C., 1988. Analysis of four Inceptisols of Holocene age, east-central Alabama. U.S. Geological Survey Bulletin 1589-C. U.S. Government Printing Office, Washington, D.C., USA, pp. C1-C29.

Markewich, H.W., Pavich, M.J., Mausbach, M.J., Johnson, R.G., Gonzalez, V.M., 1989. A guide for using soil and weathering profile data in chronosequence studies of the Coastal Plain of the eastern United States. U.S. Geological Survey Bulletin 1589-D. U.S. Government Printing Office, Washington, D.C., USA, pp. D1-D39.

Morton, R., 2006. Soil Survey of Darlington County, South Carolina. United States Department of Agriculture Natural Resources Conservation Service. US Government Printing Office, Washington, D.C. 197 p.

Murray, A.S., Wintle, A.G., 2000. Luminescence dating of quartz using an improved single-aliquot regenerative-dose protocol. Radiation Measurements 32, 57-73.

Phillips, J.D., 1993a. Chaotic evolution of some Coastal Plain soils. Physical Geography 14, 566-580.

Phillips, J.D., 1993b. Progressive and regressive pedogenesis and complex soil evolution. Quaternary Research 40, 169-176.

Phillips, J. D., 2001. Divergent evolution and the spatial structure of soil landscape variability. Catena 43, 101-113.

Phillips, J.D., Gosweiler, J., Tollinger, M., Mayeux, S., Gordon, R., Altieri, T., Wittmeyer, M., 1994. Edge effects and spatial variability in coastal plain Ultisols. Southeastern Geographer 34, 125-137.

Phillips, J. D., Perry, D., Garbee, A. R., Carey, K., Stein, D., Morde, M. B., Sheehy, J. A., 1996. Deterministic uncertainty and complex pedogenesis in some Pleistocene dune soils. Geoderma 73, 147-164.

Pitts, J.J., 1980. Soil survey of Marion County, South Carolina. United States Soil Conservation Service. US Government Printing Office, Washington, D.C. 99 pp.

Prescott, J.R., Stephan, L.G., 1982. Contribution of cosmic radiation to environmental dose. PACT 6, 17-25.

R Development Core Team, 2011. R: A Language and Environment for Statistical Computing. R Foundation for Statistical Computing, Vienna, Australia. http://www.R-project.org

Saldaña, A., Ibáñez, J.J., 2004. Pedodiversity analysis at large scales: an example of three fluvial terraces of the Henares River (central Spain). Geomorphology 62, 123-138.

Schaetzl, R. J., Anderson, S. N., 2005. Soils: Genesis and Geomorphology. Cambridge, UK: Cambridge University Press.

Schaetzl, R.J., Mikesell, L.R., M.A. Velbel, 2006. Expression of Soil Characteristics Related to Weathering and Pedogenesis Across a Geomorphic Surface of Uniform Age in Michigan. Physical Geography 27, 170-188.

Schaetzl, R. J., Barrett, L. R., Winkler, J. A., 1994. Choosing models for soil chronofunctions and fitting them to data. European Journal of Soil Science 45, 219-232.

Schwertmann, U., Taylor, R.M., 1989. Iron Oxides. In: Dixon, J.B. and Weed, S.B. (Eds.), Minerals in Soil Environments, Second Edition. Soil Science Society of America Book Series, No. 1, Soil Science Society of America, Madison, Wisconsin, USA, p. 379-438.

Segovia, A.V., 1981. Archeological Geology of the Savannah River Valley and Main Tributaries in the Richard B. Russell Multiple Resource Area. Russell Papers 1985, Archeological Services and the National Park Service, Atlanta, Georgia, USA, 93 p.

Shaw, J.N., Odom, J.W., Hajeck, B.F., 2003. Soils on Quaternary terraces of the Tallapoosa River, Central Alabama. Soil Science 168 (10), 707-717.

Soil Survey Division Staff, 1993. Soil Survey Manual. U.S. Department of Agriculture Handbook 18. U.S. Government Printing Office, Washington, D.C., USA, 437 pp.

Soil Survey Laboratory Staff, 1992. Soil Survey Laboratory Methods Manual. U.S. Department of Agriculture Soil Conservation Service Soil Survey Investigations Report No. 42, Version 2.0. U.S. Government Printing Office, Washington, D.C., USA.

Sondheim, M. W., Standish, J. T., 1983. Numerical analysis of a chronose¬quence including an assessment of variability. Canadian Journal of Soil Science 63, 501-517.

Stokes, S. and Walling, D.E., 2003. Radiogenic and Isotopic Methods for the Direct Dating of Fluvial Sediments. In: Kondolf, M. and Piegay, H. (Eds.) Tools in Fluvial Geomorphology. John Wiley and Sons, Ltd, West Sussex, England, p. 233-267.

Suther, B.E., 2006. Soil Chronosequence of the Little River valley, Atlantic Coastal Plain, North Carolina. Unpublished MS Thesis, University of Georgia, Athens, Georgia, USA.

Switzer, P. S., Harden, J. W., Mark, R. K., 1988. A statistical method for estimating rates of soil development and ages of geologic deposits: A design for soil-chronosequence studies. Mathematical Geology 20, 49-61.

USDA Natural Resources Conservation Service, 1997a. Soil temperature regimes. Soil climate map, USDA-NRCS, Soil Survey Division, World Soil Resources, Washington D.C. Website: http://soils.usda.gov/use/worldsoils/mapindex/str.html

USDA Natural Resources Conservation Service, 1997b. Soil moisture regimes. Soil climate map, USDA-NRCS, Soil Survey Division, World Soil Resources, Washington D.C. Website: http://soils.usda.gov/use/worldsoils/mapindex/smr.html

Whitley, T.G., Leigh, D.S., 2005. Evaluation of the Natural and Cultural Impacts at the Mulberry Site (38KE12) Kershaw County, South Carolina. Report Prepared for: Duke Power, a Division of Duke Energy Corporation, Charlotte, NC.

Wilding, L. P., Drees, L. R., 1983. Spatial variability and pedology. In: L. P. Wilding, N. E. Smeck, and G. F. Hall, (Eds.), Pedogenesis and Soil Taxonomy. New York, NY: Elsevier, 83-116.

Yaalon, D. H., 1975. Conceptual models in pedogenesis. Can soil-forming functions be solved? Geoderma 14, 189-205.

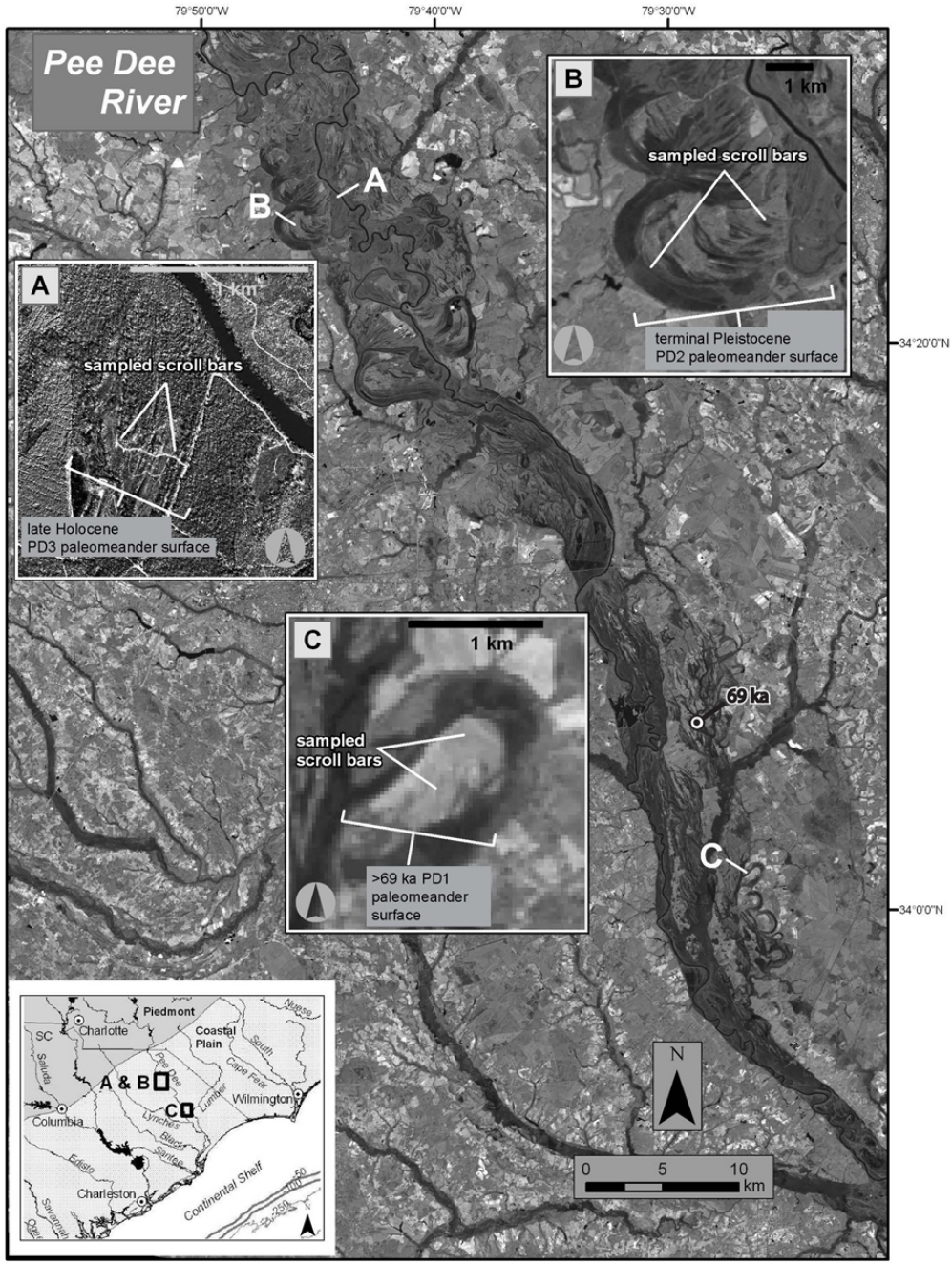

Figure 4.1. Study area. Insets A, B, and C respectively depict Holocene, terminal Pleistocene, and early-Wisconsin to Sangamon (>69 ka) age paleomeander surfaces along the Pee Dee River in South Carolina, USA. Scroll bars on these surfaces constitute long, narrow, arcuate to straight ridges that appear in lighter tones on aerial photography (Inset A) and band 4 Landsat imagery (Insets B and C; base map). Intervening swales are represented by darker tones. The 69 ka date shown about 11 km north-northwest of the PD1 site (location "C") represents an OSL age obtained by Leigh et al. (2004) for a braided river terrace that cross-cuts the PD1 paleomeander surface.

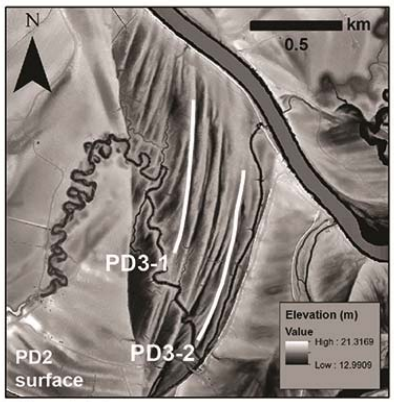

Fig. 4.2A

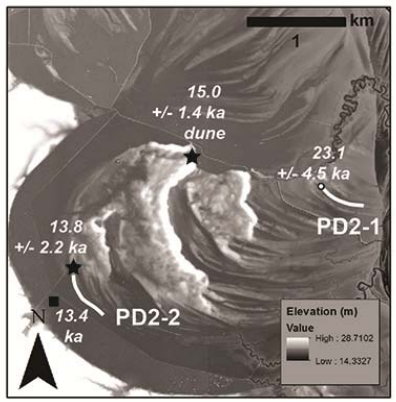

Fig. 4.2B

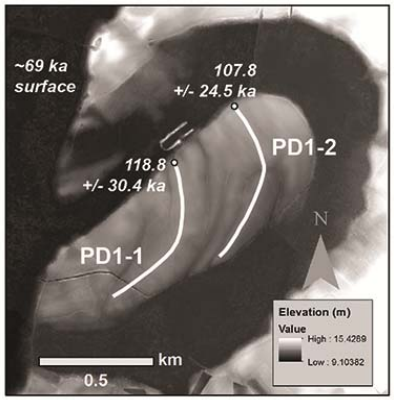

Fig. 4.2C

Figure 4.2. Locations of scroll bar study sites and sampling transects. (4.2A) PD3-1 and 3-2 scroll bars; (4.2B) PD2-1 and 2-2 scroll bars; (4.2C) PD1-1 and 1-2 scroll bars. Transects follow scroll bar ridge crests and encompass the majority of the length of each scroll bar except in areas where sampling was adjusted to avoid eolian sediments (PD2 locality, Fig. 4.2B). Circles represent the OSL dates of this study. Stars and squares respectively represent the OSL and radiocarbon dates of Leigh et al. (2004). The age estimate of the ~69 ka surface that cross-cuts the PD1 paleomeander surface (Fig. 4.2C) is based on an OSL date of Leigh et al. (2004) of braided terrace alluvium located ~11 km north-northwest of the PD1 sampling locality (see Fig. 4.1). The base maps are 2 m horizontal resolution LIDAR digital elevation models.

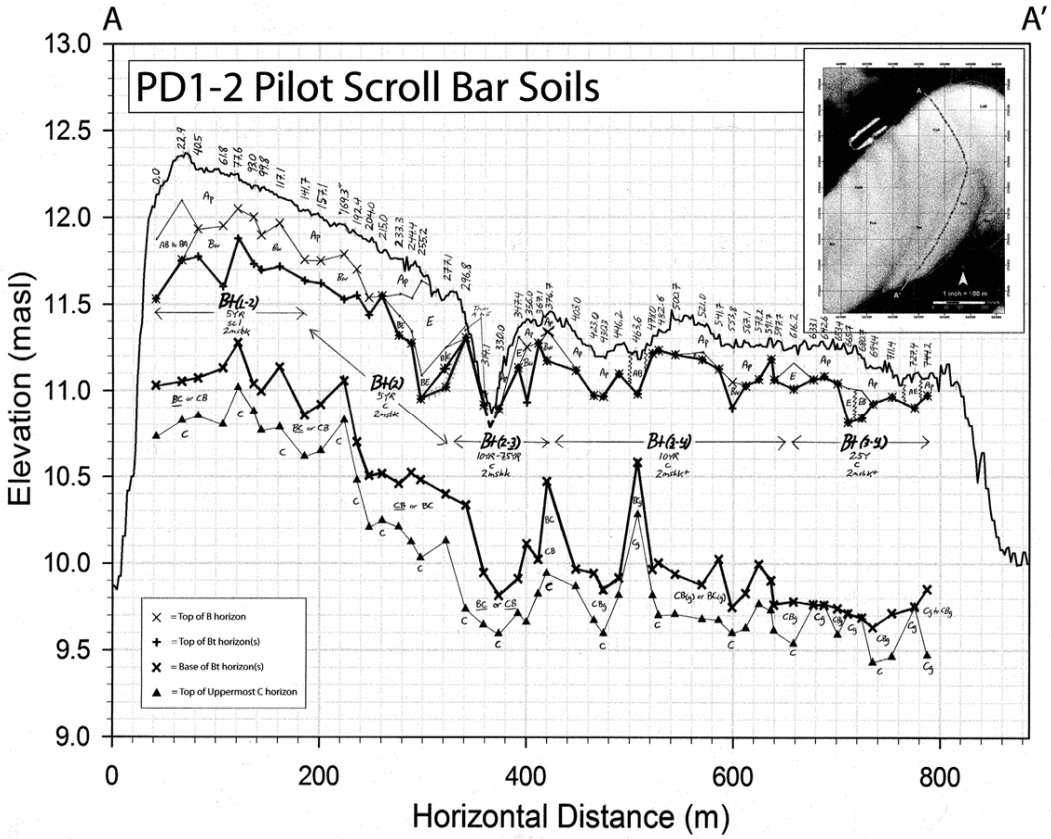

Figure 4.3. Field-sheet quality longitudinal cross-section depicting topography and soil variability along the PD1-2 pilot study scroll bar. 50 soil profiles were examined at randomly spaced intervals along a transect that followed the scroll bar ridge crest. Downstream direction is from A to A'. The transect distance of each sampling location is labeled immediately above the plot of the ground surface, but note that these distances are not referenced to the zero datum of the x-axis of the plot. Key: Bt = Bt horizon; 5YR, 7.5YR, 10YR, 2.5Y = Munsell color hues; scl = sandy clay loam; c = clay; 2msbk = moderate, medium subangular blocky structure, where + represents an intergrade between moderate and strong structure. The number following the Bt symbol represents the number of Bt-horizons typical of profiles in the area depicted, with the underlined number being dominant. Horizons overlying and underlying Bt horizons are also shown, and horizon nomenclature follows standard USDA Soil Survey terminology.

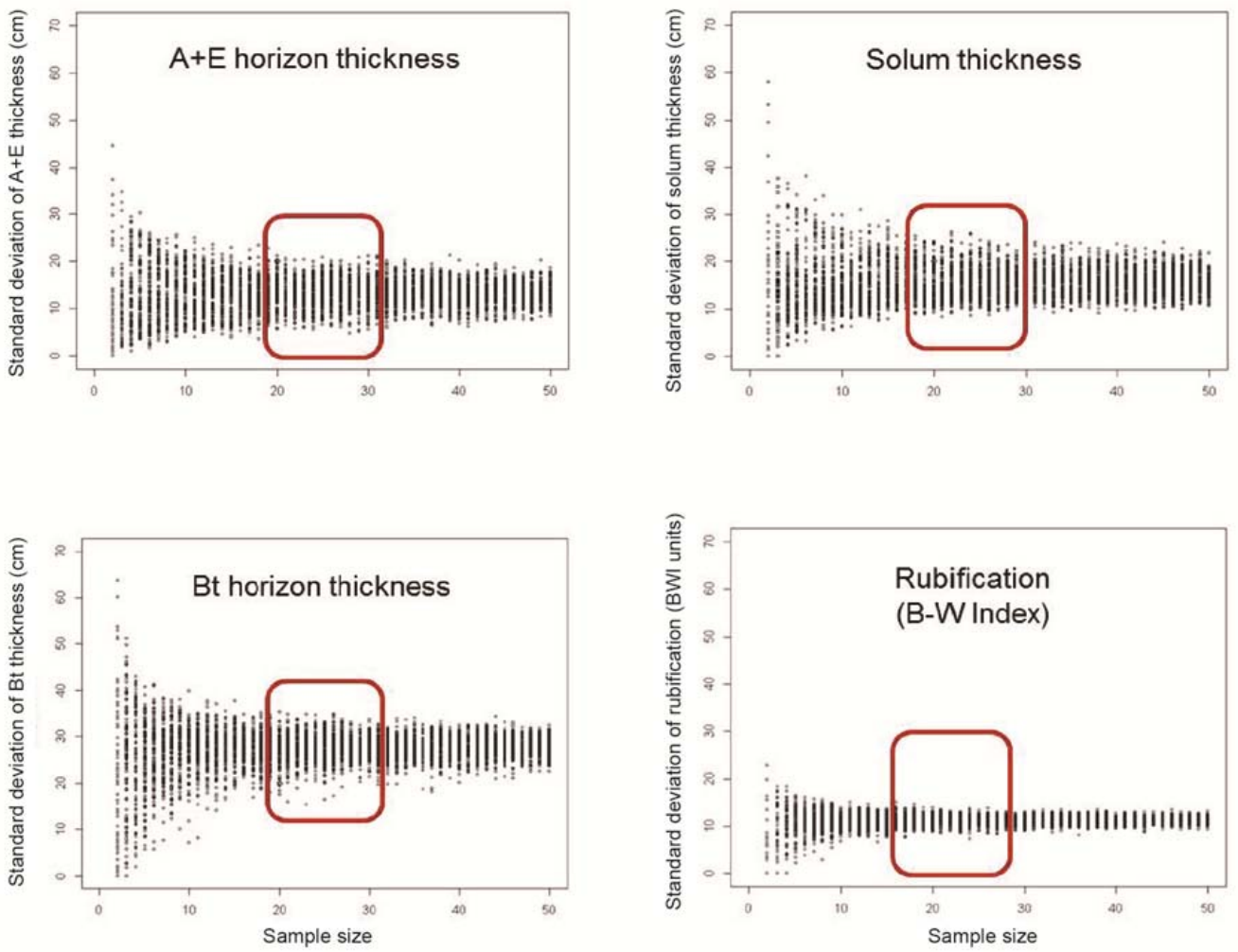

Figure 4.4. Resampled standard deviations of field-measured A+E horizon thickness, Bt horizon thickness, solum thickness, and rubification as quantified by the Buntley-Westing Index for pilot study scroll bar PD1-2 plotted against sample size. A sample size of n=20-30 appears to sufficiently characterize soil variability; larger sample sizes provide little additional benefit. Based on this information, a sample size of n =24 was used for sampling the remaining five scroll bars

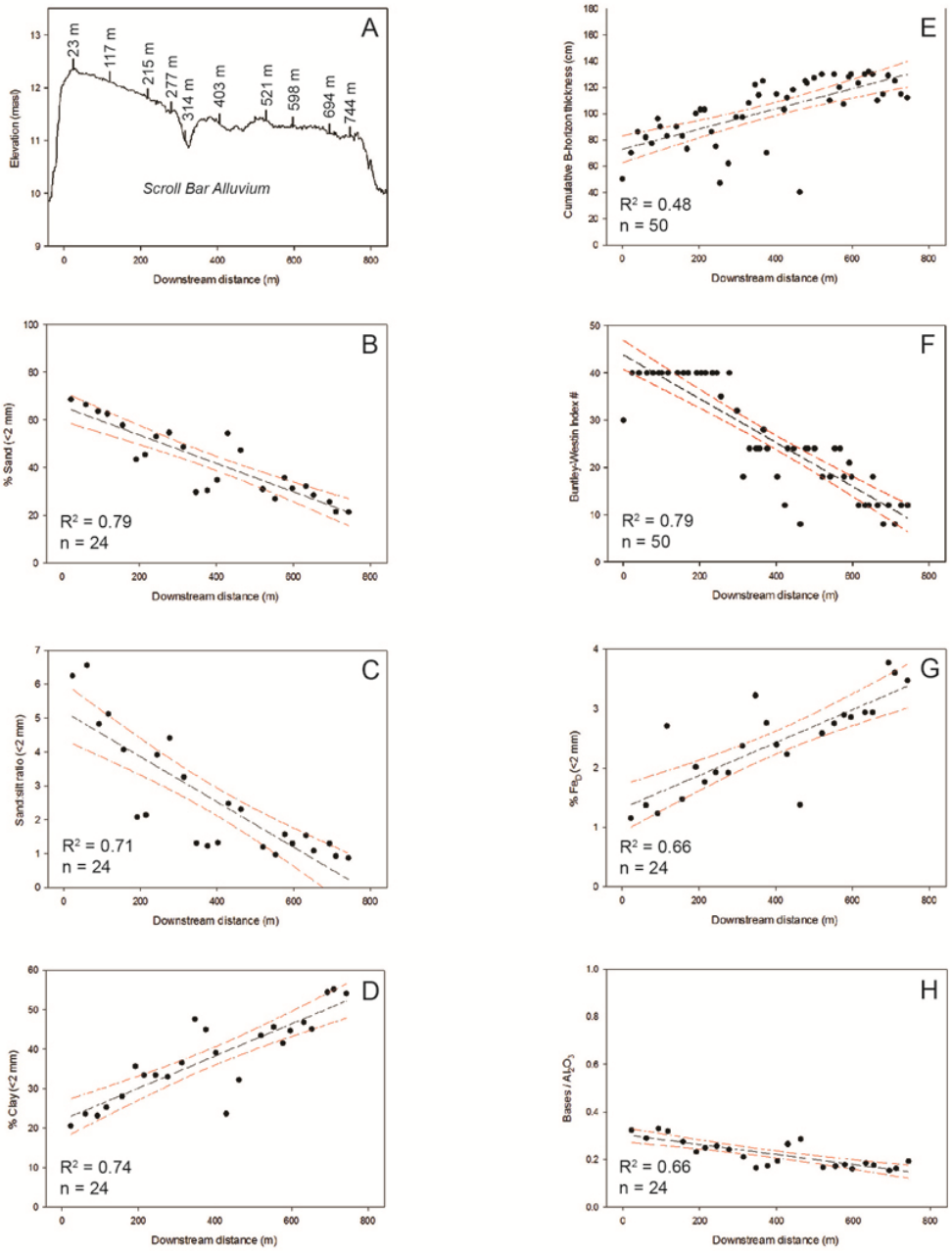

Figure 4.5. Longitudinal topographic profile of scroll bar PD1-2 (A) and selected soil morphological and chemical properties from the most well-expressed B-horizon per pedon plotted against downstream distance along the scroll bar ridge crest. (B) percent sand; (C) sand to silt ratio; (D) percent clay; (E) B-horizon thickness; (F) rubification as measured by the Buntley-Westin Index; (G) percent dithionite-extractable iron; (H) bases to alumina ratio of the <2 mm fraction. Red dashed lines indicate the 95% confidence intervals of the regressions. For locational reference, 4.5A shows the positions of 10 of the 50 sampled pedons along the scroll bar ridge. These 10 pedons constitute the soils from PD1-2 included in the chronosequence regressions depicted in Figures 4.9 and 4.10.

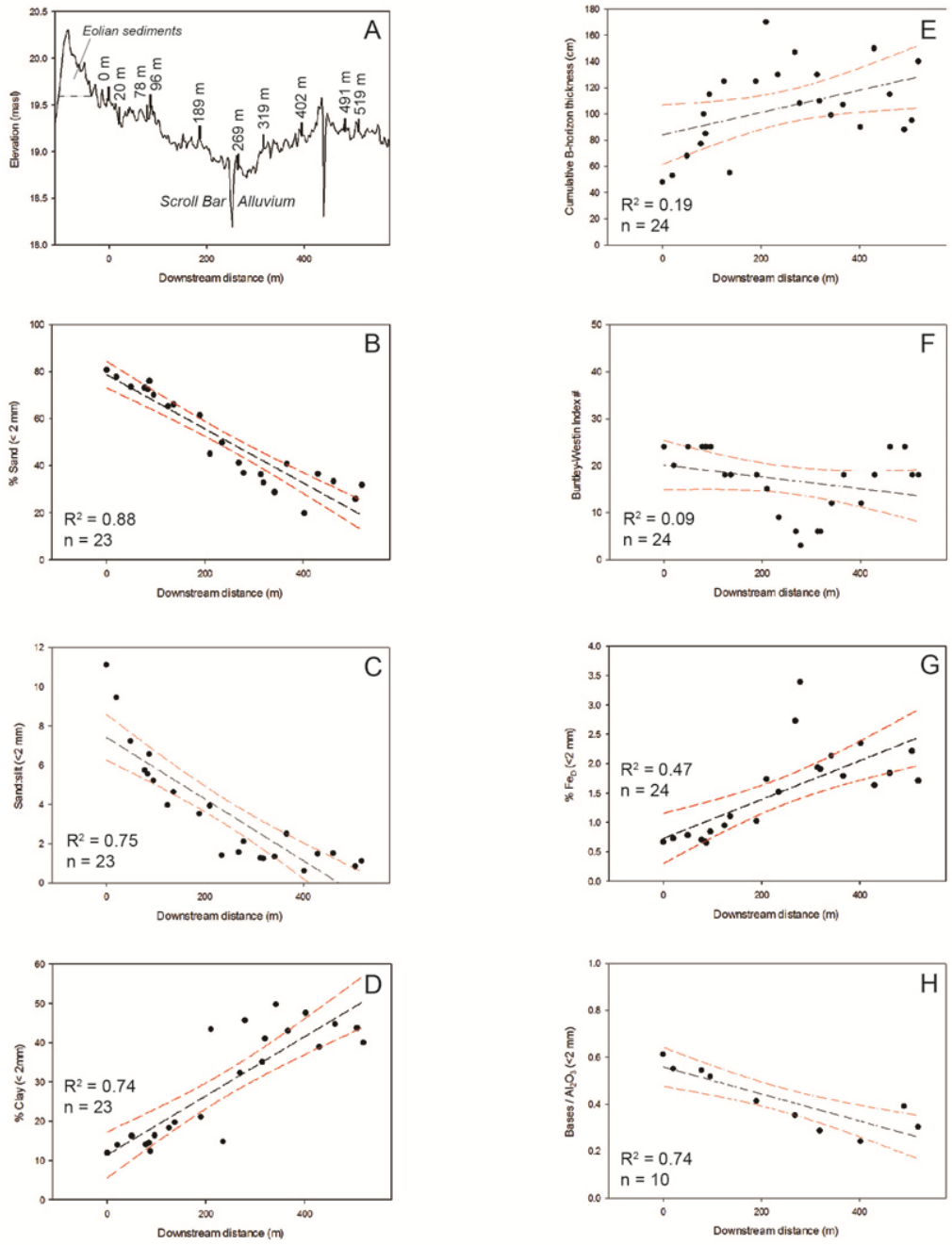

Figure 4.6. Longitudinal topographic profile of scroll bar PD2-1 (A) and selected soil morphological and chemical properties from the most well-expressed B-horizon per pedon plotted against downstream distance along the scroll bar ridge crest. (B) percent sand; (C) sand to silt ratio; (D) percent clay; (E) B-horizon thickness; (F) rubification as measured by the Buntley-Westin Index; (G) percent dithionite-extractable iron; (H) bases to alumina ratio of the <2 mm fraction. Red dashed lines indicate the 95% confidence intervals of the regressions. For locational reference, 4.6A shows the positions of 10 of the 24 sampled pedons along the scroll bar ridge. These 10 pedons constitute the soils from PD2-1 included in the chronosequence regressions depicted in Figures 4.9 and 4.10.

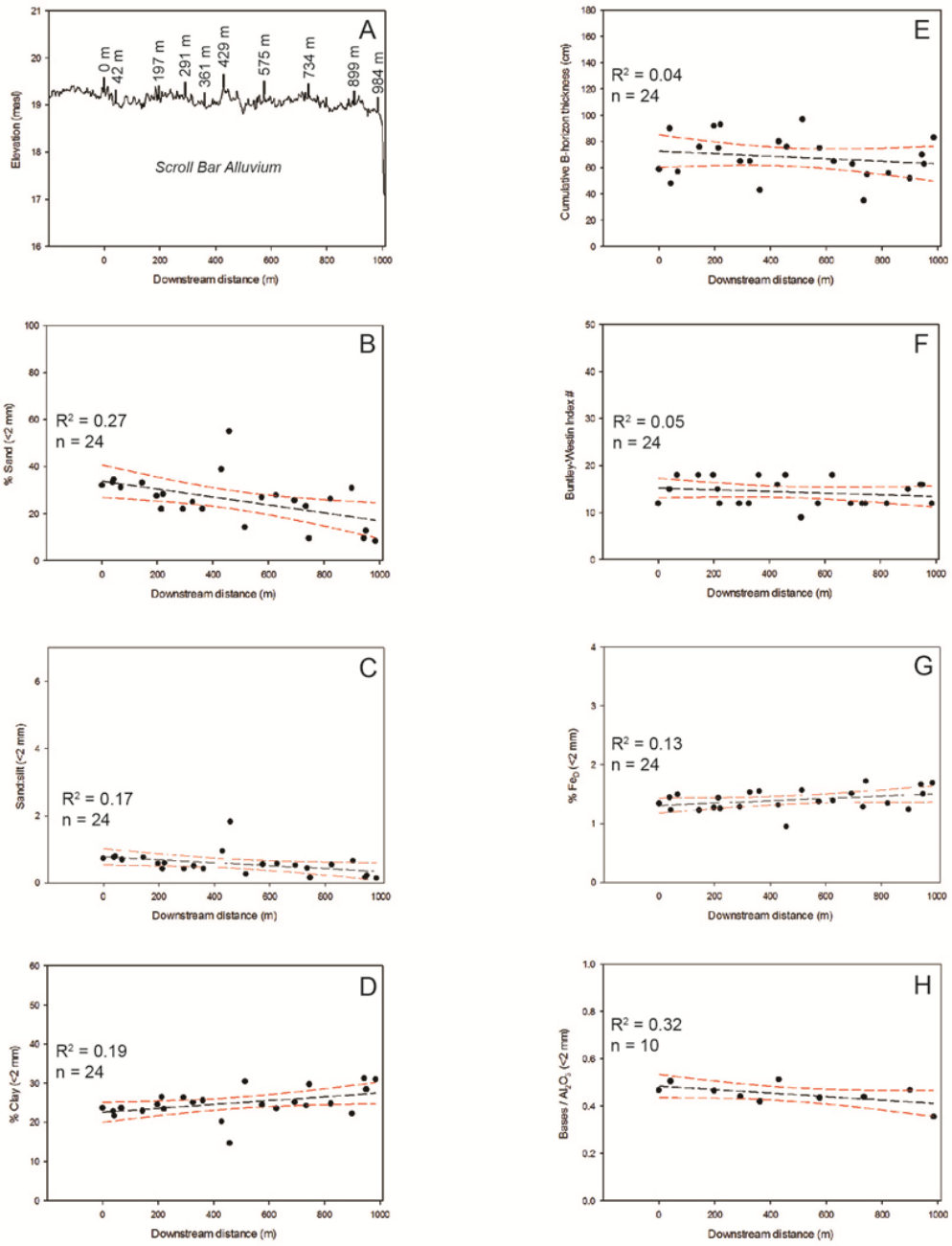

Figure 4.7. Longitudinal topographic profile of scroll bar PD3-2 (A) and selected soil morphological and chemical properties from the most well-expressed B-horizon per pedon plotted against downstream distance along the scroll bar ridge crest. (B) percent sand; (C) sand to silt ratio; (D) percent clay; (E) B-horizon thickness; (F) rubification as measured by the Buntley-Westin Index; (G) percent dithionite-extractable iron; (H) bases to alumina ratio of the <2 mm fraction. Red dashed lines indicate the 95% confidence intervals of the regressions. For locational reference, 4.7A shows the positions of 10 of the 24 sampled pedons along the scroll bar ridge. These 10 pedons constitute the soils from PD3-2 included in the chronosequence regressions depicted in Figures 4.9 and 4.10.

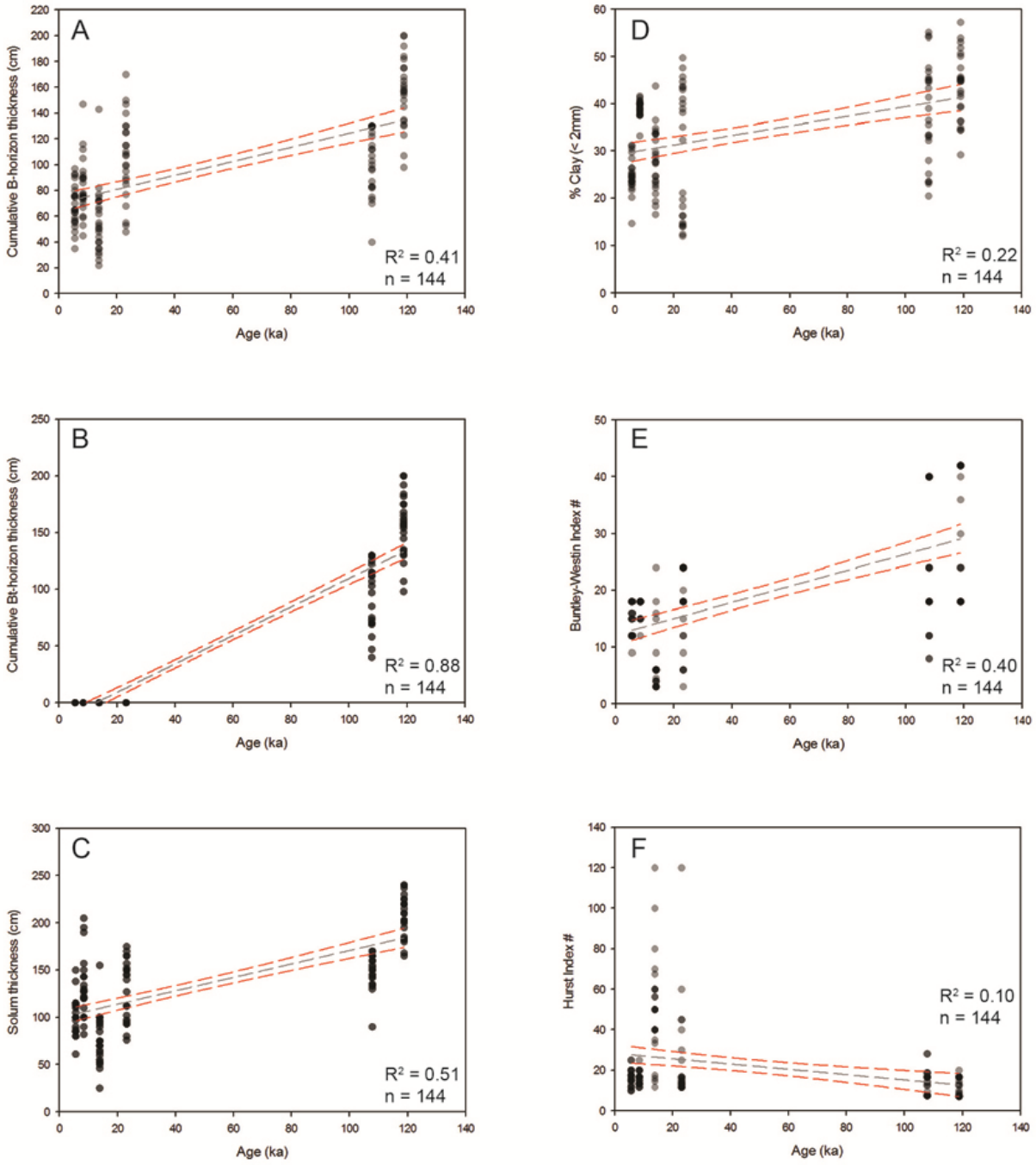

Figure 4.8. Soil morphological properties plotted as a function of age. (A) cumulative B-horizon thickness; (B) cumulative Bt-horizon thickness; (C) solum thickness; (D) percent clay based on the dry weight of the <2 mm fraction; (E) Buntley-Westin rubification index; (F) Hurst rubification index. Percent clay and rubification index data were obtained from the most pedogenically well-expressed B-horizon per pedon. Red dashed lines indicate the 95% confidence intervals of the regressions. The error bars represent two standard deviations of the age estimates.

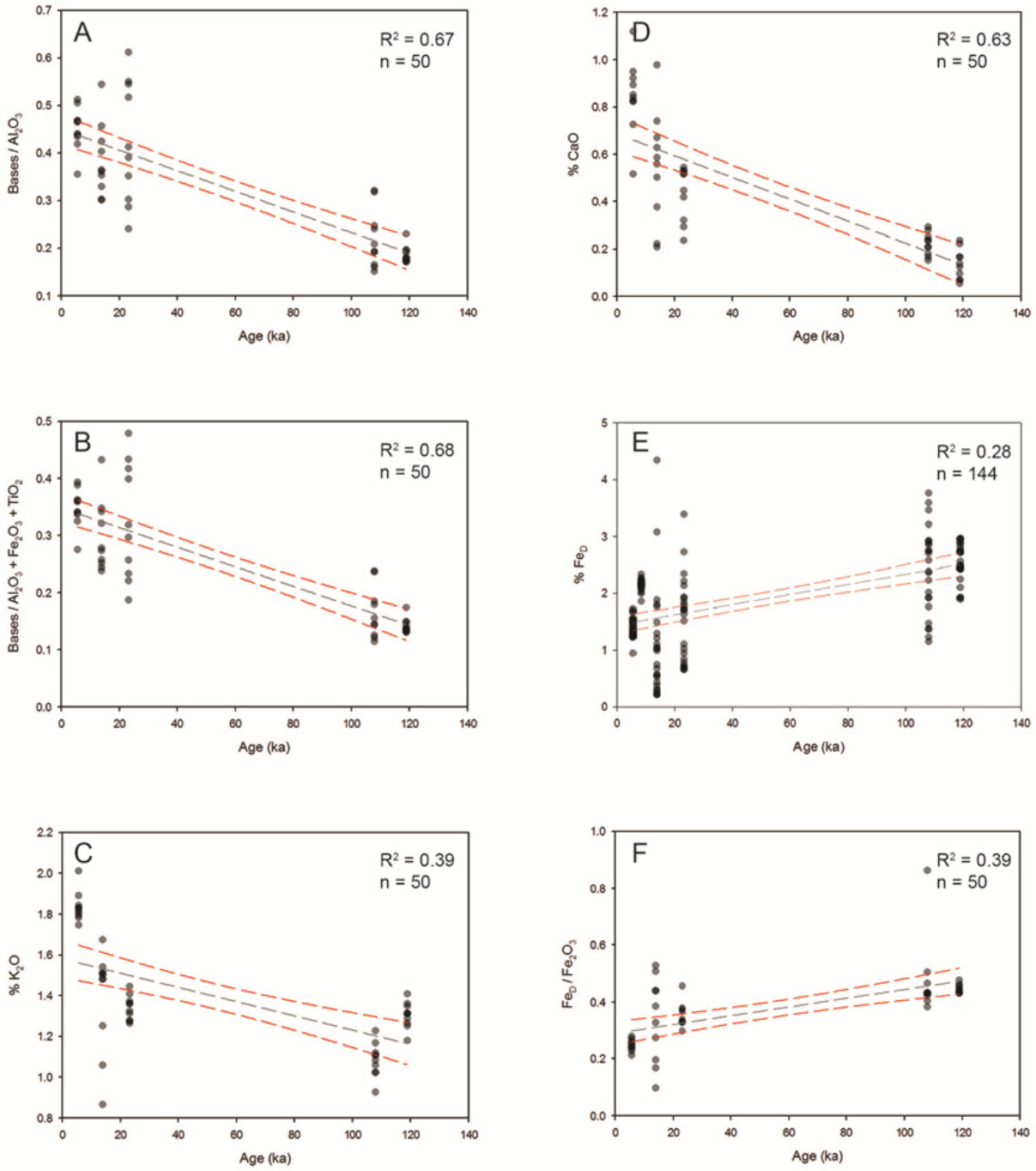

Figure 4.9. Soil chemical properties of the <2 mm fraction plotted as a function of age. (A) Bases / Al_2O_3; (B) Bases / resistant oxides; (C) % K_2O; (D) % CaO; (E) % Dithionite-extractable iron; (F) Dithionite-extractable iron / total iron. Chemical data were obtained from the most pedogenically well-expressed B-horizon per pedon. Red dashed lines indicate the 95% confidence intervals of the regressions.

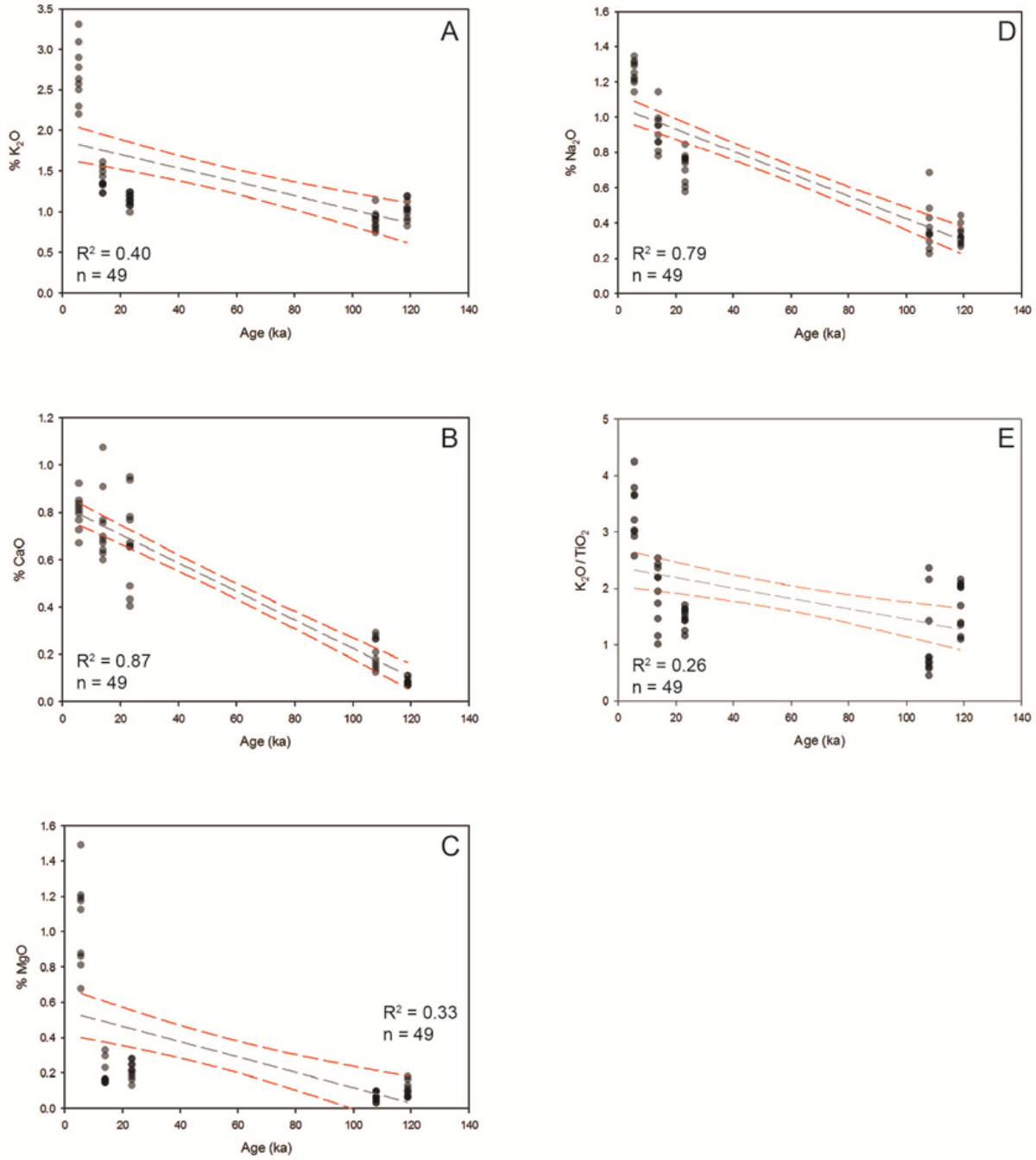

Figure 4.10. Soil chemical properties of the fine sand (0.125-250 mm) fraction plotted as a function of age. (A) % K_2O; (B) % CaO; (C) % MgO; (D) % Na_2O; (E) K_2O / TiO_2. Element oxide percentages are based on the dry weight of the fine sand fraction. Chemical data were obtained from the most pedogenically well-expressed B-horizon per pedon. Red dashed lines indicate the 95% confidence intervals of the regressions.

Table 4.1. Optically-stimulated luminescence (OSL) dates and supporting data.

Scroll bar site	Sample name/Lab No.	Age (ka) ± 2 sigma[d]	Sample depth (cm)	U (ppm)	Th (ppm)	K (%)	Water content (% by wt.)	Equivalent Dose (Gy)	Dose rate (Gy/ka)
PD2-2	DL-6[a]	**13.8±2.2**	120-150	1.0±0.3	2.2±0.9	1.19	15.0±5.0	19.9±2.7	1.4±0.1
PD2-1	UGA13OSL-877	**23.1±4.5**	150-180	1.02±0.17	2.94±0.61	1.0	15.0±5.0	31.68±0.57	1.37±0.13[b]
PD1-2	UGA13OSL-878	**107.8±24.9**	180-210	2.08±0.36	7.26±1.26	0.8	15.0±5.0	182.03±8.97	1.69±0.18[c]

[a]Previously reported in Leigh et al. (2004). Cosmic ray contribution assumed to be 0.15±0.03 Gy/ka. [b]Cosmic ray contribution assumed to be 0.165±0.02 Gy/ka. [c]Cosmic ray contribution assumed to be 0.16±0.02 Gy/ka. [d]Two times 1-sigma error.

Table 4.2. Descriptive statistics for selected soil morphological properties. Rubification and percent clay data were obtained from the most pedogenically well-expressed B-horizon per pedon. For PD1-2, statistics for field-measured morphological properties are reported for both the pilot study sample size (n=50) and a sub-sample of the pilot sample (n=24) that was analyzed for particle size distributions and dithionite iron content. Note the good agreement between the central tendencies and dispersions of the two sample sizes, which indicates a sample size of n=24 adequately represents the variability of soils on this scroll bar.

						Range	
Soil Property and Site	**n**	**Mean**	**Median**	**Std Dev**	**CV**	**Min-Max**	**25th-75th percentile**
B Thickness (cm)							
PD3-2	24	68	65	16.3	0.24	62	20
PD3-1	24	82	77	22.1	0.27	102	18
PD2-2	24	56	52	25.6	0.46	121	33
PD2-1	24	105	108	31.8	0.30	122	39
PD1-2	24	103	105	24.5	0.24	90	43
"	50	103	109	23.5	0.23	92	37
PD1-1	24	156	158	27.1	0.17	102	40
Bt Thickness (cm)							
PD3-2	24	0	0	0	---	0	0
PD3-1	24	0	0	0	---	0	0
PD2-2	24	0	0	0	---	0	0
PD2-1	24	0	0	0	---	0	0
PD1-2	24	96	105	29.1	0.30	90	53
"	50	98	108	28.0	0.29	92	52
PD1-1	24	156	158	27.1	0.17	102	40
Solum Thickness (cm)							
PD3-2	24	101	100	19.1	0.19	89	27
PD3-1	24	129	125	32.4	0.25	123	43
PD2-2	24	76	73	26.1	0.34	130	35
PD2-1	24	131	145	30.7	0.23	99	50
PD1-2	24	150	152	17.7	0.12	80	23
"	50	151	152	16.2	0.11	85	23
PD1-1	24	207	210	21.8	0.11	75	29
Rubification, Buntley-Westin Index value							
PD3-2	24	14	15	2.7	0.19	9	4.5
PD3-1	24	17	18	1.6	0.09	6	0.0
PD2-2	24	7	6	5.4	0.75	21	2.0
PD2-1	24	17	18	6.9	0.41	21	12.0
PD1-2	24	26	24	12.2	0.47	32	22.0
"	50	26	24	11.4	0.44	32	22.0
PD1-1	24	31	33	11.1	0.36	24	24.0
Rubification, Hurst Index value							
PD3-2	24	16.2	16.0	4.2	0.26	15.0	5.1
PD3-1	24	15.9	15.8	3.3	0.21	13.3	3.3
PD2-2	24	50.8	50.0	25.7	0.51	108.3	21.3
PD2-1	24	24.9	14.8	24.3	0.97	108.3	13.5
PD1-2	24	14.0	14.2	6.2	0.44	20.6	9.2
"	50	13.6	12.5	6.0	0.44	26.3	9.2
PD1-1	24	11.3	9.5	4.4	0.39	12.9	9.5
% Clay (<2 mm)							
PD3-2	24	25	25	3.7	0.15	17	3
PD3-1	24	39	39	1.7	0.04	8	2
PD2-2	24	28	28	6.6	0.24	27	10
PD2-1	24	30	34	13.8	0.46	38	27
PD1-2	24	38	38	10.5	0.28	35	14
PD1-1	24	44	45	7.1	0.16	28	10

Table 4.3. Selected statistics for linear regressions of soil properties versus downstream distance (m) along scroll bar ridge crests. Properties were measured for the most pedogenically well-expressed B-horizon per pedon, with the exception of B horizon thickness, which reflects the cumulative thickness of all B horizons in a given pedon. Regression relationships that are statistically significant at an alpha level of 0.05 are provided in bold.

Scroll bar site and soil property	R	R^2	P-value (Significance of F-ratio)	b1[a]	b1 lower limit (95% C.I.)	b1 upper limit (95% C.I.)	n
PD3-2							
% sand[b]	**-0.52**	**0.27**	**0.0094**	**-0.0169**	**-0.0291**	**-0.0046**	**24**
sand:silt ratio[b]	**-0.41**	**0.17**	**0.0473**	**-0.0004**	**-0.0009**	**-5.61E-06**	**24**
% clay[b]	**0.43**	**0.19**	**0.0337**	**0.0050**	**0.0004**	**0.0095**	**24**
B horizon thickness	-0.19	0.04	0.3703	-0.0097	-0.0316	0.0122	24
Buntley Westin Index value	-0.21	0.05	0.3186	-0.0018	-0.0055	0.0019	24
% FeD (<2 mm)[c]	0.36	0.13	0.0823	0.0002	-2.78E-05	0.0004	24
Bases:Al_2O_3 (<2 mm)[d]	-0.57	0.32	0.0867	-7.48E-05	-0.0002	1.36E-05	10
Total Bases (0.125-0.250 mm)[e]	**-0.73**	**0.53**	**0.0261**	**-0.0016**	**-0.0030**	**-0.0003**	**10**
PD3-1							
% sand	0.16	0.03	0.4446	0.0010	-0.0016	0.0036	24
sand:silt ratio	0.16	0.03	0.4536	1.84E-05	-3.15E-05	6.82E-05	24
% clay	0.13	0.02	0.5305	-0.0008	-0.0035	0.0018	24
B horizon thickness	-0.07	0.00	0.7437	-0.0054	-0.0395	0.0286	24
Buntley Westin Index value	**-0.56**	**0.31**	**0.0044**	**-0.0031**	**-0.0052**	**-0.0011**	**24**
% FeD (<2 mm)	-0.32	0.10	0.1247	-0.0001	-0.0003	3.39E-05	24
Bases:Al_2O_3 (<2 mm)	---	---	---	---	---	---	---
Total Bases (0.125-0.250 mm)	---	---	---	---	---	---	---
PD2-2							
% sand	**-0.73**	**0.53**	**<0.0001**	**-0.0668**	**-0.0947**	**-0.0389**	**24**
sand:silt ratio	**-0.66**	**0.43**	**0.0005**	**-0.0129**	**-0.0195**	**-0.0064**	**24**
% clay	**0.47**	**0.22**	**0.0206**	**0.0200**	**0.0034**	**0.0365**	**24**
B horizon thickness	0.11	0.01	0.5978	0.0185	-0.0531	0.0900	24
Buntley Westin Index value	**-0.42**	**0.18**	**0.0405**	**-0.0146**	**-0.0285**	**-0.0007**	**24**
% FeD (<2 mm)	-0.09	0.01	0.6917	-0.0005	-0.0033	0.0022	24
Bases:Al_2O_3 (<2 mm)	-0.47	0.22	0.1713	-0.0002	-0.0005	0.0001	10
Total Bases (0.125-0.250 mm)	-0.48	0.23	0.1586	-0.0011	-0.0026	0.0005	10
PD2-1							
% sand	**-0.94**	**0.88**	**<0.0001**	**-0.1152**	**-0.1350**	**-0.0955**	**23**
sand:silt ratio	**-0.87**	**0.75**	**<0.0001**	**-0.0157**	**-0.0198**	**-0.0116**	**23**
% clay	**0.86**	**0.74**	**<0.0001**	**0.0752**	**0.0548**	**0.0956**	**23**
B horizon thickness	**0.44**	**0.19**	**0.0309**	**0.0850**	**0.0086**	**0.1614**	**24**
Buntley Westin Index value	-0.30	0.09	0.1535	-0.0125	-0.0301	0.0050	24
% FeD (<2 mm)	**0.69**	**0.47**	**0.0002**	**0.0031**	**0.0016**	**0.0045**	**24**
Bases:Al_2O_3 (<2 mm)	**-0.86**	**0.74**	**0.0014**	**-0.0006**	**-0.0009**	**-0.0003**	**10**
Total Bases (0.125-0.250 mm)	**-0.82**	**0.67**	**0.0040**	**-0.0015**	**-0.0024**	**-0.0007**	**10**
PD1-2							
% sand	**-0.89**	**0.79**	**<0.0001**	**-0.0597**	**-0.0734**	**-0.0459**	**24**
sand:silt ratio	**-0.84**	**0.71**	**<0.0001**	**-0.0067**	**-0.0086**	**-0.0048**	**24**
% clay	**0.86**	**0.74**	**<0.0001**	**0.0406**	**0.0301**	**0.0511**	**24**
B horizon thickness	**0.69**	**0.48**	**<0.0001**	**0.0767**	**0.0533**	**0.1000**	**50**
Buntley Westin Index value	**-0.89**	**0.79**	**<0.0001**	**-0.0464**	**-0.0533**	**-0.0394**	**50**
% FeD (<2 mm)	**0.81**	**0.66**	**<0.0001**	**0.0028**	**0.0019**	**0.0037**	**24**
Bases:Al_2O_3 (<2 mm)	**-0.81**	**0.66**	**<0.0001**	**-0.0002**	**-0.0003**	**-0.0001**	**24**
Total Bases (0.125-0.250 mm)	0.18	0.03	0.3933	0.0002	-0.0003	0.0008	24
PD1-1							
% sand	-0.23	0.05	0.2866	-0.0096	-0.03	0.01	24
sand:silt ratio	0.06	0.00	0.7850	0.0002	0.00	0.00	24
% clay	**0.41**	**0.17**	**0.0470**	**0.0129**	**0.00**	**0.03**	**24**
B horizon thickness	**0.65**	**0.42**	**0.0006**	**0.0767**	**0.04**	**0.12**	**24**
Buntley Westin Index value	**-0.80**	**0.65**	**<0.0001**	**-0.0389**	**-0.05**	**-0.03**	**24**
% FeD (<2 mm)	-0.11	0.01	0.5987	-0.0002	0.00	0.00	24
Bases:Al_2O_3 (<2 mm)	0.04	0.00	0.9039	3.08E-06	-5.39E-05	6.01E-05	10
Total Bases (0.125-0.250 mm)	0.20	0.04	0.5767	-0.0001	0.00	0.00	10

[a]Slope of the regression line.

[b]Particle size data are given as percentages of the dry weight of the <2 mm fraction.

[c]Dithionite-extractable iron oxides of the <2 mm fraction expressed as a percentage of dry weight.

[d]The molar ratio of the sum of bases (CaO, K_2O, MgO, and Na_2O) to alumina for the <2 mm fraction.

[e]The sum of bases (CaO, K2O, MgO, and Na2O) on an oxide basis expressed as a percentage of the dry weight of the fine sand (0.125-0.250 mm) fraction.

--- = no data.

Table 4.4. Descriptive statistics for selected chemical properties of the <2 mm fraction of the most pedogenically well-expressed B-horizon per pedon. Elemental analysis was conducted on B-horizons from 24 pedons on the PD1-2 (pilot) scroll bar and 10 pedons on the remaining scroll bars. For PD1-2, descriptive statistics for chemical properties of the 24 pedons are provided along with statistics derived from a subsample of 10 of these 24 pedons to evaluate how effective the smaller sample size is at representing soil chemical variability in this setting. The relatively good agreement between the central tendencies and dispersions of the two sample sizes indicates that a sample size of n=10 provides an adequate representation of the variability in the chemical properties of soils on this scroll bar.

						Range	
Soil Property and Site	**n**	**Mean**	**Median**	**Std Dev**	**CV**	**Min-Max**	**25th-75th percentile**
Bases/Al_2O_3[a]							
PD3-2	10	0.45	0.45	0.04	0.10	0.16	0.03
PD2-2	10	0.38	0.36	0.08	0.20	0.24	0.08
PD2-1	10	0.42	0.40	0.13	0.30	0.37	0.22
PD1-2	10	0.22	0.20	0.06	0.28	0.17	0.07
"	24	0.22	0.20	0.06	0.26	0.18	0.09
PD1-1	10	0.19	0.18	0.02	0.10	0.06	0.02
Bases/R_2O_3[a]							
PD3-2	10	0.35	0.35	0.03	0.10	0.12	0.02
PD2-2	10	0.30	0.28	0.06	0.21	0.19	0.08
PD2-1	10	0.32	0.31	0.10	0.31	0.29	0.17
PD1-2	10	0.16	0.15	0.04	0.27	0.12	0.05
"	24	0.17	0.15	0.04	0.25	0.13	0.07
PD1-1	10	0.14	0.14	0.01	0.09	0.04	0.01
K_2O/TiO_2[a]							
PD3-2	10	1.55	1.54	0.04	0.03	0.15	0.04
PD2-2	10	1.54	1.47	0.24	0.16	0.65	0.32
PD2-1	10	1.64	1.55	0.42	0.26	1.22	0.44
PD1-2	10	1.00	0.94	0.20	0.20	0.65	0.14
"	24	0.99	0.91	0.19	0.19	0.68	0.22
PD1-1	10	1.08	1.08	0.06	0.05	0.20	0.03
CaO[b]							
PD3-2	10	0.85	0.85	0.16	0.18	0.60	0.09
PD2-2	10	0.55	0.57	0.24	0.43	0.77	0.25
PD2-1	10	0.44	0.48	0.11	0.26	0.31	0.18
PD1-2	10	0.22	0.22	0.05	0.21	0.14	0.06
"	24	0.24	0.24	0.05	0.20	0.17	0.07
PD1-1	10	0.14	0.13	0.06	0.47	0.18	0.09
K_2O[b]							
PD3-2	10	1.84	1.83	0.07	0.04	0.27	0.04
PD2-2	10	1.39	1.49	0.25	0.18	0.81	0.20
PD2-1	10	1.34	1.34	0.06	0.04	0.18	0.08
PD1-2	10	1.09	1.10	0.08	0.08	0.30	0.08
"	24	1.10	1.08	0.10	0.09	0.37	0.14
PD1-1	10	1.31	1.31	0.06	0.05	0.23	0.07
MgO[b]							
PD3-2	10	0.97	0.96	0.05	0.05	0.15	0.05
PD2-2	10	0.34	0.36	0.09	0.27	0.33	0.08
PD2-1	10	0.51	0.47	0.16	0.31	0.46	0.25
PD1-2	10	0.32	0.34	0.08	0.24	0.27	0.08
"	24	0.33	0.36	0.07	0.21	0.27	0.10
PD1-1	10	0.41	0.41	0.05	0.11	0.15	0.05

[a]Expressed as molar ratios on the basis of the dry weight of the <2 mm fraction.

[b]Expressed on an oxide basis as a percentage of the dry weight of the <2 mm fraction.

[c]Dithionite-extractable iron expressed as a percentage of the dry weight of the the <2 mm fraction.

[d]Dithionite-extractable / total iron.

Table 4.4, Continued. Descriptive statistics for selected chemical properties of the <2 mm fraction of the most pedogenically well-expressed B-horizon per pedon.

						Range	
Soil Property and Site	**n**	**Mean**	**Median**	**Std Dev**	**CV**	**Min-Max**	**25th-75th percentile**
Na_2O [b]							
PD3-2	10	0.81	0.80	0.10	0.12	0.36	0.07
PD2-2	10	0.62	0.67	0.23	0.37	0.74	0.29
PD2-1	10	0.49	0.53	0.08	0.16	0.27	0.09
PD1-2	10	0.28	0.26	0.08	0.29	0.30	0.03
"	24	0.28	0.26	0.09	0.30	0.34	0.07
PD1-1	10	0.20	0.21	0.04	0.22	0.16	0.04
Al_2O_3 [b]							
PD3-2	10	16.29	16.33	0.88	0.05	3.36	0.70
PD2-2	10	11.49	11.62	2.98	0.26	9.67	3.66
PD2-1	10	11.37	10.93	3.98	0.35	11.54	6.78
PD1-2	10	13.91	14.19	3.76	0.27	10.90	5.04
"	24	13.98	14.29	3.48	0.25	11.50	5.20
PD1-1	10	16.38	16.69	1.56	0.10	4.50	1.88
Fe_D [c]							
PD3-2	24	1.40	1.38	0.18	0.13	0.77	0.23
PD3-1	24	2.15	2.17	0.10	0.05	0.48	0.11
PD2-2	24	1.09	0.87	0.98	0.90	4.13	0.93
PD2-1	24	1.53	1.67	0.73	0.48	2.73	1.09
PD1-2	24	2.40	2.48	0.76	0.32	2.62	1.02
PD1-1	24	2.54	2.53	0.34	0.13	1.08	0.36
Fe_2O_3 [b]							
PD3-2	10	5.46	5.38	0.35	0.06	1.20	0.29
PD2-2	10	3.50	3.02	1.74	0.50	5.99	0.82
PD2-1	10	3.91	3.80	1.65	0.42	4.26	2.74
PD1-2	10	5.35	5.55	1.60	0.30	4.46	2.05
"	24	5.35	5.64	1.44	0.27	4.59	2.07
PD1-1	10	5.99	6.03	0.53	0.09	1.59	0.70
FeD/Fe_2O_3 [d]							
PD3-2	10	0.25	0.25	0.02	0.08	0.07	0.02
PD2-2	10	0.34	0.36	0.15	0.44	0.43	0.22
PD2-1	10	0.35	0.34	0.04	0.12	0.16	0.04
PD1-2	10	0.48	0.43	0.14	0.29	0.48	0.03
"	24	0.45	0.43	0.10	0.22	0.54	0.04
PD1-1	10	0.45	0.44	0.02	0.03	0.05	0.02

[a]Expressed as molar ratios on the basis of the dry weight of the <2 mm fraction.

[b]Expressed on an oxide basis as a percentage of the dry weight of the <2 mm fraction.

[c]Dithionite-extractable iron expressed as a percentage of the dry weight of the the <2 mm fraction.

[d]Dithionite-extractable / total iron.

Table 4.5. Descriptive statistics for selected chemical properties of the fine sand (0.125-0.250 mm) fraction of the most pedogenically well-expressed B-horizon per pedon. Elemental analysis was conducted on B-horizons from 24 pedons on the PD1-2 (pilot) scroll bar and 10 pedons on the remaining scroll bars. For PD1-2, descriptive statistics for the fine sand chemistry of the 24 pedons are provided along with statistics derived from a subsample of 10 of these 24 pedons to evaluate how effective the smaller sample size is at representing soil chemical variability in this setting. There is relatively good agreement between the central tendencies and dispersions of the two sample sizes for most parameters, indicating that a sample size of *n*=10 provides an adequate representation of the variability of most chemical properties of the fine sand fraction. However, scrutiny of the standard deviations and ranges of % K_2O and K_2O / TiO_2 suggest a sample size of 10 may slightly under-represent variability for these parameters.

						Range	
Soil Property and Site	**n**	**Mean**	**Median**	**Std Dev**	**CV**	**Min-Max**	**25th-75th percentile**
K_2O/TiO_2 [a]							
PD3-2	9	3.34	3.22	0.52	0.16	1.67	0.65
PD2-2	10	1.91	2.07	0.54	0.28	1.53	0.79
PD2-1	10	1.48	1.51	0.17	0.12	0.54	0.19
PD1-2	10	1.05	0.73	0.69	0.65	1.91	0.64
"	24	1.27	0.86	1.06	0.84	4.99	1.12
PD1-1	10	1.70	1.86	0.42	0.25	1.05	0.69
K_2O [b]							
PD3-2	9	2.70	2.64	0.36	0.13	1.11	0.40
PD2-2	10	1.39	1.35	0.13	0.09	0.39	0.15
PD2-1	10	1.15	1.15	0.08	0.07	0.24	0.11
PD1-2	10	0.90	0.90	0.11	0.13	0.40	0.13
"	24	0.95	0.95	0.19	0.20	0.80	0.20
PD1-1	10	1.03	1.03	0.12	0.12	0.36	0.17
CaO [b]							
PD3-2	9	0.80	0.81	0.07	0.09	0.25	0.07
PD2-2	10	0.74	0.69	0.15	0.20	0.48	0.12
PD2-1	10	0.68	0.66	0.19	0.28	0.55	0.25
PD1-2	10	0.21	0.20	0.06	0.30	0.17	0.11
"	24	0.22	0.21	0.08	0.35	0.27	0.13
PD1-1	10	0.09	0.08	0.02	0.18	0.04	0.02
MgO [b]							
PD3-2	9	1.05	1.13	0.26	0.24	0.81	0.33
PD2-2	10	0.20	0.17	0.07	0.34	0.18	0.06
PD2-1	10	0.22	0.22	0.05	0.23	0.15	0.06
PD1-2	10	0.07	0.07	0.03	0.39	0.07	0.04
"	24	0.07	0.08	0.03	0.38	0.08	0.05
PD1-1	10	0.11	0.10	0.04	0.39	0.12	0.06
Na_2O [b]							
PD3-2	9	1.26	1.25	0.07	0.05	0.20	0.09
PD2-2	10	0.93	0.93	0.11	0.11	0.36	0.11
PD2-1	10	0.72	0.75	0.09	0.12	0.27	0.12
PD1-2	10	0.38	0.34	0.13	0.35	0.46	0.11
"	24	0.38	0.34	0.14	0.36	0.26	0.22
PD1-1	10	0.34	0.32	0.06	0.16	0.18	0.06

[a] Expressed as a molar ratio on the basis of the dry weight of the 0.125-0.250 mm fraction.

[b] Expressed on an oxide basis as a percentage of the dry weight of the 0.125-0.250 mm fraction.

Table 4.6. Results of difference of means t-tests for selected soil morphological properties among soils of scroll bars on the same paleomeander surface. Soils that exhibited statistically significant differences at an alpha level of 0.05 with respect to a given property are provided in bold.

Soil Property and Site *(younger-older scroll bar)*	**Difference in means**	**Lower Limit, 95% Confidence Interval**	**Upper Limit, 95% Confidence Interval**	**P-value**	**n younger scroll bar**	**n older scroll bar**
B Thickness (cm)						
PD3-2 - PD3-1	**-14.4**	**-25.7**	**-3.1**	**0.0136**	**24**	**24**
PD2-2 - PD2-1	**-49.3**	**-66.0**	**-32.5**	**<0.0001**	**24**	**24**
PD1-2 - PD1-1	**-53.3**	**-68.3**	**-38.3**	**<0.0001**	**24**	**24**
Bt Thickness (cm)						
PD3-2 - PD3-1	N/A	N/A	N/A	N/A	N/A	N/A
PD2-2 - PD2-1	N/A	N/A	N/A	N/A	N/A	N/A
PD1-2 - PD1-1	**-59.5**	**-75.8**	**-43.1**	**<0.0001**	**24**	**24**
Solum Thickness (cm)						
PD3-2 - PD3-1	**-27.5**	**-43.1**	**-12.0**	**0.0009**	**24**	**24**
PD2-2 - PD2-1	**-55.5**	**-72.1**	**-38.9**	**<0.0001**	**24**	**24**
PD1-2 - PD1-1	**-57.4**	**-68.9**	**-45.8**	**<0.0001**	**24**	**24**
Rubification, Buntley-Westin Index units						
PD3-2 - PD3-1	**-2.9**	**-4.2**	**-1.6**	**<0.0001**	**24**	**24**
PD2-2 - PD2-1	**-9.7**	**-13.3**	**-6.1**	**<0.0001**	**24**	**24**
PD1-2 - PD1-1	-5.3	-12.0	1.5	0.1245	24	24
Rubification, Hurst Index units						
PD3-2 - PD3-1	0.3	-1.9	2.5	0.8084	24	24
PD2-2 - PD2-1	**25.9**	**11.3**	**40.4**	**0.0008**	**24**	**24**
PD1-2 - PD1-1	2.7	-0.5	5.8	0.0940	24	24
% Clay (<2 mm)						
PD3-2 - PD3-1	**-14.3**	**-16.0**	**-12.7**	**<0.0001**	**24**	**24**
PD2-2 - PD2-1	-1.8	-8.3	4.6	0.5659	24	24
PD1-2 - PD1-1	**-5.7**	**-10.9**	**-0.4**	**0.0357**	**24**	**24**

Notes: Bt horizons do not occur on scroll bars of the PD3 and PD2 surfaces, therefore Bt thickness was not evaluated by t-tests for these soils.

Table 4.7. Results of difference of means t-tests for selected soil chemical properties of the <2 mm fraction among soils of scroll bars on the same paleomeander surface. Groups of soils that exhibit statistically significant differences at an alpha level of 0.05 with respect to a given property are shown in bold. With the exception of dithionite-extractable iron, t-tests were not performed on chemical properties of PD3-2 and PD3-1 scroll bar soils because chemical data for PD3-1 samples are not available.

Soil Property and Site *(younger-older scroll bar)*	**Difference in means**	**Lower Limit, 95% Confidence Interval**	**Upper Limit, 95% Confidence Interval**	**P-value**	**n younger scroll bar**	**n older scroll bar**
Bases/Al_2O_3						
PD2-2 - PD2-1	-0.04	-0.14	0.06	0.4474	10	10
PD1-2 - PD1-1	0.03	-0.01	0.08	0.1296	10	10
Bases/R_2O_3						
PD2-2 - PD2-1	-0.03	-0.11	0.05	0.5088	10	10
PD1-2 - PD1-1	0.02	-0.01	0.06	0.1564	10	10
K_2O/TiO_2						
PD2-2 - PD2-1	-0.10	-0.42	0.23	0.5432	10	10
PD1-2 - PD1-1	-0.09	-0.23	0.06	0.2184	10	10
CaO						
PD2-2 - PD2-1	0.11	-0.07	0.29	0.1985	10	10
PD1-2 - PD1-1	**0.09**	**0.03**	**0.14**	**0.0030**	**10**	**10**
K_2O						
PD2-2 - PD2-1	0.05	-0.13	0.23	0.5673	10	10
PD1-2 - PD1-1	**-0.22**	**-0.29**	**-0.15**	**<0.0001**	**10**	**10**
MgO						
PD2-2 - PD2-1	**-0.16**	**-0.29**	**-0.04**	**0.0132**	**10**	**10**
PD1-2 - PD1-1	**-0.09**	**-0.15**	**-0.03**	**0.0082**	**10**	**10**
Na_2O						
PD2-2 - PD2-1	0.13	-0.04	0.29	0.1265	10	10
PD1-2 - PD1-1	**0.08**	**0.01**	**0.14**	**0.0225**	**10**	**10**
Al_2O_3						
PD2-2 - PD2-1	0.13	-3.20	3.45	0.9368	10	10
PD1-2 - PD1-1	-2.46	-5.27	0.34	0.0799	10	10
Fe_D						
PD3-2 - PD3-1	**-0.75**	**-0.83**	**-0.67**	**<0.0001**	**24**	**24**
PD2-2 - PD2-1	-0.44	-0.94	0.06	0.0847	24	24
PD1-2 - PD1-1	-0.14	-0.49	0.21	0.4164	24	24
Fe_2O_3						
PD2-2 - PD2-1	-0.42	-2.01	1.18	0.5895	10	10
PD1-2 - PD1-1	-0.64	-1.81	0.53	0.2540	10	10
Fe_D/Fe_2O_3						
PD2-2 - PD2-1	-0.02	-0.13	0.09	0.7321	10	10
PD1-2 - PD1-1	0.03	-0.07	0.13	0.5008	10	10

Notes: Differences in means for Bases/Al_2O_3, Bases/R_2O_3, and K_2O/TiO_2 are given in molar ratio units. Differences in means for Fe_D and all element oxides are given in units of percent dry weight of the <2 mm fraction.

Table 4.8. Results of difference of means t-tests for selected soil chemical properties of the fine sand (0.125-0.250 mm) fraction among soils of scroll bars on the same paleomeander surface. Soils that exhibited statistically significant differences at an alpha level of 0.05 with respect to a given property are provided in bold. T-tests were not performed on the fine sand chemistry of PD3-2 and PD3-1 scroll bar soils because chemical data for PD3-1 samples are not available.

Soil Property and Site *(younger-older scroll bar)*	**Difference in means**	**Lower Limit, 95% Confidence Interval**	**Upper Limit, 95% Confidence Interval**	**P-value**	**n younger scroll bar**	**n older scroll bar**
K_2O/TiO_2						
PD2-2 - PD2-1	**0.42**	**0.02**	**0.82**	**0.0393**	**10**	**10**
PD1-2 - PD1-1	**-0.65**	**-1.20**	**-0.11**	**0.0219**	**10**	**10**
CaO						
PD2-2 - PD2-1	0.07	-0.09	0.23	0.3820	10	10
PD1-2 - PD1-1	**0.12**	**0.08**	**0.17**	**0.0001**	**10**	**10**
K_2O						
PD2-2 - PD2-1	**0.24**	**0.14**	**0.35**	**0.0001**	**10**	**10**
PD1-2 - PD1-1	**-0.13**	**-0.24**	**-0.01**	**0.0297**	**10**	**10**
MgO						
PD2-2 - PD2-1	-0.02	-0.08	0.04	0.4594	10	10
PD1-2 - PD1-1	**-0.04**	**-0.07**	**-0.01**	**0.0172**	**10**	**10**
Na_2O						
PD2-2 - PD2-1	**0.21**	**0.12**	**0.30**	**0.0002**	**10**	**10**
PD1-2 - PD1-1	0.04	-0.06	0.14	0.3750	10	10

Notes: Differences in means for K_2O/TiO_2 are given in molar ratio units. Differences in means for FeD and all element oxides are given in units of percent dry weight of the 0.125-0.250 mm fraction.

Table 4.9. Selected statistics for linear regressions of soil properties versus mean age (ka). Properties were measured for the most pedogenically well-expressed B-horizon per pedon. B- and Bt-horizon thickness reflects the cumulative thicknesses of all B (or Bt) horizons in a given pedon.

Soil property	R	R^2	P (Significance of F-ratio)	b1[a]	b1 Lower limit, 95% C.I.	b1 Upper limit, 95% C.I.	n	Form[b]
Morphological properties								
B-horizon thickness (cm)	0.64	0.41	<0.0001	0.5439	0.4362	0.6516	144	linear
Bt-horizon thickness (cm)	0.94	0.88	<0.0001	1.2554	1.1800	1.3308	144	nonlinear (exp. grwth.)
Solum thickness (cm)	0.71	0.51	<0.0001	0.7116	0.5947	0.8285	144	linear
Percent clay (<2 mm)	0.46	0.22	<0.0001	0.1024	0.0700	0.1347	144	linear
Buntley-Westin Index value	0.63	0.40	<0.0001	0.1426	0.1137	0.1714	144	linear
Hurst Index value	-0.32	0.10	0.0001	-0.1310	-0.1963	-0.0657	144	nonlinear
Chemical properties (<2 mm)								
Bases:Al_2O_3	-0.82	0.67	<0.0001	-0.0022	-0.0026	-0.0017	50	linear to nonlinear (exp. dec.)
Bases:Resistant oxides	-0.82	0.68	<0.0001	-0.0017	-0.0021	-0.0014	50	linear to nonlinear (exp. dec.)
K_2O:TiO_2	-0.73	0.53	<0.0001	-0.0052	-0.0066	-0.0038	50	linear
% K_2O	-0.62	0.39	<0.0001	-0.0035	-0.0048	-0.0022	50	nonlinear (exp. dec.)
% CaO	-0.79	0.63	<0.0001	-0.0046	-0.0056	-0.0036	50	nonlinear (exp. dec.)
% MgO	-0.51	0.26	0.0002	-0.0027	-0.0040	-0.0014	50	nonlinear (exp. dec.)
% Na_2O	-0.83	0.68	<0.0001	-0.0042	-0.0050	-0.0034	50	nonlinear (exp. dec.)
% Al_2O_3	0.25	0.07	0.0739	0.0183	-0.0018	0.0385	50	linear
% Fe_D	0.53	0.28	<0.0001	0.0089	0.0066	0.0113	144	linear
% Fe_2O_3	0.40	0.16	0.0042	0.0128	0.0042	0.0214	50	linear
Fe_D:Fe_2O_3	0.62	0.39	<0.0001	0.0015	0.0010	0.0021	50	linear
Chemical properties (0.125-0.250 mm)								
K_2O:TiO_2	-0.51	0.26	0.0002	-0.0092	-0.0138	-0.0046	49	nonlinear (exp. dec.)
% K_2O	-0.63	0.40	<0.0001	-0.0085	-0.0115	-0.0054	49	nonlinear (exp. dec.)
% CaO	-0.93	0.87	<0.0001	-0.0060	-0.0067	-0.0053	49	linear
% MgO	-0.57	0.33	<0.0001	-0.0043	-0.0062	-0.0025	49	nonlinear (exp. dec.)
% Na_2O	-0.89	0.79	<0.0001	-0.0064	-0.0073	-0.0054	49	nonlinear (exp. dec.)

[a]Slope of the regression line.

[b]Form of the relationship between soil property and mean age estimate. Exp. dec. = exponential decay; exp.grwth. = exponential growth.

CHAPTER 5 - CONCLUSION

5.1 Conclusions

Geologic mapping of Quaternary sediments along the lower Oconee River indicates that the Oconee valley contains a far richer and more diverse array of fluvial landforms and deposits than previous mapping suggests, consisting of eight alloformations that range in age from early to middle Pleistocene to late Holocene. In terms of the complexity of late Quaternary valley fills in the southeastern Coastal Plain, results from the Oconee valley are generally consistent with the findings of Leigh et al. (2004), who documented three braided river terraces, as well as eolian dunes, located within a single map unit of Owens (1989), the fluvial facies of the upper Wando Formation.

The Oconee valley mapping provides detailed information about the three dimensional architecture of fluvial deposits and the range of variability that is possible in the surficial sediments of typical Coastal Plain alluvial valleys. This information has important implications, not only for our understanding of the geologic history of Coastal Plain river valleys, but also for modeling of groundwater movement and contaminant transport, identification of deposits with economic resource potential (e.g., clay, sand, and gravel), and geoarchaeological surveys that rely on geologic and geomorphic criteria to identify to identify deposits that require deep subsurface survey for archaeological sites buried by sedimentation. In terms of its Quaternary geology and geomorphology, the lower Oconee valley constitutes a representative setting with respect to alluvial valleys of the southeastern Coastal Plain, and findings from the Oconee should be generally correlative to other locations in the region, given the many regional similarities

exhibited by late Quaternary landforms and deposits among river valleys in the southeastern Atlantic Coastal Plain (Leigh, 2008).

Results indicate that the Oconee River had a braided morphology during the late Wisconsin interval (ca. 35-17 ka), a mega-meandering morphology during the terminal Pleistocene (ca. 17-11 ka), and a meandering morphology with more modern-like channel dimensions during the early to late Holocene (ca. 11 ka to present). These morphological phases are exhibited by rivers elsewhere in the region during this time and represent former fluvial regimes that are linked to discrete paleoenvironmental episodes (Leigh, 2008). On the Oconee River, mapping indicates that these fluvial regimes produced unique allostratigraphic units during the late Quaternary.

The geomorphic, stratigraphic, and geologic framework provided by the Oconee mapping provides a context that facilitates the study of mega-meander paleochannels both along the Oconee River and elsewhere in the southeastern Coastal Plain. Previous studies have concluded that the large planform dimensions of mega-meanders represent considerably larger-than-modern bankfull floods (Gagliano and Thom, 1967; Leigh and Feeney, 1995; Leigh, 2006, 2008). However, this study indicates that mega-meanders conveyed bankfull flood sizes that were similar to, or at most only modestly larger than, the discharge of low magnitude, high frequency floods on present-day Coastal Plain rivers.

Results of this study indicate that mega-meanders were wide and shallow, and their relatively modest discharge reflects their comparatively lower hydraulic efficiency relative to modern rivers, which resulted from a high width to depth ratio and a correspondingly reduced hydraulic radius. It appears that the exceptionally large planform dimensions of mega-meanders are more likely a product of a sediment discharge regime characterized by large quantities of

bedload sand, relatively low amounts of fine-grained vertical accretion, and the influence of these factors on bed and bank composition and channel shape, and not necessarily unusually large bankfull floods. Mega-meandering planforms were established during the terminal Pleistocene, following a late Wisconsin phase of sand-bed braiding, in response to the onset of warmer, more moist climatic conditions that drove afforestation and decrease in upland sediment yield, while simultaneously stabilizing river banks with vegetation and causing incision beneath braided floodplains (Leigh, 2006, 2008). The distinctive, scrolled floodplains of terminal Pleistocene mega-meanders, which are underlain by large volumes of lateral accretion sand but comparatively little fine-grained vertical accretion sediment (Leigh, 2006; Figs. 3.2-3.5, Chapter three), confirm that mega-meanders transported large volumes of bedload sediment and suggests that these paleochannels may represent a transitional meandering planform that was still heavily influenced by large quantities of bedload sand following sand-bed braiding during the late Wisconsin, ca. 30-17 ka (Leigh, 2006, 2008), as they laterally eroded sandy braided river deposits. This geomorphic and sedimentologic context would readily satisfy the criteria required to yield the wide, shallow sand bed channels typical of mega-meanders, given current understanding of relationships between sediment supply, bank material composition, and channel morphology, and is well-illustrated by spatial and geochronologic relationships between alloformation Qp5 (which consists of braided river deposits) and alloformation Qp6 (which consists of mega-meander deposits) in the lower Oconee River map area (Chapter two, Plates 1 and 2b). This example from the Uvalda, Georgia locality, demonstrates how the geomorphic, stratigraphic, and geochronologic relationships documented by the Oconee mapping between terminal Pleistocene mega-meander deposits and those of immediately older and younger alloformations provides useful contextual information for interpreting the morphology and

process regime of mega-meander paleochannels. This affirms the utility of conducting paleochannel analysis within the framework of a broader subsurface study.

The final component of this dissertation involved examination of soil variability and development across a chronosequence of meander channel scroll bar deposits in the Pee Dee River valley of the South Carolina Coastal Plain that range in age from Holocene to 119±30 ka. Because there are general similarities between the Oconee and Pee Dee valleys in terms of their late Quaternary landforms and deposits, findings from Oconee mapping, as well as previous studies of the geomorphology and late Quaternary history of the Pee Dee valley (Leigh et al., 2004), were useful in interpreting the geologic and geomorphic framework of the Pee Dee soil chronosequence.

Central tendencies of the morphological and chemical properties of soils in the Pee Dee chronosequence were found to become increasingly developed over the ~100 ka timescale of the chronosequence, as illustrated by increases in solum thickness, cumulative B-horizon thickness, rubification, and dithionite-iron to total iron and decreases in the concentrations of bases in both the whole soil and fine sand fractions. Some properties, like B-horizon and solum thickness appear to increase gradually with time, suggesting progressive development, while others, such as changes in the bulk chemistry of the whole soil and fine sand fractions that reflect mineral weathering trends, appear to change episodically. To varying degrees, the general directions of the age-related trends observed in Pee Dee scroll bar soils agree with those documented by other chronosequence studies in the southeastern Coastal Plain (Markewich et al., 1987, 1988, 1989; Howard et al., 1993; Shaw et al., 2003; Suther, 2006), though the magnitude and rates of change among Pee Dee soils versus those examined by previous studies may vary from property to

property, depending upon the particular geomorphic, geologic, and climatic settings and timescales involved.

Nevertheless, data indicate a large degree of soil spatial variability within the Pee Dee chronosequence, both at the scale of individual scroll bars and among older versus younger scroll bars of the same paleomeander surface. A significant component of the soil variability observed within individual scroll bars of the Pee Dee chronosequence appears to be related to systematic changes (or a lack of systematic change) in parent material and relief along scroll bar ridge crests related to the morphology, sedimentology, and stratigraphy of scroll bar deposits. Within individual scroll bars, soil variability bears a strong linkage to variation (or lack of variation) in local relief and the thickness and texture of vertical accretion deposits that is most strongly expressed by soil morphological properties, with soils exhibiting increasing B (or Bt) and solum thickness, higher B horizon clay content, and lower B horizon rubification in the downstream direction along scroll bars characterized by downstream decreases in local relief and downstream increases in the thickness and clay content of their vertical accretion sediments. Among older versus younger scroll bars of the same paleomeander surface, in some cases, variability in gross soil morphology appears to be linked to systematic spatial variation in the thickness and grain size of vertical accretion deposits across an individual paleomeander surface, with thicker, more finely textured B-horizons and sola being associated with older scroll bars located on the interior of paleomeander surfaces that have been subjected to overbank sedimentation in lower energy floodplain positions for greater durations of time. In other instances, the thicker B horizons and sola of soils on scroll bars on the interiors of paleomeanders surfaces may simply reflect a greater duration of pedogenesis.

While the variability among scroll bar soils is not so great that it invalidates the chronosequence approach in this setting, Pee Dee data demonstrate the necessity of a thorough understanding of soil variability within geomorphic surfaces of uniform age prior to undertaking a soil chronosequence study and support the recommendation of Schaetzl et al. (2006) that researchers sample large numbers of profiles and focus on central tendency values, while incorporating data pertaining to soil variability or "range of expression" within individual landforms, when developing chronosequence interpretations. In the case of the Pee Dee chronosequence, a general understanding of the stratigraphy and sedimentology of scroll bar deposits that was facilitated by the geologic mapping and paleohydrologic investigations associated with this broader dissertation research project were found to be helpful in interpreting soil variability across the chronosequence. Future research pertaining to the Pee Dee chronosequence will attempt to model scroll bar soils using multivariate statistical techniques and quantitative measures of parent material, relief, soil drainage, and age variables to better quantify the drivers and pedogenic processes responsible for soil spatial and temporal variation in this setting.

5.2 References

Gagliano, S.M., Thom, B.G., 1967. Deweyville terrace, Gulf and Atlantic Coasts. Louisiana State University, Coastal Studies Bulletin, Vol. 1, 23-41.

Howard, J.L., Amos, D.F., and Daniels, W.L., 1993. Alluvial soil chronosequence in the inner Coastal Plain, central Virginia. Quaternary Research 39, 201-213.

Leigh, D.S., 2008. Late Quaternary climates and river channels of the Atlantic Coastal Plain, Southeastern USA. Geomorphology 101, 90-108.

Leigh, D.S., Srivastava, P., Brook, G.A., 2004. Late Pleistocene braided rivers of the Atlantic Coastal Plain, USA. Quaternary Science Reviews 23, 65-84.

Leigh, D.S., 2006. Terminal Pleistocene braided to meandering transition in rivers of the Southeastern USA. Catena 66, 155-160.

Leigh, D.S., Feeney, T.P., 1995. Paleochannels indicating wet climate and lack of response to lower sea level, southeast Georgia. Geology 23, 687-690.

Markewich, H.W., Pavich, M.J., Mausbach, M.J., Hall, R.L., Johnston, R.G., Hearn, R.P., 1987. Age relationships between soil and geology on the Coastal Plain of Maryland and Virginia. U.S. Geological Survey Bulleting 1589-A. U.S. Government Printing Office, Washington DC, USA, pp. A1-A34.

Markewich, H.W., Lynn, W.C., Pavich, M.J., Johnston, R.G., Meetz, J.C., 1988. Analysis of four Inceptisols of Holocene age, east-central Alabama. U.S. Geological Survey Bulletin 1589-C. U.S. Government Printing Office, Washington, D.C., USA, pp. C1-C29.

Markewich, H.W., Pavich, M.J., Mausbach, M.J., Johnson, R.G., and Gonzalez, V.M., 1989. A guide for using soil and weathering profile data in chronosequence studies of the Coastal Plain of the eastern United States. U.S. Geological Survey Bulletin 1589-D. U.S. Government Printing Office, Washington, D.C., USA, pp. D1-D39.

Owens, J.P., 1989. Geologic Map of the Cape Fear Region, Florence 1 × 2 degree Quadrangle and Northern Half of the Georgetown 1 × 2 degree Quadrangle, North Carolina and South Carolina. US Geological Survey Miscellaneous Investigations Series Map I-1948-A (Sheet 1/2).

Schaetzl, R.J., Mikesell, L.R., and M.A. Velbel, 2006. Expression of Soil Characteristics Related to Weathering and Pedogenesis Across a Geomorphic Surface of Uniform Age in Michigan. Physical Geography 27, 170-188.

Shaw, J.N., Odom, J.W., Hajeck, B.F., 2003. Soils on Quaternary terraces of the Tallapoosa River, Central Alabama. Soil Science 168 (10), 707-717.

Suther, B.E., 2006. Soil Chronosequence of the Little River valley, Atlantic Coastal Plain, North Carolina. Unpublished MS Thesis, University of Georgia, Athens, Georgia, USA.

APPENDIX A – PROFILE DESCRIPTIONS FROM STRATIGRAPHIC CROSS-SECTIONS A, B, AND C, UVALDA, GEORGIA QUADRANGLE

KEY TO CODES USED IN SOIL AND SEDIMENT DESCRIPTIONS

(Codes are derived from the USDA-NRCS Soil Survey conventional code system)

Soil Texture

Texture Class or Subclass*	Code
sand	s
very coarse sand	vcos
coarse sand	cos
medium sand	ms
fine sand	fs
very fine sand	vfs
loamy sand	ls
loamy coarse sand	lcos
loamy medium sand	lms
loamy fine sand	lfs
sandy loam	sl
coarse sandy loam	cosl
medium sandy loam	msl
fine sandy loam	fsl
very fine sandy loam	vfsl
loam	l
silt loam	sil
silt	si
sandy clay loam	scl
fine sandy clay loam	fscl
very fine sandy clay loam	vfscl
clay loam	cl
silty clay loam	sicl
sandy clay	sc
fine sandy clay	fsc
silty clay	sic
clay	c

*Where texture is an intergrade between two classes or subclasses (e.g., sl to ls), the first texture given is the best estimate.

Texture Modifiers	Code
upper	upper half of size fraction
lower	lower half of size fraction
gravelly	15-35% gravel by volume
very gravelly	36-60% gravel by volume

Horizon Boundary

Distinctness class	Code
abrupt	a
clear	c
gradual	g
diffuse	d

Redoximorphic Features (RMF)

Quantity	Code
few	f
common	c
many	m

Size	Code
fine	no code
medium	no code
coarse	no code
very coarse	no code

Contrast	Code
faint	F
distinct	D
prominent	P

Soil Structure

Natural soil structural units	
Type	**Code**
granular	gr
angular blocky	abk
subangular blocky	sbk
platy	pl
prismatic	pr
columnar	cpr

Structureless	Code
single grain	sg
massive	m

Grade	Code
structureless	0
weak	1
moderate	2
strong	3

Size Class	Code
very fine (very thin)	vf (vn)
fine (thin)	f (tn)
medium	m
coarse (thick)	co (tk)
very coarse (very thick)	vc (vk)

*Size class for platy structure given in parentheses.

CROSS-SECTION A-A’

Table A1. Description for core 1, cross-section A-A’.

Location:	**Uvalda Quadrangle**	**Map Unit:**	Qh2
Transect:	**A**	**Geomorphic Component:**	Levee shoulder near back levee
Core #:	**1**	**Other Remarks:**	7 m from left top of bank of Oconee River.
***Easting:**	348850 m	**Date:**	12/14/2011
***Northing:**	3544028 m	**Personnel:**	BES, CSC
*UTM NAD 83		**Sampling Method:**	Hand auger

Depth (cm)	Horizon	Color	RMF	Texture	Structure	Bndy	Remarks
0-15	A	10YR 3/4	---	sil	1fsbk	g	Vertical accretion (Historical?)
15-75	C1	10YR 4/4	---	sil	m (?)	g	Vertical accretion (Historical?). Coarser than A.
75-85	C2	10YR 4/6	---	fsl	m (?)	a	Vertical accretion (Historical?)
85-100	Bwb	7.5YR 4/4	---	cl	2fsbk	g	Vertical accretion (Prehistoric?)
100-140	Bgb	7.5YR 4/1	---	c	2fsbk	a	Vertical accretion (Prehistoric?)
140-170	C'1	2.5YR 4/6	c, fine, P, 5YR 3/4	ms	sg	g	Lateral accretion. Few 1-2 mm grains.
170-190+	C'2	5YR 4/4	---	cos	sg	---	Lateral accretion. More 1-2 mm grains than C'1.

Notes:

Table A2. Description for core 2, cross-section A-A’.

Location:	**Uvalda Quadrangle**	**Map Unit:**	Qh2
Transect:	**A**	**Geomorphic Component:**	Ridge
Core #:	**2**	**Other Remarks:**	On road
***Easting:**	348937 m	**Date:**	12/14/2011
***Northing:**	3544030 m	**Personnel:**	BES, CSC
*UTM NAD 83		**Sampling Method:**	Hand auger and tile probe

Depth (cm)	Horizon	Color	RMF	Texture	Structure	Bndy	Remarks
0-20	Bw1	7.5YR 3/4	---	cl	1fsbk	no data	Vertical accretion. A horizon removed.
20-40	Bw2	7.5YR 3/4	---	scl	1fsbk	a	Vertical accretion. Fines upward from medium sand near base.
40-60	C1	7.5YR 4/6	---	upper ms	sg	c	Uppermost lateral accretion. Few granules. Moderately well sorted.
60-90	C2	7.5YR 5/4	---	upper cos	sg	g	Lateral accretion. Common granules. Moderately sorted.
90-160	C3	10YR 6/4	---	cos	sg	g	Lateral accretion. Fines upward from upper to lower coarse sand. Common granules. Moderately sorted.
160-190+	C4	10YR 6/4	---	cos	sg	---	Lateral accretion. Common granules & 8 mm gravels. Poorly sorted.

Notes: Probed to 220 cm: similar to 160-190 cm. Refusal at 220 cm on firm sand. No gravel detected at 220 cm.

Table A3. Description for core 3, cross-section A-A'.

Location:	**Uvalda Quadrangle**	**Map Unit:**	Qh2
Transect:	**A**	**Geomorphic Component:**	Paleochannel
Core #:	**3**	**Other Remarks:**	On road
***Easting:**	349008 m	**Date:**	9/23/2011
***Northing:**	3544030 m	**Personnel:**	BES, DSL
*UTM NAD 83		**Sampling Method:**	Giddings drill rig: core & flight auger

Depth (cm)	Horizon	Color	RMF	Texture	Structure	Bndy	Remarks
0-3	A	7.5YR 3.5/3	---	cl	1vfsbk	a	Vertical accretion paleochannel fill. Compacted, partially removed.
3-36	Bw	5YR 4/4	c, coarse, P, 2.5Y 5/3	c to cl	2fsbk	c	Vertical accretion paleochannel fill. Mn masses at 25-36 cm.
36-70	Bg1	10YR 6/2	c, medium, P, 10YR 5/8	c to sic	1fsbk	g	Vertical accretion paleochannel fill.
70-159	Bg2	10YR 6/1.5	c, coarse, P, 10YR 5/8	sicl to 110 cm, fsl to 159 cm	1fsbk	g	Vertical accretion paleochannel fill. Fines upward.
159-210	Bg3	2.5Y 6.5/1	c, v. coarse, P, 10YR 4/4	fsl	0 to 1fsbk	c	Vertical accretion paleochannel fill.
210-274	Cg1	N /5.5	c, coarse, P, 10YR 4/6	sicl to sic	m	a	Vertical accretion paleochannel fill. RMF at 210-231 cm. Organically enriched beds at 244-250 and 255-265 cm.
274-480	Cg2	10YR 7/1	---	cos	sg	a	Lateral accretion and bedload. Few 5-15 mm gravels from 310-480 cm.
480-600+	2Cg	5BG/1	---	c	m	---	Pre-Quaternary sediment. Abrupt contact at 480 cm.

Notes: Core refusal at 335 cm. Recovery below 288 cm by flight auger. Drilled to 600 cm but backed out to 570 cm for recovery.

Table A4. Description for core 4, cross-section A-A'.

Location:	**Uvalda Quadrangle**	**Map Unit:**	Qh1
Transect:	**A**	**Geomorphic Component:**	Ridge
Core #:	**4**	**Other Remarks:**	In planted pines south of road.
***Easting:**	349186 m	**Date:**	12/14/2011
***Northing:**	3544032 m	**Personnel:**	BES, CSC
*UTM NAD 83		**Sampling Method:**	Hand auger

Depth (cm)	Horizon	Color	RMF	Texture	Structure	Bndy	Remarks
0-5	A	10YR 4/4	---	sil	1mgr	a	Vertical accretion. Partially removed.
5-15	Bw1	10YR 4/4	---	sicl	1fsbk	c	Vertical accretion
15-45	Bw2	10YR 5/4	---	c	1 to 2fsbk	d	Vertical accretion. More angular structure than Bw1.
45-95	Bw3	2.5Y 5.5/4	c, fine, D, 10YR 6/6	c	1 to 2fsbk	a	Vertical accretion. Yellow.
95-135	C1	7.5YR 4/6	---	upper ms to lower cos	sg	c	Lateral accretion. No granules.
135-210	C2	10YR 5.5/6	---	upper ms	sg	c	Lateral accretion. Bed of 2.5Y 6/4 moderately sorted fine sand at 180-187 cm (no granules). Bed of 10YR 5.5/6 moderately sorted cos with few 5 mm gravels at 195-210 cm.
210-245	C3	10YR 7/3	---	upper ms	sg	c	Lateral accretion. Few 5 mm gravels. Moderately sorted.
245-270	C4	10YR 7/4	---	ms	sg	c	Lateral accretion. No granules. Moderately sorted.
270-310	C5	10YR 7/2	---	cos	sg	---	Lateral accretion. Few to common 6 mm gravels. Poorly sorted.

Notes: Historical/prehistoric contact uncertain but may be at 15 cm: Bw2 & Bw3 have similar texture and structure that display more development than A and Bw1. Lateral accretion at 95 cm. Below 135 cm, lateral accretion consists of stratified sands. Definite gravel lag not encountered.

Table A5. Description for core 5, cross-section A-A'.

Location:	**Uvalda Quadrangle**	**Map Unit:**	Qh1
Transect:	**A**	**Geomorphic Component:**	Ridge
Core #:	**5**	**Other Remarks:**	On road
***Easting:**	349331 m	**Date:**	9/23/2011
***Northing:**	3544035 m	**Personnel:**	BES, DSL
*UTM NAD 83		**Sampling Method:**	Giddings drill rig: core & flight auger

Depth (cm)	Horizon	Color	RMF	Texture	Structure	Bndy	Remarks
0-8	BA	7.5YR 4/3	---	c	2fsbk	c	Vertical accretion. A horizon removed.
8-40	Bw	10YR 5.5/3	---	c	2mpr parting to 3m to fsbk	g	Vertical accretion. Few Mn masses.
40-84	Bg1	10YR 6/2	m, medium, P, 10YR 5/8	c	1fsbk	g	Vertical accretion
84-164	Bg2	10YR 6/1	c, coarse, P, 10YR 5/8	c	1fsbk	a	Vertical accretion. Fines upward from sandy loam near base.
164-270	C	10YR 5/8	---	ms	sg	g	Uppermost lateral accretion. Reduced zone (10YR 7/2) at 164-180 cm.
270-480	Cg1	10YR 5/1	---	cos	sg	no data	Lateral accretion grading to possible bedload with depth. Few <10 mm gravels.
480-580	Cg2	N 4.5/	---	upper cos	sg	a	Lateral accretion and bedload. 10-15 mm gravels.
580-620	2Cg1	5G 5/1	---	sc	m	d	Pre-Quaternary sediment. Abrupt contact at 580 cm. Fine sandy clay texture.
620-700+	2Cg2	5GY 6/1	---	fsl	m	---	Pre-Quaternary sediment.

Notes: B horizons have more well-developed structure than in 349008 m hole but lack clay films.

Table A6. Description for core 6, cross-section A-A'.

Location:	**Uvalda Quadrangle**	**Map Unit:**	Qh1
Transect:	**A**	**Geomorphic Component:**	Paleochannel
Core #:	**6**	**Other Remarks:**	North of road. ^{14}C date site (UGAMS 10683).
***Easting:**	349469 m	**Date:**	12/14/2011
***Northing:**	3544040 m	**Personnel:**	BES, CSC
*UTM NAD 83		**Sampling Method:**	Hand auger and tile probe

Depth (cm)	Horizon	Color	RMF	Texture	Structure	Bndy	Remarks
0-5	Ag	10YR 3/2	c, fine, P, 10YR 3/6	c	1fsbk	no data	Vertical accretion paleochannel fill
5-75	Bg1	10YR 6.5/1	c, fine, P, 7.5YR 5/8	c	2fsbk	no data	Vertical accretion paleochannel fill. Structure has "worm cast" look to it.
75-110	BCg	10YR 6.5/1	c, fine, P, 7.5YR 5/8	c	0 to 1fsbk	no data	Vertical accretion paleochannel fill. Fines upward from sandy clay in lower part.
110-160	Cg1	N 6/	f, medium, P, 7.5YR 5/8	c	m	no data	Vertical accretion paleochannel fill. Very plastic.
160-200	Cg2	10YR 3/1.5	---	c	m	a	Vertical accretion paleochannel fill. Moderately plastic. Loses clay content with depth.
200-225+	Cg3	10YR 7/1	---	ms	sg	---	Channel bed sand.

Notes: Probed to 280 cm. Coarse sand with granules from 250-280 cm. Refusal at 280 cm on firm sand. No gravel detected at 280 cm.
Sampled at dusk under time constraints - some horizon boundaries accidentally omitted.

Table A7. Description for core 7, cross-section A-A'.

Location:	**Uvalda Quadrangle**	**Map Unit:**	Qp5
Transect:	**A**	**Geomorphic Component:**	Low ridge near terrace scarp
Core #:	**7**	**Other Remarks:**	On road. ^{14}C date site (UGAMS 9719).
***Easting:**	349560 m	**Date:**	9/23/2011
***Northing:**	3544032 m	**Personnel:**	BES, DSL
*UTM NAD 83		**Sampling Method:**	Giddings drill rig: core & flight auger

Depth (cm)	Horizon	Color	RMF	Texture	Structure	Bndy	Remarks
0-3	---	---	---	---	---	---	Road fill
3-20	A	7.5YR 4/4	---	sl	1tkpl	c	Vertical accretion. Platy from compaction.
20-57	E	7.5YR 4/6	---	ls to sl	1msbk	g	Vertical accretion
57-77	Bw	7.5YR 4.5/6	---	ls	1msbk	c	Vertical accretion
77-91	Bt	7.5YR 5/8	---	sl	1msbk	c	Vertical accretion. Few to common clay films on faces of peds and bridging sand grains.
91-222	C1	10YR 6/6	---	ms	sg	g	Mid- to lower braid bar sediment.
222-375	C2	7.5YR 5/6	---	gr vcos	sg	c	Bedload. Granules and pea gravel w/up to 12 mm grains. 290-375 cm well oxidized, with 359-375 cm = 7.5YR 5/8. 222-290 cm = 10YR 6/6.
375-680	Cg1	10YR 6/2	---	vgr cos	sg	no data	Bedload. Pea gravel w/up to 13 mm grains. 375-410 cm = 10YR 5/1.
680-920	Cg2	N /5	---	ms to cos	sg	a	Bedload. Finer than Cg1 except 720-840 cm = gravelly coarse sand. Interbedded lenses of sandy clay loam.
920-960+	2Cg	5G 5/1	---	vfsl to l	m	---	Pre-Quaternary sediment.

Notes: Only hole on Qp5 or Qp4 where pre-Quaternary sediments could be reached with the drill rig.

Table A8. Description for core 8, cross-section A-A'.

Location:	**Uvalda Quadrangle**	**Map Unit:**	Qp5
Transect:	**A**	**Geomorphic Component:**	In broad, flat braid swale
Core #:	**8**	**Other Remarks:**	Near scarp cut by more deeply incised braided paleochannel
***Easting:**	349706 m	**Date:**	12/15/2011
***Northing:**	3544039 m	**Personnel:**	BES, CSC
*UTM NAD 83		**Sampling Method:**	Hand auger

Depth (cm)	Horizon	Color	RMF	Texture	Structure	Bndy	Remarks
0-20	A	10YR 4/3	---	msl to ls	0 to 1vfsbk	g	Vertical accretion
20-35	E1	10YR 5/4	---	msl to ls	1vfsbk to sg	g	Vertical accretion
35-45	E2	10YR 5/5	---	lms	sg	g	Vertical accretion
45-72	BE	10YR 5.5/6	---	msl	1vfsbk	c	Vertical accretion
72-110	Btg	10YR 5/2	c, coarse, P, 7.5YR 5/8	scl	1msbk	g	Vertical accretion. Matrix color grades to 10YR 7/2 w/depth.
110-135	C1	10YR 7/2	c, medium, P, 10YR 7/8	upper ms	sg	g	Mid- to lower braid bar sediment.
135-165	C2	10YR 7/2	---	lower ms	sg	c	Mid- to lower braid bar sediment.
165-240+	C3	10YR 6/2	---	vgr cos	sg	---	Mid- to lower bar braid bar or bedload sediment. ≤10 mm gravel. Poorly sorted.

Notes:

Table A9. Description for core 9, cross-section A-A'.

Location:	**Uvalda Quadrangle**	**Map Unit:**	Qp5
Transect:	**A**	**Geomorphic Component:**	Braided paleochannel.
Core #:	**9**	**Other Remarks:**	Lowest part of paleochannel, no active stream channel present.
***Easting:**	349746 m	**Date:**	12/15/2011
***Northing:**	3544042 m	**Personnel:**	BES, CSC
*UTM NAD 83		**Sampling Method:**	Hand auger and tile probe

Depth (cm)	Horizon	Color	RMF	Texture	Structure	Bndy	Remarks
0-20	Ag	10YR 2/1.5	---	l	1mgr	g	Braided paleochannel fill.
20-40	Abg	10YR 2/1	---	scl	1fsbk	c	Braided paleochannel fill.
40-60	Cg1	10YR 4/2	---	upper ms	sg	c	Braided paleochannel fill. Few granules
60-80	Cg2	10YR 3/1	---	sl	m	a	Braided paleochannel fill. Few granules
80-110	Cg3	10YR 5/2	---	upper ms	sg	g	Bedload. Rare granules ≤6 mm.
110-165	Cg4	N 4.5/	---	upper ms	sg	c	Bedload. Few granules.
165-180+	Cg5	10YR 6/2	---	upper ms	sg	---	Bedload. 165-170 cm = oxidized zone, 10YR 6/8.

Notes: Stratified swale fill and channel bed sediments. Contact with braided channel sediments interpreted at 80 cm. Stratification is captured by horizons. Within horizons, sediments are uniform. There is no active stream channel in the swale at present. Swale fill appears to have been deposited during reoccupation by Oconee floodwaters rather than the product of small stream deposition.

Table A10. Description for core 10, cross-section A-A'.

Location:	**Uvalda Quadrangle**	**Map Unit:**	Qp5
Transect:	**A**	**Geomorphic Component:**	Crest of braid bar ridge w/possible eolian cover
Core #:	**10**	**Other Remarks:**	Leigh et al., 2004 CV-1 OSL date location
***Easting:**	349816 m	**Date:**	12/15/2011
***Northing:**	3544040m	**Personnel:**	BES, CSC
*UTM NAD 83		**Sampling Method:**	Hand auger

Depth (cm)	Horizon	Color	RMF	Texture	Structure	Bndy	Remarks
0-25	A	10YR 2/2	---	lower ms	sg	g	Upper braid bar or eolian (?)
25-60	CA	10YR 3/4	---	lower ms	sg	d	Upper braid bar or eolian (?)
60-120	C1	10YR 5/6	---	lower ms	sg	d	Upper braid bar or eolian (?) Finer texture than A & AC. Well to moderately well sorted.
120-240	C2	10YR 6/6	---	lower ms	sg	d	Upper braid bar or eolian (?) Texture and sorting identical to C1.
240-307	C3	10YR 6/6	---	lower ms	sg	c	Upper braid bar or eolian (?) Slightly coarser and slightly less sorted than C1 & C2.
307-315	beta-B	10YR 5/8	---	sl	1fsbk	c	Upper braid bar or eolian (?) Clay-iron band.
315-360	C4	10YR 5/8	---	lower ms	sg	g	Upper braid bar or eolian (?) Sorting similar to C3.
360-435	C5	10YR 6/8	---	ms	sg	c	Braid bar alluvium. Granules and fine gravels (≤10 mm). Moderately sorted.
435-460	C6	10YR 7/4	---	lower ms	sg	c	Braid bar alluvium. Few granules. Moderately well sorted.
460-495	C7	10YR 6/8	---	ms	sg	c	Braid bar alluvium. Rare gravels (≤12 mm). Moderately sorted.
495-530+	C8	10YR 6/5	---	cos	sg	---	Braid bar alluvium. Granules & fine gravel (≤5 mm). Moderately sorted.

Notes: Either extremely well-sorted upper braid bar sediments or a re-worked eolian cover may be present from 0-240 cm (and possibly as deep as 360 cm) based on high degree of sorting and lack of >1.0 mm grains. Fluvial gravels encountered at 360 cm. Alluvium interpreted as being deposited in a middle to lower braid bar environment occurs from 360-530+ cm.

Table A11. Description for core 11, cross-section A-A'.

Location:	**Uvalda Quadrangle**	**Map Unit:**	Qp5
Transect:	**A**	**Geomorphic Component:**	Braid bar ridge
Core #:	**11**	**Other Remarks:**	On SW side of ridge, between crest and swale, 2 m west of road.
***Easting:**	350064 m	**Date:**	5/5/2011
***Northing:**	3544044 m	**Personnel:**	BES, ZS
*UTM NAD 83		**Sampling Method:**	Hand auger

Depth (cm)	Horizon	Color	RMF	Texture	Structure	Bndy	Remarks
0-20	A	10YR 4/6	---	ms	sg	g	Upper braid bar or eolian (?). A horizon very weakly expressed.
20-75	C1	10YR 5/6	---	ms	sg	d	Upper braid bar or eolian (?).
75-135	C2	10YR 6/6	---	ms	sg	g	Upper braid bar or eolian (?). Slightly coarser than A & C1.
135-305	C3	10YR 6/7	---	upper ms	sg	g	Upper braid bar (?) 7.5YR 5/6 sandy loam clay-iron bands occur at 170-180, 195-205, 225-240, 255-260, & 280-285 cm.
305-350+	C4	10YR 5/6	---	upper ms	sg	---	Mid- to lower braid bar or bedload sediment. Common granules; ≤8 mm gravels.

Notes: Either extremely well-sorted upper braid bar sediments or a re-worked eolian cover may be present from 0-135 cm based on high degree of sorting and lack of >1.0 mm grains. Fluvial gravels encountered at 305 cm. Alluvium interpreted as being deposited in a middle to lower braid bar to bedload environment occurs from 305-350+ cm.

Table A12. Description for core 12, cross-section A-A'.

Location:	**Uvalda Quadrangle**	**Map Unit:**	Qp5
Transect:	**A**	**Geomorphic Component:**	Swale SE of nose of pronounced braid bar ridge
Core #:	**12**	**Other Remarks:**	On road
***Easting:**	350272 m	**Date:**	9/23/2011
***Northing:**	3544043 m	**Personnel:**	BES, DSL
*UTM NAD 83		**Sampling Method:**	Giddings drill rig: core & flight auger

Depth (cm)	Horizon	Color	RMF	Texture	Structure	Bndy	Remarks
0-9	Ap	10YR 3/2	---	sl	1tkpl parting to 1fsbk	a	Vertical accretion
9-44	E	2.5Y 6/3	---	sl to ls	1fsbk	c	Vertical accretion. Coarser than Ap.
44-94	Bt(g)	10YR 6/1.5	m, medium, P, 10YR 5/8	fscl	2msbk	c	Vertical accretion
94-120	BCg	10YR 7/2	f to c, fine, P, 10YR 7/6	sl	1fsbk	c	Vertical accretion
120-164	Cg	10YR 7/2	---	sl	m	g	Transitional
164-230	C1	10YR 6/6	---	lms	m	g	Mid- to lower braid bar or bedload sediment. Few granules.
230-280	C2	10YR 7/4	---	lower cs	sg	g	Bedload. ≤5 mm gravels.
280-360	C3	10YR 6/4	---	gr cos	sg	g	Bedload. ≤8 mm gravels.
360-480	C4	7.5YR 5/6	---	vgr cos	sg	g	Bedload. ≤20 mm gravels.
480-600+	C'g	10YR 5/1	---	vgr cos	sg	---	Bedload. ≤16 mm gravels.

Notes: Core refusal at 280 cm. 280-600 cm sampled by flight auger.

Table A13. Description for core 13, cross-section A-A'.

Location:	**Uvalda Quadrangle**	**Map Unit:**	Qp5
Transect:	**A**	**Geomorphic Component:**	Talf
Core #:	**13**	**Other Remarks:**	~210 m south of "hog road"
***Easting:**	350452 m	**Date:**	5/5/2012
***Northing:**	3544095 m	**Personnel:**	BES, ZS
*UTM NAD 83		**Sampling Method:**	Hand auger

Depth (cm)	Horizon	Color	RMF	Texture	Structure	Bndy	Remarks
0-21	A	10YR 4/6	---	ms1	sg	c	Vertical accretion
21-30	E	10YR 5/4	---	ms1	1fsbk	c	Vertical accretion. Finer than A horizon.
30-52	Bt1	2.5YR 4/6	c, medium, P, 10YR 5/6	c	2msbk	g	Vertical accretion. Common discontinuous clay films on faces of peds.
52-90	Bt2	5YR4/6	c, medium, P, 10YR 5/6	scl	1msbk	g	Vertical accretion. Common discontinuous clay films on faces of peds.
90-112	BC	5YR 4/6	---	sl	1fsbk	a	Vertical accretion.
112-160	C1	10YR 7/3	---	lower ms	sg	g	Mid- to lower braid bar or bedload sediment.
160-195	C2	10YR 6/1	---	lms	m	c	Mid- to lower braid bar or bedload sediment. 10YR 5/8 oxidized zone from 180-195 cm.
195-240+	C3	10YR 5.5/6	---	lower cos	sg	---	Mid- to lower braid bar or bedload sediment. Few granules.

Notes: Local and micro-topography obscured by logging impacts and vegetation. Appears to be on flat/talf component of Qp5 braided surface.

Table A14. Description for core 14, cross-section A-A'.

Location:	**Uvalda Quadrangle**	**Map Unit:**	Qp5
Transect:	**A**	**Geomorphic Component:**	Braid swale
Core #:	**14**	**Other Remarks:**	~130 m south of "hog road"
***Easting:**	350654 m	**Date:**	5/5/2012
***Northing:**	3544140 m	**Personnel:**	BES, ZS
*UTM NAD 83		**Sampling Method:**	Hand auger

Depth (cm)	Horizon	Color	RMF	Texture	Structure	Bndy	Remarks
0-40	E	10YR 5/3	---	lms	sg	g	Vertical accretion. A horizon is missing.
40-80	Btg	10YR 6/2	c, medium, P, 10YR 5/8	scl	1 to 2fsbk	c	Vertical accretion.
80-142	Cg1	10YR 6/2	c, medium, P, 10YR 6/6	ms	sg	c	Mid- to lower braid bar or bedload sediment. Coarsens to upper medium sand toward base.
142-180+	Cg2	10YR 5.5/1	---	upper ms	sg	---	Mid- to lower braid bar or bedload sediment. ≤1 mm mica flakes.

Notes:

Table A15. Description for core 15, cross-section A-A'.

Location:	**Uvalda Quadrangle**	**Map Unit:**	Qp5
Transect:	**A**	**Geomorphic Component:**	Low Ridge
Core #:	**15**	**Other Remarks:**	On road
***Easting:**	350752 m	**Date:**	12/16/2011
***Northing:**	3544253 m	**Personnel:**	BES, CSC
*UTM NAD 83		**Sampling Method:**	Hand auger

Depth (cm)	Horizon	Color	RMF	Texture	Structure	Bndy	Remarks
0-12	---	---	---	---	---	---	Road fill.
12-22	A	10YR 3.5/3	---	sl	1 to 2fsbk	c	Vertical accretion
22-30	EA	10YR 4/3.5	---	sl	1 to 2fsbk	g	Vertical accretion
30-60	Bt1	5YR 5/8	c, coarse, D, 2.5YR 4/8	c	2msbk	c	Vertical accretion. Few discontinuous clay films on faces of peds.
60-100	Bt2	10YR 6/4	c, coarse, P, 2.5YR 4/8 and c, coarse, F, 10YR 6/3	cl to scl	2msbk	g	Vertical accretion.
100-120	BC	5YR 6/4	---	sl to scl	1msbk	g	Vertical accretion. Top half redder than bottom half of horizon.
120-132	CB	5YR 5/7	---	msl	0 to 1msbk	g	Vertical accretion.
132-180	C1	7.5YR 5/6	---	lms	sg	c	Transitional. 165-180 cm = 5YR 4/6 msl clay-iron band possibly influenced by primary stratification.
180-210	C2	10YR 7/6	---	ms	sg	c	Mid- to lower braid bar or bedload sediment. Very few granules.
210-270+	Cg	10YR 7/1	---	upper ms	sg	---	Mid- to lower braid bar or bedload sediment. Fines upward from lower coarse sand in lower part.

Notes:

Table A16. Description for core 16, cross-section A-A'.

Location:	**Uvalda Quadrangle**	**Map Unit:**	Qp5
Transect:	**A**	**Geomorphic Component:**	Swale
Core #:	**16**	**Other Remarks:**	On road
***Easting:**	350825 m	**Date:**	11/21/2011
***Northing:**	3544238 m	**Personnel:**	BES, DSL
*UTM NAD 83		**Sampling Method:**	Giddings drill rig: core & flight auger

Depth (cm)	Horizon	Color	RMF	Texture	Structure	Bndy	Remarks
0-5	A	10YR 4/3	---	sl	2mpl	a	Vertical accretion
5-16	Btg1	10YR 5/2	c, medium to coarse, P, 10YR 5/6	scl to sc	1msbk	c	Vertical accretion. Few discontinuous, distinct clay films on sides of ped faces.
16-60	Btg2	10YR 6/1	c, medium, P, 7.5YR 5/6	c	2msbk	c to g	Vertical accretion. Few to common discontinuous, distinct clay films on sides and tops of ped faces and lining root channels.
60-124	BCg	10YR 6/1.5	f, fine, P, 7.5YR 5/6	scl	0 to 1fsbk	g	Vertical accretion. Much coarser than Btg2. Fines upward from sl in lower part. Sand component of texture is upper medium to lower coarse sand. 86-98 cm = oxidized zone of 50% 10YR 6/8.
124-188	Cg1	10YR 6/1	---	msl	m	g	Transitional. Textural/structure break within horizon: single grained upper medium to lower coarse sand below ~160 cm.
188-487	Cg2	10YR 6/1	---	upper cos	sg	g to d	Mid- to lower braid bar or bedload sediment. Some stratification: 188-210 cm = upper coarse to lower very coarse sand w/granules; 210-215 cm = sc bed; 215-280 cm = upper coarse sand; 280-487 cm = upper coarse sand w/6-8 mm gravels.
487-1200	Cg3	N 5/	---	upper cos	sg	---	Mid- to lower braid bar or bedload sediment. Stratified coUs grading to gravelly upper coarse sand w/depth. Scattered lenses of massive sandy clay at: 525-536 cm; 745-767 cm; 870-880 cm. Thinner lenses occur from 720-960 cm. Gravels are larger below 720 cm (≤17 mm).

Notes: Core refusal at 270 cm. Recovered by flight auger to 1080 cm. Lost auger and two Kelly bars extracting 1080-1200 cm interval, which is same material based on feel. Pre-Quaternary "clay" not encountered.

Table A17. Description for core 17, cross-section A-A'.

Location:	**Uvalda Quadrangle**	**Map Unit:**	Qp5
Transect:	**A**	**Geomorphic Component:**	Low Ridge
Core #:	**17**	**Other Remarks:**	On road
***Easting:**	350865 m	**Date:**	12/16/2011
***Northing:**	3544232 m	**Personnel:**	BES, CSC
*UTM NAD 83		**Sampling Method:**	Hand auger

Depth (cm)	Horizon	Color	RMF	Texture	Structure	Bndy	Remarks
0-20	A	10YR 3/3	---	sl	1vfsbk	g	Vertical accretion
20-35	EA	10YR 4/3	---	sl	1vfsbk to sg	c	Vertical accretion
35-60	E	10YR 5/6	---	sl	1fsbk	g	Vertical accretion. Some BE characteristics: some fsbk to msbk peds.
60-90	Bt1	10YR 5/6	c, fine, P, 7.5YR 5/8	sl to scl	1 to 2fsbk	g	Vertical accretion. Faint clay films bridging grains. Mn masses.
90-110	Bt2	10YR 6/6	c, coarse, P, 7.5YR 5/8 and c, coarse, P, 10YR 6/2	sl to scl	1 to 2fsbk	c	Vertical accretion. Faint clay films bridging grains.
110-140	C1	10YR 7/4	f, fine, P, 7.5YR 5/8	ms	sg	g	Transitional
140-160	C2	7.5YR 5/6	---	sl	m	c to a	Transitional. Strongly oxidized.
160-205	C3	10YR 7/1	---	msl	m	c to a	Transitional.
205-225	C4	10YR 6/8	---	upper ms	sg	c to a	Lens of sandy loam at 205-210 cm.
225-270+	Cg	10YR 8/1	---	lower cos	sg	---	Mid- to lower braid bar or bedload sediment. Scattered 1-2 mm grains.

Notes:

Table A18. Description for core 18, cross-section A-A'.

Location:	**Uvalda Quadrangle**	**Map Unit:**	Qp5
Transect:	**A**	**Geomorphic Component:**	In depression within probable braid swale
Core #:	**18**	**Other Remarks:**	On over-grown logging road
***Easting:**	351157 m	**Date:**	5/5/2012
***Northing:**	3544269 m	**Personnel:**	BES, ZS
*UTM NAD 83		**Sampling Method:**	Hand auger

Depth (cm)	Horizon	Color	RMF	Texture	Structure	Bndy	Remarks
0-15	BAg	10YR 5/2	c, fine, P, 10YR 6/8	scl	1fsbk	c	Vertical accretion.
15-60	Btg1	10YR 5/1.5	c, fine, P, 10YR 5/8	c	2msbk	g	Vertical accretion. Common, discontinuous, distinct clay films on ped faces.
60-135	Btg2	10YR 5/1.5	m, medium, P, 10YR 5/8	c	2msbk	g	Vertical accretion. Common, discontinuous, distinct clay films on ped faces. Slickensides/pressure faces.
135-170	Btg3	10YR 6/1	f, fine, P, 10YR 5/8	c to sc	1msbk	c	Vertical accretion. Few, discontinuous, distinct clay films on ped faces. Slickensides/pressure faces.
170-207	Cg1	10YR 6/1	---	upper ms	sg	g	Mid- to lower braid bar or bedload sediments.
207-240+	Cg2	10YR 7/1	---	lower cos	sg	---	Mid- to lower braid bar or bedload sediments.

Notes:

Table A19. Description for core 19, cross-section A-A'.

Location:	**Uvalda Quadrangle**	**Map Unit:**	Qp5
Transect:	**A**	**Geomorphic Component:**	Edge of swale
Core #:	**19**	**Other Remarks:**	On road. ^{14}C date site (UGAMS 10684).
***Easting:**	351398 m	**Date:**	9/24/2011
***Northing:**	3544328 m	**Personnel:**	BES, DSL
*UTM NAD 83		**Sampling Method:**	Giddings drill rig: core & flight auger

Depth (cm)	Horizon	Color	RMF	Texture	Structure	Bndy	Remarks
0-4	Ap	10YR 2/2	---	fsl to l	1vfsbk	a	Vertical accretion.
4-13	E	10YR 6/3	c, fine, P, 10YR 5/8	sl	1fsbk	c	Vertical accretion.
13-27	Btg1	10YR 5/2	f to c, medium, P, 10YR 5/6	c	2fsbk	g	Vertical accretion. Few discontinous distinct clay films on faces of peds.
27-112	Btg2	10YR 5/1	m, coarse, P, 2.5YR 4/8 & 7.5YR 5/8	c	2 to 3fsbk	g	Vertical accretion. Sand content increases with depth. Few discontinous distinct clay films on faces of peds.
112-143	BCx	2.5Y 5/2	c, fine, P, 7.5YR 5/6	sl	1fsbk	g	Vertical accretion. Fragic properties most pronounced from 112-125 cm. Difficult to drill with flight auger.
143-189	Cg	10YR 7/1	---	msl	m	g	Vertical accretion.
189-240	Co	10YR 6/8	c, coarse, P, 10YR 7/1	msl	m	c	Vertical accretion. RMF (reduced zones) are horizontally oriented and slightly finer textured than matrix.
240-310	C	see remarks	---	ms	sg & m	g	Transitional. Bedded: 240-270 cm = 2.5Y 6/3 single-grain coarse sand w/5 mm gravels; 270-280 cm = 10YR 7/1 massive loamy medium sand; 280-296 cm = 10YR 6.5/6 single-grain coarse sand w/5 mm gravels; 296-302 cm = 10YR 7/1 massive loamy medium sand.
310-355	C'g1	10YR 6/1	---	gr cos	sg	d	Braid bar and bedload sediment. Granules.
355-600	C'g2	10YR 6/2	---	gr cos	sg	d	Braid bar and bedload sediment. ≤5 mm gravels. Clay bed at 487-490 cm.
600-1020	C'g3	10YR 6/1	---	gr cos	sg	d	Braid bar and bedload sediment. Stratified gravelly coarse sand w/≤5 mm gravels. Lens of N 5/ sandy clay at 465-485 cm. Thinner lenses occur within 910-960 cm and 1010-1020 cm intervals.
1020-1320	C'g4	N 5.5/	---	gr cos	sg	---	Braid bar and bedload sediment. Few 10 mm gravels. Gley color main difference from C'g3.

Notes: Core refusal at 112 cm. Recovered by flight auger to 1200 cm. Used every Kelly bar but one. Pre-Quaternary sediment never reached.

Table A20. Description for core 20, cross-section A-A'.

Location:	**Uvalda Quadrangle**	**Map Unit:**	Qp5
Transect:	**A**	**Geomorphic Component:**	Swale
Core #:	**20**	**Other Remarks:**	On eastern edge of swale.
***Easting:**	351600 m	**Date:**	5/6/2012
***Northing:**	3544466 m	**Personnel:**	BES, ZS
*UTM NAD 83		**Sampling Method:**	Hand auger

Depth (cm)	Horizon	Color	RMF	Texture	Structure	Bndy	Remarks
0-45	BAg	10YR 3/1	---	scl	1fsbk	g	Vertical accretion.
45-105	Btg1	10YR 4/1	c, fine, P, 10YR 5/8	c	1 to 2msbk	g	Vertical accretion. Common, distinct, discontinuous clay films on faces of peds.
105-208	Btg2	10YR 5/1	c, coarse, P, 10YR 5/8	c	2msbk	c	Vertical accretion. Common, distinct, discontinuous clay films on faces of peds.
208-238	Btg3	10YR 6/1	---	c	1msbk	a	Vertical accretion. Grades to scl with depth. Few, faint, discontinuous clay films on faces of peds. More weakly developed than Btg1&2.
238-270+	Cg	10YR 7/1	---	lower cos	sg	---	Mid- to lower braid bar or bedload sediment. Few fine gravels.

Notes:

Table A21. Description for core 21, cross-section A-A'.

Location:	**Uvalda Quadrangle**	**Map Unit:**	Qp4
Transect:	**A**	**Geomorphic Component:**	No distinct fluvial topography - flat terrace tread
Core #:	**21**	**Other Remarks:**	Beside unimproved road
***Easting:**	351811 m	**Date:**	5/6/2012
***Northing:**	3544595 m	**Personnel:**	BES, ZS
*UTM NAD 83		**Sampling Method:**	Hand auger

Depth (cm)	Horizon	Color	RMF	Texture	Structure	Bndy	Remarks
0-20	Ap	10YR 3/2	---	sl	0 to 1fsbk	a	Vertical accretion.
20-60	E	10YR 6/4	---	sl	1fsbk	c	Vertical accretion.
60-90	Bt	10YR 5/6	c, medium, P, 10YR 6/2	sl to scl	1msbk	g	Vertical accretion.
90-142	Btg1	10YR 6/2	m, medium, P, 10YR 6/8	sl	1fsbk	c	Vertical accretion.
142-247	Btg2	10YR 3/2	c, medium, P, 10YR 5/8	c	2msbk	d	Vertical accretion. Backswamp or paleochannel fill clays.
247-307	Btg3	10YR 7/2	c, fine, P, 10YR 5/8	c	2msbk	c	Vertical accretion. Backswamp or paleochannel fill clays.
307-352	Cg1	10YR 7/2	f, medium, P, 10YR 6/6	sl	m	a	Vertical accretion.
352-365	Cg2	10YR 6/1	---	lower cos	sg	a	Lateral accretion.
365-390+	C	10YR 6/4	---	lower cos	sg	---	Lateral accretion.

Notes: About 40 m inside Qp4 from ~1.5 m scarp at lateral boundary with Qp5.

Table A22. Description for core 22, cross-section A-A'.

Location:	**Uvalda Quadrangle**	**Map Unit:**	Qp4
Transect:	**A**	**Geomorphic Component:**	flat/talf
Core #:	**22**	**Other Remarks:**	On road
***Easting:**	351919 m	**Date:**	9/24/2011
***Northing:**	3544659 m	**Personnel:**	BES, DSL
*UTM NAD 83		**Sampling Method:**	Giddings drill rig: core & flight auger

Depth (cm)	Horizon	Color	RMF	Texture	Structure	Bndy	Remarks
0-24	A	10YR 2.5/1	---	sl	2tkpl	g	Vertical accretion. Platy from compaction.
24-48	AEg	10YR 4/1	f, fine, P, 10YR 4/6	sl	2vkpl	c	Vertical accretion. Platy from compaction.
48-99	Eg	10YR 6.5/2	f, fine, P, 10YR 4/6	sl to ls	1msbk to sg	g	Vertical accretion.
99-143	Btg1	10YR 5.5/1	c, fine, P, 10YR 5/8	sc to scl	1fsbk	g	Vertical accretion backswamp or paleochannel fill clay. Sand grains coated and bridged with clay.
143-212	Btg2	10YR 6/1	m, medium, P, 7.5YR 5/8	c	2tkpl	g	Vertical accretion backswamp or paleochannel fill clay. Common, distinct discontinuous 10YR 6/1 and 7.5YR 5/8 clay films. Becomes more sandy towards base.
212-485	Btg3	see below	see below	see below	see below	see below	Vertical accretion backswamp or paleochannel fill clays. Mega Btg horizon w/higher clay content than Btg1 & 2. Parent sediments appear stratified resulting in horizon subdivisions (below).
212-290	"	10YR 7/1	c, coarse, P, 7.5YR 5/8	sc	2f to msbk	---	Sand & granules from 212-266 cm. Common prominent 1-3 cm wide clay films on vertical ped faces.
290-333	"	10YR 7/1	---	scl	1 f to msbk	---	No granules. 7.5YR 5/8 oxidized zone from 310-333.
333-446	"	10YR 6/1	---	c	2msbk	---	Common prominent 1-3 cm wide clay fims on vertical ped faces that become thinner and more discontinuous below 420 cm. 7.5YR 5/8 oxidized zones at 400-425 cm & 446-485 cm.
446-485	"	10YR 6/1	---	c	2msbk	c	Slightly sandier than 333-446 cm interval.
485-528	Cg1	2.5Y 7/1.5	---	vfscl	m	g	Vertical accretion.
528-608	Cg2	10YR 8/1	---	ms	sg	g	Lateral accretion. Sandy clay bed at 590-608 cm.
608-750	Cg3	10YR 8/2	---	cos	sg	no data	Lateral accretion.
750-840+	Co	2.5YR 5/6	---	gr upper ms to lower cos	sg	---	Lateral accretion.

Notes: A distinct ~1.5 m scarp separates T5 from the braid terrace. The red color of the gravelly medium to coarse sand at the base of this profile may indicate the unit below (possibly "pre-Quaternary" blue/green clay) is perching water.

Table A23. Description for core 23, cross-section A-A'.

Location:	**Uvalda Quadrangle**	**Map Unit:**	Qp3
Transect:	**A**	**Geomorphic Component:**	flat/talf
Core #:	**23**	**Other Remarks:**	On road
***Easting:**	352099 m	**Date:**	11/21/2011
***Northing:**	3544795 m	**Personnel:**	BES, DSL
*UTM NAD 83		**Sampling Method:**	Giddings drill rig: core & flight auger

Depth (cm)	Horizon	Color	RMF	Texture	Structure	Bndy	Remarks
0-11	AE	2.5Y 4/2	---	msl	2mpl	c	Alluvium. A removed. Platy from compaction.
11-40	E	2.5Y 6/4	f, fine, P, 10YR 6/8	msl	2m to tkpl	g	Alluvium. Finer textured than AE.
40-111	Btg1	10YR 6/2	c, medium, P, 2.5YR 4/8 and c, coarse, p, 10YR 6/6	c to sc	2msbk	g	Alluvium. Few discontinuous distinct clay films on ped sides and faces.
111-144	Btg2	10YR 7/2	c, coarse, P, 7.5YR 5/8 and f, coarse, d, 2.5Y 6/3	scl	2tkpl	g	Alluvium. Oxidized zone at base of horizon (140-144 cm). 3-4 mm subrounded granules.
144-195	BC(x)	10YR 6/2	f, medium, P, 10YR 5/8 and f, medium, D, 10YR 6/4	scl	2tk to vkpl	g	Alluvium. 2-3 mm subrounded granules. Incipient fragipan development (some slaking in water).
195-330	Cx	2.5Y 7/4 grading to 10YR 6/2 w/depth	---	sl	no data*	g	Alluvium. Few subrounded granules and 4-6 mm gravels. Fines upward from coarse sandy loam in lower part. 300-330 cm is texturally similar to Cg1 but not pink. Readily slakes in water.
330-370	C	7.5YR 6/2	---	cosl	no data*	c	Alluvium. Few 1-2 mm particles. Pinkish gray.
370-425	2C1	7.5YR 5/2	---	c	m(?)	c	Scattered 1-2 mm particles. Difficult to determine structure due to disruption by auger. It is possible this is a buried A horizon within a paleosol (thus alternative horizon name would be 2Ab).
425-490	2C2	10YR 5.5/8	---	scl	m(?)	no data	Well oxidized. Difficult to determine structure due to disruption by auger. It is possible this is a buried B horizon within a paleosol (thus alternative horizon name would be 2Bb).
490-550	2C3	10YR 6/3	---	mls to cls	m	---	Subangular to subrounded granules. Little pedogenic development.

Notes: Cored to 195 cm. Augered below 195 cm. 0-370 cm interpreted as fining upward Oconee River Quaternary alluvium. 370-550 cm is possibly Pre-Quaternary Coastal Plain sediment -or- older Oconee River-derived alluvium. Oxidized color 425-490 cm appears pedogenic, and 370-490 cm interval may contain a paleosol. *Asterisk indicates structure destroyed by flight auger.

Table A24. Description for core 24, cross-section A-A'.

Location:	**Uvalda Quadrangle**	**Map Unit:**	Qp3
Transect:	**A**	**Geomorphic Component:**	flat/talf
Core #:	**24**	**Other Remarks:**	Beside logging road near small field
***Easting:**	352268 m	**Date:**	5/6/2012
***Northing:**	3544841 m	**Personnel:**	BES, ZS
*UTM NAD 83		**Sampling Method:**	Hand auger

Depth (cm)	Horizon	Color	RMF	Texture	Structure	Bndy	Remarks
0-45	A	10YR 2/1	---	sl	1fsbk to sg	c	Alluvium. Thickness probably due to agriculture. 40-45 cm interval is very dark, may represent incipient spodic development or buried topsoil.
45-75	E	10YR 5/4	---	sl	1fsbk to sg	c	Alluvium.
75-90	Eg(x)	10YR 6/1	---	sl	1fsbk to sg	c	Alluvium. Some brittle peds and incipient fragic properties.
90-145	Btxg	10YR 5/2	c, medium, P, 10YR 5/8	sl	2csbk	a	Alluvium. Fragipan. Extremely difficult to hand auger. True structure of horizon destroyed by auger.
145-210	Bt(x)g	10YR 5/2	c, medium, P, 10YR 5/8	sl	1msbk	d	Alluvium. Coarser than Btxg. Fragic properties much less pronounced than in Btxg. RMF restricted to 145-165 cm interval.
210-250	BC or C	10YR 6/2	c, medium, P, 10YR 5/8	cosl	1fsbk to m	a	Alluvium. Up to 10 mm rounded quartz gravels. Lowest 10 cm of horizon is oxidized (10YR 5/8).
250-290	2Cg1	10YR 5/2	---	c	2msbk	g	Appears to have common, discontinuous, distinct clay films on ped faces. Possible clay films and pedogenic structure indicate this may be a B horizon within a paleosol (thus alternative horizon name would be 2Btg1).
290-330+	2Cg2	10YR 3/1	---	c	2mabk	---	Nearly black. Appears to have common, discontinuous, distinct clay films on ped faces. Contains more clay and has higher plasticity than 2Cg1. Possible clay films and pedogenic structure indicate this may be a B horizon within a paleosol (thus alternative horizon name would be 2Btg2).

Notes: 0-250 cm interpreted as fining upward Oconee River alluvium. 250-330+ cm lower stratum may be pre-Quaternary Coastal Plain sediment or older Oconee River-derived alluvium. Similar to hole #23 at 352099 m East.

Table A25. Description for core 25, cross-section A-A'.

Location:	**Uvalda Quadrangle**	**Map Unit:**	TQu
Transect:	**A**	**Geomorphic Component:**	On subtle nose slope just below 45 m contour
Core #:	**25**	**Other Remarks:**	On logging road immediately south of McArthur tract road
***Easting:**	352546 m	**Date:**	11/21/2011
***Northing:**	3544775 m	**Personnel:**	BES, DSL
*UTM NAD 83		**Sampling Method:**	Giddings drill rig: core & flight auger

Depth (cm)	Horizon	Color	RMF	Texture	Structure	Bndy	Remarks
0-9	A	10YR 3/2	---	sl	1fsbk	c	
9-62	E	2.5Y 6/4	---	sl	1msbk	c	
62-110	Bt	10YR 5/8	c, coarse, P, 2.5YR 4/8 and c, coarse, P, 10YR 6/4	scl	2msbk	d	
110-170	Btg	10YR 7/1	c, v. coarse, P, 10YR 5/8 and c, v. coarse, P, 2.5YR 4/8	c	2msbk	d	
170-310	BCg	10YR 7/1	c, v. coarse, P, 10YR 5/8 and c, v. coarse, P, 2.5YR 4/8	c	1msbk to m	c to a	Slightly sandier than Btg. Base of horizon (307-310 cm) is bright red (2.5YR 5/8) sandy loam that sits atop contact with underlying orange sandy clay/sandy clay loam of C horizon. Boundary disturbed by auger but probably abrupt.
310-390	(2?)C	10YR 4/6	---	scl to sc	m (?)	c to a	Possible lithologic boundary at 310 cm (difficult to determine). Structure disturbed by auger but probably massive. Boundary disturbed by auger but probably abrupt.
390-480	(3 or 2?)Cg	10YR 8/1	---	c	m (?)	---	"White clay"

Notes: Soil parent material difficult to determine. Profile may be developed entirely in stratified pre-Quaternary Coastal Plain sediments, or the 0-310 cm interval may consist of a cap of Quaternary surficial material of indeterminate origin. The 310-390 cm may have different origin and lithology than over- and underlying sediments. The "white clay" appears morphologically and lithologicaly distinct from overlying sediments and is separated from them by an abrupt contact.

Table A26. Description for core 26, cross-section A-A'.

Location:	**Uvalda Quadrangle**	**Map Unit:**	TQu
Transect:	**A**	**Geomorphic Component:**	Lower nose slope in uplands, just below 54 m CI
Core #:	**26**	**Other Remarks:**	South side of power line easement at woodline
***Easting:**	353073 m	**Date:**	5/6/2012
***Northing:**	3544959 m	**Personnel:**	BES, ZS
*UTM NAD 83		**Sampling Method:**	Hand auger

Depth (cm)	Horizon	Color	RMF	Texture	Structure	Bndy	Remarks
0-20	A	10YR 4/2	---	lfs to lms	sg	c	
20-45	E1	2.5Y 6/3	---	lfs to lms	sg	d	
45-97	E2	2.5Y 6.5/3	---	lfs to lms	sg	c	Slightly coarser than A & E1.
97-127	Bt1	10YR 6/6	c, medium, P, 7.5YR 5/8	sl	1 to 2msbk	g	
127-150	Bt2	7.5YR 5/8	c, medium, F, 5YR 5/8 and c, medium, P, 10YR 6/2	sl	1 to 2msbk	c	
150-255	2Btg	10YR 7/2	c, medium, P, 2.5YR 3/6	c	2msbk	g	Few to common, discontinuous, distinct clay films on ped faces.
255-300+	2Cg	2.5Y 7/2	---	c	m	---	Little pedogenic alteration.

Notes: Interpreted as sandy cap of indeterminate origin (0-150 cm) overlying pedogenically altered pre-Quaternary Coastal Plain sediments. Boundary between the two strata is overprinted by pedogenesis, forming one soil profile.

Table A27. Description for core 27, cross-section A-A'.

Location:	**Uvalda Quadrangle**	**Map Unit:**	TQu
Transect:	**A**	**Geomorphic Component:**	Upper nose slope of upland, just above 60 m CI
Core #:	**27**	**Other Remarks:**	On fire break immediately north of McArthur tract road
***Easting:**	353312 m	**Date:**	11/22/2011
***Northing:**	3545011 m	**Personnel:**	BES, DSL
*UTM NAD 83		**Sampling Method:**	Giddings drill rig: core & flight auger

Depth (cm)	Horizon	Color	RMF	Texture	Structure	Bndy	Remarks
0-9	A	10YR 3/2	---	sl	1tkpl	c	
9-20	EA	10YR 5/3	---	sl	1fsbk to sg	g	
20-85	E1	2.5Y 6/3	---	msl	0 to 1 fsbk to sg	d	Few granules. Two 15 mm ironstones.
85-152	E2	10YR 7/3	---	upper ms to lower cos	sg	a	2-8 mm gravels.
152-175	Btx1	7.5YR 5/6	c, medium, D, 7.5YR 5/8 and c, medium, P, 10YR 6/4	scl	2msbk to 1tkpl	g	≤12 mm gravels.
175-217	Btx2	Variegated: 2.5YR 4/8, 7.5YR 5/8, and 10YR 7/2	see remarks	scl	1msbk to 1tkpl	c to a	Matrix color is variegated due to redox processes. ≤12 mm gravels.
217-250	(2?)C	Variegated: 2.5YR 3/6, 10YR 6/8, and 10YR 6/1	see remarks	c	no data*	a	Matrix color is variegated due to redox processes. Some fine to medium sand can be felt in clay. No gravels, less sand than Btx2. May be of different lithology than overlying sediments.
~250-300+	(2 or 3?)C	10YR 8/1	---	indurated & chalky	no data*	---	Different lithology than overlying sediments. Upper boundary is approximate.

Notes: Soil parent material is difficult to determine. 0-217 cm may be an alluvial cap, but this is uncertain. The profile below 217 cm is interpreted to consist of pre-Quaternary Coastal Plain sediments. The chalky white sediment from 250-300 cm appears morphologically and lithologicaly distinct from overlying sediments and is separated from them by an abrupt contact. This material was indurated and crunched during drilling, making the bit hot. *Asterisk indicates structure destroyed by flight auger, which was used from ~185-300 cm.

Table A28. Description for core 28, cross-section A-A'.

Location:	**Uvalda Quadrangle**	**Map Unit:**	TQu
Transect:	**A**	**Geomorphic Component:**	Knob of upland summit
Core #:	**28**	**Other Remarks:**	On roadside
***Easting:**	353560 m	**Date:**	11/22/2011
***Northing:**	3545029 m	**Personnel:**	BES, DSL
*UTM NAD 83		**Sampling Method:**	Giddings drill rig: core & flight auger

Depth (cm)	Horizon	Color	RMF	Texture	Structure	Bndy	Remarks
0-6	A	10YR 4/3	---	sl	1tkpl	c	"Natural" A horizon removed.
6-44	E	10YR 6/4	---	msl	2tkpl	c	~35 cm of E removed when road cut.
44-107	Btx1	10YR 5/8	c, coarse, P, 2.5YR 3/6 & 10YR 6/1 and c, coarse, D, 10YR 6/8	scl	2msbk	g	RMF occur below 75 cm and result in variegated color. Few discontinuous distinct clay films on vertical faces and tops of peds.
107-150	Btx2	see remarks	see remarks	dominantly scl (see remarks)	2 to 3tkpl	a	Three "subhorizons" present distinguished by color (from redox processes) and illuvial clays (see below).
107-123		10YR 3/4		scl	3tkpl	---	Sand grains partially coated and bridged with clay.
123-138		10YR 6/8		scl	2tkpl	---	Few distinct clay films on tops of peds.
138-150		5R 4/6		sl	2tkpl	a	Sand grains partially coated and bridged with clay.
150-405+	Btx3	Variegated: 10R 3/3 and 10YR 8/1	see remarks	c	2 to 3f to msbk	---	Redox processes have resulted in variegated horizon with purple (10R 3/3 is most similar chip) and white (10YR 8/1) zones. Both zones are oriented vertically and occur in bodies 5-6 cm wide and up to 20 cm high. Purple zones have strong (3) structure and are surrounded by 10YR 5/8 RMF "haloes". White zones have moderate (2) structure. Common, distinct clay films occur on vertical faces and tops of peds in both zones but are more pronounced and abundant in purple zones.

Notes: Cored to ~360 cm then augered to 405 cm. This entire profile probably consists of pre-Quaternary sediments. An road gulley in 50 m west of this hole contains rounded gravels that are probably fluvial in origin, but more likely derive from the Miocene Altamaha Formation, which immediately underlies uplands in this area, than Oconee River alluvium. The contact between the Btx2 and Btx3 is abrupt. Whether this is of sedimentologic significance is unclear, as the boundary may be pedogenic in origin.

CROSS-SECTION B-B’

Table A29. Description for core 29, cross-section B-B’.

Location:	**Uvalda Quadrangle**	**Map Unit:**	Qh1
Transect:	**B**	**Geomorphic Component:**	Swale
Core #:	**29**	**Other Remarks:**	On dirt road. ^{14}C date site (UGAMS 9554).
***Easting:**	348968 m	**Date:**	8/25/2011
***Northing:**	3546142 m	**Personnel:**	BES, DSL
*UTM NAD 83		**Sampling Method:**	Giddings drill rig

Depth (cm)	Horizon	Color	RMF	Texture	Structure	Bndy	Remarks
0-10	BA	10YR 5/2.5	c, medium, D 10YR 5/6	c	1fsbk	c	Vertical accretion. A horizon probably removed during road construction.
10-80	Bg	10YR 5/2	m, medium, P 7.5YR 5/8	c	2fsbk	a	Vertical accretion.
80-250	C1	10YR 7/3	---	ms	sg	g	Transitional. Fines upward to loamy sand in upper 30 cm. Interstratified sand and organic beds from 4-15 cm in thickness from 110-250 cm, with some indiviual beds containing thinner mm-scale internal bedding. Pronounced N 2.5/, black humate stratum at 155-168 cm that has weak cementation in places. Interpreted as vertical accretion overbank sands.
250-360	C2	10YR 7/2&3	f, medium, F 10YR 7/4	cos	sg	g	Lateral accretion. Fines upward to medium sand. Up to 6 mm gravels.
360-600+	Cg	10YR 6/1	---	gr vcos	sg	---	Lateral accretion and bedload. Fines upward to coarse sand. 10-12 mm gravels in 480-600 cm interval.

Notes: 250 cm is top of lateral accretion sediments.

Table A30. Description for core 30, cross-section B-B’.

Location:	**Uvalda Quadrangle**	**Map Unit:**	Qh1
Transect:	**B**	**Geomorphic Component:**	Backswamp
Core #:	**30**	**Other Remarks:**	Recently timbered
***Easting:**	349172 m	**Date:**	5/11/2012
***Northing:**	3545986 m	**Personnel:**	BES, ZS
*UTM NAD 83		**Sampling Method:**	Hand auger

Depth (cm)	Horizon	Color	RMF	Texture	Structure	Bndy	Remarks
0-15	A	7.5YR 4/4	---	sil	1fsbk	c	Vertical accretion.
15-60	Bw1	10YR 5/6	c, medium, P & D, 10YR 6/2 & 10YR 5/8	cl	1 to 2msbk	g	Vertical accretion.
60-105	Bw2	10YR 5/6	c, medium, P & D, 10YR 6/2 & 10YR 5/8	scl	1 to 2msbk	g	Vertical accretion. Fines upward from sandy loam near base.
105-145	Cg	2.5Y 6/2	c, medium, P, 10YR 5/8	cl to scl	m	g	Vertical accretion. Contains clay lenses.
145-160	C1	10YR 5/8	---	msl	sg	a	Transitional. Interpreted as overbank sands. Contains clay lenses. Upper 5 cm is reduced (10YR 6/2).
160-165+	C2	10YR 5/8	---	gr s	sg	---	Lateral accretion and bedload. 5-18 mm gravels.

Notes: 160 cm is top of lateral accretion and bedload.

Table A31. Description for core 31, cross-section B-B'.

Location:	**Uvalda Quadrangle**	**Map Unit:**	Qp6
Transect:	**B**	**Geomorphic Component:**	Indeterminate
Core #:	**31**	**Other Remarks:**	Distinct fluvial topography destroyed by silvicuture.
***Easting:**	349350 m	**Date:**	5/11/2012
***Northing:**	3545866 m	**Personnel:**	BES, ZS
*UTM NAD 83		**Sampling Method:**	Hand auger

Depth (cm)	Horizon	Color	RMF	Texture	Structure	Bndy	Remarks
0-45	E	10YR 5/6	---	sl to ls	0 to 1fsbk	g	Vertical accretion. A horizon absent, probably destroyed or eroded due to silviculture.
45-95	Bt	7.5YR 5/8	---	scl to sl	1 to 2msbk	g	Vertical accretion. Few discontinuous clay films on some ped faces. Most of horizon lacks clay films.
95-160	C	7.5YR 4.5/6	---	ls to sl	sg	c	Transitional.
160-210	Cg	10YR 7/2	m, medium, P, 10YR 6/8	sl	m	c	Transitional.
210-245	C'1	7.5YR 4/6	---	upper ms	m to sg	a	Transitional. Contains pockets of sandy loam.
245-285+	C'2	7.5YR 4/6	---	lower cos	sg	---	Lateral accretion. Matrix color is 10YR 5/4 in lower part.

Notes: 245 cm is top of lateral accretion.

Table A32. Description for core 32, cross-section B-B'.

Location:	**Uvalda Quadrangle**	**Map Unit:**	Qp6
Transect:	**B**	**Geomorphic Component:**	Shoulder of subtle scrollbar near scrollbar crest
Core #:	**32**	**Other Remarks:**	Beside dirt road. Some compaction & erosion.
***Easting:**	349555 m	**Date:**	8/25/2012
***Northing:**	3545719 m	**Personnel:**	BES, DSL
*UTM NAD 83		**Sampling Method:**	Giddings drill rig

Depth (cm)	Horizon	Color	RMF	Texture	Structure	Bndy	Remarks
0-10	BA	7.5YR 4/6	---	sl	1 to 2msbk to pl	c	Vertical accretion. A horizon likely destroyed or eroded by silviculture or other land uses.
10-57	Bw	7.5YR 4.5/6	---	sl	2tkpl	g	Vertical accretion. More clay and redder than BA.
57-160	C1	7.5YR 5/8	---	ls	sg	g	Transitional. Fines upward from medium lower sand in 110-160 cm interval. 57-70 cm interval has 1f-msbk structure and may be incipient BC horizon.
160-240	C2	10YR 6/6	---	upper ms	sg	no data - destroyed by flight auger bit	Lateral accretion. Contains more coarse sand than C1. 210-225 cm = 7.5YR 5/8, oxidized medium upper sand with pebbles. 225-240 cm = 10YR 8/1, white coarse sand with granules.
240-360	C3	7.5YR 4/4	---	cos	sg	no data - destroyed by flight auger bit	Lateral accretion. Contains granules and a few darker, oxidized beds of sandy clay.
360-630	C4	10YR 5.5/6	---	vcos	sg	no data - destroyed by flight auger bit	Lateral accretion and bedload. Oxidized and markedly coarser than C3, especially from 460-630 cm. Up to 10 mm gravels. Fines upward to coarse sand in 360-460 cm interval.
630-680	Cg1	10YR 6.5/2	---	ms	sg	no data - destroyed by flight auger bit	Lateral accretion and bedload. Markedly finer than C4. Contains few granules.
680-840	Cg2	N 5/	---	cos & vcos	sg	---	Lateral accretion and bedload. Fines upward to medium sand near top. Up to 5-6 mm gravels.

Notes: 160 cm is top of lateral accretion.

Table A33. Description for core 33, cross-section B-B'.

Location:	**Uvalda Quadrangle**	**Map Unit:**	Qp6
Transect:	**B**	**Geomorphic Component:**	Swale on mega-meander paleochannel scrollwork
Core #:	**33**	**Other Remarks:**	
***Easting:**	349755 m	**Date:**	5/11/2012
***Northing:**	3545562 m	**Personnel:**	BES, ZS
*UTM NAD 83		**Sampling Method:**	Hand auger

Depth (cm)	Horizon	Color	RMF	Texture	Structure	Bndy	Remarks
0-5	A	10YR 4/3	---	l	1mgr	a	Vertical accretion.
5-20	Bt	7.5YR 4/4	c, fine, P, 5YR 5/8	c	1 to 2fsbk	c	Vertical accretion. Few, faint, discontinuous clay films on ped faces and along root channels.
20-60	Btg	10YR 5/2	c, fine, P, 7.5YR 5/8	c	2msbk	g	Vertical accretion. Few, faint, discontinuous clay films on ped faces and along root channels.
60-100	Bw	2.5Y 5/6	c, coarse, P, 2.5Y 6/2	c to fsc	1fsbk	a	Vertical accretion. No macroscopic clay films. Less clay and more sand than Bt and Btg.
100-150	Cg1	10YR 7/1	---	upper ms	sg	g	Lateral accretion.
150-185+	Cg2	10YR 6/1	---	upper ms	sg	---	Lateral accretion. Coarser than Cg1.

Notes: 100 cm is top of lateral accretion. Vertical accretion has a finer upper stratum (0-60 cm) and a coarser lower stratum (60-100 cm).

Table A34. Description for core 34, cross-section B-B'.

Location:	**Uvalda Quadrangle**	**Map Unit:**	Qp6
Transect:	**B**	**Geomorphic Component:**	Crest of point bar of Uvalda mega-meander
Core #:	**34**	**Other Remarks:**	271 m from left top of bank (LTB). OSL date site
***Easting:**	349962 m		(UGA11OSL-789).
***Northing:**	3545419 m	**Date:**	8/24/2011
*UTM NAD 83		**Personnel:**	BES, DSL
		Sampling Method:	Hand auger

Depth (cm)	Horizon	Color	RMF	Texture	Structure	Bndy	Remarks
0-20	A	10YR 4/3	---	l	1 to 2fsbk	no data	Vertical accretion
20-38	Bw	10YR 5/4	---	l to cl	2f to msbk	no data	Vertical accretion
38-60	Bt	10YR 5/4	c to m, medium, D, 10YR 5/6	cl	2f to msbk	no data	Vertical accretion. Markedly stronger structure and more clay than Bw.
60-105	B'w1	10YR 5/3	c, fine to medium, P, 10YR 5/8	fsl to l	1f to msbk	no data	Vertical accretion
105-125	B'w2	10YR 5/4	f to c, fine, P, 2.5Y 6/8	sil	1f to msbk	a	Vertical accretion
125-130	C1	10YR 5/1	---	ls to fs	sg	no data	Transitional
130-237+	C2	10YR 7/1	---	ms to cos	sg	---	Upper lateral accretion

Notes: OSL sample obtained from 205-237 cm. Some horizon boundaries accidentally omitted from description. Vertical accretion contains a finer upper stratum (0-60 cm) and a slightly coarser lower stratum (60-130).

Table A35. Description for core 35, cross-section B-B'.

Location:	**Uvalda Quadrangle**	**Map Unit:**	Qp6
Transect:	**B**	**Geomorphic Component:**	Mid-point bar position of Uvalda mega-meander
Core #:	**35**	**Other Remarks:**	250 m from LTB
***Easting:**	349983 m	**Date:**	8/24/2011
***Northing:**	3545409 m	**Personnel:**	BES, DSL
*UTM NAD 83		**Sampling Method:**	Hand auger

Depth (cm)	Horizon	Color	RMF	Texture	Structure	Bndy	Remarks
0-60	Bw1	10YR 5/4	c, fine, P, 10YR 5/8	sil to l	1 to 2fsbk	no data	Vertical accretion
60-85	Bw(t)2	2.5Y 5/3	c, fine, D, 2.5Y 5/6	cl	1 to 2fsbk	no data	Vertical accretion. Incipient argillic development.
85-130	C1	10YR 5.5/1	---	sl	m	a	Vertical accretion
130-185+	C2	10YR 6.5/1	---	ms to cos	sg	---	Upper lateral accretion. Granules below 150 cm.

Notes: Vertical accretion contains a finer upper stratum (0-85 cm) and a slightly coarser lower stratum (85-130). Top of lateral accretion is 130 cm. Some horizon boundaries accidentally omitted from description.

Table A36. Description for core 36, cross-section B-B'.

Location:	**Uvalda Quadrangle**	**Map Unit:**	Qp6
Transect:	**B**	**Geomorphic Component:**	Toe of point bar of Uvalda mega-meander
Core #:	**36**	**Other Remarks:**	224 m from LTB
***Easting:**	350006 m	**Date:**	8/24/2011
***Northing:**	3545402 m	**Personnel:**	BES, DSL
*UTM NAD 83		**Sampling Method:**	Hand auger

Depth (cm)	Horizon	Color	RMF	Texture	Structure	Bndy	Remarks
0-115	Cg1	5GY 5/1	c, fine, P, 10YR 4/6 & 10YR 5/3	c	m	no data	Vertical accretion paleochannel fill.
115-205	Cg2	10YR 5/1	---	sl & ls	m to sg	a	Vertical accretion paleochannel fill. Interstratified sandy loam, loamy sand, and organic material.
205-220+	Cg3	10YR 5.5/1	---	cos to vcos	sg	---	Bedload.

Notes: 205 cm is top of bedload. Some horizon boundaries accidentally omitted from description.

Table A37. Description for core 37, cross-section B-B'.

Location:	**Uvalda Quadrangle**	**Map Unit:**	Qp6
Transect:	**B**	**Geomorphic Component:**	Mega-meander paleochannel
Core #:	**37**	**Other Remarks:**	200 m from LTB
***Easting:**	350025 m	**Date:**	8/24/2011
***Northing:**	3545388 m	**Personnel:**	BES, DSL
*UTM NAD 83		**Sampling Method:**	Tile probe

Depth (cm)	Horizon	Color	RMF	Texture	Structure	Bndy	Remarks
0-160	no data	no data	---	c	m	a	Vertical accretion paleochannel fill.
160-165+	no data	no data	---	cos	sg	---	Bedload.

Notes: 160 cm is top of bedload. A tile probe was used to determine depths of stratigraphic boundaries. Sample material was not recovered by hand auger. Therefore, horizons, colors, and structures (where not obvious from probing) were not described. This technique was reliable because auger borings revealed that the fill in this paleochannel is very uniform.

Table A38. Description for core 38, cross-section B-B'.

Location:	**Uvalda Quadrangle**	**Map Unit:**	Qp6
Transect:	**B**	**Geomorphic Component:**	In swale within mega-meander paleochannel
Core #:	**38**	**Other Remarks:**	173.7 m from LTB
***Easting:**	350051 m	**Date:**	8/24/2011
***Northing:**	3545380 m	**Personnel:**	BES, DSL
*UTM NAD 83		**Sampling Method:**	Tile probe

Depth (cm)	Horizon	Color	RMF	Texture	Structure	Bndy	Remarks
0-125	no data	no data	no data	c	m	a	Vertical accretion paleochannel fill.
125-130+	no data	no data	no data	cos	sg	---	Bedload.

Notes: 125 cm is top of bedload. A tile probe was used to determine depths of stratigraphic boundaries. Sample material was not recovered by hand auger. Therefore, horizons, colors, and structures (where not obvious from probing) were not described. This technique was reliable because auger borings revealed that the fill in this paleochannel is very uniform.

Table A39. Description for core 39, cross-section B-B'.

Location:	**Uvalda Quadrangle**	**Map Unit:**	Qp6
Transect:	**B**	**Geomorphic Component:**	Mega-meander paleochannel
Core #:	**39**	**Other Remarks:**	150 m from LTB
***Easting:**	350072 m	**Date:**	8/24/2011
***Northing:**	3545369 m	**Personnel:**	BES, DSL
*UTM NAD 83		**Sampling Method:**	Tile probe

Depth (cm)	Horizon	Color	RMF	Texture	Structure	Bndy	Remarks
0-139	no data	no data	no data	c	m	a	Vertical accretion paleochannel fill.
139-150+	no data	no data	no data	cos	sg	---	Bedload.

Notes: 139 cm is top of bedload. A tile probe was used to determine depths of stratigraphic boundaries. Sample material was not recovered by hand auger. Therefore, horizons, colors, and structures (where not obvious from probing) were not described. This technique was reliable because auger borings revealed that the fill in this paleochannel is very uniform.

Table A40. Description for core 40, cross-section B-B'.

Location:	**Uvalda Quadrangle**	**Map Unit:**	Qp6
Transect:	**B**	**Geomorphic Component:**	Mega-meander paleochannel
Core #:	**40**	**Other Remarks:**	126 m from LTB
***Easting:**	350092 m	**Date:**	8/24/2011
***Northing:**	3545358 m	**Personnel:**	BES, DSL
*UTM NAD 83		**Sampling Method:**	Tile probe

Depth (cm)	Horizon	Color	RMF	Texture	Structure	Bndy	Remarks
0-138	no data	no data	no data	c	m	a	Vertical accretion paleochannel fill.
138-145+	no data	no data	no data	cos	sg	---	Bedload.

Notes: 138 cm is top of bedload. A tile probe was used to determine depths of stratigraphic boundaries. Sample material was not recovered by hand auger. Therefore, horizons, colors, and structures (where not obvious from probing) were not described. This technique was reliable because auger borings revealed that the fill in this paleochannel is very uniform.

Table A41. Description for core 41, cross-section B-B'.

Location:	**Uvalda Quadrangle**	**Map Unit:**	Qp6		
Transect:	**B**	**Geomorphic Component:**	Mega-meander paleochannel		
Core #:	**41**	**Other Remarks:**	99 m from LTB		
***Easting:**	350119 m	**Date:**	8/24/2011		
***Northing:**	3545349 m	**Personnel:**	BES, DSL		
*UTM NAD 83		**Sampling Method:**	Hand auger and tile probe		

Depth (cm)	Horizon	Color	RMF	Texture	Structure	Bndy	Remarks
0-130	Cg1	5G 6/1	f, fine, P, 10YR 4/6	c	m	a	Vertical accretion paleochannel fill.
130-205+	Cg2	10YR 5/1	---	cos to vcos	sg	---	Bedload.

Notes: 130 cm is top of bedload.

Table A42. Description for core 42, cross-section B-B'.

Location:	**Uvalda Quadrangle**	**Map Unit:**	Qp6		
Transect:	**B**	**Geomorphic Component:**	On ditch dug in mega-meander paleochannel		
Core #:	**42**	**Other Remarks:**	75 m from LTB		
***Easting:**	350140 m	**Date:**	8/24/2011		
***Northing:**	3545340 m	**Personnel:**	BES, DSL		
*UTM NAD 83		**Sampling Method:**	Hand auger and tile probe		

Depth (cm)	Horizon	Color	RMF	Texture	Structure	Bndy	Remarks
0-40	---	---	---	---	---	---	Air & water. Base of ditch at 40 cm.
40-160	C	no data	no data	no data	no data	a	Ditch spoil
160+	Cg1	no data	no data	cos to vcos	sg	---	Bedload

Notes: 160 cm is top of bedload. 40-160 cm interval contains loose ditch spoil with air pockets.

Table A43. Description for core 43, cross-section B-B'.

Location:	**Uvalda Quadrangle**	**Map Unit:**	Qp6		
Transect:	**B**	**Geomorphic Component:**	On ditch dug in mega-meander paleochannel		
Core #:	**43**	**Other Remarks:**	50.5 m from LTB		
***Easting:**	350160 m	**Date:**	8/24/2011		
***Northing:**	3545328 m	**Personnel:**	BES, DSL		
*UTM NAD 83		**Sampling Method:**	Hand auger and tile probe		

Depth (cm)	Horizon	Color	RMF	Texture	Structure	Bndy	Remarks
0-30	---	---	---	---	---	---	Air & water. Base of ditch at 30 cm.
30-150	C	no data	no data	no data	no data	a	Ditch spoil
150+	Cg1	no data	no data	cos to vcos	sg	---	Bedload. Granules.

Notes: 150 cm is top of bedload. 30-150 cm interval contains loose ditch spoil with air pockets.

Table A44. Description for core 44, cross-section B-B'.

Location:	**Uvalda Quadrangle**	**Map Unit:**	Qp6
Transect:	**B**	**Geomorphic Component:**	Mega-meander paleochannel thalweg
Core #:	**44**	**Other Remarks:**	25 m from LTB
***Easting:**	350185 m	**Date:**	8/24/2011
***Northing:**	3545319 m	**Personnel:**	BES, DSL
*UTM NAD 83		**Sampling Method:**	Hand auger and tile probe

Depth (cm)	Horizon	Color	RMF	Texture	Structure	Bndy	Remarks
0-188	Cg1	10YR 5.5/1	c, fine, D, 10YR 5/3.5	c	m	a	Vertical accretion paleochannel fill. Matrix color changes to N 4.5/ with common, medium 5GY /1 redoximorphic features below 120 cm. Clay has high plasticity and is pottery grade.
188-305+	Cg2	10YR 5/1	---	cos to vcos	sg	---	Bedload. Very coarse sand below 240 cm. Granules scattered throughout 188-305 cm.

Notes: 188 cm is top of bedload

Table A45. Description for core 45, cross-section B-B'.

Location:	**Uvalda Quadrangle**	**Map Unit:**	Qp6
Transect:	**B**	**Geomorphic Component:**	Mega-meander thalweg
Core #:	**45**	**Other Remarks:**	24.3 m from LTB. ^{14}C date site (UGAMS 9553).
***Easting:**	~350185 m	**Date:**	8/24/2011
***Northing:**	~3545319 m	**Personnel:**	BES, DSL
*UTM NAD 83		**Sampling Method:**	Hand auger and tile probe

Depth (cm)	Horizon	Color	RMF	Texture	Structure	Bndy	Remarks
0-203	Cg1	10YR 5.5/1	c, fine, D, 10YR 5/3.5	c	m	a	Vertical accretion paleochannel fill. Matrix color changes to N 4.5/ with common, medium 5GY /1 redoximorphic features below ~120 cm. Clay has high plasticity and is pottery grade.
203+	Cg2	10YR 5/1	---	cos to vcos	sg	---	Bedload.

Notes: 203 cm is top of bedload.

Table A46. Description for core 46, cross-section B-B'.

Location:	**Uvalda Quadrangle**	**Map Unit:**	Qp6
Transect:	**B**	**Geomorphic Component:**	Mega-meander paleochannel, toe of cut bank
Core #:	**46**	**Other Remarks:**	17.1 m from LTB
***Easting:**	350198 m	**Date:**	8/24/2011
***Northing:**	3545320 m	**Personnel:**	BES, DSL
*UTM NAD 83		**Sampling Method:**	Tile probe

Depth (cm)	Horizon	Color	RMF	Texture	Structure	Bndy	Remarks
0-42	no data	no data	no data	c	no data	a	Vertical accretion paleochannel fill.
42+	Cg	no data	no data	cos to vcos	sg	---	Bedload.

Notes: 42 cm is top of bedload. A tile probe was used to determine depths of stratigraphic boundaries. Sample material was not recovered by hand auger. Therefore, horizons, colors, and structures (where not obvious from probing) were not described. This technique was reliable because auger borings revealed that the fill in this paleochannel is very uniform.

Table A47. Description for core 47, cross-section B-B'.

Location:	**Uvalda Quadrangle**	**Map Unit:**	Qp5
Transect:	**B**	**Geomorphic Component:**	Adjacent to scarp cut by Qp6 mega-meander
Core #:	**47**	**Other Remarks:**	-4.23 m from mega-meander LTB in dirt road
***Easting:**	350218 m	**Date:**	8/24/2011
***Northing:**	3545312 m	**Personnel:**	BES, DSL
*UTM NAD 83		**Sampling Method:**	Giddings drill rig

Depth (cm)	Horizon	Color	RMF	Texture	Structure	Bndy	Remarks
0-18.5	A(p?)	10YR 4/3	---	sl	3vkpl	c	Vertical accretion. Color is 10YR 5/2 near base.
18.5-101.5	Bt	5YR 5/8	---	c	3msbk	g	Vertical accretion. Texture fines upward from sandy loam at 80-101.5 to clay in upper part. 5YR 4/6, thick, discontinuous clay films on ped faces that become diffuse below 80 cm. Structure is angular blocky in places.
101.5-204	C1	7.5YR 6/8	---	ms	sg	g	Mid- to lower braid bar or bedload sediments. Few 2.5YR 5/8 clay-iron bands 1-2 cm thick.
204-250	C2	10YR 6.5/4	---	ms	sg	g	Mid- to lower braid bar or bedload sediments. One clay-iron band at 222-227 cm.
250-350	Cg	10YR 7/2	---	ms	sg	g	Mid- to lower braid bar or bedload sediments. 10YR 6/1 color and faint, thinly bedded strata with granules near base.
350-480	C'1	10YR 6/6	---	ms to cos	sg	---	Mid- to lower braid bar or bedload sediments. Boundary destroyed by flight auger so it was not described. Few granules.
480-550	C'2	10YR 6/4.5	---	vocs	sg	---	Bedload. Scattered granules and fine and medium granules. Boundary destroyed by flight auger so it was not described.
550-585	C'3	10YR 6/4.5	---	cos	sg	---	Bedload. Banded with a few 7.5YR 4/6, oxidized zones. Boundary destroyed by flight auger so it was not described.
585-620	C'4	10YR 6/4.5	---	vocs	sg	---	Bedload. Granules and fine gravels up to 6 mm. Boundary destroyed by flight auger so it was not described.

Notes: 101.5 cm is top of braid bar/bedload sediments.

CROSS-SECTION C-C'

Table A48. Description for core 48, cross-section C-C'.

Location:	**Uvalda Quadrangle**	**Map Unit:**	Qh2
Transect:	**C**	**Geomorphic Component:**	Crest of point bar of paleochannel
Core #:	**48**	**Other Remarks:**	50 m from left top of bank (LTB). OSL date site
***Easting:**	349886 m		(UGA11OSL-805).
***Northing:**	3543294 m	**Date:**	9/3/2011
*UTM NAD 83		**Personnel:**	BES, ATW
		Sampling Method:	Hand auger

Depth (cm)	Horizon	Color	RMF	Texture	Structure	Bndy	Remarks
0-4	A	10YR 4/2	---	fsl	1vfgr	no data	Vertical accretion (coarse drape).
4-24	Bw	7.5YR 4/6	---	c	2vfsbk	no data	Vertical accretion. No clay films.
24-75	Bg	2.5Y 6/2	c, medium to coarse, P, 10YR 5/8	scl	1fsbk	no data	Vertical accretion.
75-100	BC	10YR 5/6	---	sl	1vfsbk to sg	no data	Vertical accretion. Fines upward; coarser at base.
100-135	C1	10YR 7/2	---	ms	sg	no data	Transitional.
135-150	C2	10YR 7/1	---	cos	sg	no data	Bedload.
150-180+	C3	10YR 6/1	---	cos to vcos	sg		Predominantly bedload. Granules. Few interbedded clay lenses.

Notes: 135 cm is top of bedload. 185-217 cm sampled for OSL dating. Some horizon boundaries accidentally omitted from description.

Table A49. Description for core 49, cross-section C-C'.

Location:	**Uvalda Quadrangle**	**Map Unit:**	Qh2
Transect:	**C**	**Geomorphic Component:**	Upper-mid point bar of paleochannel
Core #:	**49**	**Other Remarks:**	45.5 m from LTB
***Easting:**	349890 m	**Date:**	9/3/2011
***Northing:**	3543298 m	**Personnel:**	BES, ATW
*UTM NAD 83		**Sampling Method:**	Hand auger

Depth (cm)	Horizon	Color	RMF	Texture	Structure	Bndy	Remarks
0-5	A	no data	---	sl	no data	no data	Vertical accretion (coarse drape).
5-75	Bg	10YR 5/2	m, medium, P, 10YR 5/8 & f, medium, F, 10YR 6/1	scl	no data	no data	Vertical accretion.
75-90	BC	no data	---	cosl	no data	no data	Vertical accretion. Oxidized but color not noted. Interbedded clay lenses.
90-102	Cg1	10YR 7/1	---	ms	sg	no data	Transitional.
102-135+	Cg2	10YR 7/1	---	cos	sg	no data	Bedload. Granules.

Notes: 102 cm is top of bedload. Some horizon boundaries accidentally omitted from description.

Table A50. Description for core 50, cross-section C-C'.

Location:	**Uvalda Quadrangle**	**Map Unit:**	Qh2
Transect:	**C**	**Geomorphic Component:**	Lower-mid point bar of paleochannel
Core #:	**50**	**Other Remarks:**	41 m from LTB
***Easting:**	349892 m	**Date:**	9/3/2011
***Northing:**	3543299 m	**Personnel:**	BES, ATW
*UTM NAD 83		**Sampling Method:**	Hand auger

Depth (cm)	Horizon	Color	RMF	Texture	Structure	Bndy	Remarks
0-5	A	no data	---	sl	no data	no data	Vertical accretion (coarse drape).
5-80	Bg	no data	no data	sc	no data	no data	Vertical accretion. RMF more oxidized than in paleochannel fill but Munsell color not noted.
80-108	C1	no data	---	ms	sg	no data	Transitional.
108-150+	C2	no data	---	cos	sg	no data	Bedload

Notes: 108 cm is top of bedload. Some horizon boundaries accidentally omitted from description.

Table A51. Description for core 51, cross-section C-C'.

Location:	**Uvalda Quadrangle**	**Map Unit:**	Qh2
Transect:	**C**	**Geomorphic Component:**	Toe of point bar/ right bank edge of paleochannel
Core #:	**51**	**Other Remarks:**	37.7 m from LTB
***Easting:**	349901 m	**Date:**	9/3/2011
***Northing:**	3543301 m	**Personnel:**	BES, ATW
*UTM NAD 83		**Sampling Method:**	Hand auger

Depth (cm)	Horizon	Color	RMF	Texture	Structure	Bndy	Remarks
0-60	BCg	10YR 5/2	m, coarse, P, 10YR 5/8	c	1fsbk	no data	Vertical accretion paleochannel fill. Fines upward from sandy clay near base to clay.
60-82	CBg	10YR 5/1	---	scl	1fsbk to m	no data	Vertical accretion paleochannel fill. Fines upward - sandier near base.
82-100	Cg1	10YR 6/1	---	sl	sg	no data	Vertical accretion paleochannel fill. Fines upward from loamy sand at base.
100-105	Cg2	10YR 7/1	---	ms	sg	no data	Bedload.
105-150+	Cg3	10YR 7/1	---	cos	sg	---	Bedload. Few granules.

Notes: 100 cm is top of bedload. Some horizon boundaries accidentally omitted from description.

Table A52. Description for core 52, cross-section C-C'.

Location:	**Uvalda Quadrangle**	**Map Unit:**	Qh2
Transect:	**C**	**Geomorphic Component:**	Paleochannel
Core #:	**52**	**Other Remarks:**	32 m from LTB
***Easting:**	349903 m	**Date:**	9/3/2011
***Northing:**	3543303 m	**Personnel:**	BES, ATW
*UTM NAD 83		**Sampling Method:**	Hand auger

Depth (cm)	Horizon	Color	RMF	Texture	Structure	Bndy	Remarks
0-70	BCg	10YR 5/1	c, medium, P, 7.5YR 5/8	c	1fsbk to m	no data	Vertical accretion paleochannel fill. No sedimentary structures evident.
70-75	CBg	10YR 5/1	---	sc	m to 1fsbk	no data	Vertical accretion paleochannel fill to transitional.
75-90	Cg1	10YR 6/1	---	msl	m	no data	Transitional.
90-150+	Cg2	10YR 6/1	---	cos	sg	no data	Bedload. Fines upward from very coarse sand at base. ≤5 mm gravels.

Notes: 90 cm is top of bedload. Some horizon boundaries accidentally omitted from description.

Table A53. Description for core 53, cross-section C-C'.

Location:	**Uvalda Quadrangle**	**Map Unit:**	Qh2
Transect:	**C**	**Geomorphic Component:**	Paleochannel
Core #:	**53**	**Other Remarks:**	28.9 m from LTB
***Easting:**	349906 m	**Date:**	9/3/2011
***Northing:**	3543305 m	**Personnel:**	BES, ATW
*UTM NAD 83		**Sampling Method:**	Hand auger

Depth (cm)	Horizon	Color	RMF	Texture	Structure	Bndy	Remarks
0-10	Ag	10YR 5/2	c, medium, P, 7.5YR 4/6	c	2fsbk	no data	Vertical accretion paleochannel fill. No sedimentary structures evident.
10-105	BCg to CBg	10YR 6/1	c, medium, P, 7.5YR 5/8	c	1fsbk to m	a	Vertical accretion paleochannel fill. No sedimentary structures evident.
105-160+	Cg1	10YR 6/1	---	vcos	sg	---	105-120 cm contains few clay lenses and may represent stratum of interbedded post channel abandonment flood sands and clays. Top of bedload at 120 cm, where granules encountered.

Notes: 120 cm is top of bedload. Some horizon boundaries accidentally omitted from description.

Table A54. Description for core 54, cross-section C-C'.

Location:	**Uvalda Quadrangle**	**Map Unit:**	Qh2
Transect:	**C**	**Geomorphic Component:**	Paleochannel
Core #:	**54**	**Other Remarks:**	24 m from LTB
***Easting:**	349910 m	**Date:**	9/3/2011
***Northing:**	3543305 m	**Personnel:**	BES, ATW
*UTM NAD 83		**Sampling Method:**	Tile probe

Depth (cm)	Horizon	Color	RMF	Texture	Structure	Bndy	Remarks
0-136	no data	no data	no data	c	no data	a	Vertical accretion paleochannel fill.
136-153	no data	no data	no data	cos to vcos	sg	a	Loose sand interpreted as post channel abandonment flood sands.
153-155+	no data	no data	no data	cos to vcos	sg	---	Bedload. Firm when probed.

Notes: 153 cm is top of bedload. A tile probe was used to determine depths of stratigraphic boundaries. Sample material was not recovered by hand auger. Therefore, horizons, colors, and structures (where not obvious from probing) were not described. This technique was reliable because auger borings revealed that the fill in this paleochannel is very uniform.

Table A55. Description for core 55, cross-section C-C'.

Location:	**Uvalda Quadrangle**	**Map Unit:**	Qh2
Transect:	**C**	**Geomorphic Component:**	Paleochannel
Core #:	**55**	**Other Remarks:**	20 m from LTB
***Easting:**	349915 m	**Date:**	9/3/2011
***Northing:**	3543311 m	**Personnel:**	BES, ATW
*UTM NAD 83		**Sampling Method:**	Tile probe

Depth (cm)	Horizon	Color	RMF	Texture	Structure	Bndy	Remarks
0-145	no data	no data	no data	c	no data	a	Vertical accretion paleochannel fill.
145-150	no data	no data	no data	cos	sg	a	Loose sand interpreted as post channel abandonment flood sands.
150-160+	no data	no data	no data	vcos to cos	sg	---	Bedload. Firm when probed.

Notes: 150 cm is top of bedload. A tile probe was used to determine depths of stratigraphic boundaries. Sample material was not recovered by hand auger. Therefore, horizons, colors, and structures (where not obvious from probing) were not described. This technique was reliable because auger borings revealed that the fill in this paleochannel is very uniform.

Table A56. Description for core 56, cross-section C-C'.

Location:	**Uvalda Quadrangle**	**Map Unit:**	Qh2
Transect:	**C**	**Geomorphic Component:**	Paleochannel
Core #:	**56**	**Other Remarks:**	16 m from LTB
***Easting:**	349917 m	**Date:**	9/3/2011
***Northing:**	3543305 m	**Personnel:**	BES, ATW
*UTM NAD 83		**Sampling Method:**	Hand auger and tile probe.

Depth (cm)	Horizon	Color	RMF	Texture	Structure	Bndy	Remarks
0-15	Ag	10YR 5/2	c, fine, P, 10YR 4/6	c	1fsbk	no data	Vertical accretion paleochannel fill.
15-80	Cg1	10YR 5.5/1	m, fine, P, 10YR 5/8	c	m	no data	Vertical accretion paleochannel fill. Hint of gley color.
80-177	Cg2	10YR 5/1	f, fine, P, 10YR 5/8	c	m	a	Vertical accretion paleochannel fill. Fines upward from sandy loam near base. Abundant organic materials near base.
177-315+	Cg3	10YR 5/2	---	gr vcos	sg	---	Bedload. Granules and ≤6 mm gravels.

Notes: 177 cm is top of bedload. Some horizon boundaries accidentally omitted from description.

Table A57. Description for core 57, cross-section C-C'.

Location:	**Uvalda Quadrangle**	**Map Unit:**	Qh2
Transect:	**C**	**Geomorphic Component:**	Paleochannel thalweg
Core #:	**57**	**Other Remarks:**	15.8 m from LTB. ^{14}C date site (UGAMS 9718).
***Easting:**	~349917 m	**Date:**	9/3/2011
***Northing:**	~3543305 m	**Personnel:**	BES, ATW
*UTM NAD 83		**Sampling Method:**	Hand auger

Depth (cm)	Horizon	Color	RMF	Texture	Structure	Bndy	Remarks
0-15	Ag	10YR 5/2	c, fine, P, 10YR 4/6	c	1fsbk	no data	Vertical accretion paleochannel fill.
15-80	Cg1	10YR 5.5/1	m, fine, P, 10YR 5/8	c	m	no data	Vertical accretion paleochannel fill. Hint of gley color.
80-174	Cg2	10YR 5/1	f, fine, P, 10YR 5/8	c	m	a	Vertical accretion paleochannel fill. Fines upward from sandy loam near base. Abundant organic materials near base.
174-176+	Cg3	10YR 5/2	---	gr vcos	sg	---	Bedload. Granules and ≤6 mm gravels.

Notes: 174 cm is top of bedload. Some horizon boundaries accidentally omitted from description.

Table A58. Description for core 58, cross-section C-C'.

Location:	**Uvalda Quadrangle**	**Map Unit:**	Qh2
Transect:	**C**	**Geomorphic Component:**	Paleochannel
Core #:	**58**	**Other Remarks:**	12 m from LTB
***Easting:**	349922 m	**Date:**	9/3/2011
***Northing:**	3543309 m	**Personnel:**	BES, ATW
*UTM NAD 83		**Sampling Method:**	Tile probe

Depth (cm)	Horizon	Color	RMF	Texture	Structure	Bndy	Remarks
0-60	no data	no data	no data	c	no data	a	Vertical accretion paleochannel fill.
60-120	no data	no data	no data	s & c	no data	a	Interstratified post channel abandonment sands and clays.
120+	no data	no data	no data	s	sg	---	Bedload. Firm when probed.

Notes: 120 cm is top of bedload.

Table A59. Description for core 59, cross-section C-C'.

Location:	**Uvalda Quadrangle**	**Map Unit:**	Qp5
Transect:	**C**	**Geomorphic Component:**	Adjacent to scarp cut by Qh2 paleochannel.
Core #:	**59**	**Other Remarks:**	-3.1 m from LTB
***Easting:**	349936 m	**Date:**	9/3/2011
***Northing:**	3543313 m	**Personnel:**	BES, ATW
*UTM NAD 83		**Sampling Method:**	Hand auger

Depth (cm)	Horizon	Color	RMF	Texture	Structure	Bndy	Remarks
0-10	A	10YR 4/4	---	fsl	1vfsbk	no data	Vertical accretion.
10-45	E	10YR 5/6	---	sl	1vfsbk	no data	Vertical accretion.
45-77	Bt1	2.5YR 4/6	---	scl	2fsbk	no data	Vertical accretion. Clay films present.
77-98	Bt2	2.5YR 4/7	---	sl	1fsbk	no data	Vertical accretion. "Color BC" in upper 30 cm?
98-165	C1	5YR 4.5/6	---	lms	sg	no data	Bedload or mid- to lower braid bar sediment.
165-220+	C2	10YR 6/6	---	ms	sg	---	Bedload or mid- to lower braid bar sediment. Coarser than C1; some of sand is in very coarse sand fraction.

Notes: Horizon boundaries accidentally omitted from description.

APPENDIX B – PROFILE DESCRIPTIONS FROM ALLOFORMATIONS Qp2 AND Qp1, UVALDA QUADRANGLE, GEORGIA

Table B1. Description for Qp2 alloformation, McBride Tract locality.

Location:	**Uvalda Quadrangle**	**Map Unit:**	Qp2
Site:	**McBride Tract**	**Geomorphic Component:**	No distinct fluvial topography - flat terrace tread
		Other Remarks:	On highest part of tread in clearing
***Easting:**	347434 m	**Date:**	6/26/2012
***Northing:**	3543795 m	**Personnel:**	BES
*UTM NAD 83		**Sampling Method:**	Hand auger

Depth (cm)	Horizon	Color	RMF	Texture	Structure	Bndy	Remarks
0-20	Ap	10YR 4.5/3	---	sl	0 to 1vfsbk	a	Alluvium. Sand component is medium sand.
20-30	EA	10YR 5/3	---	sl	0 to 1fsbk	c	Alluvium. Sand component is medium sand.
30-70	E	10YR 6/4	---	sl	0 to 1fsbk	g	Alluvium. Sand component is medium sand.
70-95	Bt1	10YR 6/6	---	scl	1msbk	g	Alluvium. Grains coated and bridged with clay. Rare granules.
95-127	Bt2	10YR 6/7	---	sl to scl	1 to 2msbk	g	Alluvium. Distinct, discontinuous clay films on some ped faces; some grains coated and bridged with clay. Common, medium 5YR 5/8 Fe-oxide masses. Rare subrounded to subangular granules.
127-180	Bt3	7.5YR 6/8	f, fine, P, 10YR 4/8	sl	1msbk	g	Alluvium. Sand component is coarser. Up to 10 mm subrounded to subangular quartz gravels. Pockets of 10YR 7/2 sandy clay loam and some ≤2 chroma reduced zones.
180-270	Bt4	10YR 4/6	c, medium, D, 10YR 6/8	sl	1csbk	c	Alluvium (?). Common, subangular quartz granules and fine gravels. Grains of sandy loam matrix coated and bridged with clay. Many pockets of reduced, 10YR 7/2 sandy clay loam and sandy clay give horizon a variegated color. Horizon is heavily weathered.
270-300+	C	10YR 7/6	---	sl	sg	---	Alluvium (?). Coarser than Bt4, with upper coarse sand as sand component of the sandy loam texture. Up to 15 mm subrounded and subangular quartz gravels. Looks more like alluvium than Bt4.

Notes: 0-180 interval interpreted as Oconee River-derived alluvium. 180-300+ cm interval is likely also alluvium, but possibility exists that it consists of weathered pre-Quaternary Coastal Plain sediments.

Table B2. Description for Qp2 alloformation, Chapman Tract locality.

Location:	**Uvalda Quadrangle**	**Map Unit:**	Qp2
Site:	**Chapman Tract**	**Geomorphic Component:**	Flat terrace tread
		Other Remarks:	In pre-existing borrow pit near 6 m scarp that forms lateral boundary with Qp5
***Easting:**	349165 m	**Date:**	7/13/2012
***Northing:**	3540718 m	**Personnel:**	BES, JMM
*UTM NAD 83		**Sampling Method:**	Pit face

Depth (cm)	Horizon	Color	RMF	Texture	Structure	Bndy	Remarks
0-20	Ap	10YR 5/3	---	sl	0 to 1fsbk	c	Vertical accretion
20-55	E	10YR 6/3	---	sl	nearly m	c	Vertical accretion
55-87	Bt	10YR 6/5	f, medium, P, 2.5YR 4/8	cl	2msbk	g to d	Vertical accretion. Distinct, discontinuous clay films on tops and faces of peds.
87-125	Btg	10YR 6/1	c, coarse, P, 2.5YR 4/8	c	3mabk	a	Vertical accretion. Distinct, nearly continuous clay films on tops and faces of peds. There is no sand or gravel lag overlying the abrupt contact with the C at the base of this horizon.
125-230+	C	7.5YR 7/1	m, coarse, P, 10R 6/3 conforming to beds	sl to ls	sg	---	Lateral accretion and bedload sediment. Moderately to poorly sorted; sand fraction component of texture is medium to coarse sand. Infrequent granules. Indeterminant cross-bedding, with trough cross-bedding evident elsewhere in pit. Individual beds range from 5-15 cm thick. Many zones oxidized to ~10R 6/3. In rare cases, weathering in the form of redox features overprints abrupt contact with overlying Btg horizon. Face of pit is weakly cemented.

Notes: Entire profile interpreted as Oconee River-derived alluvium. The contact between what are interpreted to be vertical and lateral accretion sediments is surprisingly abrupt, given how old and weathered these deposits are. Sedimentary structures in the C horizon are relatively well preserved.

Table B3. Description for Qp1 alloformation, Allen Tract, boring 1.

Location:	**Uvalda Quadrangle**	**Map Unit:**	Qp1
Site:	**Allen Tract, boring 1**	**Geomorphic Component:**	Terrace tread, just above 55 m contour
		Other Remarks:	Tread is dissected to the north and south by streams
***Easting:**	344413 m	**Date:**	7/14/2012
***Northing:**	3544887 m	**Personnel:**	BES, JMM
*UTM NAD 83		**Sampling Method:**	Hand auger

Depth (cm)	Horizon	Color	RMF	Texture	Structure	Bndy	Remarks
0-20	Ap	10YR 3/2	---	sl	0 to 1f to msbk	a	Surface covered in 5-20 mm rounded to subrounded ironstones.
20-35	BE	10YR 4/6	---	sl	1msbk	c	Common 5-20 mm rounded to subrounded ironstones.
35-150	Bt	10YR 5/8	---	scl	2msbk	g	Common, distinct, discontinuous clay films on ped faces. Common 5-20 mm rounded to subrounded ironstones above 105 cm.
150-180	Btv	2.5YR 4/6	c, coarse P, 10YR 8/1	sl to scl	2 to 3mabk	g	10YR 4/8 plinthite averaging 10 mm thick (b-axis) with 10YR 6/8 "haloes".
180-240	B't or BC	2.5YR 4/7	see remarks	gr sl	1msbk	d	10YR 8/1 reduced zones at 195-200 cm and 210-225 cm. No plinthite, but weakly cemented iron masses occur. Weathered enough to be a Bt horizon, but structure and argillans hard to verify due to sample destruction by auger. Subrounded to rounded 2-16 mm quartz gravels present.
240-330	C1	7.5YR 5/6	---	gr lower cos	sg	d	Contains pockets of loamy sand. Subrounded to rounded 2-16 mm quartz gravels present.
330-400+	C2	10YR 6/6	---	lower cos	sg	---	Gravels less abundant and smaller on average than in overlying horizons - only present in thin lenses. Sand predominates, fewer fines than in C1. Yellower than C1 and less weathered. Looks like sandy alluvium.

Notes: Entire profile interpreted as extremely weathered alluvium. Origin of ironstones in 0-105 cm interval unclear.

Table B4. Description for Qp1 alloformation, Allen Tract, boring 2.

Location:	**Uvalda Quadrangle**	**Map Unit:**	Qp1
Site:	**Allen Tract, boring 2**	**Geomorphic Component:**	Terrace tread, just below 52 m contour
		Other Remarks:	Tread is dissected to the north and south by streams
***Easting:**	345237 m	**Date:**	7/14/2012
***Northing:**	3545307 m	**Personnel:**	BES, JMM
*UTM NAD 83		**Sampling Method:**	Hand auger

Depth (cm)	Horizon	Color	RMF	Texture	Structure	Bndy	Remarks
0-10	Ap	10YR 4/3	---	sl	0 to 1fsbk	a	Surface covered in 5-20 mm rounded to subrounded ironstones that persist to depth of 120 cm.
10-25	E	10YR 5/4	---	sl	1fsbk	c	
25-90	Bt1	10YR 5.5/8	---	scl to cl	2msbk	g	Few, distinct, discontinuous clay films on ped faces.
90-120	Bt2	10YR 5.5/8	c, medium, P 10YR 6/3	scl	2msbk	g	Few to no clay films.
120-165	Btv	7.5YR 5/8	m, medium, P 10YR 7/1	sl to scl	2msbk	g	Contains 10YR 4/6 plinthite. Few 8-12 mm subrounded quartz gravels occur from 160-165 cm.
165-255	(2?)BC to CB	10YR 7/1	c, medium, P 10R 3/6	sic & sl	1msbk to m	c	Horizon consists of silty clay from 165-225 cm and contains 10R 3/6 bodies of plinthite up to 10 mm thick in the 180-195 cm interval. 225-255 cm interval consists of sandy loam and is variegated in color (equal parts 10YR 7/1 and 10R 4/6).
255-270+	(2?)C	5YR 5/6	---	gravelly lower cos	sg	---	Contains subrounded to rounded 5-15 mm quartz gravels.

Notes: Profile has been extremely altered by weathering and pedogenesis. 0-165 cm interval is interpreted as highly weathered alluvium. 165-270+ cm interval probably also consists of highly weathered alluvium, but the possibility that this interval contains older Coastal Plain sediments cannot be ruled out. Refusal on gravels at 270 cm. Origin of ironstones in 0-120 cm interval is unclear.